UNIVERSITÉ DE STRASBOURG

ÉCOLE DOCTORALE 414

Sciences de la vie et de la santé

INSERM 1118

THÈSE présentée par :

Jelena SCEKIC-ZAHIROVIC

soutenue le : **11 Janvier 2016**

pour obtenir le grade de : **Docteur de l'université de Strasbourg**

Discipline/ Spécialité : **Neurosciences**

Troncation conditionnelle de la protéine FUS chez la souris: un nouveau modèle animal du continuum sclérose latérale amyotrophique/démence fronto-temporale

DIRECTEURS DE THESE :

M DUPUIS Luc	Directeur de recherches, Université de Strasbourg
M CARONI Pico	Professeur, University of Basel
Mme BARTOS Marlene	Professeur, University of Freiburg

RAPPORTEURS :

Mme NEUMANN Manuela	PR PUPH, University of Tubingen
M BUEE Luc	Directeur de recherchés, Inserm UMR_S 1172

EXAMINATEURS :

M CHELLY Jamel	PR PUPH, Université de Strasbourg/IGBMC
M ROTTER Stefan	Professeur, University of Freiburg

Jelena SCEKIC-ZAHIROVIC

Troncation conditionnelle de la protéine FUS chez la souris: un nouveau modèle animal du continuum sclérose latérale amyotrophique/démence fronto-temporale

Résumé

La sclérose latérale amyotrophique (SLA) et la démence fronto-temporale (DFT) sont deux maladies qui constituent un continuum clinico-pathologique. La mutation de FUS, une protéine nucléaire à fonctions multiples, provoque des cas familaux de SLA, et ces mutations provoquent une redistribution sub-cellulaire de FUS, du noyau vers le cytoplasme. Certains cas de DFT présentent une telles distribution anormale en l'absence de mutations de FUS. Il n'est pas connu si la maladie est provoquée par une perte de la fonction nucléaire de FUS et/ou un gain de fonction cytoplasmique.

Nous avons généré et caractérisé une lignée de souris exprimant une forme cytoplasmique de FUS (*Fus-ΔNLS)*. La localisation exclusive de FUS dans le cytoplasme provoque la mort des motoneurones *via* un gain de fonction dans les motoneurones eux-mêmes. Une localisation cytoplasmique partielle de FUS est suffisante pour développer un phénotype de la SLA et de DFT.

Les mécanismes élucidés permettront de comprendre les bases des SLA/DFT et de

Mots-clés : SLA/DFT, FUS, cytoplasmique localisation, gain de fonction

Résumé en anglais

Amyotrophic lateral sclerosis (ALS) and Frontotemporal dementia (FTLD) are now considered as a unique clinicopathological spectrum referred to as ALS/FTLD. Cytoplasmic aggregation of the physiologically nuclear FUS protein is a hallmark feature of a subset of ALS/FTLD. It remains unknonwn whether the critical pathogenic event relies on a loss of FUS normal nuclear functions, a toxic gain of function of FUS in the cytoplasm, or a combination of both.

To answer this question we have generated a conditional mouse model expressing truncated FUS without nuclear localization signal - *FusΔNLS*. Our data showed that complete cytoplasmic mislocalization of truncated FUS protein within spinal motor neurons is a major determinant of motor neuron degeneration via toxic gain of function. A partial mislocalization of truncated FUS protein was sufficient to trigger key features of ALS and of FTLD.These studies allowed the elucidation of mechanisms underlying FUS role in ALS/FTLD, and will hopefully lead to development of therapies for these devastating diseases.

Key words: ALS/FTLD, FUS, cytoplasmic mislocalization, toxic gain of function

ACKNOWLEDGMENTS

This thesis could not have been completed without the great support that I have received from so many people over the years. I wish to offer my most heartfelt thanks to the following people.

Firstly, I would like to express my sincere gratitude and deepest thanks to my supervisor Dr Luc DUPUIS for the continuous support of my PhD study and related research, for his patience, motivation, and immense knowledge. His guidance helped me in all the time of research and writing of this thesis. I could not have imagined having a better advisor and mentor for my PhD study.

My sincere thanks also go to Director Dr Jean-Phillippe LOEFFLER who provided me an opportunity to join his team, and who gave access to the laboratory and research facilities. Without his precious support it would not be possible to conduct this research.

I would like to thank to my thesis co-supervisors Prof. Pico CARONI and Prof. Marlene BARTOS for their help and encouragement.

I also wish to express my sincere gratitude and appreciation to Dr Caroline ROUAUX, who has taught me many of the techniques used in this project, and for being a friend.

I am grateful to Dr Frédérique RENE and Dr Jose-Luis GONZALEZ DE AGUILAR, for their insightful comments but also for the hard question which incented me to widen my research from various perspectives.

I am thankful to other members of my committee, Pr Manuela NEUMANN, Dr Luc BUEE, Pr Jamel CHELLY and Prof. Stefan ROTTER for finding the time in their busy schedules to review my thesis.

I am indebted to Hajer ELOUSSINI, for her love and encouragement. Thank you for your support when I have needed it the most. You really let me feel like at home. You are a great friend and a rock of stability in my life and I hope our strong friendship will continue in the future. Thank you with all my heart!

My work has greatly benefited from suggestions and kind encouragement from Sylvie DIRRIG-GROSCH and Jérôme SINNIGER. Your technical depth and attention to the detail, which I experienced, are amazing.

I thank my fellow lab mates Lavinia PALAMIUC, Aurélia VERNAY and Alexandre HENRIQUES, Pauline VERCRUYSSE, Gina PICCHIARELLI, Stéphane DIETERLE, Christine MARQUES and Laura ROBELIN for the stimulating discussions, for the sleepless nights we were working together before deadlines, and for all the fun we have had in the last three years.

To Mme Brigitte KUENEMANN, thank you for keeping your office door open and available for all the times when I needed it.

Thank you goes to all the other members of the LOEFFLER lab Annie PICCHINENNA and Marie-Jo RUIVO for providing a pleasant and productive working atmosphere.

The work of this thesis was supported by the Erasmus Mundus Neurotime program. My greatest thank to wonderful people in this unique program Dr Paul PEVET and Dr Domitille BOUDARD.

Last but not the least, I would like to thank my family: my husband, my brother and to my mother for supporting me spiritually throughout writing this thesis and in my life in general.

To anyone that may I have forgotten, I apologize. Thank you as well.

TABLE OF CONTENT

ABBREVIATIONS

AAVs	Adeno-associated viruses
ALS	Amyotrophic lateral sclerosis
ALSbi	ALS with behavioural impairment
ALSci	ALS with cognitive impairment
AOS	Apraxia of speech
BIBD	Basophilic inclusion body disease
bvFTD	Behavioural variant frontotemporal dementia
CHCHD10	Coiled-coil-helix-coiled-coil-helix domain-containing protein 10
CHMP2B	Charged multivesicular body protein 2B
CLIP	Crosslinking and immunoprecipitation
CNS	Central nervous system
CSF	Cerebrospinal fluid
DPR	Essential tremor
ET	Dipeptide repeat proteins
EWSR1	Ewing RNA-binding protein
FTD	Frontotemporal dementia
FTLD	Frontotemporal lobar degeneration
FUS	Fused in sarcoma
GFAP	Glial Fibrillary Acidic Protein
GWAS	Genome wide associated studies
HDAC1	Histone deacetylase 1
IBMPFD	Inclusion body myopathy and Paget's disease of the bone
LMN	Lower motor neuron
MND	Motor neuron disease
MAPT	Microtubule-associated protein tau
NCI	Neuronal cytoplasmic inclusions
NES	Nuclear export signal
NII	Neuronal nuclear inclusions
NIFID	Neuronal intermediate filament inclusion disease
NLS	Nuclear localization signal
NMJ	Neuromuscular junction
OPTN	Optineurin
PGRN	Progranulin
PLS	Primary lateral sclerosis
PNFA	Progressive nonfluent aphasia

PMA	Progressive muscular atrophy
POMC	Pro-opiomelanocortin neurons
PRMT1	Protein arginine methyl transferases 1
RGG	Glycine rich region
RIP	RNA immunoprecipitation
RRM	RNA recognition motif
SBT	Somatic brain transgenesis
SD	Semantic dementia
SOD1	Superoxidedismutase 1
SQSTM1	Sequestosome 1
TAF-15	TATA-binding protein-associated factor 15
TARDBP	Transactive response DNA-binding protein
TBK1	TANK-binding kinase 1
TLS	Translocated in liposarcoma
UBQLN2	Ubiquilin 2
UMN	Upper motor neuron
UPS	Ubiquitin proteasome system
VAPB	Vesicle-associated membrane protein-associated protein B
VCP	Valosin-containing protein
VE neurons	Von Economo neurons
WES	Whole-exome sequencing
WGS	Whole-genome sequencing

FOREWORD

The general topic of my PhD work was the understanding of the molecular mechanisms of amyotrophic lateral sclerosis (ALS). During these last 3 years, I pursued two major objectives.

First, I sought to understand the consequences of loss of function of ALS8/VAPB, a gene that has been reported as mutated in a few familial ALS cases. When I arrived in the laboratory, it had already been shown that VAPB knock-out mice did not develop ALS, but showed a mild rotarod defects. I went further into the analysis of these mice and showed that they developed abnormal muscle response to fasting (Han et al, 2013, PLOS Genet). In collaboration with Dr Niels Decher, we also showed that VAPB knock-out mice suffered from heart defects (manuscript in preparation). While the analysis of VAPB knock-out mice led to interesting insights into the physiological function of VAPB, we concluded from our work that the loss of function of VAPB has likely little relevance to ALS. I have also participated in another study investigating a role of the hypothalamus in ALS (manuscript submitted). I included these papers in the Annex of the manuscript.

A second objective was initiated in parallel to understand the mechanisms of ALS mediated by FUS mutations. FUS mutations are a much more frequent cause of familial ALS than VAPB mutations, and lead to typical ALS. In the present manuscript, I describe our two step analysis of a novel knock-in model of FUS-ALS, with a first study focusing on the phenotype of homozygous mice (Publication N°1), and a second study in preparation describing the early characterization of heterozygous knock-in mice (Publication N°2).

INTRODUCTION

INTRODUCTION

Neurodegenerative diseases are a group of diverse disorders characterized by progressive loss of specific populations of neurons. In the vast majority of cases, etiology is unknown. Although, these diseases affect different neuronal populations, lead to widely different clinical manifestations, and are characterized by disparate pathological findings, they share a common characteristic, the presence of misfolded and aggregated proteins in and/or around neurons.

Over the past few years, several clinical, genetic (molecular), and neuropathological features have been recognized as shared by different neurodegenerative diseases. As a typical example, an important scientific interest has been driven toward the DNA/RNA-binding protein FUS (fused in sarcoma). This growing interest in FUS arose after the discovery of variants in the FUS gene causing or contributing to multiple neurodegenerative diseases, including amyotrophic lateral sclerosis (ALS), rare forms of frontotemporal lobar degeneration (FTLD), polyglutamine diseases as well as essential tremor (ET). Additionally, abnormal aggregation of FUS protein has been reported in *postmortem* material of patients suffering from these neurodegenerative diseases in the absence of somatic *FUS* mutations. These findings suggest an important role of FUS in the pathogenesis of these diseases.

Although several lines of evidence indicate that cytoplasmic mislocalization of FUS, is a key event in disease pathogenesis, definitive *in vivo* evidence is lacking. The respective contributions of gain *vs.* loss of function, as well as the cell types in which the critical pathogenic events occur are still undefined.

More generally, the links between FUS dysregulation and pathophysiological processes leading to neurodegeneration in ALS/FTD are poorly understood.

Despite worldwide efforts in the research field, current understanding of the normal function of FUS, and its role in the pathology of ALS, FTLD and other neurodegenerative diseases, are still insufficient. Further understanding of the underlying pathogenic mechanisms of these FUS-related disorders might lead to improvements in the treatment and prevention of such disorders.

In this introduction, I will first describe ALS and FTLD as the major diseases involving FUS. I will then present the structure and physiological functions of FUS. The pathology of FUS, and the effects of FUS mutations, will be detailed to discuss the currently existing models of FUS diseases.

I. ALS AND FTLD: clinical, genetic and pathological link

ALS and FTLD were traditionally considered as two completely different neurological disorders with discordant clinical features. Over the years, however, several observations have suggested that there is a link connecting these disorders. Multiple lines of emerging evidence showed that these disorders share mutual clinical, pathological and genetic features and led to establishment of ALS/FTLD disease spectrum.

A. Clinical presentations

1. Amyotrophic lateral sclerosis (ALS)

Classical concept – a single disease vs. new concept – heterogeneous syndrome

Amyotrophic lateral sclerosis (ALS) is the most frequent adult onset degenerative disease of the motor neuron (motor neuron disease) with an incidence of 2.6/100 000.It is characterized by progressive loss of **cortical-upper (UMN)** and **spinal-lower (LMN)** motor neurons (1–3).The name describes the key features of the disease: muscle wasting (*amyotrophic*) due to the degeneration of the lower motor neurons and their axons and degenerationof the upper motor neurons and their corticospinal axonal tracts (*lateral sclerosis*) (4). Clinically, gradual loss of motor neurons leads to muscle weakness, fasciculation, spasticity and paralysis with a devastatingly rapid disease progression and respiratory failure as the cause of death for most patients (**Figure 1**) (3). Disease onset, generally in adulthood, peaks at 60–70 years of age. Half of the affected individuals die within 3-5 years. The genetics of ALS comprises only 5-10% of cases due to identified genetic mutations while nearly 90-95% remains of unknown origin. Regardless of the genetics, ubiquitin-positive inclusions are found in dying motor neuronsin almost all ALS cases. More than a century after Jean-Martin Charcot first description of the disease in 1869, and in spite of many efforts towards the elucidation its etiology and the search for a treatment for ALS remains an incurable disease of unknown origin.

One possible reason for this failure could be due to the fact that for a long period, ALS has been identified as a single nosological entity, characterized by a pattern of progressive motor neuron degeneration.Textbook neurology addresses ALS as a degenerative disease that **selectively affects upper and lower motor neurons**– a description which suggests that the clinical presentation of ALS is very **homogenous**. This may explain why the disease was expected to have a single cause, a single pathogenesis and a single phenotype. However, with growing knowledge of profound clinical, neuropathological and now genetic **heterogeneity**, the concept of ALS as one disease appears increasingly unsustainable.

1.1. Phenotypic heterogeneity: from motor neuron disease to neurodegenerative disease

Clinical examination usually reveals atrophy and weakness of muscles, fasciculation, hyperreflexia and often a mild to severe hypertonia. Clinicians designate weakness, muscle atrophy and fasciculation as **lower motor neuron signs**, whereas hyperreflexia and hypertoniaindicate **upper motor neuron involvement** (**Figure 1**).

Figure 1. Different patterns of MN involvement in ALS

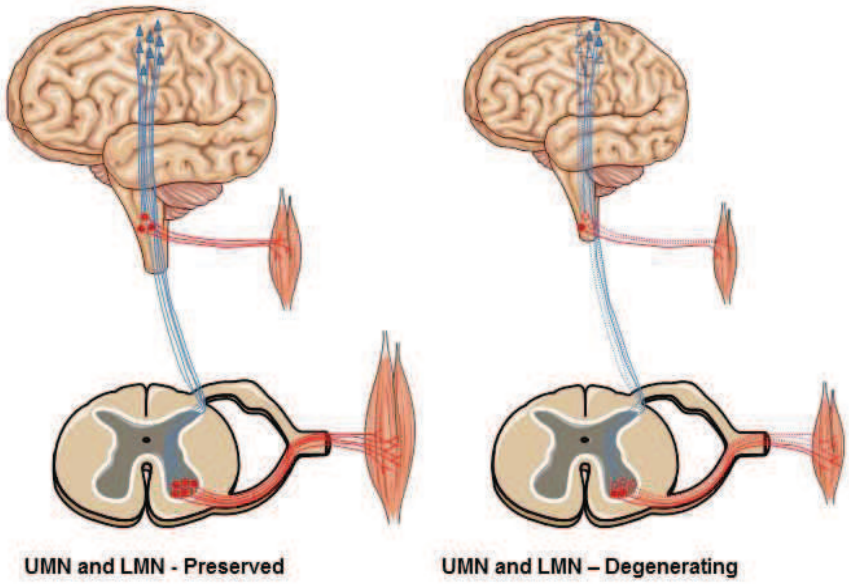

UMN involvement	
Muscle bulk	Grossly normal
Weakness	Mild to moderate
Fasciculation	Absent
Tone	Hypertonia
Reflex	Bisk
Hoffman"s reflex	Present
Babinski reflex	Present

LMN involvement	
Muscle bulk	Atrophic
Weakness	Severe
Fasciculation	Present
Tone	Hypotonia
Reflex	Reduced or absent
Hoffman"s reflex	Absent
Babinski reflex	Absent

Schematic representation of LMN (red) and UMN (blue) degeneration with clinical signs (red and blue boxes) in ALS

The evidence of both upper and lower motor neuron involvement is required for the diagnosis of ALS, and have been incorporated in the so-called revised El Escorial criteriaor the newer Awaji criteria (**Table 1**) (5). Using these criteria ALS itself can be classified as **definite, probable or possible.**

Table 1. Diagnostic criteria for amyotrophic lateral sclerosis (ALS) derived from the revised El Escorial and Awaji criteria

Principles of revised El Escorial CriteriaFi	Principles of the Awaji-Shima consesus recommendations
1. Evidence of LMN loss (reduced interferential pattern on full conrtaction and increased firing rate)	1. Evidence of LMN loss (reduced interferential pattern on full conrtaction and increased firing rate)
2. Evidence of reinnervation (motor units of large amplitude and longer duration)	2. Evidence of reinnervation (motor units of large amplitude and longer duration)
3. Fibrillation and sharp waves	3. Fibrillation and sharp waves or fasciculation potentials (fibrillation and sharp waves are required in weak limb muscles)

The presence of:	The absence of:
(a) evidence of lower motor neuron degeneration by clinical, electrophysiological, or neuropathological examination; (b) evidence of upper motor neuron degeneration by clinical examination; and (c) progression of the motor syndrome within a region or to other regions, as determined by history or examination;	(a) electrophysiological and pathological evidence of other disease processes that might explain the signs of lower or upper motor neuron degeneration; and (b) neuroimaging evidence of other disease processes that might explain the observed clinical and electrophysiological signs.

Clinically definite	▪ UMN + LMN signs in bulbar region + 2 or more spinal regions ▪ UMN + LMN signs in 3 spinal regions
Clinically probable	▪ UMN + LMN signs 2 or more spinal regions and with UMN signs above the LMN signs
Clinically possible	▪ UMN + LMN signs in 1 spinal region;or ▪ UMN signs in 2 or more spinal regions; or ▪ LMN signs are found above to UMN sign

Reproduced from Costa et al., J. Arch. Neurol.,2012.

In spite of the precise clinical description of ALS, there is a considerable **variability in its phenotypic expressions,** with regard to the site and age of onset, the rate of progression, disease duration and clinical presentation, and the presence and degree of cognitive dysfunction. Among other parameters, **phenotypic heterogeneity** arises due to pattern of motor neuron involvement and extent of extra-motor involvement.

1.1.1. Multiple sites of onset

There are several classification systems in place for ALS. The first one relies on the **site of onset of the disease : spinal, bulbar or respiratory** (**Figure 2**) (6). Most of the patients present first with asymmetric and painless weakness in a limb, which is referred as spinal-onset ALS. In contrast, about 20% of patients present first with weakness in bulbar muscle causing, dysarthria, dysphagia and tongue fasciculations. Finally 3–5% of patients present first with a respiratory onset, characterized by orthopnea or dyspnea (7). Compared to spinal-onset

patients, with bulbar- and respiratory-onset patients have a worse prognosis and a decreased disease duration and long term survival (7), reviewed in(6).

Figure 2. Site of onset in ALS

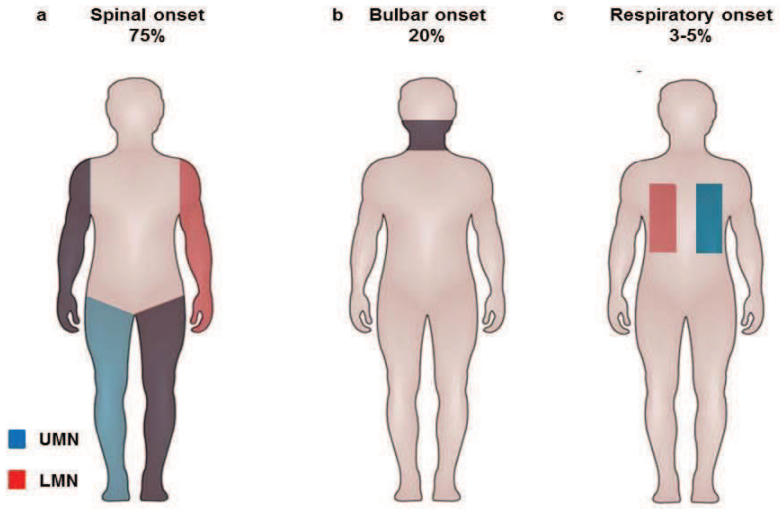

Red indicates LMN involvement, blue indicates UMN involvement. Darker shading indicates more-severe involvement.
(a) In spinal-onset ALS, patchy UMN and LMN involvement is observed in all limbs.
(b) In bulbar-onset ALS, UMN and LMN involvement is observed in the bulbar muscles.
(c) In spinal-onset ALS, UMN and LMN involvement is observed in the respiratory muscles
Reproduced from : Swinnen & Robberecht, Nat. Rev.Neurol., 2014.

1.1.2. Variability in age of onset

The age of clinical onset of ALS is usually between the fourth or sixth decade of life. However, onset at almost any age has been described. Juvenile ALS is rare and defined as ALS with age at onset before 25 years, and the course of progression is generally slower than in other forms of ALS. Onset after 80 years is associated with a particularly faster progression (8). Biological onset of the disease is unknown. In rodent models of ALS, which admittedly are overexpression models, abnormalities are present as early as embryonic development (9–11). Nevertheless, these animals develop no clinical abnormalities until adulthood. Thus, biologically, the disease may start early in life and become clinically apparent much later.

1.1.3. Diversity of disease progression and survival

The range of **disease progression** is wide. Although median **survival** in ALS is generally around 3 years from diagnosis, variability in survival is remarkable with some patients die within months after onset and others surviving for more than two decades (**Figure 3**). Less than 20% of patients survive over 5 years from the disease onset (10). Long survival is seen

more frequently in patients with juvenile ALS and upper motor neuron-predominant ALS (8). Large differences in survival and age at disease onset exist even between individuals from a same family, in whom ALS is caused by the same mutation, suggesting that other factors may modify the phenotype (12).

Figure 3. Variability of disease progression in ALS

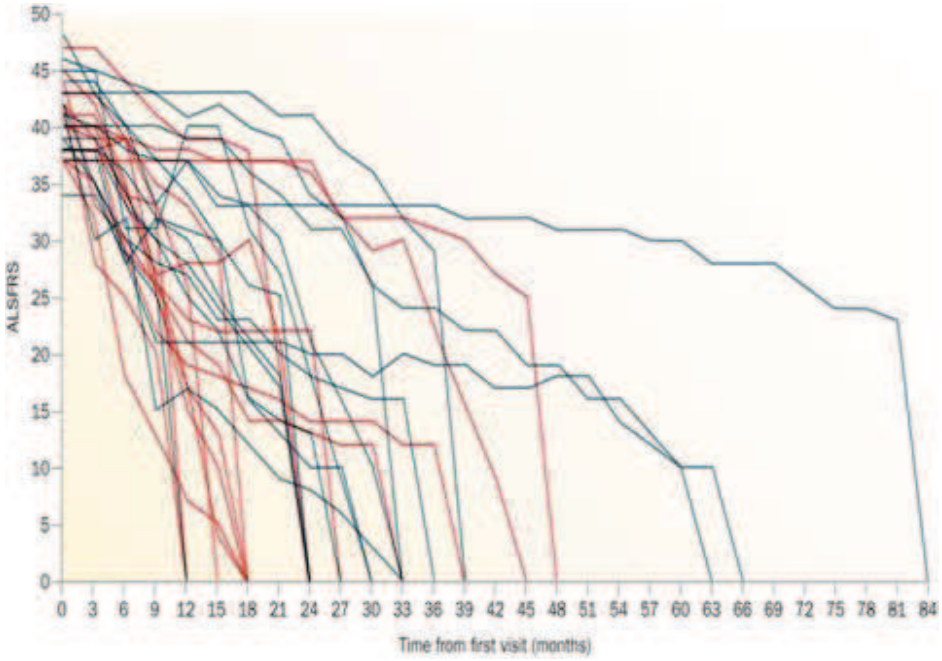

Reproduced from: Swinnen & Robberecht, Nat. Rev.Neurol., 2014.

1.1.4. Heterogenous clinical presentation

Neurodegeneration of motor neuron

Depending on the overall pattern of upper or lower motor neuron involvement and the degree of asymmetry, first **clinical presentation** could vary in between two opposite extremes (**Figure 4**). On the one hand, patients in whom only the lower motor neurons are initially found affected, usually asymmetrically, are classified as progressive muscular atrophy (PMA). On the other hand, if only evidence of upper motor neuron degeneration is initially found, often symmetrically, a diagnosis of primary lateral sclerosis (PLS) is made. Both PMA and PLS progress over time to ALS in a significant proportion of patients (about 5% in each case). The main reason for distinguishing these phenotypes is the difference in prognosis. The patients with PMA fare slightly better than those with clinical evidence of both lower and upper motor neuron involvement while patients with PLS survive longer than both (13).

Further to this, a causal primacy of lower motor neuron over upper motor neuron degeneration remains an issue of debate. Many of the initial pathological changes in rodent models of ALS occur in the lower motor neurons, supporting a dying-back view of pathogenesis (14). However, ALS can also be viewed primarily as a disease of the upper motor neurons, which connect monosynaptically, only in humans and not rodents, with anterior horn cells. This is supported by the clinical observation that the oculomotor, abducens, and Onuf's motor nuclei, which all lack direct cortical motor neuron connections, are strikingly resistant to degeneration (15).

Figure 4. ALS, pattern of motor neuron involvement.

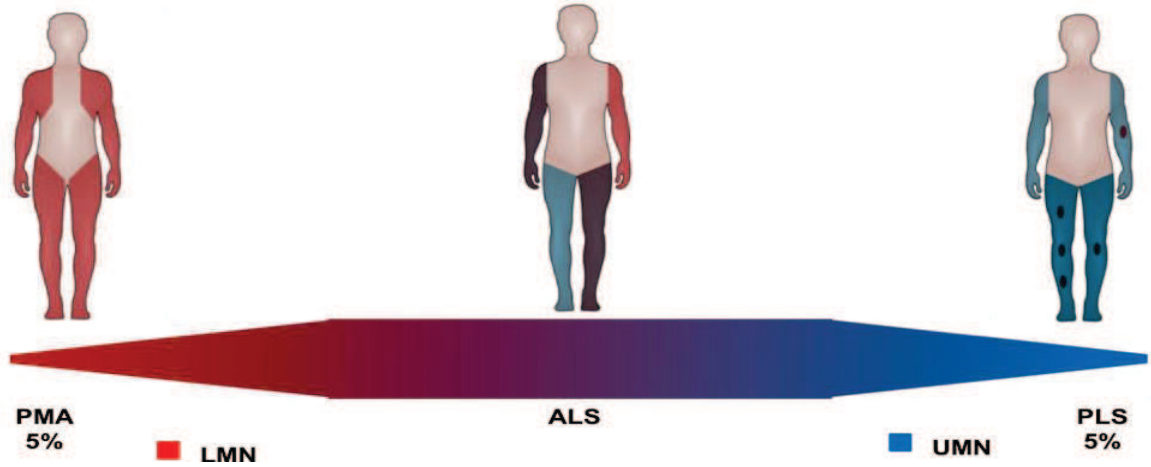

Red indicates LMN involvement, blue indicates UMN involvement. Darker shading indicates more-severe involvement. PMA (isolated LMN involvement) and PLS (isolated UMN involvement) constitute the ends of a spectrum of LMN and UMN involvement; intermediate phenotypes are considered to be different expressions of ALS
PMA- In progressive muscular atrophy, LMNs in arms and legs are involved, often proximally.
PLS- In primary lateral sclerosis, UMNs of arms and legs are primarily involved, but later in the disease, discrete LMN involvement can be detected.
Reproduced from :Swinnen & Robberecht, Nat. Rev.Neurol., 2014.

Neurodegeneration of extramotor neurons

ALS phenotypic variability becomes more apparent when it combines different motor and extramotor involvement. In some patients, neurons in the prefrontal and temporal cortexare affected. This leads to cognitive and/or behavioural problems. ALS patients with mild behavioural dysfunction are classified as having ALS with behavioural impairment (ALSbi), whereas patients with mild executive and language dysfunction are said to have ALS with cognitive impairment (ALSci). In total, around 30% of ALS (16). However, in about 15% of ALS cases, patients who meet the Neary criteria for frontotemporal dementia (FTD), the main symptom of frontotemporal lobe degeneration (FTLD) are considered to have ALS-FTLD (17).

On the other hand, up to 50% of patients with a diagnosis of FTLD have some motor neuron involvement and are said to have FTLD–MND (16,17). Of note, 15% of FTLD patients show signs of motor neuron degeneration that meet criteria for ALS and are classified as ALS–FTLD (**Figure 5**) (17). This suggests that ALS and FTLD are at the ends of a same disease spectrum.

Although, there are extremes of relatively isolated involvement of each of these compartments PLS, PMA and FTLD, all of these **overlap** with classic ALS on post-mortem neuropathological examination, by showing **protein inclusions**.

Figure 5. ALS, a spectrum disorder.

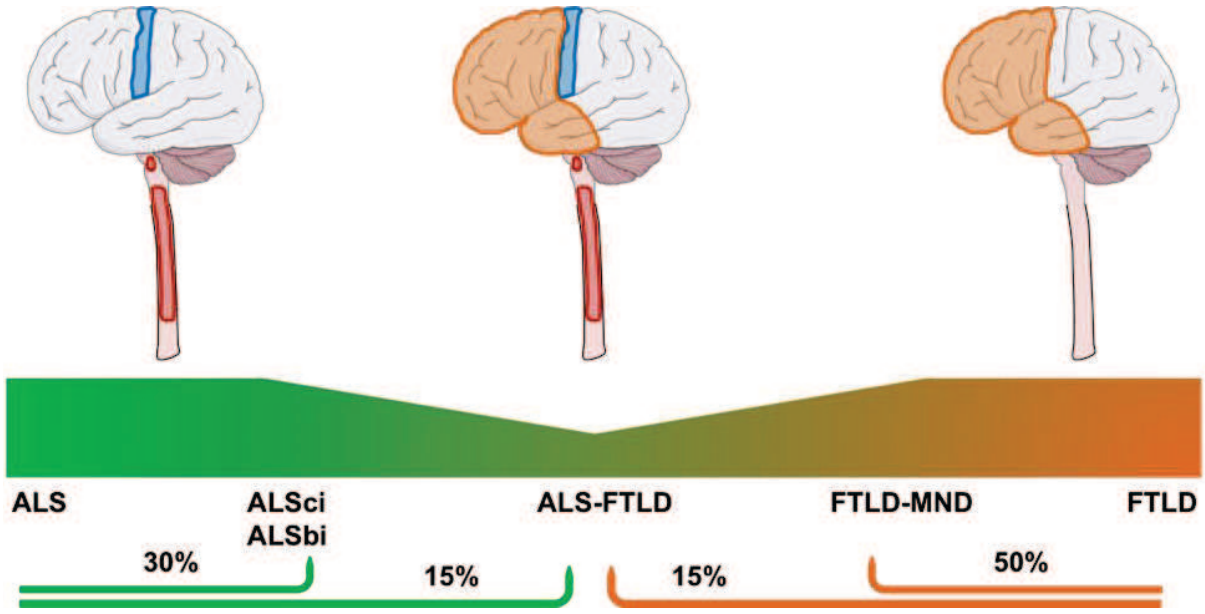

ALS and FTD constitute the ends of a spectrum of motor neuron and frontotemporal neuron involvement. This spectrum includes patients with ALS who express isolated ALSci or ALSbi, and patients with ALS who meet the Neary criteria for FTLD and are, thus, diagnosed with ALS–FTLD. Some patients with FTLD have insufficient motor neuron involvement for a diagnosis of ALS, and are classified as FTLD–MND
Reproduced from :Swinnen & Robberecht, Nat. Rev.Neurol., 2014.

Following examples of extramotor involvement comes from research that has been done in our laboratory. In ALS, spasticity is traditionally thought to be the result of degeneration of the upper motor neurons (18,19), although degeneration of other neuronal types, in particular serotonergic neurons, might also represent a cause of spasticity (20). A pathological study in ALS patients as well as in mice confirmed hypothesis that degeneration of serotonergic neurons could at least in part underlie spasticity (20). It was observed in patients that central serotonergic neurons suffer from a degenerative process with prominent neuritic degeneration, and sometimes loss of cell bodies. More recently, serotonergic degeneration has been observedin a

mouse model of ALS, further confirming the data from patients (H. Eloussini et al, Unpublished data). Another ongoing study from our laboratory, suggests that hypothalamic pro-opiomelanocortin neurons (POMC) are lost in different ALS animal models (SOD1 G86R, TDP43 A315T, FUSΔNLS mice). The decrease of POMC caused abnormal food intake behavior, and could be implicated in ALS hypermetabolism problems, frequently observed in patients (P. Vercruysse et al, manuscript submitted).

2. Frontotemporal lobar degeneration (FTLD)

Frontotemporal lobar degeneration (FTLD) is a neurodegenerative disease first described by Arnold Pick in 1892, originally called Pick's disease. This initial description reported upon a patient with progressive aphasia and anterior temporal lobar atrophy (21). FTLD encompasses a group of heterogeneous diseases characterized by relatively selective **atrophy of the frontal and temporal lobes**, (**Figure 6**) sometimes bilateral. Atrophy is due to progressive degeneration of neurons particularly in the superficial layers of the frontotemporal cortex and in the dentate gyrus of the hippocampus (21).

(21)(21)FTLD is the second most common cause of early onset dementia, after Alzheimer's disease (22) and occurs with an incidence of 3.5–4.1/100 000 per year in individuals under 65 (23) and accounts for 20% of young onset dementia cases (24).

The term FTLD is often used to describe pathological conditions that are clinically predominantly or commonly presented by frontotemporal dementia (FTD). It is a syndrome that is characterized by progressive alteration in behaviour, language, sociability and personality, with relative preservation of memory at early disease stages (25,26). Signs and symptoms typically manifest in late adulthood, more commonly between the ages of 55 and 65, approximately equally affecting men and women.The median survival from the onset of symptoms is 6–11 years, independent of age at onset or gender (27).

For FTLD, a stronger genetic contribution, compared to ALS, is reflected by the higher percentage (up to 30-50%) of patients with a familial history, while etiology of the rest remains unknown.

Like in other neurodegenerative diseases, detailed neuropathological studies have elicited proteinopathies defined by **ubiquitin positive inclusions and/or aggregates** (28–31).

Currently, there is no cure for FTLD, but there are treatments that help alleviate symptoms.

Figure 6. Brain atrophy in patients with FTLD

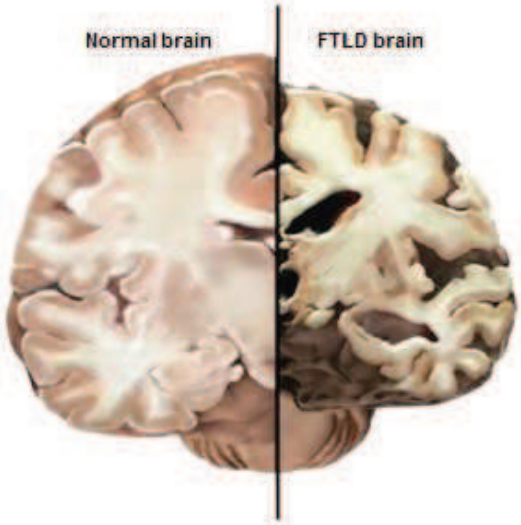

Reproduced from: Presentation for RNA Virtual Institute VH-VI-510 reevaluation: Dysmetabolism in Amyotrophic Lateral Sclerosis and Frontotemporal Dementia. Berlin, 201

2.1. Phenotypic heterogeneity

FTD is traditionally difficult to diagnose due to the heterogeneity of the associated symptoms. Clinical subtypes of FTD include the behavioural variant (bvFTD) and two forms of primary progressive aphasia (PPA): progressive nonfluent aphasia (PNFA) and semantic dementia (SD) (32). Signs and symptoms are classified into three groups based on the functions of the frontal and temporal lobes (33):

The behavioural variant frontotemporal dementia (bvFTD) is characterized by changes in social behaviour and conduct, with loss of social awareness and poor impulse control (24), such as disinhibition, apathy, loss of empathy, or stereotypic behavior, leading to a loss of social competence (26,34). When executive functions are impaired, patients become unable to perform skills that require complex planning or sequencing.

Semantic dementia (SD) is characterized by the loss of semantic understanding, conceptual knowledge resulting in impaired word comprehension, although speech remains fluent and grammatically faultless (24). Concomitant development of anomia is frequent (26).

Progressive nonfluent aphasia (PNFA) is characterized by progressive difficulties in speech production and grammatical error-making, with relatively preserved language comprehension (24). Apraxia of speech (AOS) or orofacial apraxia is frequently accompanying the aphasia (34).

At least in the initial stages of FTD, the following abilities are preserved: perception, spatial skills, memory and praxis (24). In the later stages of the disease, patients tend to struggle with binge eating and present compulsive behaviors including overeating, stuffing oneself with food, changes in food habits (35).

Recent studies over several years have developed new criteria for the diagnosis of behavioral variant frontotemporal dementia (bvFTD). Six distinct clinical features have been identified as symptoms of bvFTD (36).

1. Disinhibition
2. Apathy/Inertia
3. Loss of Sympathy/Empathy
4. Perseverative/compulsive behaviors
5. Hyperorality
6. Dysexecutive neuropsychological profile

Of the six features, three must be present in a patient to diagnose one with possible bvFTD.

bvFTD accounts for more than 50 % of the FTLD cases, while PNFA and SD correspond each to 25 % of the cases (37). Overlap between the clinical syndromes of bvFTD, PNFA and SD can occur during the progression of the disease and clinical distinction between them is often complicated in advanced disease stages.

The comorbidity of behavioural alterations, cognitive impairment or dementia with ALS has been noticed since the early 20th century (38). Additionally, FTD is often associated with an extrapyramidal movement disorder (parkinsonism or corticobasal syndrome) (32).

3. Clinical link among ALS and FTLD

The clinical overlap between ALS and FTLD is now well established and increasingly recognized. As already noted above 30-50% of ALS patients show at least some executive function deficits, and 15% meet the clinical criteria for FTLD(16,17,32); likewise, up to 50% of FTLD patients present with some forms of motor neuron dysfunction and 15% meet criteria of ALS (16,17,32). However, before the recent genetic revolution in ALS and FTLD, the background of this clinical overlap was completely ignored (**Figure 7**).

Figure 7. ALS-FTLD clinical overlap

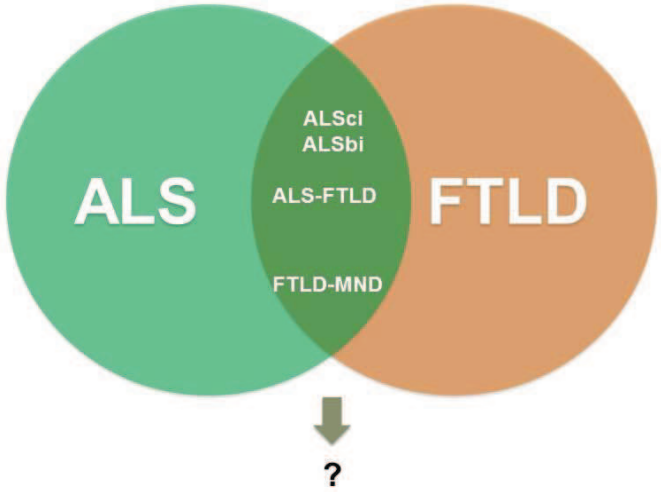

Reproduced from :Presentation for RNA Virtual Institute VH-VI-510 reevaluation: Dysmetablism in Amyotrophic Lateral Sclerosis and Frontotemporal Dementia. Berlin, 2015.
ALS with behavioral impairment (ALSbi), ALS with cognitive impairment (ALSci).

B. Molecular basis

1. Heterogenous molecular basis of ALS:

The increasingly blurred boundary between sporadic to familial forms

There are three recognized forms of ALS: **sporadic**, **familial** and the **endemic** ALS–Parkinson dementia syndromes of Guam and the Kii peninsula (39).

Most ALS cases, about 90-95 % (40) are isolated in nature, and are referred to as “sporadic” ALS (sALS) with unknown etiology. A subset of ALS cases (remaining 5-10%) is inheritedand referred to as “familial” ALS (fALS). Most of the inherited cases rely on an autosomal dominant way, but autosomal recessive and X-linked forms also exist (41).

It is believed however that fALS incidence is underestimated due to flaws in patient history and reduced genetic penetrance of certain mutations. FALS is clinically indistinguishable from sporadic cases (sALS), except the mean age of onset for fALS occurs about 10 years earlier.

The early substrate for ALS is likely to involve **genetic**, **developmental**, and **environmental factors**. For most apparently sporadic cases, multiple genetic factors with small individual effects might in part affect development and maturation of the nervous system. This process might result in a motor system architecture that is more permissive to pathological

changes later in life, for example. Environmental triggers might then operate on an already primed system (**Figure 8**). Head injuries, cigarette smoking, exposure to toxic substances (e.g. heavy metals, pesticides) and other including diet (42,43) have all been linked to detrimental effects on the human body, however only recently these factors have been associated with sALS (44).One of the most cited environmental risk factor is physical activity. An active sports-oriented life stile has been associated with ALS patients (45) and increased incidence amongst professional athletes has also been reported (46).

As with other neurodegenerative diseases, given the **genetic predisposition** and the proper **environmental conditions**, the probability of developing familial or sporadic form of ALS increases with **age** (**Figure 8**) (47). Gender has been documented to be a factor in the likelihood of developing ALS, with male:female ratio of 1.5:1 (47).

Figure 8. Early supstrat of ALS – factors to consider in aethiology of ALS

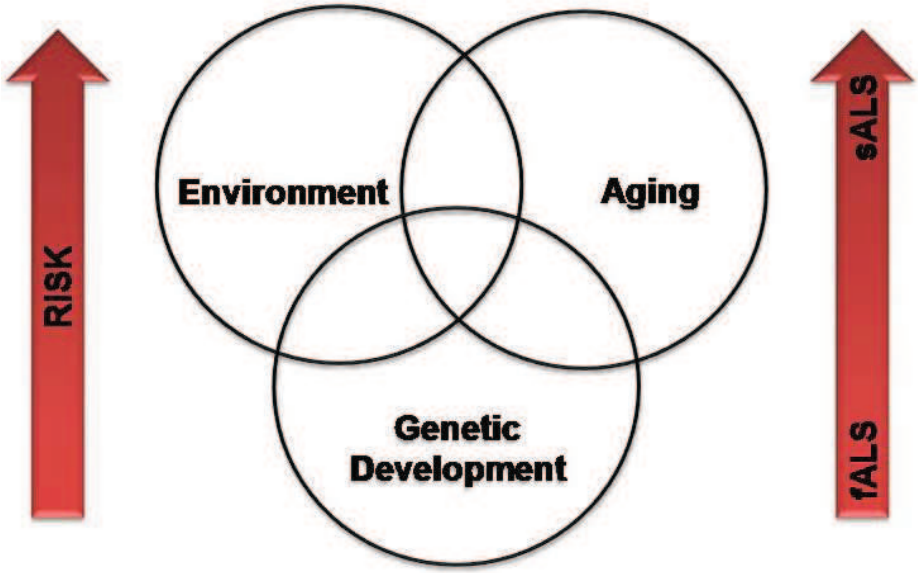

As seen in several other neurodegenerative diseases, ALS is believed to occur due to a convergence of factors: genetic variation in genes, late disease onset age, in the 50s, indicates that the risk of getting ALS increases with age and several environmental factors are known to increase the risk of getting this disease: head trauma, smoking and exposure to diets rich in heavy metals.

The most significant advances in understanding of the etiology of neurodegenerative disorders come from the identification of disease-causing genes. For almost two decades, only one gene was known to have a role in ALS pathogenesis, superoxide dismutase 1 (*SOD1)*. Today, the pace of gene discovery has greatly accelerated, fuelled in large part by advances in

new technologies like genome wide associated studies (GWAS), whole-exome (WES) and whole-genome sequencing (WGS) in relation to previous linkage gene analysis (**Figure 9**).

Figure 9. Progress of genetic findings related to ALS etiology and pathogenesis

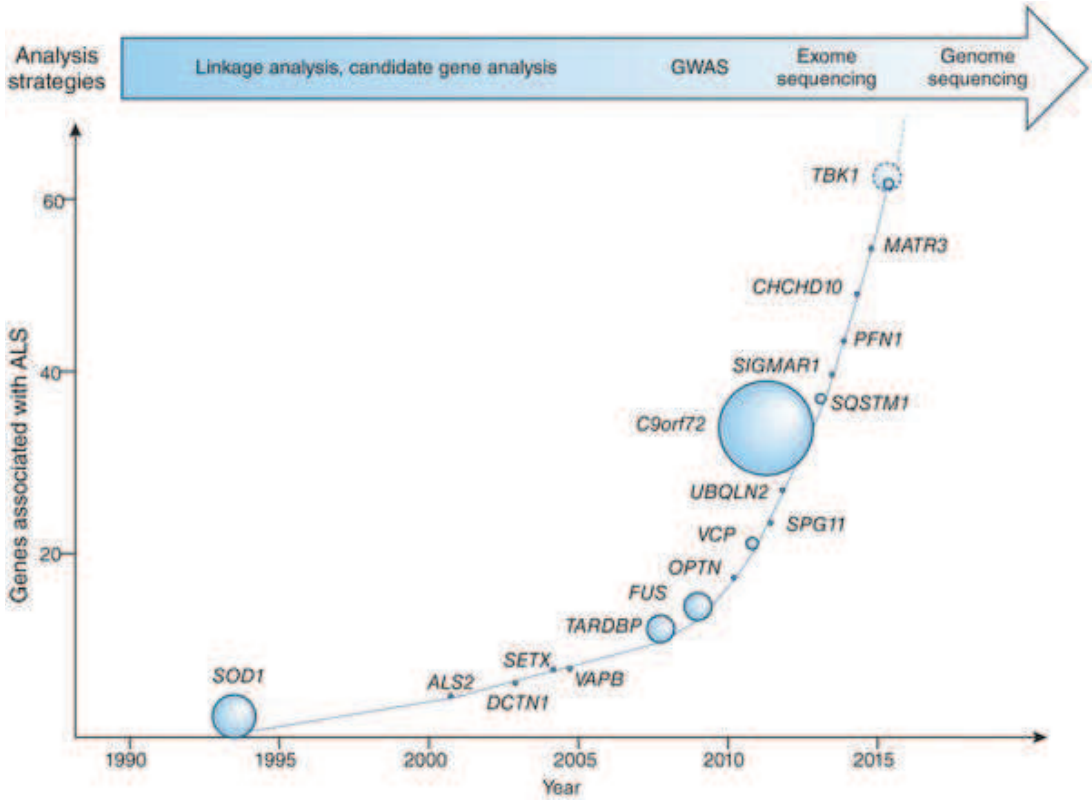

Mendelian ALS genes are shown, with the sizes of the circles indicating the relative contribution of each gene toward the explanation of ALS cases. The effect of *TBK1* is likely to expand, as indicated by the dashed circle outline, in the near future as additional studies emerge.
Reproduced from :Bettencourt & Houlden.Nat. Neurosci., 2015.

Mutations in almost **40** genes have been identified to be implicated in or associated with ALS pathogenesis (48). In the last 3 years alone, six new ALS genes have been discovered (40). In parallel this indicates ALS as **genetically heterogenous disease**. Mutations of all these genes account for 68% of fALS and surprisingly 11% of sALS patients (**Figure 10**) (40), while the rest of the cases remain of **unknown cause.** Among these, the most common ones, representing over 50% of the fALS cases (4), are found in the four major genes encoding superoxide dismutase 1 (*SOD1*; ~20%) (49), fused in sarcoma (*FUS*; 1-5%) (50,51) and trans-active response (TAR) DNA-binding protein TDP-43 (*TARDBP*; 1-5%) (52). Recently, a hexanucleotide repeat expansion $(GGGGCC)_n$ in the *C9ORF72* gene was identified as the most frequent cause of fALS (~40%) (53,54).

Figure 10. Frequency distribution of genes involved insALS and fALS. Blurred line between sALS and fALS

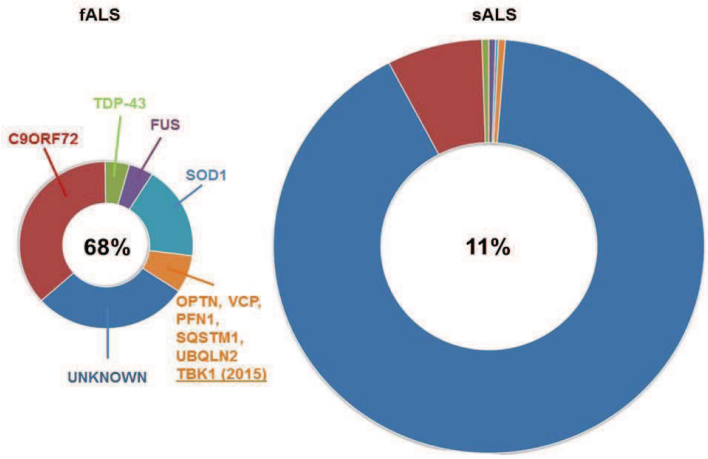

Reproduced from : Renton, Chio & Traynor. Nat. Neurosci.,2014.

A rapid advance in knowledge of the genetic architecture of ALS, reveals missing links between the **genetic subtypes** with **clinical subtypes** and **pathological phenotypes**. Despite the fact that each new genetic discovery is broadening the phenotype associated with the clinical entity we know as ALS, it also underlies multiple common points which are nowadays emerging themes: 1) **genetic convergence** that unifies the etiology, 2) a **final common pathway** of diverse proposed pathogenic mechanisms, 3) an **oligogenic rather then monogenic** nature of disease, and 4) overlapping phenotypes of the **disease spectrum**.

The early studies of the *C9ORF72* hexanucleotide repeat expansion suggest that it is also present in a sizeable minority of apparently sALS cases (53,54) outlining the **genetic convergence** between fALS and sALS. Likewise, mutations of the other genes *SOD1* (49),*FUS* (50,51), *TARDBP* (52), optineurin (*OPTN*) (55) and newly discovered TANK-binding kinase 1(*TBK1*) (56,57) are as well detectable in a small but significant proportion of the 90–95% of sALS reporting no family history (**Figure 10**). All together, the current macrogenetic landscape in ALS, highlights the **increasingly blurred boundary between familial and apparently sporadic disease.**

2. Heterogenous molecular basis of FTLD:

Given this variability in phenotype, it is not surprising that the molecular basis of FTLD is also heterogeneous. Unlike ALS cases, about 30-50% of patients have a familial history of

disease, and referred to as “familial” FTLD (fFTLD). When considering clinical FTLD subtypes, family history is most prominent in bvFTD (45%), especially when concomitant symptoms of MND are present (60%), while SD appeared to be the least hereditary FTLD subtype (<20%) (58). Otherwise, the remaining cases are with unknown etiology and are referred to as “sporadic” FTLD (sFTLD). Combinations of genetic variants and environmental factors are likely to be responsible for the disease in the majority of patients with sporadic FTLD.

In the FTLD, disease causative mutations were identified in 9 genes and represent 30-50% of fFTLD with two major genes firstly described: the microtubule-associated protein tau (*MAPT*) (59) and the progranulin (*PGRN*) (60). Together, they account for 10%–20% of FTLD (**Figure 11**).

In the past few years, remarkable advances have been made in the molecular genetics of FTLD. Today, the genetic causes responsible for the majority of autosomal dominant cases have been determined (61).

Figure 11. Frequency distribution of genes involved in fFTLD

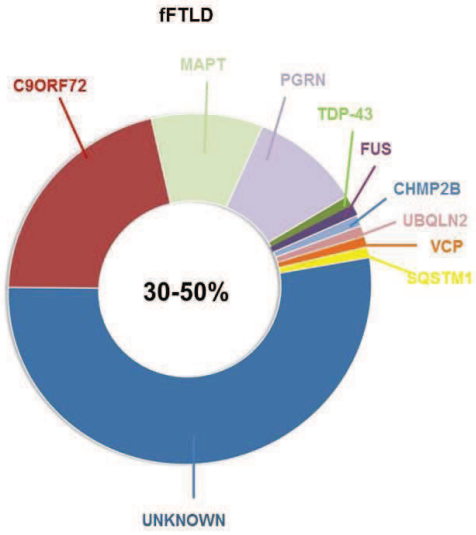

Data taken from: Ling, Polymenidou and Cleveland. Neuron., 2013.

3. Genes linked to ALS and FTLD:

In this chapter causative genes linked to ALS and FTLD are presented divided in three groups (**Table 2**):

Pure ALS genes – found only associated with classical ALS and characterized by predominantly motor phenotype.

Overlapping genes – involved in ALS and overlapping with other diseases, characterized by the presence of overlapping motor and extramotor phenotypes and and with particular emphasis on genes found in both diseases ALS-FTLD.

Pure FTLD genes – found only associated with cognitive and behavioral phenotype – FTD

Table 2. Genes linked to ALS and FTLD

DISEASE	LOCUS	GENE	PROTEIN FUNCTION	HEREDITY	ONSET	fALS %	sALS %	FTLD %	PATHOLOGY	OTHER DISEASES
TYPICAL ALS										
ALS1	21q22.1	*SOD1*	Detoxification enzyme	AD	Adult	20%	2%	-	SOD1	
ALS6	16-11.2	*FUS*	RNA processing	AD, AR	Adult, Juvenile	5%	‹ 1%	‹ 1%	FUS	FTLD
ALS10	1p36.2	*TARDBP*	RNA processing	AD	Adult	5%	‹ 1%	‹ 1%	TDP-43	FTLD
ALS12	10p15-p14	*OPTN*	Multifunction	AD, AR	Adult	4%	‹ 1%	-	TDP-43	POAG, PDB
ALS14	9p13.3	*VCP*	Protein quality control	AD	Adult	‹ 1%	‹ 1%	‹ 1%	TDP-43	FTLD, PDB, IBM
PDB	5q35.3	*SQSTM1*	Protein degradation	AD	Adult					PDB
ALS with FTLD										
ALS/FTLD	9q21-22	*C9ORF72*	Unknown	AD	Adult	25%	5%	10%	TDP-43	
ALS/FTLD -X	Xp11,21	*UBQLN2*	Protein degradation	AX	Adult	‹ 1%		‹ 1%	TDP-43 FUS	
FTLD										
FTLD-TAU	17Q21	*MAPT*	Cytosceleton	AD	Adult			10%	TAU	
FTLD-TDP	17q21.31	*PGRN*	Inflammation	AD	Adult			10%	TDP-43	
FTLD-UPS	3p11.2	*CHMP2B*	Vesicle trafficing	AD	Adult		‹ 1%	‹ 1%	P62	

Reproduced from : Ling , Polymenidou and Cleveland. Neuron., 2013.
AD: autosomal dominant, AR: autosomal recessive, POAG: Primary open angle glaucoma, PDB: Paget's disease of the bone, IBM: inclusion body myositis.

3.1. Pure ALS genes

3.1.1. Superoxidedismutase 1 (*SOD1*)

SOD1 mutations were found to cause familial ALS in 1993, representing the first demonstration that linkage analysis could successfully pinpoint the underlying genetic cause of a rare neurodegenerative disease (49).

There are now more than 160 recorded mutations in this 153 amino-acid protein, mostly missense, all apparently resulting in fALS (20%) or sALS (1-2%) (40).

Considerable **phenotypic heterogeneity** occurs across the various *SOD1*mutations. For instance, the *SOD1* A4V mutation can induce very aggressive disease while long survival has been reported in association with the *SOD1* D90A mutation (40). In general, patients have almost exclusively **lower motor neuron signs** and almost never bulbar onset of disease (62). Although, cognitive impairment is not a prominent feature of *SOD1* disease, patients with D90A manifest **FTLD** at the later stages of the disease (63).

SOD1 main physiological function is to protect cells from oxidative damage by metabolizing superoxide radicals (64).The molecular basis of the toxicity of mutant SOD1 is multifactorial. Because SOD1 detoxifies superoxide anion, it is likely that mutant SOD1 **provokes oxidative stress** (65). Whatever the molecular underpinnings of its cytotoxicity, SOD1 can disrupt a wide set of cellular functions. While a complete recounting of these pathways is beyond the scope of this manuscript, some of the adverse effects include: provocation of cellular hyperexcitability (66), disruption of mitochondrial function (67), induction of the unfolded protein response (UPR) and endoplasmic reticulum (ER) stress (68), impairment of molecular motors and axonal transport (69), and early disruption of the neuromuscular synaptic structures (70).

Whatever the pathway is, it ends with misfolded proteins, having toxic effects on the cell's degradation machinery, impairing its two major components: the proteasomal pathway and the autophagy, and triggering its deposition in **inclusion bodies** within spinal motor neurons (71). Mutant SOD1 also spontaneously forms oligomers (72) as well as visible **aggregates** (73).

Neuropathologically, ALS patients with *SOD1* mutation show loss of spinal cord neurons but while there is immunopositivity for **ubiquitin and p62 inclusions** in the spinal neurons and glia cells, there is usually negativity for TDP-43 (74).The protein appears **to gain a novel, toxic function** that leads to motor neuron degeneration (75).

The *SOD1* mutations discovery in ALS led directly to the development of the SOD1 transgenic mouse (76). Though important in elucidating the cellular mechanisms by which mutationof this gene predispose to motor neuron degeneration, the **use of this model to select agents for human trials has been increasingly called into question** (77).

3.2. Overlapping genes

3.2.1. TAR DNA-binding protein (*TARDBP*)

In 2006 the protein TDP-43 was identified by Neumann and colleagues as **major component of the ubiquitin-positive neuronal inclusions** that are the pathological hallmarks of both ALS and frontotemporal dementia FTLD (28).This finding provided strong evidence that

FTLD and ALS are closely related conditions with overlapping molecular pathogenesis. Importantly, in 2008 it was shown that mutations in *TARDBP* caused a fraction of familial is causative gene mutated in ALS cases (52).

This presented a landmark event in our understanding of both diseases pathogenesis.

There have now been more than 40 mutations found in *TARDBP* accounting for ~4% of fALS cases and a smaller percentage of sALS cases and rare FTLD (78). Most are missense mutations, but there are a few deletion mutations that give rise to a protein truncated at the very C-terminal (79).

Bulbar involvement was originally reported more frequently than might be expected, but assimilation of all published phenotypes suggests that the proportion is about the same as for all ALS. Phenotype is usually **ALS with or without FTLD but only rarely isolated FTLD** (78).

Under normal conditions, TDP-43 is located in the nucleus, where it is involved as all DNA/RNA binding proteins in multiple steps of RNA metabolism (80). The data imply that TDP-43 causes pathogenesis in a two-step manner. The first step involves the exit of TDP-43 from the nucleus and the second step involves the irreversible formation of stress granule-based aggregates. Disease-associated mutations cause a shift of TDP-43 location from nucleus to cytoplasm and increase its aggregation propensity (81), but it is uncertain whether these changes are sufficient to initiate this vicious circle *in vivo*. TDP-43–mediated toxicity may reflect either **loss of its function in the nucleus**, an acquired adverse effect of its pathological presence in the cytoplasm (**gain-of-function**), or **both**. Indeed, in a recently developed mouse model, the expression of mutant TDP-43 induced a phenotype even without formation of aggregates or abnormal processing of the cytoplasmic mutant protein and with no loss of TDP-43 from the nucleus which suggested a **toxic gain of function** (82). In line with this are findings from the very recent study that, by comparing the pathological changes in TDP-43^{WTxQ331K} (with cytoplasmic aggregation and nuclear clearing) and TDP-43^{Q331K} mice (with only cytoplasmic aggregation) showed that the **loss of nuclear** TDP-43 may accelerate, but it was not essential for the disease. Whereas cytoplasmic aggregation of TDP-43 seen in aged TDP-43^{Q331K} and TDP-43^{WTxQ331K} mice, was sufficient to cause neurodegeneration (83). Thus, while nuclear clearance of TDP-43 may accelerate disease it does not appear to be essential to cause neurodegeneration and loss of nuclear TDP-43 function may not be a primary or disease-critical event.

Neuropathology in cases of ALS with *TARDBP* mutations tends to reveal features similar to those of sALS, with neuronal loss and gliosis in the anterior horns of the spinal cord, and pallor of the corticospinal tracts. Immunohistochemically, there are **TDP-43 positive**

cytoplasmic inclusions in upper and lower motor neurons, but also in other regions of the central nervous system including frontal and temporal cortex (84). In the brain, cytoplasmic TDP-43 undergoes secondary modifications such as hyperphosphorylation, ubiquitylation and processing into smaller fragments (28).

The discovery of the central role of TDP-43 in ALS pathogenesis has highlighted the importance of RNA processing. Additional support for this hypothesis comes from the discovery of *FUS*, another RNA-binding protein.

3.2.2. Fused in sarcoma (*FUS*)

In 2009, shortly after the identification of TDP-43, a second RNA-binding protein functionally homologous and structurally comparable with TDP-43, FUS was linked to familial ALS (50,51). FUS is discussed in more details afterwards (see below).

3.2.3. Hexanucleotide repeat expansion in *C9ORF72*

In 2011, a duo of teams made the discovery of a massive hexanucleotide repeat expansion in *C9ORF72* as the cause of ALS and FTLD. The distinctive mutation in this gene is an expansion of an intronichexanucleotide GGGGCC (G_4C_2) repeat motif (53,54). Normally present in 30 or fewer copies, in *C9ORF72*-associated ALS, the repeat domain expands to encompass hundreds of tandem repeats (85). The expanded segment is transmitted as a dominant trait. Intriguingly, in several patients with *C9ORF72* mutations, a second mutation has been found in another gene (*TARDBP*, for example) (86). The biological significance of this finding is unknown, but it suggests that in some families, ALS may be **oligogenic in etiology** (87)**.**

It has reinvigorated the ALS and FTLD research field for a variety of reasons. First, the pathogenic expansion accounts for a remarkable percentage of both fALS (~37%) and familial FTLD (~21%) and **genetically explains the majority of the overlap** of these two disparate clinical syndromes (88). Second, the repeat expansion has been found to account for ~6% of apparently sALS cases and 6% of patients with supposed sFTLD (53,54,88).

C9ORF72 linked diseases clinically present with a widely variable phenotype including **ALS** or **FTLD-ALS** or **FTLD** (53). **Bulbar onset** is frequent in C9ORF72-associated ALS, as is frontotemporal involvement, which is usually of the **behavioural variant,** but patients with primary progressive aphasia (PPA) have been described (53,54,89–92).

The normal function of the presumably cytoplasmic protein C9ORF72 is unknown. However, it has recently been demonstrated that C9ORF72 regulates endosomal trafficking and

colocalizes with Rab proteins that are implicated in autophagy and endocytic transport. C9ORF72 also colocalizes with ubiquilin-2 and microtubule-associated protein light chain 3 (LC3) positive vesicles, and co-migrates with lysosome-stained vesicles in neuronal cell lines, providing further evidence that C9ORF72 regulates autophagy (93).

How repeat expansions in *C9ORF72* cause ALS remains to be elucidated. In the ALS patients with a *C9ORF72* expansion that have been studied, the levels of *C9ORF72* mRNA were reduced by 50% (53), suggesting that the expanded allele does not generate mature mRNA. Thus, the *C9ORF72* expansion may result ina **loss-of-function**. The expanded hexanucleotide repeats form nuclear **RNA foci** in neurons in the frontal cortex and spinal cord in patients with *C9ORF72* mutations (53). Pre-mRNA containing the expansion may thus exert a deleterious **gain-of-function** effect.These two mechanisms (**haplo-insufficiency versus gain-of-function**) are not mutually exclusive and do not exclude other mechanisms for the repeat expansion to cause fALS.

Neuropathologically, patients with ALS who carry *C9ORF72* hexanucleotide expansions present with typical features such as **TDP-43-positive inclusions** within the remaining motor neurons, as well as in the cortex and the hippocampus (91). Interestingly, two recent reports have indeed identified **dipeptide repeat (DPR) proteins**, which are most likely generated through RAN translation from expanded G_4C_2 RNA, within **aggregates** of patients with *C9ORF72* expansion-associated ALS and/or FTLD (94,95). The pathogenic significance of these DPR proteins remains to be demonstrated, but a study in *Drosophila* suggested that the DPR proteins could represent, by themselves the toxic agents (96).

3.2.4. Valosin-containing protein (*VCP*)

In the same year than *C9ORF72*, mutations in the valosin-containing protein (*VCP*) gene responsible for 1–2% of fALS cases were also reported (97). This is important given that these mutations provide **another genetic link** between motor neuron degeneration and FTLD, where *VCP* mutations are rare and represent less than 1 % of the fFTLD cases (most frequently **bvFTD and SD)** (98).

Today, 17 different mutations have been identified, and underlie an unusual clinical syndrome characterized by FTLD, inclusion body myopathy and Paget's disease of the bone (IBMPFD) (99). The existence of inclusion body myopathy in these patients was similarly interesting because it demonstrated that mutations in a single gene could result in pathology on both sides of the neuromuscular junction. This has given rise to the concept of **multisystem proteinopathy**, in which multiple tissues are affected.

Physiologically, VCP interacts with a large number of ubiquitinated proteins to enable degradation or recycling and functions in multiple protein clearance pathways, including extracting misfolded proteins from the ER and sorting of endosomal proteins for proper trafficking. Depletion of VCP leads to accumulation of immature autophagosomes, similar to what is observed upon expression of IBMFD-linked mutations (100), suggesting that VCP is required for proper autophagy. Most intriguingly, TDP-43 is apparently mislocalized to the cytosol upon VCP-mediated autophagic dysfunction (100).

FTLD patients with a *VCP* mutation have **TDP-43-positive inclusions** (98).

The best supported hypotheses of the disease mechanism of *VCP* mutations are disturbed ubiquitin–proteasome mediated protein degradation, autophagy, or both (101).

3.2.5. Ubiquilin 2 (*UBQLN2*)

In 2011, missense mutations in *UBQLN2*, located on the short arm of chromosome X, were initially identified in autosomal dominant ALS (41). Nevertheless, ubiquilin 2 pathology has been observed in ALS patients who do not carry mutations in the gene.

Although, isolated **ALS was the predominant phenotype**, occasional patients had **concomitant symptoms of FTLD** with abnormalities in both behaviour and executive functions; however, none of these patients presented with FTLD alone.

Ubiquilin 2 is a member of the ubiquilin family, with unknown exact function. It has been implicated in ubiquitinated proteins degradation via both ubiquitin-proteasome system (UPS) and autophagy, in G-protein coupled receptor endocytosis , and may be an important component of the final common pathway mediating motor neuron degeneration (41).

In human spinal cord autopsy material of *UBQLN2* ALS mutation carriers, inclusions were positive for UBQLN2, ubiquitin, p62, TDP-43, FUS and OPTN but not SOD1 (41,102). In cases with ALS-FTLD with or without *UBQLN2* mutations, UBQLN2-positive inclusions are found in the hippocampus which are absent in ALS cases without dementia indicating that UBQLN2 aggregation and neurodegeneration are linked (41). Inclusions in spinal cord tissue from sALS and fALS patients with unknown mutations or mutations in *SOD1*, *TDP-43* or *FUS* also stain positive for UBQLN2 (41,102).

3.2.6. Charged multivesicular body protein 2B (*CHMP2B*)

A mutation in the gene encoding charged multivesicular body protein 2B (*CHMP2B*), was found in a large Danish FTLD pedigree at chromosome 3 (103,104). Mutations affect the C-terminal end of the protein due to aberrant splicing.

CHMP2B encodes a protein with functions in the endosomal–lysosomal and the autophagic protein degradation pathway.

Ubiquitin-immunoreactive inclusions do not stain for tau, TDP-43 or FUS antibodies (105) (106).

3.2.7. Optineurin (*OPTN*)

OPTN autosomal recessive mutations were described in a few ALS families in 2010 (55). This has become interesting because of the intriguing phenotypic pleiotropy associated with such mutations. Indeed, the *OPTN* locus has been previously implicated in Paget's disease of bone (107). Dominant missense, recessive deletion and nonsense mutations of OPTN have been identified in both patients with fALS and with sALS.

Physiologically, OPTN functions as an inhibitor of NFκB-signaling (108), acts as an autophagy receptor(109) and participates in the regulation of vesicular trafficking and maintenance of the Golgi apparatus(110).

In sALS cases, OPTN is present in **cytoplasmic inclusions** and colocalizes with **ubiquitin**, **TDP-43**, and possibly **FUS** (108,111–113).

3.2.8. Sequestosome 1 (*SQSTM1*)

SQSTM1 encodes p62 protein and mutations in this gene are known to cause Paget's disease of bone (114). A candidate gene screening approach identified missense and deletion variants in ~1% of in familial and sporadic ALS patients (115–117).

Similar to ubiquilin, p62 has been shown to interact with polyubiquitinated proteins (118) and with LC3, allowing p62 to target polyubiquitinated proteins to the proteasome or autophagy. Therefore, both p62 and ubiquilin-2 link the ubiquitin-proteasome and autophagy pathways.

p62-positive inclusions have also been reported as **deposited** in neurons and glia of a wide array of other neurodegenerative diseases (91). While the way these ALS-associated variants in p62 contribute to pathogenesis has not been established, autophagy/proteasome disturbance seems likely to play a role.

3.2.9. Other genes

Mutations in several other genes have been reported as rare causes of ALS or ALS-like syndromes. In 2014, whole-exome sequencing led to the identification of one mutation in the gene **coiled-coil-helix-coiled-coil-helix domain-containing protein 10 (*CHCHD10*)** in two families presenting with ALS/FTLD (119).

A large collaborative effort in 2015, by Cirulli et al., involving researchers from more than two dozen laboratories, recently led to the identification of a genome-wide association between rare, non-benign variants in TANK-binding kinase 1 (*TBK1*) and ALS (56). Most importantly, mutation in familial cases of ALS were recently identified in the *TBK1* gene (57). Notably, the new ALS gene (*TBK1*) converges, together with previously known ALS genes (such as *OPTN* and *SQSTM1*) on autophagy pathway (56,57).

3.3. Pure FTLD genes

Two causal genes firstly identified: the microtubule-associated protein tau (*MAPT*) (59) and the progranulin (*PGRN*) (60) together account for 10%–20% of FTLD cases (22).

3.3.1. Microtubule-associatedprotein TAU (*MAPT)*

In 1998, mutations in the *MAPT* gene located on chromosome 17 were identified in a number of families with FTLD and parkinsonism (59). Since then, 44 different *MAPT* mutations have been reported, accounting for 5–20% of cases of familial FTLD (120).

MAPT encode the four microtubule-binding domains of TAU. In normal brain, the tau protein occurs as six isoforms of which three contain three microtubule-binding domains (3R TAU) and three contain four microtubule-binding domains (4R TAU). A substantial number of missense mutations affecting the splicing of exon 10 result in aberrant ratios of 3R and 4R TAU. Consequently, the binding of TAU to tubulin is impaired either due to an increased expression of 4R tau relative to 3R TAU isoforms, or due to the altered binding properties of the mutant TAU protein (120). In addition, coding *MAPT* mutations increase the tendency of TAU to form **neurotoxic aggregates** that are pathological characterictic of the more then 40% of **FTLD** cases (121).

FTLD with **tau-positive inclusions** is mainly associated with **bvFTD**. However, forms of **PPA** are also reported. Symptoms of associated motor neuron diseases are rare. On average, FTLD-TAU is characterized by the **earliest onset** age in the FTLD syndromes (38).

3.3.2. Progranulin (*PGRN)*

A major breakthrough occurred in 2006 when the progranulin (*PGRN*) gene was identified as the second FTLD-related located gene on the same chromosome 17 (60). Indeed, *PGRN* mutations account for an even larger proportion of FTLD families than do mutations in *MAPT*(120). To date, 69 different *PGRN* mutations have been reported (122) distributed across

the complete coding region and splice sites of the gene. They are **loss-of-function mutations** leading to **reduced functional protein** and resulting in **haplo-insufficiency** (123).

The characteristic pathological inclusions were **tau-negative, ubiquitin-positive**. It is now known that these inclusions are **TDP43-positive.**

Despite the fact that haplo-insufficiency is the common disease mechanism in all patients carrying a *PGRN*mutation, the associated clinical phenotype is variable, including **bvFTD and PNFA**(124). Parkinsonism symptoms are often observed, but motor neuron symptoms are rare (125).

4. Genetic link among ALS and FTLD

The description of mutations for several genes that are common to both ALS and FTLD provided a genetic link between them. Around six-seven genes that have been identified since nowadays represent a strong genetic proof of the continuum between these two pathologies (**Figure 12**).

The genetic link between ALS and FTLD was first established when *TARDBP* was found to be mutated in both diseases (52). This first gene was rapidly followed by a second one, *FUS* (50,51). A third, notable example was the identification of a hexanucleotide expansion in the *C9ORF72* gene, among both ALS and FTLD cases (53,54,126).The average mutation frequencies reported in European populations are 37% for fALS, 6% for sALS, 21% for fFTLD, and 6% for sFTLD patients, which make *C9ORF72* the strongest genetic link between these two diseases (61). Importantly, all these genes are involved in **multiple steps of RNA metabolism** (4)**.**

Figure 12. ALS-FTLD genes

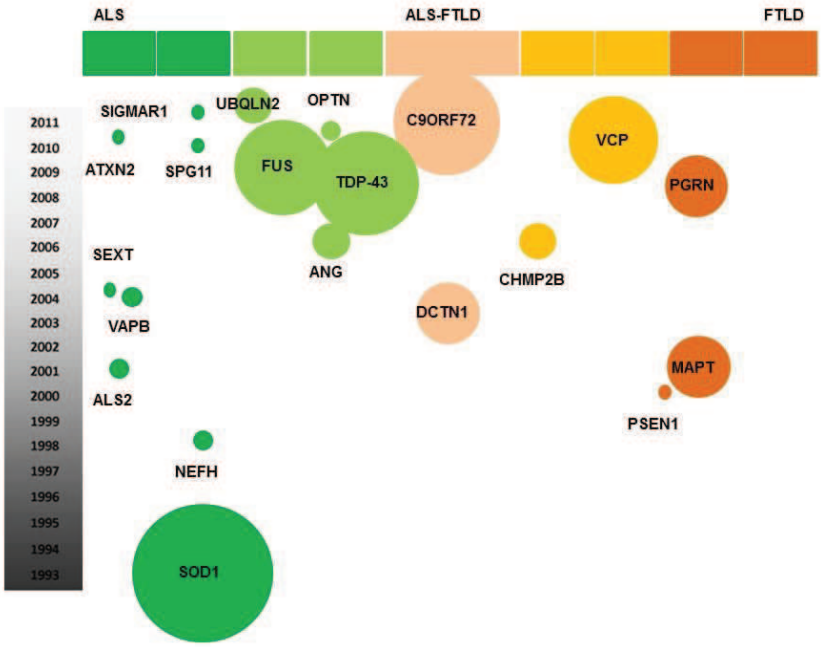

ALS-FTLD genes plotted to show phenotype, year of discovery and importance gauged by research outputs. The X axis is a score representing the involvement of each gene in ALS or FTLD. The Y axis represents year of mutation identification. The circle size represents the level of research on each gene.
Reproduced from: Al-Chalabi A et al., Acta Neuropathol.,2012

ALS, ALS/FTLD and/or FTLD causing mutations were also identified in genes involved in **protein clearance pathways or in maintaining proper protein homeostasis**, including ubiquilin-2 (*UBQLN2*) (41), vasolin-containing protein (*VCP*) (97,99), vesicle-associated membrane protein-associated protein B (*VAPB*) (127), p62/sequestosome (*SQSTM1*) (115–117), optineurin (*OPTN*) (55), and charged multivesicular body protein 2B (*CHMP2*) (103,104).

Interestingly, these genes are associated with two major categories of cellular function: protein homeostasis and RNA metabolism. Together with the toxic protein aggregation that represent a classical pathological hallmark of both ALS and FTLD, these convergent genetic findings indicate that protein and RNA metabolisms are key cellular pathways systematically impaired in both diseases (**Figure 13**).

Figure 13. ALS-FTLD genetic overlap and converging underlying cellular pathways

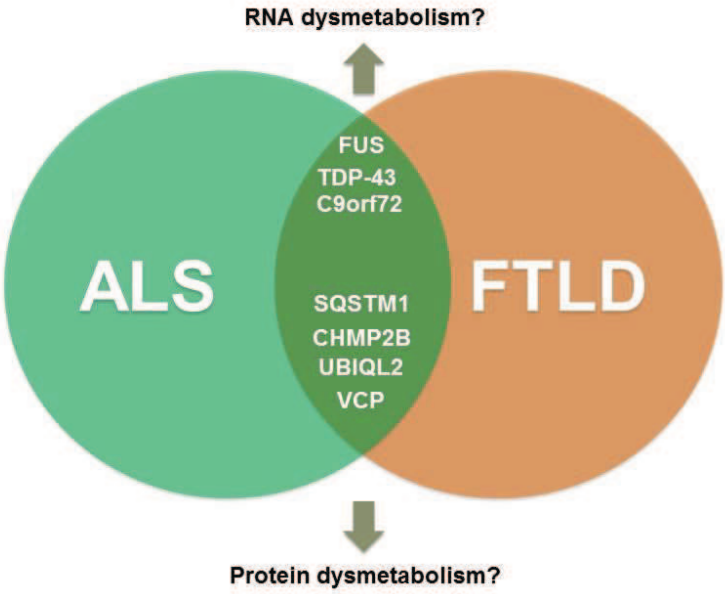

Taken from: Presentation for RNA Virtual Institute VH-VI-510 reevaluation: Dysmetablism in Amyotrophic Lateral Sclerosis and Frontotemporal Dementia. Berlin, 2015

C. Pathological characteristics

1. Pathological overlap between ALS and FTLD

Along with **neuronal degeneration**, **neuronal insoluble protein deposits/inclusions/aggregates** are a histopathological hallmark of several neurodegenerative disorders. Inclusions are mostly cytoplasmic (NCI, neuronal cytoplasmic inclusions) and less frequently with nuclear localisation (NII, neuronal intranuclear inclusions). However, the role played by inclusions in neurodegenerative pathogenesis remains enigmatic and the published data are currently not sufficient to conclude if aggregation is directly responsible for neurodegeneration.

Hence, ALS and FTLD are neuropathologically characterized by accumulation of **ubiquitin-positive protein inclusions** in affected cells of the central nervous system (neurons and glia) (29,128). For instance, **p62 positive aggregates** are systematically found in inclusions (129). In ALS patients, inclusions are not restricted to the spinal cord but also present in other brain regions such as the frontal and temporal cortices, hippocampus and cerebellum (130). As well, FTLD patients have inclusion detected outside brain, in the brainstem and spinal cord (131).

Recent advances in the identification of the exact protein composition of the inclusion further supported the clinical ALS/FTLD continuum by a pathological overlap.

A last shared pathological feature is activation of immune system and signs of **neuroinflammation.**

In all, pathological links between ALS and FTLD include three main characteristics: protein inclusions, neuronal degeneration and neuroinflamation.

1.1. Protein deposits/inclusions/aggregates in ALS and FTLD

The presence of protein aggregates in and around affected neurons is a hallmark of ALS and FTLD. It is remarkable that the proteins encoded by genes linked to ALS/FTD (TARDBP, FUS, CHMP2B, VCP, UBQLN2 and MAPT) are almost all present in protein aggregates in a large proportion of sporadic patients indicating a more widespread role for their abnormal localization in disease pathogenesis.

Following the identification of SOD1 aggregates in *SOD1*-ALS patients, a greatest breakthrough was finding that TDP-43 is the major ubiquitinated protein in inclusions in both ALS and FTLD diseases (28). Mutations in *TARDBP* are unique to ALS and are not found in other neurodegenerative disorders (52,84) with the exception of a small number of FTLD cases (132–137). TDP-43 positive inclusions are found in almost all sALS patients (non-mutated TDP-43) and in the vast majority of fALS patients with associated genes *TARDBP, VCP, C9ORF72, UBQL2, OPTN*, but not in *SOD1* and *FUS* related fALS (74,138) (**Table 3**). FTLD with TDP-43 aggregates includes sporadic and genetic forms, with mutations having been identified in *PGRN*, *VCP* and *TARDBP*, along with the *C9ORF72* repeat expansion and *UBIQLN2* (139,140). Before TDP-43 was discovered this the most common subtype of the disease, was known as FTLD with ubiquitinated inclusions (28). Furthermore, the distribution of the TDP-43-positive aggregates is disease-specific: they are present in spinal cord motor neurons, hippocampal and frontal cortex neurons and glial cells in ALS, and have a more widespread distribution in the brain of FTLD patients (141).

Pathological modifications of TDP-43 in these disorders include a redistribution of the protein from the nucleus to the cytoplasm in cells with inclusions, as well as hyperphosphorylation, ubiquitination and N-terminal truncation of the protein (28).

In all, based on these findings, ALS and FTLD with TDP-43 positive inclusions are now grouped as **TDP-43 proteinopathies** (ALS-TDP and FTLD-TDP) according to the major deposited protein within inclusion (**Table 3**). On the basis of the morphology and anatomical distribution of TDP-43 pathology, four distinct FTLD-TDP subtypes have been identified (142),

supported by genetic and clinical correlations (**Table 3**), as well as distinct biochemical properties of TDP-43 in the different subtypes (28).

More recently, FUS was found as accumulating in remaining TAU/TDP-43-negative, rare ALS and FTLD subtypes (29,50,51). Indeed, the identification of mutated *FUS* within ubiquitin-positive neuronal cytoplasmic inclusions (NCI) in a portion of ALS cases led to the reexamination of other neurological diseases with NCI of unknown origin. Pathological examination of post-mortem tissue of *FUS* mutation carriers showed predominant degeneration of lower motor neurons with FUS-positive cytoplasmic inclusions and a normal distribution of TDP-43, thereby distinguishing them from other ALS cases (50,51). The precise pattern of FUS-immunoreactivity in ALS cases without *FUS* mutations is still unclear. Some studies report that FUS is not present in sALS patients and SOD1 fALS (29,50,143), while others show FUS-positive inclusions with signals for TDP-43, p62 and ubiquitin in all sALS and fALS cases, except for *SOD1* mutation carriers (113,144).

Subsequently, abnormal FUS was detected within inclusion bodies in neuronal cytoplasm NCI and nucleus NII, as well as glial inclusions, in several uncommon forms of frontotemporal lobar degeneration (FTLD) (29,145–147). These rare subsets of FTLD, previously referred to as atypical FTLD with ubiquitinated inclusions (aFTLD-U), neuronal intermediate filament inclusion disease (NIFID) and basophilic inclusion body disease (BIBD) (29,145–147). However, in contrast to ALS, FTLD patients with FUS inclusions only rarely harbor genetic alterations in *FUS* (148). Interestingly, FUS-positive inclusions in FTLD cases are immunoreactive for Ewing RNA-binding protein (EWSR1), and TATA-binding protein-associated factor 15 (TAF-15), two other members (along with FUS as third) of the FET family of RNA binding proteins, and for transportin-1, while inclusionsin ALS cases with *FUS* mutations do not stain for these proteins(149,150).

Biochemical analyses show that mutant FUS protein itself is not ubiquitinated, hyperphosphorylated or cleaved (29). However, FUS is enriched in the insoluble fraction of FTLD brains (29). Deposited FUS is arginine methylated in ALS, but not in FTLD (151). Furthermore, nuclear clearing of FUS is not as evident as observed for TDP-43 (29).

ALS and FTLD that share FUS aggregation as common pathological feature and a presumed underlying disease mechanism have now been grouped together as the **FUS proteinopathies.** The two major clinical and pathological types are known as FTLD with FUS pathology (FTLD-FUS) and ALS with FUS pathology (ALS-FUS). This nomenclature is analogous to the classification that has been developed for the TDP-43 proteinopathies (**Table**

3). FTLD-FUS is additionally divided in three subtypes corresponding to previously known rare subsets of FTLD: aFTLD-U, NIFID and BIBD.

Subsequent confirmation that FUS is present in the pathological inclusions in most of the FTLD patients without TDP-43-containing inclusions has led to a proposed reclassification of ALS and FTLD based on the main protein component of inclusion (30,31) (**Table 3**).

Table 3. Pathological and clinical features of ALS and FTLD subtypes

Disease	ALS				FTLD				
Subtype	ALS-TDP	ALS-DPR	ALS-FUS	ALS-SOD	FTLD-Tau	FTLD-TDP	FTLD-DPR	FTLD-FUS	FTLD-UPS
Deposited Protein (s)	TDP-43	DPR TDP-43	FUS	SOD1	Tau	TDP-43	DPR TDP-43	FET/TR	Ub+
Associated genes	*TARDBP VCP ATXN2 ANG OPT UBQLN2 PFN1*	*C9ORF72*	*FUS*	*SOD1*	*MAPT*	*GRN VCP TARDBP# UBQLN2#*	*C9ORF72*	*FUS#*	*CHMP2B*
Pathological subtype	UMN, LMN, Bulbar	UMN, LMN, Bulbar	UMN, LMN, Bulbar	UMN, LMN, Bulbar	Pick disease, CBD, MSTD, dementia	Types A-D	FTDL-TDP types A and B	Atypical FTLD with Ub, NIFID, BIBD	FTD linked to chromosome 3
Clinical features	Bulbar, FTLD, parkinsonism	Bulbar, FTLD, parkinsonism	FTLD, parkinsonism	PMA, bulbar, autonomic dysfunction, ALSci	bvFTD, PNFA*, SD*, ALS*, PLS*, parkinsonism*	bvFTD, PNFA*, SD*, ALS*, parkinsonism*	bvFTD, PNFA*, SD*, ALS*, parkinsonism*	bvFTD, ALS*, PLS*, parkinsonism*	bvFTD, ALS*, parkinsonism*

New molecular classification of FTLD and ALS. FTLD and ALS are divided into different neuropathological subtypes based on the disease-signifying deposited protein in pathological inclusions and genetic defects associated with a certain pathological and clinical subtype.
*clinical features present in some, but not all, pathological subtypes. #Rare case reports of patients with clinical FTLD, but no description of pathology, ALS, amyotrophic lateral sclerosis; BIBD, basophilic body disease; CBD, corticobasal degeneration; DPR, dipeptide repeat proteins; FTD, frontotemporal dementia; FTLD, frontotemporal lobar degeneration; LMN, lower motor neuron; MSTD, multiple system taupathy with dementia; NIFID, neuronal intermediate filament inclusion disease; PNFA, progressive non fluent aphasia,;SD, semantic dementia; Ub, ubiquitin inclusions; UMN, upper motor neurons; UPS, ubiquitin proteasome system.
Reproduced from Dormann D & Haass C Mol. Cell. Neurosci. 2013. and Reproduced from Deng, H. et al., Nat. Rev. Neurol.2014

Although, the majority of inclusions from cases with the *C9ORF72* intronic expansion stain positive for TDP-43 (with exception of rare TDP43-negative but ubiquitin and p62-positive), neurons also develop another type of inclusions. Cytoplasmic aggregates composed of dipeptide repeat proteins (DPR) encoded by the intronic hexanucleotide repeats that are produced through non-canonical, repeat-associatednon-ATG–mediated (RAN-mediated) translation. These atypical peptides reflect translation of amino acids from all possible reading frames of the G_4C_2 expanded domains (94,95). These are now classified accordingly to ALS-DPR and FTLD-DPR representing **DPR proteinopathies**.

Other proteins could be found co-aggregated with the main ones in both diseases. In cases ofALS-FTLD, with or without UBQLN2 mutations, UBQLN2-positive inclusions are found in the hippocampus. These inclusionsare absent from pureALS cases (i.e. without dementia), which indicates that UBQLN2 aggregation and neurodegeneration are linked (41,102). In cases with ALS-FTLD with or without *UBQLN2* mutations, UBQLN2-positive inclusions are found in the hippocampus which are absent in ALS cases without dementia indicating that UBQLN2 aggregation and neurodegeneration are linked (41). Inclusions in spinal cord tissue from sALS and fALS patients with unknown mutations or mutations in *SOD1*, *TARDBP* or *FUS* also stain positive for UBQLN2(41,102).

In all, TDP-43 and FUS are the major components of pathological inclusions observed in almost 100% of ALS and over 50% of FTLD patients. In the remaining TDP-43 and FUS negative inclusions found in ALS cases, SOD1 positive inclusions were detected in less than 2% (ALS-SOD1). In less than 50% inclusions identified in FTLD cases that were negative for both proteins, the main component was TAU protein encoded by corresponding *MAPT* gene (FTLD-TAU), or proteins of ubiquitin-proteasome system named FTLD-UPS (around 1%) (Figure 14).

Figure 14. Pathological protein inclusions in ALS and FTLD, according to the major misaccumulatedprotein. Inclusions of TDP-43 and FUS/TLS in ALS and FTD reflect the pathological overlap of ALS and FTD

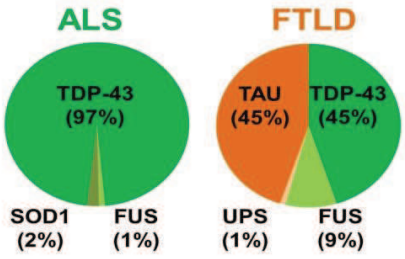

Reproduced from : Ling , Polymenidou and Cleveland. Neuron., 2013.

When all inclusions negative for TDP-43 and FUS are substracted from ALS and FTLD cases, the distribution looks then like presented in **Figure 15**.

Figure 15. Frequency of TDP-43 and FUS pathological protein inclusions in ALS and FTLD

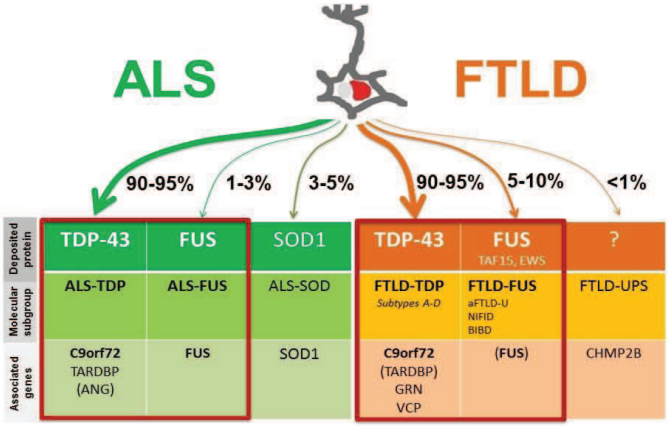

Reproduced from: Presentation for RNA Virtual Institute VH-VI-510 reevaluation: Dysmetablism in Amyotrophic Lateral Sclerosis and Frontotemporal Dementia. Berlin, 2015

Altogether, linking the different types of protein aggregates to specific genetic alterations uncovered the converging cellular pathological processes affected in both ALS and FTLD.

1.1.1. Common cellular pathomechanisms among ALS and FTLD protheinopathies: from proteinopathy to ribonucleopathy

The consistent presence of ubiquitin and p62 in ALS and FTLD aggregates regardless of the main deposited protein, implicated a role of the protein quality control system in ALS and FTLD pathophysiology. Ubiquitin proteasome system (UPS) and the autophagy-lysosome system function to monitor protein quality and protect cells from dysfunctional, misfolded or denatured proteins, by degradation.

Ubiquitination marks proteins for degradation and p62 is an important participant in autophagy (152) (**Figure 16**). It has been already postulated that ubiquitinated proteins form aggregates when dysfunctional protein levels exceed cell protein capacity for clearance. As previously mentioned and in line with this, mutations in genes encoding autophagy regulators have been associated with ALS and FTLD: *VCP*, *p62*, *CHMP2B* and *UBQLN2* (41,97,103,115–117). This fact further underlined the notion that **proteasomal degradation might play a causative role in ALS and FTLD pathogenesis and reinforced the notion that ALS/FTLD is a 'proteinopathy'**.

Meanwhile, many genes linked to ALS and FTLD were found to encode for DNA/RNA binding proteins and/or to influence RNA metabolism. Indeed, in addition to already known TDP-43, FUS and C9ORF72,mutations in several other RBPs were recently identified, in particular

TAF15 (153) and EWSR1(154), two proteins from the same family as FUS, and some that are less closely related RBPs such as ataxin 1, ataxin 2, hnRNPA2B1, hnRNPA1, matrin-3 and CREST(155–159). Consequently, the aberrant RNA metabolism was proposed as crucial in the pathogenesis (reviewed in(160)) (**Figure 16**).

Under physiological conditions, these DNA/RNA-binding proteins are largely nuclear, and a fraction of the mere known to also translocate to the cytoplasm. Disease-associated mutations are either located in highly unstructured protein domains with prion-like properties, resulting in a **higher propensity to aggregate** (155), or in the vicinity of the nuclear localization signal (NLS) impairing nuclear import of the mutant protein, with concomitant sequestration of the endogenous wild-type protein into **cytoplasmic aggregates**, often leaving the nucleus entirely depleted of the affected protein (161).

Altogether, these findings highlight that errors in RNA metabolism may be central to ALS and FTLD pathogenesis.

These insights shifted the focus from **'ALS/FTLD as a proteinopathy'** to '**ALS/FTLD as a ribonucleopathy'**(162).

However, these two pathways are not mutually exclusive. Indeed, the failure to maintain proper protein and RNA homeostasis drives a feed-forward cycle that leads to perturbation of many aspects of protein and RNA functions (**Figure 16**). This became clear when it was discovered that both TDP-43 and FUS regulates expression of genes involved in protein clearance. For instance FUS binds to the mRNAs encoded by genes like *OPTN* (163,164), *UBIQUILIN-2* (164,165), and *VCP* (163–165). As for TDP-43, it affects the mRNAs levels of *CHMP2B*, *OPTN*, *VAPB*, and *VCP* (4,166) (**Figure 16**).

Thus far, altered RNA granule formation, self-aggregating properties of prion-like domains and dysfunction of the protein quality control system, have been suggested to contribute to protein aggregation in ALS and FTLD.

Figure 16. Common cellular pathomechanisms among ALS and FTLD protheinopathies

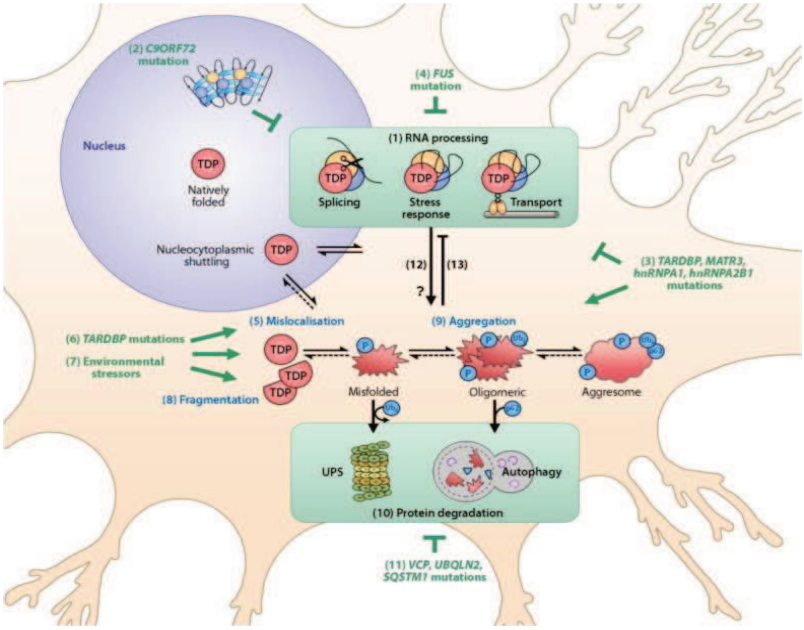

(1) TDP-43 is a DNA- and RNA-binding protein involved in RNA processing. Natively folded TDP-43, shown in the nucleus, regulates RNA splicing. As a nucleocytoplasmic shuttling protein, TDP-43 is also involved in cytoplasmic RNA processing including the stress granule response and RNA transport. (2) *C9ORF72* mutation causes the sequestration of RNA-binding proteins, which impairs RNA processing. *C9ORF72*-mediated ALS also manifests with accumulation and aggregation of TDP-43. (3) *MATR3*, *hnRNPA1* and *hnRNPA2B1* mutations also impair RNA processing and induce TDP-43 proteinopathy, likely through direct binding interactions with TDP-43 which influence its folding and function. (4) *FUS* mutations are thought to cause ALS, independent of TDP-43 proteinopathy, via impaired processing of transcripts that may be common to those targeted by TDP-43. (5) Mislocalization of excess TDP-43 to the cytoplasm can be promoted by (6) *TARDBP* mutations and (7) environmental stressors, both of which also promote (8) TDP-43 fragmentation. (9) Cleaved and mislocalized TDP-43 species are prone to misfolding and aggregation, which is associated with the addition of phosphorylation and ubiquitin chains. (10) The ubiquitin proteasome system (UPS) and autophagy ordinarily serve to maintain TDP-43 homeostasis; however, in ALS these protein degradation systems fail to prevent the accumulation of TDP-43, thus favoring the formation of large protein complexes called aggresomes. (11) Mutations in *VCP*, *UBQLN2*, and *SQSTM1* can impair protein degradation. (12) Aberrant RNA processing, and particularly stress granule formation, may promote the aggregation of TDP-43. (13) Conversely, TDP-43 misfolding and aggregation impairs RNA processing function, and sequesters TDP-43 in a dominant-negative fashion. Strategies that prevent TDP-43 misfolding and/or enhance clearance of pathological TDP-43 have the potential to prevent RNA processing deficits and pathogenesis in the majority of ALS cases. P = phosphorylation; Ub_4 = tetra-ubiquitin chain

Reproduced from : Scotter, Chen & Shaw. Neurotherapeutics., 2015

1.2. Degeneration of neurons in ALS and FTLD

Motor neuron death was the first histopathological phenomenon described in ALS and FTLD. To date, the disease mechanisms behind this neurodegeneration remain unknown. While for a long period motor neuron death has been considered as an intrinsic neuronal process, it is now accepted that other cells are involved including astrocytes and microglia and skeletal muscle cells (167–172).

The role of astrocytes in ALS has been shown using *in vitro* co-cultures of healthy motor neurons with astrocytes from either transgenic ALS mouse models (167) or from patients bearing a *SOD1* mutations (168). Astrocytes expressing mutant *SOD1* induced motor neuron death via the secretion of toxic factors. This showed that the toxicity of astrocytes in ALS is a general process that is not specific to the expression of a mutant *SOD1* gene.

Furthermore, the muscle tissue appears as a player in the pathology (169).This hypothesis is supported by the fact that the muscle exerts a direct influence on the neurons from which it receives innervation (170). More specifically, muscle hypermetabolism is sufficient to induce a partial denervation and motor neuron disease (171). Muscle-specific expression of a double mutant of SOD1 (G37R and G93A),or of the wild human SOD1, is sufficient to trigger muscle atrophy, degradation of the neuromuscular junction (NMJ), axonopathy and degeneration of the motoneurons (MN) (172).

In FTLD, the massive atrophy of frontal and temporal lobes suggests a massive loss of neurons and/or glial cells. Only one type of degenerative neurons in FTLD have been identified: the Von Economo neurons (VE neurons). VE neurons are large bipolar neurons present in the layer V of the anterior cingulate cortex, and representing approximately 5% of the neurons in this area (173). Although, the function is not precisely known, their location suggests a role in complex social interactions. This selective degeneration of VE neurons has been recently described in a small group of patients with sFTLD and having a type of FTLD-TAU histopathology or FTLD-U. The authors showed a loss of 74% VE neurons compared to control subjects (174). The loss of VEN neurons in FTLD patients has been confirmed in two other studies and seems to occur in early stages of FTLD, suggesting that these neurons are among the neuronal population targeted by the disease (175,176).

1.3. Neuroinflammation in ALS and FTLD

Neuroinflammation is characterized by the activation of glial cells astrocytes and microglia, the release inflammatory factors such as cytokines and the infiltration of immune cells into the cerebrospinal fluid (CSF) upon blood brain barrier injury.

Microglias are the principal inflammatory cells of the central nervous system (CNS) and are considered as the macrophages of CNS. Their activationis defined as a proliferation, a change in morphology, and an increased capacity of phagocytosis (177).

Astrocytes have a supporting role in the physiology of neurons, especially in the formation and the maintenance of synapses, the recycling of neurotransmitters and the energy intake (reviewed in (178)). Under condition of neuroinflammation, the activation of astrocytes results in their proliferation, their migration to an injured area and the overexpression of the Glial Fibrillary Acidic Protein (GFAP).

The presence of neuroinflammation in ALS was demonstrated by revealing the presence of activated astrocytes in the brain (179), and in the spinal cord of patients (180). Because these studies were conducted on *post mortem* tissues from patients that had reached the final stage of the disease, it was not possible, at the time, to determine whetherthe observed neuroinflammation was a consequence of the death of motor neurons or whether it had actively participated to the neurodegeneration process.

On the opposite, the ALS transgenic models indicates an active role of astrocytes and microglia in neurodegeneration. Firstly, overexpression of GFAP has been reported in the spinal cord of G93A SOD1 mice prior to motor neurons death (181). Second, a couple of studies elegantly showed that the targeted decrease of conditional SOD1 G37R expression either in microglia, or in astrocytes, was sufficient to increase mutant mice survival (182,183). Thus, expression of the mutant gene in these two cell populations affects disease onset and progession.

Neuroinflammation was also highlighted in FTLD. The presence of activated microglia and astrocytes was reported in the brains of patients (184,185). It was published that astrocytic activation in the frontal cortex is positively correlated with the level of atrophy and that microglial activation in the white matter is present from the early stages of the disease (186). Another study confirmed that astrocytic activation is present at stages that proceed pathology, before the massive neurodegeneration (187). More generally, an increase in pro and anti-inflammatory cytokines was demonstrated in the CSF of FTLD patients (188). These studies suggest an important role of glial activation and inflammation in the disease. However, they did not show whether neuroinflammation is beneficial or detrimental to neurons. Alongside to astrocytic activation, several studies showed degeneration of astrocytes in the brain of FTLD patients (189).

The role of microglia and astrocytes in the FTLD has also been studied in animal models. Neuroinflammation has been observed in many transgenic FTLD models, including those based

on the mapping expression *TDP-43* (190), *MAPT* (191), *CHMP2B* (192), *PGRN* (193) and *FUS* (194–198). Yoshiyama et al. showed that microglial activation appears early in the pathology in a mouse model of FTLD based on the expression of tau P301S. They also showed that immunosuppression in this model is beneficial for the survival of neurons. Furthermore, a study published in 2005 showed that a conditional overexpression of *MAPT* in astrocytes induced the accumulation of hyperphosphorylated and ubiquitinated TAU in these, accompanying the neurodegeneration (199). These studies therefore indicate involvement of astrocytes in neurodegeneration at least in the FTLD positive TAU inclusions. Conversely, another study using a model based on PGRN inhibition showed that the behavioural impairment observed in these mice was independent of astrocyte activation and inflammation (200).

Altogether ALS and FTLD are now considered as two extremes of a clinic-pathological disease spectrum commonly referred to as ALS/FTLD and set forth FUS as one of the important common key player between both diseases.

II. FUS – A MULTIFUNCTIONAL RNA/DNA BINDING PROTEIN

A. FUS structure and physiological role

FUS was identified about 20 years ago as a fusion oncogene in human myxoid liposarcomas, hence its name (FUSed in sarcoma) (201). FUS is also known as Translocated in liposarcoma (TLS). Mutations in *FUS* were reported to cause ALS in 2009, and deposition of FUS in pathological protein inclusions in ALS cases carrying *FUS* mutations was also observed (50,51). Immediately after these initial genetic pathological discoveries linking FUS to ALS, FUS inclusions were also found in the brains of a subset of FTLD patients despite the absence of *FUS* mutations in these patients (29,146,202).

1. Gene structure of *FUS*

The *FUS* gene is located on chromosome 16 and contains 15 exons encoding a multidomain protein consisting of 526 amino acids (**Figure 17**). It belongs to a group of DNA/RNA binding proteins that share typical structures, including a N-terminal transcriptional activation domain (QGSY, 165 amino acids), adjacent to a glycine rich region (RGG1), followed by RNA recognition motif region (RRM, 86 amino acids). This RRM contains a nuclear export signal (NES) of eleven amino acids, located near by the N-terminal end. In C-terminal, a 31 amino acid-zinc finger domain (ZnF) is found embedded in between two glycine rich regions (RGG2 and RGG3) creating a 130 amino acids-domain. The last 19 C-terminal amino acids of FUS delineate an atypical nuclear localization signal, containing proline and tyrosine residues (PY-NLS, later referred to as NLS) (203,204) (**Figure 17**).

At least one specific role for each protein domain of FUS has been documented. The N-terminal QGSY-rich domain functions as a potent transcriptional activation domain (205,206). This specific role as transcriptional activator has been well described since FUS was recognized to have an oncogenic properties .In addition, the QGSY-rich domain is directly implicated in the aggregation of FUS *in vitro* (207,208), and this has been linked to its prion-like features (209).(207,208)(207,208) The three glycine rich regions (RGG), together with the RNA recognition motif (RRM) and the zinc finger domain (ZnF) are required for nucleic acid binding (210,211). However, the way FUS binds to nucleic acids and the amino acids involved in this process still remain to be determined. Yet, different *in vitro* studies suggested that the RGG2-ZnF-RGG3 domain is most likely the major RNA binding domain and has a preference for GU-rich sequences (212,213).

Although, FUS predominantly resides within the nucleus, it constantly shuttles between the nucleus and the cytoplasm. FUS nuclear import is mediated by the binding of this PY-NLS

(204) to the nuclear import receptor Transportin (also known as Karyopherinβ2) (151,203) (**Figure17**).

Figure 17. FUS gene structure :schematic representation of the *FUS* transcript and its specific domains

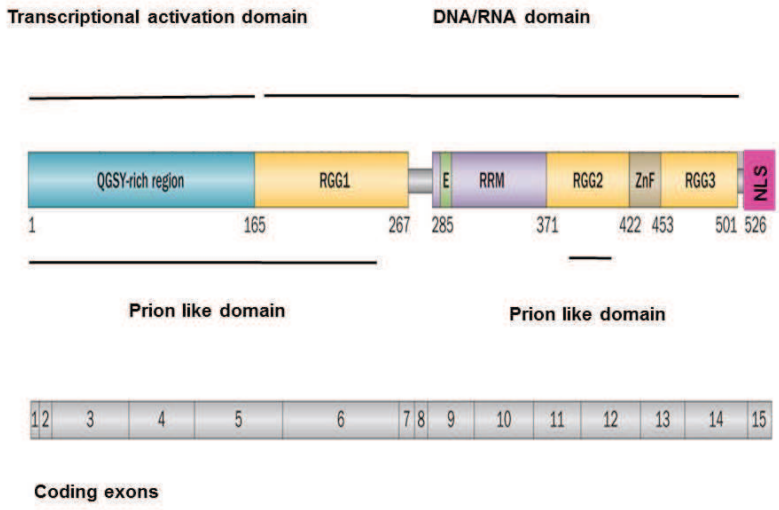

FUS has 526 amino acids and contains several conserved domains: SYGQ, RGG, RRM, E, NLS and ZnF. Numbers under the protein line indicate the boundaries of each domain. The putative prion domain of FUS comprises amino acids 1–239 and 391–407. E, nuclear export signal; NLS, nuclear localization signal; RGG, Arg–Gly–Gly-rich motifs; RRM, RNA-recognition motif; QGSY, Ser–Tyr–Gly–Gln; ZnF, zinc-finger motif
Reproduced from Deng, H. et al., Nat. Rev. Neurol.2014

2. Physiological role of FUS

FUS is ubiquitously expressed during embryogenesis, but its expression is rapidly downregulated in the peripheral organs during postnatal development. FUS remains expressed at significant levels in neurons throughout the lifetime, suggesting that FUS may exert important functions in the central nervous system (214).

FUS protein has been now recognized to play a role in a number of critical cellular functions. These include nuclear functions, such as DNA repair and maintaining of genomic integrity, regulation of transcription, and pre-mRNA processing, as well as cytoplasmic functions such as RNA transport, local translation, microRNA biosynthesis as well as multiple protein-protein interactions. These different functions are detailed below.

2.1. DNA repair

DNA repair is defined as the processes by which a cell identifies and corrects damage to the DNA molecules that encode its genome. Many proteins were shown to be involved in DNA damage response, repair and protection (215).

FUS binds to denatured single-stranded DNA and promotes its annealing to complementary single stranded DNA and D-loop formation (216) (**Figure 18, a**). Moreover, FUS is also phosphorylated by ATM following the induction of double strand breaks and is involved in regulation of gene expression induced by DNA damage (217,218). FUS does not only take part to DNA damage response has also a pivotal role in neuronal DNA repair via its direct interaction with the histone deacetylase 1 (HDAC1) (218).

Consistent with a major role in genomic stability, *Fus* knockout mice show genomic instability as well as enhanced radiation sensitivity (219–221).

Defects in DNA repair have been extensively linked to neurodegenerative diseases (218). **Together, these emerging findings suggest that FUS plays an important role in the preservation of genomic integrity trough DNA repair mechanism, which could be affected by disease associated *FUS* mutations.**

2.2. Transcriptional regulation and gene expression

Transcriptional regulation is the means by which a cell regulates the synthesis of RNA from the DNA matrix, thereby controlling gene expression. The regulation of transcription is a vital process in all living organisms and is orchestrated by transcription factors and other accessory proteins working in concert to finely tune the nature and the amounts of RNA being produced through a variety of mechanisms.

The N-terminal QGSY-rich domain of FUS functions as a potent transcriptional activation domain in oncogenic fusion proteins (205,206), suggesting a fundamental role in **transcription initiation and/or elongation**. Indeed, several studies identified an interaction of the FUS protein with integral components of the transcriptional pre-initiation complex (PIC), including RNA polymerase II and the TFIID complex (**Figure 18, b,c**) (222,223). FUS has been reported as acting as **co-regulator**, by modulating the transcription of target genes through association with nuclear hormone receptors and gene-specific transcription factors (such as Spi-1/PU.1, NF-κB and Runx2) (224–226). In addition, by binding to non-coding RNAs,and by inhibiting the acetyl-transferase activities of CREB-binding protein (CREB) and p300, FUS interferes with **transcriptional repression** of cyclin D1 and RNA polymerase III (227,228). FUS also

associates with TBP and TFIIIB to repress transcription of small structural and catalytic RNAs by RNAP III (227).

Last, FUS is able to **bind to the promoter region** of several genes transcribed by RNA polymerase II to regulate their expression (229). Indeed, a recent study identified potential FUS-response elements of many target genes, indicative of transcriptional activation or repression directly by FUS (229). Additionally, FUS and protein arginine methyl transferases (PRMT1) synergistically coactivate transcription initiation at the survivin promoter (230). The extent of FUS targets remains to be identified, and is likely to be different from one cell type to another.

Thus, FUS strongly affects expression of specific target genes, that remain to be fully identified.This suggests that critical patterns of gene expression could be changed upon *FUS* mutations, contributing to the FUS related pathology.

2.3. mRNA Splicing

Splicing is a modification of the nascent pre-messenger RNA (pre-mRNA) transcript in which introns are removed from the pre-mRNA, leading to the generation of a mature mRNA consisting exclusively of exons. For nuclear encoded genes, splicing takes place within the nucleus after or concurrently with transcription. Splicing is needed for the messenger RNA (mRNA) before it can be used to produce a correct protein through translation. Splicing is performed by a large complex of small nuclear ribonucleoproteins (snRNPs) called spliceosome.

FUS has been identified as part of the spliceosome machinery with a role in splicing regulation of pre-mRNA by three independent proteomic studies (231–233) (**Figure 18, d, e**). Recently, it was shown that FUS directly associates with several components of the spliceosomal complex, among which SMN protein was the major partner (234,235). As well, FUS was required for the formation of nuclear gems, substructures that are involved in the final stages of snRNP modification and assembly (234,235).

The identification of RNAs bound to FUS is a first step to understand the role of FUS in RNA splicing. Using crosslinking and immunoprecipitation (CLIP) followed by high-throughput sequencing or RNA immunoprecipitation (RIP) and then by microarray analysis, several groups published global RNA targets of FUS (163–165,236,237). These studies reveal that FUS binds to several thousand different pre-mRNAs, preferentially to long introns and less frequently to exons and 3′UTRs. Full length FUS was bound to mRNAs introns 70% of the time, while mutant FUS only interacted with the intronic regions 13% of the time, and with 3′ UTRs 61% of the time.

RIP-chip analysis, showed that the mature mRNA targets or “targetome” of FUS in the cytoplasmic compartment of the motor neuron-like cells are related to general cellular activities, including DNA repair, cell cycle, and RNA processing (163).

Furthermore, FUS also regulates its own expression by alternative splicing of exon 7 and nonsense-mediated decay (238).

In all, these findings suggest that splicing alterations in response to *FUS* mutations may be relevant and possibly contribute to neurodegeneration.

2.4. RNA biogenesis and processing

FUS is a component of the large Drosha complex, an RNase III enzyme that is required for microRNA biogenesis (239) (**Figure 18, f**). FUS might stimulate microRNA biogenesis by facilitating co-transcriptional Drosha recruitment. In one suggested paradigm, processing of specific miRNA families requires interaction with RNA-binding proteins (240). FUS is recruited to chromatin at sites of their transcription and binds the corresponding pre-microRNAs. Moreover, **FUS depletion** leads to decreased Drosha levels at the same chromatin loci and to a reduced microRNA biogenesis. Many of microRNA species modulated by FUS depletion are involved in neuronal function, differentiation and synaptogenesis.

A possible link between *FUS* mutations and altered neuronal microRNA biogenesis in neurodegeneration was suggested (241). **However, the precise function of FUS in these cellular processes is still poorly characterized.**

2.5. RNA transport and local translation

A function of FUS in RNA transport was first suggested by the observation that FUS shuttles between the nucleus and cytoplasm while bound to RNA (211). In addition, complexes of FUS and mRNA is translocate to neuronal dendrites and spines in response to neuronal activity. Dendritic transport of FUS seems to depend both on microtubules and actin filaments (**Figure 18, g,h,i**) (211,242). This process seems to be essential for local protein synthesis (local translation) (**Figure 18, i**) and synaptic plasticity (243). As noted above, RNA immunoprecipitation (RIP) followed by microarray analysis identified several hundred cytosolic mRNA targets of FUS in the motor neuron-like cell line NSC-34 (163).

Whether *FUS* mutations impact RNA transport remain to be determined by further studies.

2.6. Protein interactions

A number of direct **protein-protein interactions** are required for FUS functions in RNA metabolism, including SMN (234,235), HDAC1 (218) or PRMT1 (244) and have been detailed earlier.

Figure 18. FUS displays diverse physiological roles

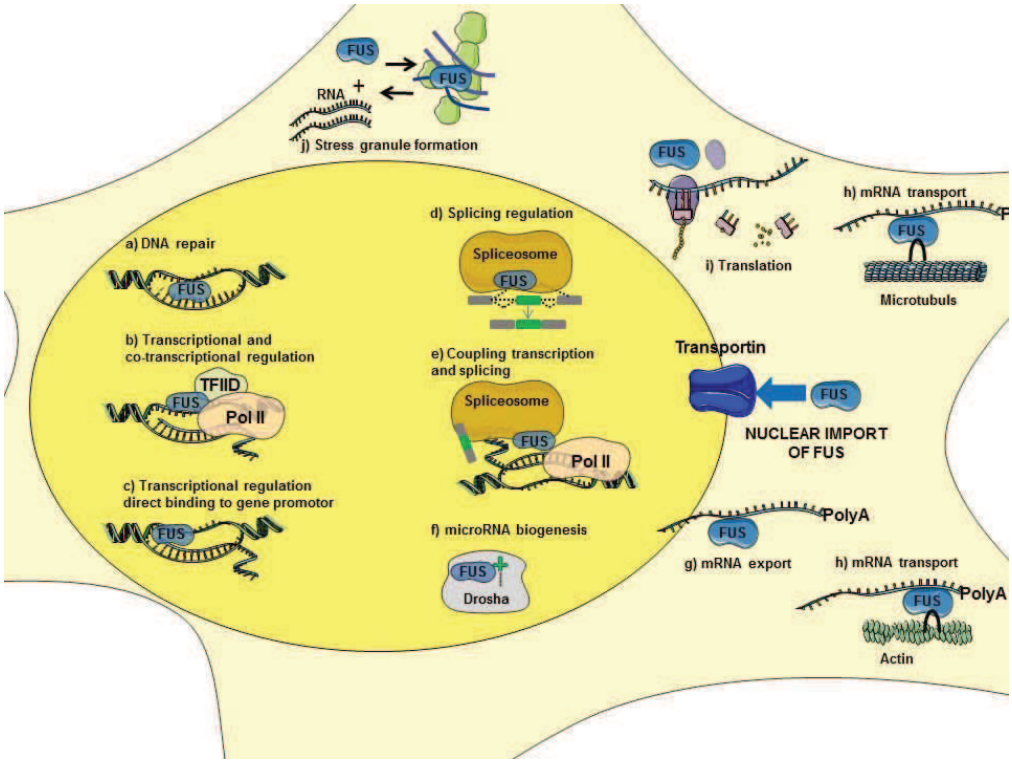

(a) FUS has DNA homologous pairing activity and is important for the repair of DNA double strand breaks. (b) FUS interacts with the transcriptional pre-initiation complex (*e.g.* RNA pol II and the TFIID complex) and with gene-specific transcription factors. (c) FUS also directly binds to specific DNA sequences in the promoter region of certain target gene. (d)FUS affects alternative splicing by interacting with intronic regions near splice sites and subsequently recruiting the spliceosome or other splicing factors, such as hnRNPs or SR proteins, to the nascent pre-mRNA. (e) FUS interacts with both the transcriptional machinery and the splicing machinery and therefore has been proposed to couple transcription to splicing. (f) FUS is a component of the large Drosha complex, an RNase III enzyme that is required for microRNA biogenesis (g) FUS shuttles between the nucleus and cytoplasm and thus might play a role in mRNA export. From the cytoplasm FUS, is imported back to nucleus via TRANSPORTIN (h) In neurons, FUS is involved in the transport of specific mRNAs, to dendrites and dendritic spinesvia an associationwith actin or microtubules. (i) This may regulate local translational of localized mRNAs and may be important for synaptic function. (j) FUS is involved in stress granule formation, however it is still not clear if it is physiological function. Yellow color represents FUS subcellular localization which is predominantly nuclear.
Reproduced from Dormann D & Haass C Mol. Cell. Neurosci. 2013.

In general, an important issue in understanding the FUS pathogenic mechanisms in neurodegeneration is to get detailed insight of FUS physiological role. Of outmost importance is to define the full set of transcripts that are directly bound and post-transcriptionally regulated by FUS in association with splicing, in particular in neuronal cells.

B. Neurodegenerative disorders with FUS pathology

Alongside with involvement in ALS and FTLD, immunostaining for FUS revealed intense reactivity in some other neurological diseases like in Huntington's diseaseas well as spinocerebellar ataxias 1 and 3, and neuronal intranuclear inclusion body disease (245–247).

1. FUS mutations related to FUS proteinopathies - ALS-FUS / FTLD-FUS

At the time of writing more than 50 mutations in the *Fus* gene have been identified in ALS and very rarely in FTLD (**Figure 19**). This gene accounts for a small percentage of fALS cases (~4%), and fFTLD cases (~1%), and it is also found in sALS cases (~1%).

The majority of ALS-linked mutations of *FUS* are clustered in or around the nuclear localisation signal (NLS). By causing the disruption of the binding of FUS protein to transportin, these mutations prevent the nuclear import of FUS and result in the cytoplasmic accumulation of the mutant *FUS* (203,248,249). Along with these dominantly inherited missense mutations, several truncating or frameshift mutations of *FUS* have been identified in ALS that result in the complete deletion of the NLS (250).The inheritance pattern of these mutations is **autosomal dominant**, except in one family of Cape Verdean origin, FUSH517Q, which seems to display a **recessive pattern** (50) (**Figure 19**). Recently, a second mutation in a homozygous state was identified, a single base deletion in the *FUS* gene (FUSc.1486delG) leading to a frameshift and a premature codon termination (251).

Reports of *FUS* mutations in patients with clinical FTLD are rare, and only four *FUS* mutations have so far been identified in patients with ALS/FTLD or in their families. Two patients with *FUS* mutations (p.R521H, and p.G156E) had ALS with FTLD features (252,253), and a two additional mutations (p.G206S and p.R521C) were identified in families affected by ALS/FTLD (254). One patient with a p.M254V mutation and another patient with a p.P106L mutation presented with FTLD without motor neuron signs (255). However, no autopsy data or functional analyses from mutation carriers were available to confirm FUS pathology in any of these patients with FTLD. Until now, no *FUS* mutations have been found in any patient with pathologically confirmed FTLD-FUS (29,144).

Although, ALS is the most common **phenotype** observed upon *FUS* mutation, ALS-FTLD or FTLD alone also occur.

Amongst the ALS-FUS patients, the proportion of **bulbar** and **spinal** onsets are similar to that of typical ALS. **An aggressive phenotype** is associated with FUSP525L, FUSc.1554−1557delACAG, FUSG478LfsX23 and, to a lesser degree, FUSR495X. Of note all these mutations are located in the NLS, affect patients in the first or second decade of life and are fatal after half of a year (143,256,257).The newly described homozygous frameshift deletion in *FUS* (p.Gly496Glyfs*31) was observed in a male patient with an upper limb onset at 39 years (251). His family history was negative for ALS or other neurodegenerative disorders. The patient died 12 months after the disease onset because of a rapidly worsening respiratory failure. This *FUS* mutation causes a frameshift in the 3′ end of the gene, coding for the NLS, which once again confirms that the NLS of FUS represents a mutational hot-spot in ALS patients. This further corroborates the link between mutations leading to NLS deletion and aggressive ALS phenotype.

Although, clinical presentation is widely variable, patients with the FTLD-FUS usually develop a **rapidly evolving FTD syndrome**, mostly bvFTD, sometimes in combination with motor neuron symptoms (258).

Histologically, brain and spinal cord tissue from patients with *FUS* mutations showed severe motor neuron loss in the spinal cord, and to a lesser extent in the brain stem. Mild to moderate upper motor neuron loss was seen in the motor cortex. FUS-immunoreactive cytoplasmic **inclusions, ubiquitin- and p62-positive** were found in spinal cord of FUS patients (50,51).

Pathologically, FTLD-FUS was characterized by severe, usually asymmetric atrophy of the frontotemporal cortex in patients. As already mentioned, an accumulation of FUS protein in inclusions was associated with this clinicopathological type of FTLD (29,145–147)(**Table 3, Figure 19**). FUS-immunoreactive cytoplasmic **inclusions** are usually **ubiquitin- and p62-positive** (29,128,256). However, FUS protein itself is not ubiquitinated, hyperphosphorylated or cleaved, yet insoluble (29). FUS immunohistochemistry also shows normal nuclear levels in many neurons and glial cells(29). It is important to repeat that inclusions in a subset of sporadic FTLD-FUS casesare immunoreactive for the full-length FUS protein, together with TAF15, EWSR1and transportin-1 (149,150).

Figure 19. Schematic representation of the *FUS* gene mutations identified in patients with neurodegenerative diseases

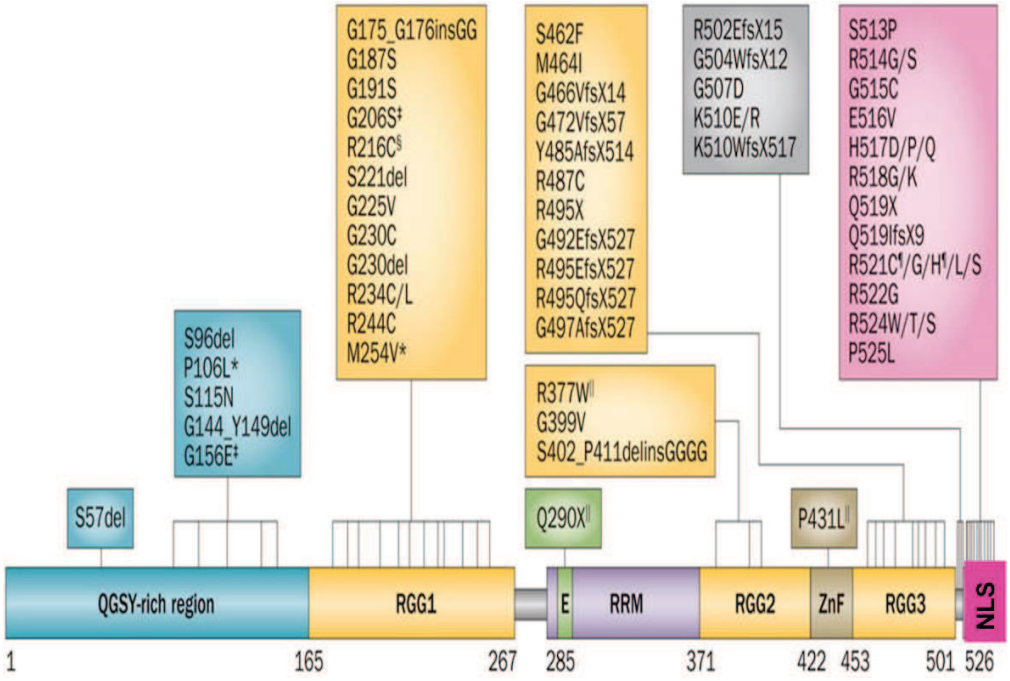

*The pathogenicity of many mutations identified in patients with FTLD still needs to be validated. ‡Mutations identified in patients with ALS and FTLD, or in their families. §Mutations identified in patients with ALS, and in those with essential tremor. ||Mutations identified in patients with essential tremor. ¶Mutations identified in patients with ALS, and in those with both ALS and FTLD. Abbreviations: ALS, amyotrophic lateral sclerosis; E, nuclear export signal; FTLD, frontotemporal lobar degeneration; NLS, nuclear localization signal; RGG, Arg–Gly–Gly-rich motifs; RRM, RNA-recognition motif; SYGQ, Ser–Tyr–Gly–Gln; ZnF, zinc-finger motif
Reproducedfrom Deng, H. et al. Nat. Rev. Neurol.2014

2. Similarities and differences related to FUS proteinopathies - ALS-FUS/FTLD-FUS

Although, FUS accumulation is the common denominator of ALS-FUS and FTLD-FUS, significant genetic and pathological differences have been observed for ALS-FUS and FTLD-FUS.

First, ALS-FUS was always associated with a genetic defect in the *FUS* gene (50,51), while FTLD-FUS was only rarely associated with *FUS* mutations (29,252–255,259,260).

Second, ALS-FUS was characterized by the selective deposition of FUS, while FTLD-FUS showed co-accumulation together with TAF15, EWSR1 and their nuclear import receptor Transportin (149,150) reviewed in (262). In all FTLD-FUS subtypes, FUS-positive pathology was also labeled for TAF15 and EWRS1 and cells with inclusions showed a reduction in the normal

nuclear staining of all FET proteins. In contrast, in cases of ALS-FUS, TAF15 and EWSR1 remained localized to the nucleus and did not label FUS-positive inclusions (149,150).

Third, in ALS-FUS, deposited FUS was methylated on arginine residues, but not in FTLD-FUS (151,262).

Together, these findings strongly suggest that **neurodegeneration is directly related to the subcellular redistribution of FUS rather than only due to mutations**.

3. Possible mechanisms of FUS toxicity - Loss vs gain of function

A two-hit model, which is similar to the one mentioned above for TDP-43, has been proposed to underlie FUS toxicity (203,248). The first step involves the exit of FUS from the nucleus and the second step involves the irreversible formation of stress granule-based inclusions. Indeed, most mutations in *FUS* disrupt nuclear import and cause a cytoplasmic mislocalization of FUS. It seems that nuclear import defect is a key event in ALS pathogenesis, since mutations that cause a very severe nuclear import block (e.g. P525L) are characterized by an unusually early disease onset and rapid disease progression (203,248) (**Figure 19**).

FUS–mediated toxicity could either rely on a reduced ability of FUS to perform its normal nuclear functions referred to as **loss of function**, or on a **toxic gain of function** of FUS in the cytoplasm - an acquired adverse effect of its pathological presence in the cytoplasm.

As ALS caused by mutated *FUS* is most often inherited in an autosomal dominant manner, it suggests that the toxicity is the result of **a gain-of-function** for FUS. However, if mutated *FUS* has lost a function or if mutated *FUS* is binding to DNA, RNA, or protein and abrogating their normal functions, then **a loss of function** would be indicated. The third possibility is **a combination of these two mechanisms.**

However, it is currently unknown whether mutant *FUS* causes toxicity owing to a toxic **gain-of-function mechanism**, a **loss-of-function mechanism** or both.

Current evidence suggest that FUS-induced pathology could arise from one of the following aspects.

3.1. Alteration of gene expression and splicing

Gene expression andsplicing alteration may be involved in FUS toxicity (**Figure 20, a-f**). As already mentioned above several groups published results for the global RNA targets of FUS (163–165,236,237).

ALS-associated FUS mutants expressed in HEK 293 cell lines bind to very different RNA targets compared to wild type FUS (165). It was shown that mRNAs for endoplasmic reticulum

and ubiquitin proteasome-related target gene categories were overrepresented in transcripts bound by mutant FUS proteins with cytosolic mislocalization (165). In a motor neuron-like cell line, FUS has been preferentially bound to cytoplasmic mRNAs that are involved in the ubiquitin-proteasome pathway, in particular the cullin-RING E3 ubiquitin ligases (163). As well as, other studies confirmed that FUS binds to the mRNAs encoding genes responsable for protein clearance and involved in ALS and/or FTLD: *OPTN* (163,164), *UBIQUILIN-2* (42),and *VCP* (42,44).

The role of FUS in splicing has also been shown by performing loss of function studies. Indeed, shRNA-mediated knockdown of FUS in primary mouse neurons revealed 78 FUS-responsive exons (236), while a similar number of splicing changes were detected in embryonic brains of *Fus* knockout mice (237). Last, antisense oligonucleotide-mediated depletion of FUS in adult mouse brain or in embryonic brains of *Fus* knockout mice found splicing changes in >300 genes (164).

Interestingly, a common finding from different groups was that FUS-regulated splicing events are essential for neuronal integrity and function. For instance, one neuronal gene whose splicing was consistently altered by the loss of FUS in all three studies is the microtubule associated protein TAU (encoded by *MAPT*, known to be one of the major genes mutated in FTLD). This is in accordance with a results published by Orozco and colleagues (263) that showed that in the absence of FUS, inclusions of *Tau* exons 3 and 10 increase in *Tau* mRNA leading to a shift in TAU isoform in an analogous manner like in *TAU* mutations associated with FTLD (59).

Altogether, the evidence strongly suggests that *FUS* mutations alter gene expression and splicing. The underlying mechanisms of FUS toxicity might be either nuclear loss of function of FUS or toxic gain of function of *FUS* mutants.

3.2. Defective stress granule and protein aggregation

Stress granules are dense cytosolic ribonucleoprotein (RNP) complexes that negatively control mRNA translation in condition of cellular insults. Stress granules might help to protect RNAs from harmful conditions, thus their appearance under stress (264). Environmental stress triggers a series of signals, which early on involve phosphorylation of eukaryotic translation initiation factor eIF2α, then downstream-prion-like aggregation of the proteinTIA-1 leads to the formation of stress granules.

Localization of mutant FUS in stress granules, has been recently and widely demonstrated suggesting a new pathological mechanism of FUS (161,212,249,265–267)

(**Figure 20, j**). Moreover co-deposition of stress granule marker proteins with FUS is a common finding in ALS-FUS and FTLD-FUS supporting a role for stress granules in their pathogenesis (203).

Some authors proposed an interesting hypothesis whereby cytoplasmic mislocalization under cellular stress induces FUS incorporation into stress granules together with several RNA-binding proteins and RNA molecules. This physiologic reaction might lead to irreversible aggregates due to defects in stress granule disassembly that occurr : upon chronic cellular stress or with aging (as a second hits), or facilitated by disease causing *FUS* mutations (203).

In all, mutated FUS by gaining toxic function eventually could lead trough stress granule to irreversible pathological aggregation or cytoplasmic aggregates may sequester normal FUS (268)**, disrupt RNA processing and initiate motor neuron degeneration trough FUS loss of function.**

3.3. Prion-like properties

A prion is a protein that can fold in multiple, structurally distinct ways, at least one of which is transmissible to other prion proteins. It is this form of replication that leads to disease that is similar to viral infection. While several yeast proteins have been identified as having prionogenic properties, the first prion protein was discovered in mammals and is referred to as the major prion protein (PrP). While PrP is considered the only mammalian prion, prion-like domains have been found in a variety of other mammalian proteins. Some of these proteins have been implicated in the ontogeny of age-related degenerative disorders such as ALS, FTLD, Alzheimer's disease, and Huntington's disease (269). This has given rise to the 'prion paradigm', where otherwise harmless proteins can be converted to a pathogenic form by a small number of misfolded, nucleating proteins (270).

By scouring the human genome with an algorithm designed to detect RNA-binding proteins harboring a canonical RNA recognition motif (RRM) and a putative prion domains FUS and TDP-43, were rank as 1stand 10th among RRM-bearing prion candidates (270). Afterwards, it was proposed that misfolded FUS propagating from cell to cell in a prion-like fashion, might be involved in neurodegeneration (270,271).The FUS prion-like domains are located in the N-terminal QGSY region of the protein (residues 1–239) and in the C-terminal RGG2 domain (residues 391–407) and both are required for FUS misfolding, aggregation and toxicity (208,209).

Despite this hypothesis is tempting it is not known yet how FUS mutations affect these prion-like properties as well how that contribute to the disease, through loss or gain of function.

3.4. Post-translational modifications of FUS

A major post-translational modification of FUS protein is methylation on arginin residues (R216, R218, R242 and R394), catalyzed by individual protein arginine methyl transferases (PRMT), in particuar PRMT1 (151,272). More important, FUS arginine methylation affects nuclear–cytoplasmic localization of FUS (151,272). One study showed that chemical or genetic inhibition of arginine methylation restored nuclear import of ALS-associated *FUS* mutants in HeLa cells or primary hippocampal neurons (151). Also, depletion of PRMT1 in mouse embryonic fibroblasts by gene knockout, or in human HEK293 cells by siRNA knockdown, diminished the ability of ALS-linked *FUS* mutants to localize to the cytoplasm. In murine spinal cord motor neurons, after shRNA-mediated PRMT1 knockdown ALS-linked *FUS* mutants were sequestered in the nucleus and cytoplasmic inclusions were reduced (272). Interestingly, only the inclusions seen in patients with ALS-FUS contain methylated FUS, whereas FUS aggregates in patients with FTLD-FUS are not methylated (151,262).

In all, these findings suggest that arginine methylation might be important in FUS pathogenesis, further elucidation is however necessary.

Figure 20. Possible mechanisms of FUS toxicity

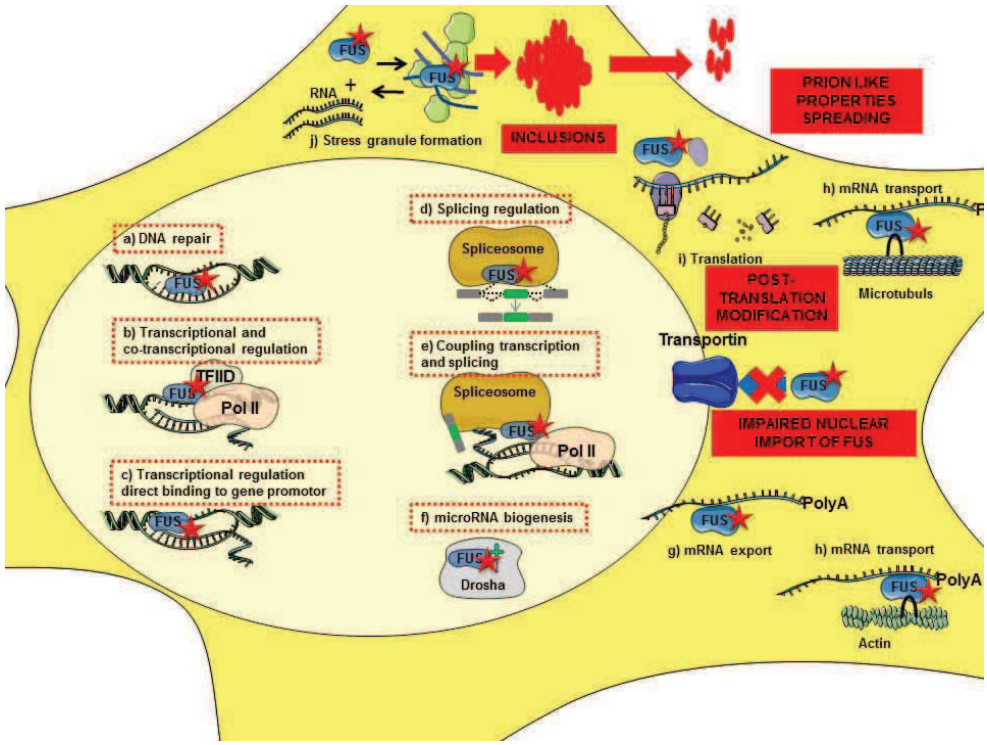

(a-f) Mutation of *Fus* (represented with red star) might alter gene expression and/or splicing, as well as RNA microbiogenesis (red dashed boxes), (g-i) Transport of specific mRNAsand local translational of localized mRNAs and may be disrupted by *Fus* mutations, j) Cytoplasmic mislocalization of mutated FUS protein, followed by cellular stress, might contributes to the transformation of stress granule to cytoplasmic aggregates that may sequester FUS or other proteins and disrupt RNA processingk) Possible cell to cell spread (not yet tested for FUS) of prion-like aggregates may underlie (contribute to) disease spreading from a focal initiation, l)Post-translational modificiation could contribute to Fus toxicity (yet, it is still unknown how precisely).
Yellow color represents FUS subcellular localization which is mostly mislocalized to cytoplasm if mutated due to impaired nuclear import by TRANSPORTIN.
Reproduced from Dormann D & Haass C Mol. Cell. Neurosci. 2013.

C. Animal models of FUS related protheinopathies ALS/FTLD – remaining questions

A key question in the field is how mutations in FUS cause neurodegeneration in ALS or FTLD. Different pathogenic mechanisms for FUS mutants including toxic gain-of-function, loss-of-function, or a combination of effects have been hypothesized. Indeed, does the disease arise from a lack of normal FUS or some new, toxic action by the mutant protein? As in the case of TDP-43, either a gain of toxic properties or a loss of function owing to sequestration of these proteins in aggregates is plausible.

Worldwide research effort is focus in answering this crucial question by generating different animal model.

1. Non-rodent models

Experiments in yeast (273,274), drosophila (275–279) and C. elegans (280,281) **support the concept that cytoplasmic accumulation of FUS is toxic**.

A study conducted in yeast found that overexpression of human wild type WT FUS is toxic (273). In an independent study, ectopic expression of human full length FUS or ALS mutant FUSR524S and FUSP525L in yeast cells led to the formation of FUS punctate immunoreactive aggregates and dose-dependent cytotoxicity. Expression of N-terminal fragments or the C-terminal fragment was sufficient for aggregate formation but did not cause any cytotoxicity (274).

Taken together, these yeast models suggest that overexpression of either WT or mutant FUS is toxic in yeast cells, both N-terminal and C-terminal sequences are required for aggregation and cytoplasmic localization of FUS.

Neuron-specific overexpression of full length FUS in Drosophila resulted in a dose-dependent decrease in life span, and an impaired locomotor phenotype (276). Ectopic expression of either WT or mutant FUS in the motor neurons caused age dependent and progressive neurodegeneration such as axonal loss and functional defects including locomotive defects and tail lifting phenotypes. Yet, mutant FUS caused more toxicity as compared to WT FUS, suggesting that ALS-linked mutations of FUS acquired toxic gain of functions (277). By deleting the nuclear export signal (NES) FUS is trapped inside the nucleus. Deletion of the nuclear export signal strongly suppressed mutant FUS toxicity, suggesting that the cytoplasmic localization of FUS is a necessary step in causing the toxicity (275). In contrast, Xia et al. reported that FUS toxicity in Drosophila requires nuclear localization (278).

Taken together, these studies demonstrate that, in Drosophila, the expression of mutant FUS is more toxic than that of WT FUS.

However, a recent study brought new insights in the problematic of FUS toxicity. Storkebaum et al., introduced cell-type-specific endogenous gene inactivation of *cabeza* (*caz*) (the Drosophila ortolog of human FUS). Neuron-selective *caz* inactivation was performed under temporal control; during development and in adult stage. Inactivation during development resulted in failure of pharate adult flies to eclose from the pupal case, and adult escapers displayed motor performance defects and reduced life span. Remarkably, selective *caz* inactivation in adult neurons did not affect motor performance and life span, indicating that neuronal *caz* is required during development, but not for maintenance of adult neuronal function.

Together, these findings indicate that loss of neuronal caz function during development is necessary and sufficient to induce adult motor performance defects and shorten life span while later in life (partial) loss of neuronal FUS function may not be sufficient to cause adult motor neuron degeneration(279).

Recently, a C.elegans model was generated by expressing WT or mutant FUS with ALS linked mutations using a pan neuronal promoter (280). Mutant FUS was predominantly localized in the cytoplasm and formed cytoplasmic aggregates as seen in human patients, while WT FUS was localized exclusively in the nucleus. The degree of cytoplasmic mislocalization of mutant FUS was correlated with the type of FUS mutations and the degree of neurodegenerative phenotypes seen in human ALS patients. Animals expressing mutant FUS demonstrated progressive motor defect and had a shorter life span as compared to WT FUS-expressing animals. Interestingly animals expressing WT FUS also showed motor defect, but that remained mild, suggesting that the mutant protein is more toxic than the wild type one (280). Transgenic worms expressing mutant FUS displayed adult-onset, age-dependent loss of motility, progressive paralysis and neuronal degeneration that was distinct from wild type alleles. Additionally, mutant FUS proteins are highly insoluble while wild type proteins remain soluble suggesting that protein misfolding may contribute to toxicity (281).

In summary, these findings suggest that ALS-linked mutations in FUS cause neuronal dysfunction via a dominant gain-of-function mechanism and that mutant FUS aggregates lead to neurotoxicity in C. elegans.

2. Rodent models

2.1. FUS knockout and knockdown models

So far three independent FUS knockout mouse models have been generated (219,220,234). Two independent groups reported FUS knockout (KO) mouse models long

before the identification of ALS-linked mutations in FUS but did not analyze their neurological phenotype.

Back in 2000, Kuroda et al., developed the first FUS knockout model, the *TLS–/–* mice (hence its other name *TLS* for translated in liposarcoma), by disrupting the FUS gene in embryonic stem cells. In these mice, the coding region was interrupted inside the exon 8 (immediately upstream of the RNA recognition motif) by a promoterless insertion cassette that created an allele encoding a truncated TLS–NEO fusion protein. Cells derived from the *TLS–/–* animals express no intact TLS protein, yet the TLS–NEO fusion protein encoded by the targeted allele is expressed at very low levels. Homozygous *TLS–/–,* male mice were completely sterile while females were less fertile. Mice exhibited increased sensitivity to ionizing irradiation that was consistent with a role for FUS in homologous DNA recombination, nowadays widely proven. More important, on the inbred 129svev background, rare mutant animals were alive at weaning, but none reached adulthood. The survival of *TLS–/–* animals of partially outbred background (with equal contribution of genes from the 129svev and CD1 strains) was virtually unimpaired. Other than their reduced size, the mutant animals appeared developmentally normal. The authors did not examine the neuronal phenotype and, to my knowledge, these mice were not further studied. Information about any phenotype related to ALS or FTD, at least in the surviving outbred mice, are lacking (220).

Around the same time, Hicks et al., succeeded in making FUS knockouts. In their *Fus–/–* mice, the U3NeoSV1 gene-trap retrovirus was integrated into a region of genomic DNA homologous to exon 12 of human *FUS.* In this case, the provirus disrupted exon 12 of *Fus*, resulting in a null mutation and subsequently in the loss of wild-type Fus expression. Although, low levels of truncated Fus protein was also present, the authors claimed that it was unlikely to retain wild-type activity because the truncation removed essential domains that bind nucleic acids. Mice homozygous for the *Fus* mutation failed to suckle, and died within 16 hours of birth, only one *Fus–/–* mouse survived 2.5 days. Newborn *Fus–/–* mice were typically the smallest in the litter, otherwise, *Fus–/–* mice appeared to develop normally and histological examination of serial sections confirmed normal structure and development of all major organs and tissues (except smaller thymus gland). Interestingly, the *Fus–/–* mice demonstrated a reduction in the number of white blood cells. Furthermore, a majority of animals showed chromosomal abnormalities. These homozygous FUS-null mice died too soon to look for signs of an aging disease (219).

In 2013, a third knockout model was published by Yamanaka et al., which were obtained by inserting b-Gal-neo cassette in between exons 2 and 3 of FUS gene (234).

FUS knockout mice were used to assess the importance of FUS for spliceosome integrity and gem formation. Their findings indicated that loss of FUS altered these processes, and suggested one more possible cellular mechanism for FUS loss of function. However, no other data regarding the phenotype of these mice are available.

These findings describe physiological functions for FUS in a mouse model and indicate that FUS is essential for development and viability of neonatal animals, for the maintenance of genomic stability, DNA repair and splicing.

Results from these models, as well as potential remaining truncated FUS protein, have made it unclear whether FUS loss of function is required for ALS/FTLD pathology.

A paper in April 2015, by Kino and Nukina (221), partially solved the problem. Authors started their experiments with Hicks' black-6 animals that were missing just one copy of the *Fus* gene. To shuffle the background genotype, Kino out bred them to another strain – white ICR mice.The heterozygous offsprings were then intercrossed to obtain total *Fus* knockouts with a hodgepodge of black-6/ICR genomes. Unlike the original Hicks homozygotes, these mixed-background knockout pups survived more than a day, but they could not compete with their *Fus*-positive littermates for milk. When those robust siblings were removed from the cages, the *Fus* knockouts survived to adulthood and did not present anymotor phenotype. At a rotating rod – a common challenge for ALS mouse models, the knockouts performed same as their control littermates. At 90 weeks, Kino collected their spinal cords, and observed that the knockouts had similar numbers of motor neurons than controls. Mice missing the *Fus* gene lived to nearly two years with no signs of motor neuron disease. The authors concluded that the lack of motor neuron deficits suggests that FUS gain of function rather then FUS loss of function is the main pathophysiology in ALS.

However, as evident by their small size and difficulty scrambling for milk after birth, the knock-out mice were not entirely normal. Homozygous knockout mice did not manifest ALS-like phenotype; instead they showed distinct behavioral and histological alterations. Compared to control mice, knockout mice were unusually active, they roved their cages more frequently, and spent more time exploring open and lighted areas. Thus, *Fus* knock-out mice developed some kind of hyperactivity disorder and reduction in anxiety-like behavior, as speculated by the authors. Their brains looked grossly normal, but some developed vacuoles in the hippocampus (221).

This observation was strengthened by a group studying the consequences of FUS depletion. Udagawa et al., evaluated *in vivo* consequences of FUS depletion on synaptic functions. To this end, adeno-associated viruses (AAVs) expressing a shRNA targeting FUS

were stereotaxically injected into the mouse hippocampus. This area was chosen because the hippocampus is one of the most degenerated brain regions in FTLD/ALS patients and is involved in multiple aspects of behavior including learning and memory, emotions, anxiety, hyperactivity and social interactions. FUS knockdown mice interacted with the unfamiliar wild type intruder mouse as long as control mice did. The interaction time of the control mice gradually decreased over the course of four sessions. However, FUS knockdown mice interacted with the intruder to a similar extent over the four sessions, indicating that the FUS knockdown animals were deficient in social behavior. Thus, hippocampal FUS depletion caused a novelty-induced hyperactivity which might be responsible for social impairment, and could be reminiscent of typical FTLD symptoms (282).

Altogether, these results suggest that that deficiency of FUS leads to behavioral and pathological abnormalities that might be relevant to neurodegenerative disorders, including FTLD. This suggests at least some contribution of FUS loss-of-function to neurodegenerative disorders.

The major characteristic of FUS knockout and knockdown models are summarized in the Annex (Table 4) .

2.2. Models with overexpression of wild type or mutant FUS

Currently several rodent models stably overexpressing wild type FUS or expressing ALS-linked mutations in FUS have been published (194–198,283) (**Table 5**).

To study the consequences of mutation in the *FUS* gene, transgenic rats ubiquitinously expressing the human *FUS* gene, with or without mutation, were generated (195). Transgenic lines expressing the human *FUS*, under tight control by Doxycycline (Dox) at substantial levels, were crossed with a CAG-tTA transgenic line to produce double transgenic offspring that expressed human *FUS* transgene in the absence of Dox. Breeding female rats were given Dox in their drinking water until delivery such that expression of the *FUS* transgenes was recovered postnatally, after Dox withdrawal. Overexpression of a mutant *FUS* (FUSR521C substitution) induced progressive paralysis resembling ALS. Mutant *FUS* transgenic rats developed a progressive paralysis secondary to severe axonopathy of otherwise preserved spinal motor neurons, an atrophy of the skeletal muscles, and displayed a substantial loss of neurons in the cortex and hippocampus. Within neuronal cells FUSR521C subcellular distribution was affected to a minimal extent and was accompanied by FUS-negative ubiquitin-positive aggregates. Glial reaction was observed in the brain and spinal cord (195).

While transgenic rats that overexpressed the wild-type human *FUS* (WTFUS) were asymptomatic at young ages, they showed a deficit in spatial learning and memory and a significant loss of cortical and hippocampal neurons at advanced ages. Immunoreactivity to human FUS was detected in the brain and spinal cord where FUS mainly resided in the nucleus, but was also diffusely located in the cytoplasm. WT FUS rats accumulated ubiquitin; however FUS did not co-localize with ubiquitin (195).

These results suggest that mutant *FUS* is more toxic to neurons than normal *FUS* and that increased expression of normal *FUS* is sufficient to induce neurodegeneration (195).

Transgenic mice overexpressing wild-type human *FUS* (WTFUS), under the control of the mouse prion protein (PrP), central nervous system promoter developed an aggressive age- and dose- dependent phenotype with an early onset tremor followed by progressive hind limb paralysis and death by 12 weeks in homozygous animals. Large motor neurons were lost from the spinal cord accompanied by neurophysiological evidence of denervation and focal muscle atrophy. Surviving motor neurons in the spinal cord had greatly increased nuclear and cytoplasmic expression of FUS, with globular and skein-like FUS-positive and ubiquitin-negative inclusions. This was associated with astroglial and microglial reactivity. In the brain of the transgenic mice FUS inclusions together with diffuse cytoplasmic staining were also detected in the neurons without apparent neuronal loss and little astroglial or microglial activation. The increased expression of human *FUS* however was associated with a down-regulation of endogenous murine *Fus* in transgenic animals. Hemizygous FUS overexpressing mice showed no evidence of a motor phenotype or pathology after two years of age (196).

Although, this phenotype recapitulates many behavioural and pathological aspects of ALS-FUS, deciphering if *FUS* overexpression is toxic in nucleus or in cytoplasm is hardly possible. Loss of endogenous murine *Fus* further complicates our understanding of the mechanism. Nevertheless, neurodegeneration observed in both mice and rats transgenic models somehow demonstrate that FUS overexpression per se is pathogenic. Both models support a toxic gain of function due to the accumulation of FUS rather than a loss of nuclear function.

To investigate how *FUS* mutations lead to neurodegeneration, a technique called somatic brain transgenesis (SBT) was utilized to overexpress either WTFUS, FUS R521C, or FUS Δ14 throughout the brain, with the highest levels in the cerebral cortex and the hippocampus, and no detectable glial expression. SBT uses recombinant adeno-associated virus (rAAV) through bilateral intracerebroventricular injection to express a cDNA predominantly

in neurons beginning a few weeks after birth. Expression of both *FUS* mutants led to increased FUS protein in the neuronal cytoplasm, to the degree which correlated with the severity of the mutation as reflected by disease onset in humans. Despite increased cytoplasmic levels of FUSR521C, no obvious inclusions or aggregates of FUS were observed in mice injected with WTFUS or FUSR521C. Only, mice expressing the most aggressive mutation, FUSΔ14, showed histological features of human FUS proteinopathies, including insoluble FUS protein, basophilic and eosinophilic neuronal cytoplasmic inclusions, and presence of other pathologic markers, including ubiquitin, p62/SQSTM1, α-internexin, and the polyadenylate-binding protein 1 (PABP-1). Any evidence of TDP-43 redistribution from the nucleus to the cytoplasm or presence of TDP-43 within inclusions in WTFUS, FUSR521C and FUSΔ14 mice was not find. Astrocytosis or microglial activation were absent. These mice were sacrificed at 3 months of age and untill then no motor or other behavioural phenotype relevant for ALS or FTLD was observed (283).

However, results obtained for truncated form FUSΔ14 support the hypothesis that cytoplasmic FUS is toxic. The finding that FUSΔ14 expression can reproduce many pathologic features observed in subtypes of FTLD and ALS patients provides additional evidence that these diseases may share common mechanisms

To examine FUS in the pathogenesis of FTLD, a rat model expressing human *FUS* with pathogenic mutation restrictedly in the neurons of the forebrain was developed. To induce expression Camk2a-tTA transgenic rat line were crossed with mutant FUS transgenic rats carring TRE-FUS-R521C. In the double-transgenic rats, expression of the mutant human FUS was observed only in the neurons, but not in the glia. This novel rat model showed progressive loss of neurons particularly in the superficial layers II and III of the frontal cortex accompanied with severe loss of neurites and dendritic spines. Accordingly, reactive microglia and astrocytes were first detected in the layers II and III of frontal cortex. Mislocalization of the FUS to the cytoplasm and ubiquitin aggregates developed primarily in the neurons of the entorhinal cortex of the temporal lobe. Intriguingly, aggregated ubiquitin was not colocalized with mutant *FUS*, but neurons with ubiquitin aggregates were deprived of endogenous TDP-43. Overexpression of mutant *FUS* in the forebrain neurons impaired rats' spatial memory, which was detected by Barnes maze assay. By the age of 18 weeks most of the rats had difficulty in locating the escaping hole in the Barnes maze and reached disease end-stages (194).

This mouse model shows that overexpression of mutated human *FUS* restricted to the rat forebrain and accompanied by the cytoplasmic mislocalization of FUS reproduces some bahavioural and histological charactheristic consistent with the findings in the FTLD patients.

However, from the aforementioned models it appears extremely hard to achieve aggregation in models with expression of full-length FUS or FUS lacking functional NLS like FUSR521C.

To overcome these limitations and to answer the question whether FUS aggregation is sufficient to cause pathological changes typical for FUSopathies, Shelkovnikova et al., generated a new mouse model expressing a fragment of human FUS1–359 cDNA cloned into Thy-1 promoter. The truncated human protein FUS1–359 lacked RNA binding site, NLS and was highly aggregate-prone. In the central nervous system of hemizygous FUS1–359 transgenic mice, the truncated human protein was expressed in spinal cord, brainstem and cortex at a lower level than the endogenous mouse FUS protein. These animals abruptly developed a severe neurological phenotype early in their life. A typical motor dysfunction pattern included gait impairment caused by asymmetrical paresis and eventual complete paralysis of limbs, atrophy and denervation of the musle. Multiple FUS-positive inclusions were revealed primarily in the lower motor neuron cell bodies and axons. Unexpectedly, nuclear localization and aggregation of *FUS* variants completely lacking the C-terminal NLS were observed in a significant number of mouse neurons. Similar inclusions were observed in other neurons including upper motor neurons in the motor cortex. Only a fraction of FUS-positive inclusions was ubiquitinated, and in some cells, non-overlapping FUS and ubiquitin inclusions were present. In the late stage of the disease profound neuroinflammation was seen (198).

This study produce the first direct *in vivo* evidence that aggregation of FUS protein can *per se* trigger ALS like FUSopathy with severe damage to susceptible neurons. However, because the truncated form of FUS was able to seed aggregation of normal FUS protein, secondary loss of function, along with direct toxicity induced by the aggregates, might play a role in the development of the neurodegenerative changes in the nervous system.

Another study provided insight into how gain-of-function of FUS mutations affected critical neuronal functions. Transgenic mice expressing FLAG-tagged FUS-R521C mutant proteins using the Syrian hamster prion promoter, exhibited postnatal lethality and early onset motor behavioral deficits characterized by gait and motor coordination defects. The majority of the mice showed growth retardation, spastic paraplegia, severe muscle wasting and denervation. Loss of spinal cord motor neurons was progressive, age-dependent while cortical motor neurons were spared. Prominent microgliosis and modest astrogliosis was found. FUSR521C mutant protein was predominantly nuclear but also found in the cytoplasm. Interestingly, in FUSR521C transgenic mice the distribution of endogenous FUS was affected. A

reduction of FUS was observed in neuronal nuclei, as well as in punctate structures that resembled synapse at the nerve terminals within spinal cord and sensorimotor cortex (197).

Mutant FUSR521C proteins failed to interact with histone deacetylase 1 (HDAC1) and prevented the normal interaction of the remaining endogenous FUS with HDAC1. Consequently, FUSR521C mice exhibited evidence of DNA damage in selective genetic loci, followed by severe dendritic and synaptic defects in spinal motor neurons and cortical neurons. The results suggested that the dendritic defects in FUSR521C motor neurons most likely preceded neuron loss and could contribute to spinal motor neuron degeneration in FUSR521C mice. DNA damage was not widespread in FUSR521C mice, but can be detected in 5′noncoding exons of the *Bdnf* gene in both spinal cord and brain. Indeed, these results identified BDNF as target of FUSR521C–associated DNA damage and RNA splicing defects in mice. RNA-seq analyses of FUSR521C spinal cords revealed additional transcription and splicing defects in genes that regulate dendritic growth and synaptic functions (197).

Together, these results indicate that mutant FUSR521C protein present abnormal gain-of-function properties in protein-protein and protein-RNA interactions that contribute to the severe defects restricted to neurons.

The major characteristic of transgenic models with overexpression of wild type or mutant FUS are summarized in the Annex (Table 5).

2.3. Summary of current results in available Fus models

- Models of Fus knockout show early lethality in inbred strains (219,220)
- Mixed-background knockout mice survive birth to adulthood but do not manifest ALS-like phenotype (221)
- FUS knockout as well hippocampal FUS knockdown leads to behavioural phenotypes related to typical FTLD symptoms (221,282)
- Two out of three existing models show potential remaining of truncated FUS protein (219,220)
- There is no available Fus conditional knockout mouse model.
- Transgenic models with overexpression of wild type or mutant FUS in general recapitulates some features of ALS (195–198) and FTLD (194,283), however it is unclear whether the phenotypes were caused by overexpression per se or were specific to the FUS mutation.
- Transgenic FUS expression leads to downregulation of endogenous FUS (196,197).

- Transgenic models show both nuclear and cytoplasmic FUS staining (194–198,283). All models failed to achieve total nuclear clearance with complete cytoplasmic mislocalization of FUS.
- It is unclear to which extent the observed pathology is due to **FUS loss of function** or **FUS gain of function.**

Therefore no clear picture has yet emerged on whether mutated FUS is more toxic than similar levels of wild type FUS. Similarly, it is unclear whether the phenotypes were caused by the overexpression per se or were specific to the FUS mutation.

There have been several major hurdles indiscriminating the pathophysiological effects. First, models with ALS-associated mutations failed to achieve complete loss of nuclear import and **total nuclear clearance** of FUS (194–198,283). Despite showing FUS **inclusions in the cytoplasm** to varying degrees a substantial FUS nuclear staining as well as **nuclear aggregations** were present (195,198). Second, since FUS protein levels are very tightly regulated by an auto-regulatory mechanism involving alternative splicing of exon 7 (238), transgenic FUS expression leads to **downregulation of endogenous *Fus*** as a consequence, (196,197), making the interpretation of results even more complicated.

In all, results from initial *in vivo* models of ALS-FUS have been inconsistent and the mechanisms remain unresolved. Thus, the debate between loss-of-function and gain-of-function hypotheses for FUS is not settled. Better mechanistic insights and animal models are crucial for a better understanding of the underlying mechanism(s). Transgenic models overexpressing FUS may not adequately mimic the human FUS-opathies from a genetic point of view, and more sophisticated genetic approaches may be required. For example, knock-in animal models, where expression is upon the control of the endogenous FUS promoter, would therefore represent a better option to study the FUS pathology, and to determine the nature of FUS mutations.

Furthermore, given the diversity of FUS functions, the generation of animal models of FUS-opathies fully recapitulating the human pathology and phenotype remains quite challenging. Thus, in order to address **the spectrum of possible pathomechanisms in genetic and sporadic FUS-opathies (toxic gain of mutated FUS in nucleus; toxic gain of increased cytoplasmic FUS; loss of nuclear and/or cytoplasmic functions due to FUS mutations)** comparative analysis of distinct model systems are necessary.

III. STATE OF ART - AIMS OF THE THESIS

Although several lines of evidence indicate that cytoplasmic mislocalization of FUS, is a key event in disease pathogenesis, definitive *in vivo* evidence is lacking. The respective contributions of gain *vs.* loss of function, as well as the cell types in which the critical pathogenic events occur are still undefined.

More generally, the links between FUS dysregulation and pathophysiological processes leading to neurodegeneration in ALS/FTD are poorly understood.

We hypothesize that there are at least three ways in which aberrant subcellular distribution of FUS could impact on neurons leading to disease:

1) Loss of function. The loss of FUS DNA/RNA processing properties may prevent the production of some “RNA X” or “Protein Y” that is required for proper regulation of neuronal function and survival. This could be a possible mechanism not only for nuclear but also for cytoplasmic function

2) Gain of function. In addition to its RNA-binding domains, FUS also contains glycine-rich protein-protein interactiondomains. Their presence in the cytoplasm could lead to “RNA X” dysregulation or/and misfolding of “Protein Y” via direct interaction at the protein level or through indirect biochemical pathways involving these proteins.This could be a possible mechanism not only for cytoplasmic but also for nuclear gain of function.

3) A combination of **gain and loss of function** resulting from the mislocalization.

We postulated that FUS related diseases develop cell autonomously through a two-step pathogenic pathway. First, in vulnerable neurons, loss of nuclear import of FUS and cytoplasmic mislocalization leads to toxic functions, potentially involving aggregation, upon the action of modifierssuch asaging. Second, this culminates in neuronal death and the subsequent development of symptoms (**Figure 21**). If these pathogenic events appear in the LMN and UMN motor neurons, motor neuron disease resembling ALS will develop while, if the events occur in the neurons of frontal cortex, the resulting disease will be FTLD.

Figure 21. Working hypotesis

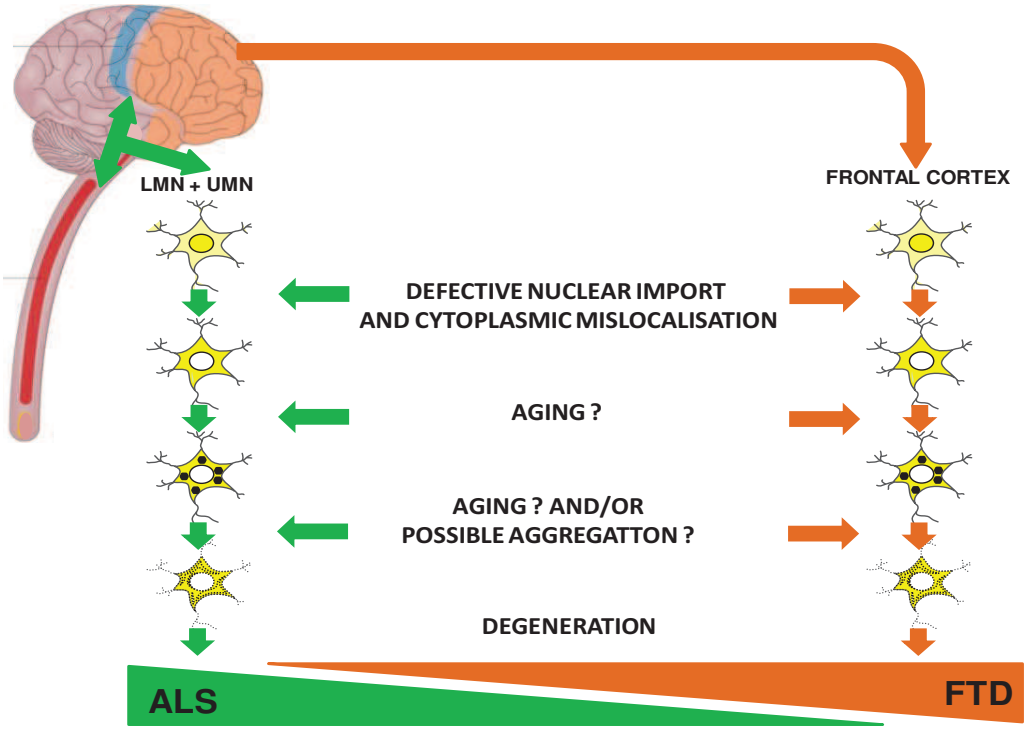

Schematically represented working hypothesis that FUS diseases originate from a cell-autonomous defect in nuclear import. This defect, upon the action of modifyers, like ageing, will lead to neuronal death. In this model, loss of nuclear import of FUS in LMN and UMN motor neurons, will cause ALS, while when same defect occure in the neurons of frontal cortex, the disease will mostly be FTLD.

If this working model stands true, then the following assumptions should also stand true:

- Cytoplasmic mislocalization of FUS in motor neurons should be both necessary and sufficient to drive motor neuron loss.
- Cytoplasmic mislocalization of FUS in frontal cortex should be both necessary and sufficient to drive neuronal loss and cortical atrophy
- Aging should precipitate ALS and/or FTLD upon cytoplasmic FUS mislocalization, even partially

The goal of my PhD work was to test experimentally these assumptions.

Based on the previous working model, we derived four questions to be addressed:

1) Does complete cytoplasmic mislocalization of FUS recapitulate ALS and/or FTLD in mice?

2) Is complete cytoplasmic mislocalization of FUS in selected neuronal types *necessary* to trigger the disease?

3) Does partial cytoplasmic mislocalization of FUS recapitulate ALS and/or FTLD in mice?

4) Is partial cytoplasmic mislocalization of FUS in selected neuronal types *necessary* to trigger the disease?

The answers to these questions relied on the generation and characterization of relevant animal models to overcome the drawbacks detected in the currently existing animal models. In particular we generateda conditional knock-in mouse model to overcome well-known problems regarding transgenic models.

RESULTS

I. PUBLICATION Nº1

(Manuscript submitted)

A. Summary –publication Nº1

To investigate the in vivo consequences of altered FUS localization, we generated a conditional mouse model FusΔNLS, with targeted ablation of the whole PY-NLS, encoded by the last exon (exon 15) of the Fus gene, as occurs in ALS-associated truncating mutations of FUS. Complete deletion of NLS led toeither complete (homozygous) or partial (heterozygous) cytoplasmic mislocalization depending on the number of mutant alleles (**Figure 22**). These mice have been be extensively characterized for neurodegeneration related phenotypes as well as for consequences of FUS subcellular redistribution.

Figure 22. New knock-in mouse model- FusΔNLS

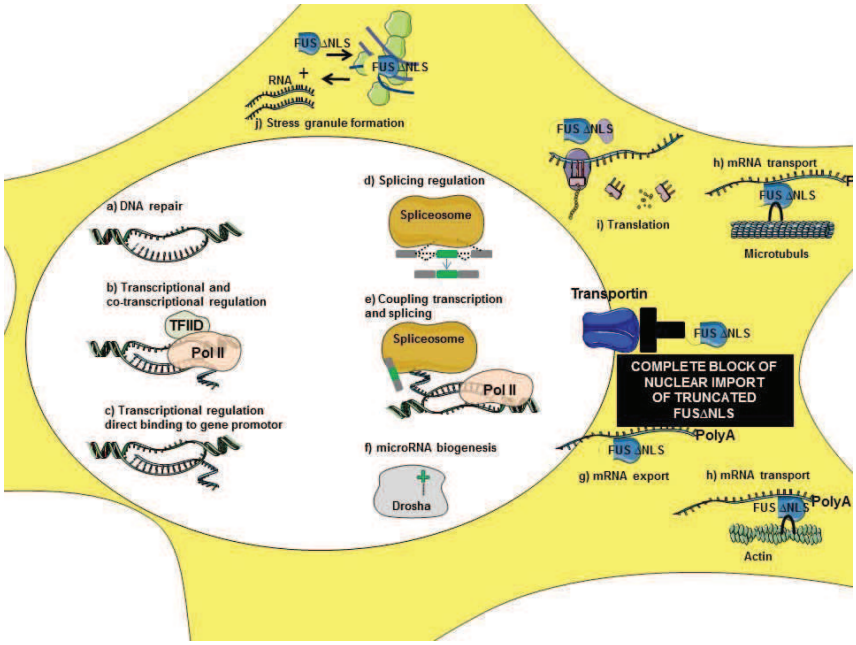

Schematically represented subcellular localization of truncated FUS in our novel knock-in mouse modelFusΔNLS inhomozygous animalsFus$^{\Delta NLS/\Delta NLS}$.Yellow color representstruncated FUS subcellular localization which is entirely mislocalized to cytoplasm upon complete block of nuclear import by TRANSPORTIN, due to NLS deletion.

In addition, we performed parallel and comparative analysis of phenotype characteristics and pathological changes in between our FUS knock-in model and a new FUS knockout mouse model. These mice were generated by our collaborator Erik Storkebaum (Munster, Germany). As this new model is a represent of loss of FUS function we were able to decipher the respective contributions of FUS gain vs. loss of function (**Figure 23**).

Moreover, here, we determined if genomewide RNA processing alterations associated with FUS truncation reflected loss or toxic gain of the FUS protein function. To this purpose we

used a combination of approaches linked to high-throughput sequencing. Expression and splicing changes were determined by RNA-seq and RASL-seq, respectively, in both Fus models. RNA profiles were defined by using two complementary methods linked to high-throughputsequencing for unbiased identification of RNA expression and splicing changes: strand-specificRNA-seq (284) and RNA-directed oligo Annealing, Selection, and Ligation or RASL-seq (285).

Figure 23. Comparative analysis of distinct models

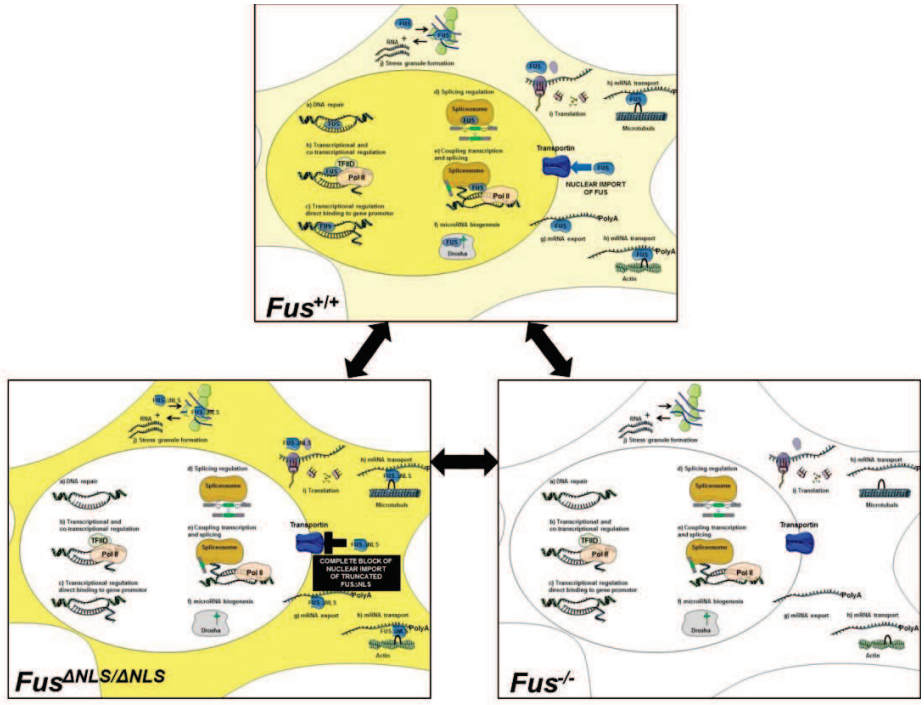

Schematically represented subcellular localization of FUS in wild type animals $Fus^{+/+}$, in two other models we introduced here homozygous ΔNLS$Fus^{\Delta NLS/\Delta NLS}$and homozygous knockout animals $Fus^{-/-}$. Yellow color represents FUS subcellular localization which is normally distributed in $Fus^{+/+}$,entirely mislocalized to cytoplasm in $Fus^{\Delta NLS/\Delta NLS}$and completely absent $Fus^{-/-}$.

More importantly, our genetic strategy allows us to restore the expression of the full-length protein, in a cell-, tissue- or region- specific manner upon crossing with chosen CRE-expressing mouse lines.

Since one of our aims was to determine whether selected neuronal types were amajor site of toxicity for FUS truncation, we took advantage of the conditionality of our FusΔNLS model, to restore wild type FUS expression in the spinal motor neurons and check whether this genetic manipulation rescues the phenotype. To do this, we cross-bred FusΔNLS mice with mice expressing the CRE recombinase from the ChATlocus, active in cholinergic neurons among which are the spinal motor neurons.

The cross-breeding was achieved through a two step breeding strategy (**Figure 24**).

Figure 24. Cross-breeding strategy

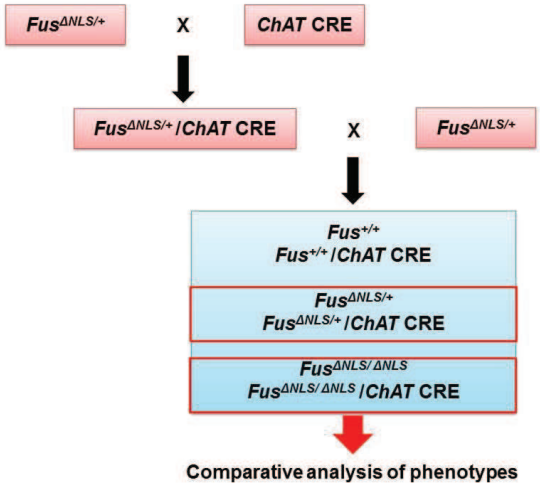

Schematically represented cross–breeding strategy. We crossed heterozygous FusΔNLSmice with ChAT CRE mice to obtain heterozygous $Fus^{\Delta NLS/+}$/ChAT-CRE mice. The resulting F1 generation was intercrossed to generate F2 homozygous $Fus^{\Delta NLS/\Delta NLS}$/ChAT-CRE mice.

In the litters of these F2 generations, we will checked for phenotypical and pathological phenotypes between mice with or without ChAT transgene (**Figure 25**).

Figure 25. Comparative analysis of FusΔNLS mice with or without ChAT transgene

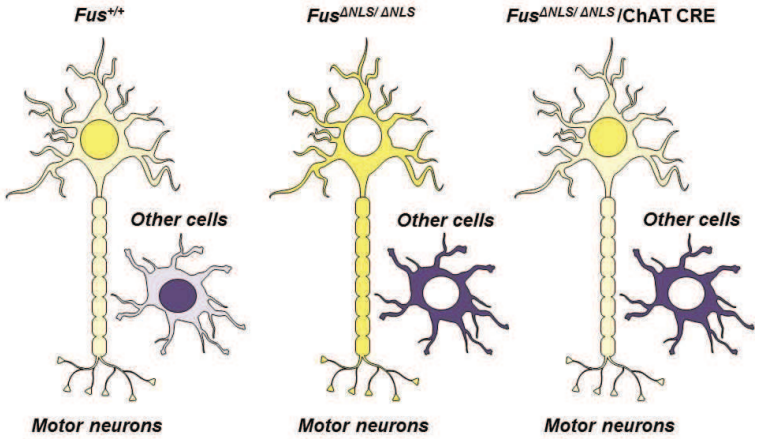

Schematically represented FUS subcellular localization inneuronal cell expressing ChAT and all other cell.Yellow color represents FUS subcellular localization in neuronal cells and violet in all other cells. FUS is normally distributed in $Fus^{+/+}$, entirely mislocalized to cytoplasm in $Fus^{\Delta NLS/\Delta NLS}$in both cell types. Whereas in $Fus^{\Delta NLS/\Delta NLS}$/ChAT-CRE normal nuclear FUS localization is restored in neuronal but not in other cells.

Toxic gain of function from mutant FUS protein is crucial to trigger cell autonomous motor neuron loss

Jelena Scekic-Zahirovic[1,2], Oliver Sendscheid[3,4], Hajer El Oussini[1,2], Mélanie Jambeau[5,6], Sun Ying[5,6], Sina Mersmann[3,4], Marina Wagner[3,4], Stéphane Dieterlé[1,2], Jérome Sinniger[1,2], Sylvie Dirrig-Grosch[1,2], Kevin Drenner[5,6], Marie-Christine Birling[7], Jinsong Qiu[8], Yu Zhou[8], Hairi Li[8], Xiang-Dong Fu[8], Caroline Rouaux[1,2], Tatyana Shelkovnikova[9], Anke Witting[10], Albert C. Ludolph[10], Friedemann Kiefer[11], Erik Storkebaum[3,4#], Clotilde Lagier-Tourenne[5,6#] & Luc Dupuis[1,2#]

1- INSERM U1118, Faculté de médecine, 11 rue Humann, 67085 Strasbourg, France
2- Université de Strasbourg UMR_S1118, Strasbourg, France
3- Molecular Neurogenetics Laboratory, Max Planck Institute for Molecular Biomedicine, Muenster, Germany
4- Faculty of Medicine, University of Muenster, Muenster, Germany
5- Department of Neurosciences, University of California, San Diego, La Jolla CA 92093 USA
6- Ludwig Institute for Cancer Research, University of California, San Diego, La Jolla CA 92093 USA
7- Institut Clinique de la souris, Illkirch-Graffenstaden, France
8- Department of Cellular and Molecular Medicine, University of California, San Diego, La Jolla CA 92093 USA
9- University of Cardiff, UK
10- Department of Neurology, Ulm, Germany
11- Mammalian Cell Signaling Laboratory, Department of Vascular Cell Biology, Max Planck Institute for Molecular Biomedicine, Münster, Germany

corresponding authors
Luc DUPUIS: ldupuis@unistra.fr; Clotilde LAGIER-TOURENNE: clagiertouren@ucsd.edu; Erik STORKEBAUM: erik.storkebaum@mpi-muenster.mpg.de

Abstract

FUS is an RNA-binding protein involved in amyotrophic lateral sclerosis (ALS) and frontotemporal dementia (FTD). Cytoplasmic FUS-containing aggregates are often associated with concomitant loss of nuclear FUS. Whether loss of nuclear FUS function, gain of a cytoplasmic function, or a combination of both lead to neurodegeneration remains elusive. To address this question, we generated knock-in mice expressing mislocalized cytoplasmic FUS and complete FUS knock-out mice. Both mouse models display similar perinatal lethality with respiratory insufficiency, reduced body weight and length, and largely similar alterations in gene expression and mRNA splicing patterns, indicating that mislocalized FUS results in loss of its normal function. However, FUS knock-in mice, but not FUS knock-out mice, display reduced motor neuron numbers at birth, associated with enhanced motor neuron apoptosis, which can be rescued by cell-specific CRE-mediated expression of wild-type FUS within motor neurons. Together, our findings indicate that cytoplasmic FUS mislocalization not only leads to nuclear loss of function, but also triggers motor neuron death through a toxic gain of function within motor neurons.

Introduction

Mutations in several aggregation-prone RNA binding proteins (RBPs) are increasingly linked to various neurodegenerative diseases. Such mutations constitute a major cause of amyotrophic lateral sclerosis (ALS), the most frequent adult-onset motor neuron disease, with mutations in TDP-43 (Gitcho et al, 2008; Kabashi et al, 2008; Sreedharan et al, 2008) and FUS (Kwiatkowski et al, 2009; Vance et al, 2009) accounting each for about 5% of familial ALS cases. Even in absence of mutations, abnormal cytoplasmic inclusions of TDP-43 represent a pathological hallmark of sporadic ALS, non-SOD1 familial ALS and frontotemporal dementia (FTD) (Neumann et al, 2009; Neumann et al, 2006), a neurodegenerative condition characterized by behavioral and language deficits. Similarly, compromised FUS nuclear localization and cytoplasmic FUS aggregates are found in ALS patients carrying *FUS* mutations, as well as in a subset of FTD patients without TDP-43 pathology (Mackenzie et al, 2010). Consistent with a central role of RNA processing misregulation in ALS and FTD pathogenesis, mutations in several other RBPs were recently identified, in particular TAF15 and EWSR1, two proteins from the same family as FUS (Couthouis et al, 2012; Couthouis et al, 2011), and other less closely related RBPs such as ataxin 2 (Elden et al, 2010), hnRNPA2B1 (Kim et al, 2013), hnRNPA1 (Kim et al, 2013) and matrin-3 (Johnson et al, 2014).

Disease-associated mutations in RBPs typically disrupt the normal nuclear localization of mutant proteins, with concomitant sequestration of the endogenous wild-type protein into cytoplasmic aggregates (Neumann et al, 2006; Vance et al, 2013). Mutations are either located in highly unstructured prion-like protein domains, resulting in a higher propensity to aggregate (Kim et al, 2013), or in the vicinity of the nuclear localization signal (NLS), impairing nuclear import of the protein. For instance, the NLS of FUS is an atypical PY-NLS (Dormann et al, 2010) located at the C-terminus of the protein that represents a mutational hot-spot in ALS patients. Along with missense mutations, several truncating or frameshift mutations deleting the FUS NLS have been identified in ALS patients (**Supplementary Fig. 1**), and are often associated with juvenile onset and rapid disease progression (Baumer et al, 2010; Calvo et al, 2014; Deng et al, 2014; Waibel et al, 2010; Waibel et al, 2013; Zou et al, 2013). In most instances *FUS*

mutations are dominantly inherited, however it is noteworthy that a recessive inheritance pattern is occasionally observed in ALS patients (Bertolin et al, 2014; Kwiatkowski et al, 2009).

FUS and TDP-43 normally shuttle between the nucleus and cytoplasm, and defective nuclear import may lead to both loss of their nuclear functions and dysregulation of their cytoplasmic roles. In the nucleus, FUS and TDP-43 are involved in regulation of pre-mRNA splicing, transcription, and microRNA biogenesis, all processes that may be affected by their depletion from the nucleus (Ling et al, 2013; Morlando et al, 2012). Consistently, reductions of TDP-43 or FUS were associated with altered expression and splicing of several hundreds of genes (Ishigaki et al, 2012; Lagier-Tourenne et al, 2012; Polymenidou et al, 2011; Rogelj et al, 2012; Tollervey et al, 2011), and both proteins are critically involved in the processing of long pre-mRNAs (Lagier-Tourenne et al, 2012; Ling et al, 2013; Polymenidou et al, 2011). Cytosolic functions of FUS and TDP-43 include transport (Alami et al, 2014) and/or storage (Han et al, 2012) of mRNA in the cytoplasm with a crucial role in the formation of stress granules (Li et al, 2013).

Although several lines of evidence indicate that cytoplasmic mislocalization of RBPs is a key event in disease pathogenesis, definitive *in vivo* evidence is lacking and the relative contributions of loss and gain of function still need to be established. Indeed, it remains unknown whether loss of nuclear function of mutant RBPs is sufficient to trigger motor neuron disease, or whether a cytosolic gain of function is also involved. There have been two major hurdles in answering these questions. First, ALS-associated RBPs are crucial for cell physiology, and overexpression of wild type proteins causes widespread phenotypes (Huang et al, 2011; Mitchell et al, 2013; Sephton et al, 2014). This represents a major drawback when attempting to discern the pathophysiological effects of disease-causing mutations in overexpression models. Second, potent auto-regulatory mechanisms control cellular levels of RBPs. For instance, both TDP-43 (Ayala et al, 2011; D'Alton et al, 2015; Polymenidou et al, 2011) and FUS (Dini Modigliani et al, 2014; Lagier-Tourenne et al, 2012; Zhou et al, 2013) control their own levels by binding to their mRNAs. As a consequence, the levels of endogenous TDP-43 or FUS proteins are strikingly reduced in animal models overexpressing wild type or mutant TDP-43 and FUS (Arnold et al, 2013;

Huang et al, 2011; Mitchell et al, 2013; Sephton et al, 2014; Wegorzewska et al, 2009).

Here, we use homologous recombination techniques to circumvent issues inherent to overexpression animal models. We systematically compare the pathological and molecular features of two novel mouse models either expressing a truncated FUS protein that lacks the NLS and localizes within the cytoplasm (knock-in mice) or harboring a genomic mutation associated with complete absence of FUS protein (knock-out mice). Both mice expressing mutant cytoplasmic FUS and mice completely devoid of FUS died at birth of respiratory insufficiency. Using genomic approaches, we determined that FUS knock-in mice display expression and splicing alterations consistent with loss of FUS nuclear function. However, mice expressing truncated cytoplasmic FUS, but not FUS knock-out mice, exhibit perinatal motor neuron loss, which can be rescued by motor neuron-restricted reversal of the mutant FUS gene to wild-type FUS. This finding demonstrates that cytoplasmic FUS leads to loss of nuclear FUS function, yet exerts a toxic gain of function within the cytoplasm of motor neurons necessary to trigger neuronal death.

Results

Cytoplasmic mislocalization of mutant FUS in *Fus*$^{\Delta NLS/\Delta NLS}$ mice

With the aim to investigate *in vivo* consequences of altered FUS localization, we generated a mouse model with targeted deletion of the PY-NLS, encoded by the last exon of the *Fus* gene (exon 15). This mutation closely mimics ALS-causing truncating mutations of *FUS* (**Supplementary Fig. 1**). We opted for a strategy that would not only result in ablation of exon 15, but also allow for CRE-mediated reversal to the wild type locus. Due to the small size of intron 14, we engineered the *Fus* locus to include, in intron 12, a floxed cDNA encoding exons 13 and 14 of *Fus*, followed by 3 transcription stop cassettes and a poly-adenylation signal (**Figure 1A**). Germline transmission of the recombinant allele was obtained (**Figure 1B**) and mice heterozygous and homozygous for the targeted allele will hereafter be referred to as *Fus*$^{\Delta NLS/+}$ and *Fus*$^{\Delta NLS/\Delta NLS}$, respectively. Homozygous *Fus*$^{\Delta NLS/\Delta NLS}$ mice die shortly after birth, and tissues dissected at birth (P0) were analyzed for expression and localization of FUS$^{\Delta NLS}$ mRNA and protein. The ΔNLS mRNA could be detected by RT-PCR in tissues of *Fus*$^{\Delta NLS/+}$ and *Fus*$^{\Delta NLS/\Delta NLS}$ mice (**Figure 1C and Supplementary Fig. 2A**). FUS protein was detected by immunoblotting in *Fus*$^{\Delta NLS/+}$ and *Fus*$^{\Delta NLS/\Delta NLS}$ brain, spinal cord and muscle protein extracts using antibodies targeting the internal or N-terminal parts of FUS (**Figure 1D** and **Supplementary Fig. 2B**). Contrastingly, no signal was detected in *Fus*$^{\Delta NLS/\Delta NLS}$ protein extracts when using two different antibodies that recognize the C-terminal NLS of FUS (**Figure 1D** and **Supplementary Fig. 2B**), demonstrating that the engineered *Fus* gene leads to the generation of a FUS protein devoid of NLS. As expected, FUS protein localized to the nucleus in cultured mouse embryonic fibroblasts (MEF) of *Fus*$^{+/+}$ mice. In striking contrast, FUS redistributed from the nuclear compartment to the cytoplasm in *Fus*$^{\Delta NLS/\Delta NLS}$ MEFs (**Supplementary Fig. 2C**) and was detected in both the nucleus and the cytoplasm of *Fus*$^{\Delta NLS/+}$ MEFs (**Supplementary Fig. 2C**). Consistently, in *Fus*$^{\Delta NLS/\Delta NLS}$ newborn mice, immunostaining revealed that mutant FUS is localized to the cytoplasm of spinal motor neurons, contrasting with the normal nuclear localization in *Fus*$^{+/+}$ motor neurons (**Figure 1E).** In *Fus*$^{\Delta NLS/+}$ mice, FUS is detected in both the nucleus and the cytoplasm of motor neurons (**Figure 1E**).

Thus, the *Fus*$^{\Delta NLS}$ allele effectively leads to the expression of a truncated FUS protein that lacks the NLS and localizes predominantly to the cytoplasm.

Cytoplasmic mislocalization of FUS and complete loss of FUS both result in perinatal lethality

Fus$^{\Delta NLS/\Delta NLS}$ mice were born alive, but died within minutes after birth, while *Fus*$^{\Delta NLS/+}$ mice survived the perinatal period. The body length and weight of *Fus*$^{\Delta NLS/\Delta NLS}$ pups was slightly but significantly reduced as compared to *Fus*$^{+/+}$ and *Fus*$^{\Delta NLS/+}$ newborn mice (**Supplementary Fig. 3A-C).** The cause of death appeared to be respiratory insufficiency, as *Fus*$^{\Delta NLS/\Delta NLS}$ animals showed poor respiratory movements and cyanosis, and H&E staining of sections through the lung revealed uninflated lungs with complete alveolar atelectasis (**Supplementary Fig. 3D**).

Cytoplasmic FUS mislocalization could have detrimental effects either through toxicity resulting from increased cytoplasmic FUS levels or through loss of its normal nuclear function. To distinguish between these possibilities, we investigated whether complete loss of FUS recapitulates the perinatal lethality phenotype of *Fus*$^{\Delta NLS/\Delta NLS}$ mice. Mice with a gene trap insertion in exons 8 or 12 of the *Fus* gene have been described previously (Hicks et al, 2000; Kuroda et al, 2000), yet both of these *Fus* gene trap lines express low amounts of truncated FUS protein, thus precluding their use to discriminate between loss *versus* gain of function mechanisms. To tackle this issue, we generated a novel *Fus* knock-out model (hereafter referred to as *Fus* $^{-/-}$) that was systematically compared to *Fus*$^{\Delta NLS/\Delta NLS}$ mice in the same C57Bl6 background. In this new *Fus* knock-out allele, a trap cassette was inserted in intron 1 to completely disrupt transcription of the endogenous *Fus* gene (**Figure 2A**). Southern blot and direct sequencing confirmed the position and orientation of the gene trap insertion, and excluded additional insertion events elsewhere in the genome (not shown). FUS protein was undetectable in the central nervous system of *Fus*$^{-/-}$ newborn mice by western blot using antibodies raised against the N-terminal and C-terminal parts of the protein (**Figure 2B-C**) and *Fus* mRNA could not be detected by quantitative real-time PCR (**Figure 2D)**. Consistently, immunostaining for FUS on spinal cord sections of E18.5 *Fus*$^{-/-}$ mice did not detect FUS protein (**Figure 2E**). These data confirm that *Fus*$^{-/-}$ mice are FUS protein null. Depending on the genetic

background, previously described *Fus* gene trap mice were reported either to be adult viable, to die before the age of weaning or within 16 hours after birth (Hicks et al, 2000; Kino et al, 2015; Kuroda et al, 2000). In contrast, $Fus^{-/-}$ mice died within 30 minutes after birth due to respiratory insufficiency. Similar to $Fus^{\Delta NLS/\Delta NLS}$ pups, the body weight and body length of $Fus^{-/-}$ newborn mice was significantly reduced as compared to litermate controls **(Supplementary Figure 3E-F).** Thus, both complete loss of FUS or its cytoplasmic mislocalization trigger a similar perinatal phenotype in C57Bl6 mice.

Substantial overlap of RNA expression changes induced by cytoplasmic FUS mislocalization and complete loss of FUS

The phenotypic similarity of $Fus^{\Delta NLS/\Delta NLS}$ and $Fus^{-/-}$ newborn mice suggests that FUS cytoplasmic mislocalization leads to loss of FUS nuclear function. FUS has been involved in the regulation of gene expression and alternative splicing of its mRNA targets (Ishigaki et al, 2012; Lagier-Tourenne et al, 2012; Polymenidou et al, 2011; Rogelj et al, 2012; Tollervey et al, 2011). In addition, FUS interacts with several proteins, including U1-snRNP (Sun et al, 2015; Yamazaki et al, 2012), SMN (Groen et al, 2013; Tsuiji et al, 2013; Yamazaki et al, 2012), HDAC1 (Wang et al, 2013), Drosha (Morlando et al, 2012), RNA polymerase II (Schwartz et al, 2012) or PRMT1 (Tibshirani et al, 2014), known to have profound effects on splicing and gene expression. Hence, the expression of a truncated cytoplasmic form of FUS may primarily lead to loss of nuclear FUS function and defective regulation of direct FUS RNA targets. In addition, cytoplasmic accumulation of FUS may also alter the function and/or subcellular localization of FUS-interacting proteins, and result in additional gene expression and splicing alterations. To discriminate between gain- and loss-of-function changes, we systematically compared RNA profiles in brains from $Fus^{\Delta NLS/\Delta NLS}$ and $Fus^{-/-}$ mice. First, we used strand-specific, genome wide sequencing of RNAs (Parkhomchuk et al, 2009) (RNA-seq) to evaluate RNA expression levels in brains of $Fus^{\Delta NLS/\Delta NLS}$ and $Fus^{-/-}$ mice. Total RNA was extracted from E18.5 embryonic brains of $Fus^{\Delta NLS/\Delta NLS}$ mice (N=5) and wild-type littermates (N=4), as well as homozygous $Fus^{-/-}$ (N=5) and their control $Fus^{+/+}$ littermates (N=5). Expression levels for each annotated protein-coding gene were determined by the number of mapped

fragments per kilobase of exon, per million mapped reads (FPKM) (Mortazavi et al, 2008; Trapnell et al, 2012). The FPKM ratio of the *Fus* gene confirmed that *Fus* was expressed in $Fus^{\Delta NLS/\Delta NLS}$ mice, but not in $Fus^{-/-}$ mice (**Supplementary Fig. 4A**). Inspection of the reads mapped on the *Fus* gene demonstrated the absence of reads throughout all exons for the $Fus^{-/-}$ mice while only exon 15 was not integrated in *Fus* transcripts of $Fus^{\Delta NLS/\Delta NLS}$ mice (**Figure 3A**). Unsupervised hierarchical clustering with all genes reliably discriminated mutant genotypes from their controls (**Supplementary Fig. 4B-C**), indicating that both *Fus* mutation and *Fus* deletion displayed RNA expression profiles divergent from wild-type. Statistical comparison of FPKM values identified 237 genes upregulated and 549 genes downregulated (**Supplementary Table 1**) in $Fus^{\Delta NLS/\Delta NLS}$ mice (as defined by $P<0.05$ adjusted for multiple testing) (**Figure 3B**). Of note, only 9 genes and 56 genes were upregulated and downregulated more than 1.5 fold, respectively (**Supplementary Table 1**). Identical analysis in $Fus^{-/-}$ mice identified 669 upregulated genes (29 genes more than 1.5 fold) and 889 downregulated genes (72 genes more than 1.5 fold) (**Supplementary Table 2 and Figure 3C**). Comparison of both models identified 353 genes that were altered in the same direction, consistent with loss of FUS nuclear function underlying the altered levels of these transcripts (**Figure 3D** and **Supplementary Table 3**).

Downregulation of selected genes in both mouse models was confirmed by qRT-PCR (**Supplementary Fig. 5A**), yielding data similar to the RNA-seq results (**Figure 3E**). Out of these, several genes have been previously involved in neurological diseases such as the *Abelson helper integration site 1* (*Ahi1*) gene mutated in the neurodevelopmental Joubert syndrome (Ferland et al, 2004), the *Dystrophia myotonica protein kinase* (*Dmpk*) gene implicated in myotonic dystrophy type 1, the *low* and *medium* molecular weight *neurofilamen*t subunits (*Nefl* and *Nefm*) (Bergeron et al, 1994)and the gene encoding tubulin alpha 4A (*Tuba4a*) that was recently implicated in ALS (Smith et al, 2014). Similarly, selected upregulated genes were confirmed by qRT-PCR (**Figure 3E** and **Supplementary Fig. 5A**), including *Taf15,* a FUS family member also mutant in ALS (Couthouis et al, 2011). Increased levels of *Taf15* in $Fus^{\Delta NLS/\Delta NLS}$ and $Fus^{-/-}$ mice is consistent with the presence of FUS binding sites on the *Taf15* transcript (Lagier-Tourenne et al, 2012) and may illustrate a mechanism of compensation induced by loss

of FUS nuclear function. Overall, a substantial overlap in RNA expression changes was found in *Fus*$^{\Delta NLS/\Delta NLS}$ and *Fus*$^{-/-}$ brains consistent with loss of FUS nuclear function in knock-in mice.

Cytoplasmic mislocalization of FUS leads to unique RNA expression changes

A number of the genes identified by RNA-seq as uniquely regulated in *Fus*$^{\Delta NLS/\Delta NLS}$ mice displayed similar trends in both mouse models when evaluated by qRT-PCR (**Supplementary Fig. 5B-C**), suggesting that the set of genes commonly regulated by truncation and loss of FUS was underestimated. However, a subset of transcripts were altered uniquely in *Fus*$^{\Delta NLS/\Delta NLS}$ animals **(Figure 3F** and **Supplementary Fig. 5D**),, including the *Vitronectin* (*Vtn)* gene, the *small nuclear ribonucleoprotein polypeptides B and B1* (*Snrpb)* gene*,* the *Trove2* gene encoding for the 60 kDa SS-A/Ro ribonucleoprotein and the *U2AF homology motif kinase 1 (Uhmk1)* gene encoding for the Kinase interacting with Stathmin (KIS) protein that was implicated in schizophrenia and the regulation of splicing (Manceau et al, 2008) and local translation in neuritic projections (Cambray et al, 2009; Pedraza et al, 2014). Interestingly, *Fus*$^{\Delta NLS/\Delta NLS}$ animals displayed increased mRNA levels of *Ephb3*, a member of Eph/Ephrin signalling pathways crucial in synaptogenesis and previously involved in Alzheimer's disease (Sheffler-Collins & Dalva, 2012), while *EphA4,* another member of Eph/ephrin system has been recently involved in ALS (Van Hoecke et al, 2012) **(Figure 3F** and **Supplementary Fig. 5D**). Thus, *Fus*$^{\Delta NLS/\Delta NLS}$ expression profiles largely recapitulated expression profiles of *Fus*$^{-/-}$ brains, yet a subset of genes was found specifically associated with the expression of cytoplasmic truncated FUS in *Fus*$^{\Delta NLS/\Delta NLS}$ brains.

Gene ontology analysis showed that transcripts whose expression was upregulated in *Fus*$^{\Delta NLS/\Delta NLS}$ animals were enriched for genes involved in mRNA translation and extracellular matrix constituents (**Supplementary Table 4**). In contrast, transcripts upregulated in *Fus*$^{-/-}$ brains revealed an enrichment for nuclear and nucleolar proteins involved in the regulation of transcription, DNA replication or regulation of RNA metabolic processes (**Supplementary Table 5**). Gene ontology analysis revealed a similar enrichment for synaptic activity and function among transcripts downregulated in *Fus*$^{\Delta NLS/\Delta NLS}$ and *Fus*$^{-/-}$ animals (**Supplementary Tables 4 and 5**). Altogether, these data suggest that cytoplasmic

mislocalization of FUS alters expression of genes involved in synaptogenesis, as a direct consequence of FUS loss of function. Contrastingly, gain of function elicited by cytoplasmic FUS might be more related with alterations in genes related with mRNA translation, especially in neurites, and extracellular matrix.

Widespread splicing alterations induced by cytoplasmic mislocalization and loss of FUS

To further compare the molecular changes elicited by cytoplasmic FUS mislocalization and FUS loss of function, we asked whether regulation of mRNA splicing was commonly affected in E18.5 brains of $Fus^{\Delta NLS/\Delta NLS}$ mice and $Fus^{-/-}$ mice. To characterize mRNA splicing, we exploited the RNA-mediated oligonucleotide Annealing, Selection, and Ligation with Next-Generation sequencing (RASL-seq) method (Li et al, 2012; Zhou et al, 2012). This approach allowed us to quantitatively profile 3859 unique alternative splicing events that correspond to exon inclusion or skipping events conserved between mouse and human (**Supplementary Fig. 6A**). After filtering, ratios of shorter to longer isoform counts were calculated and used to statistically compare the splicing changes between different groups. Unsupervised hierarchical clustering for all splicing events showed that both mutant *Fus* genotypes clustered apart from their controls (**Supplementary Fig. 6B-C**). Thus, both *Fus* deletion and expression of truncated FUS led to splicing profiles distinct from controls. In $Fus^{\Delta NLS/\Delta NLS}$ brains, 9.3% (173 events) of the 1852 detected splicing events were different from controls, with 101 increased long splicing isoforms and 72 enhanced short isoforms (defined by t-test with $p<0.05$ and average fold change >1.5) (**Figure 4A** and **Supplementary Table 6**). In $Fus^{-/-}$ brains, 17.9% (252 events) of the 1406 detected splicing events were different from control littermates, with 118 increased long isoforms and 134 enhanced short isoforms (**Figure 4B** and **Supplementary Table 7**).

Comparison of the splicing changes between $Fus^{\Delta NLS/\Delta NLS}$ and $Fus^{-/-}$ mice revealed a striking overlap between both models. Seventy-five splicing events were commonly regulated in $Fus^{\Delta NLS/\Delta NLS}$ and $Fus^{-/-}$ mice, 100% of which were differentially included or excluded in the same direction (**Supplementary Fig. 6D-E** and **Supplementary Table 8**).

Semi-quantitative RT-PCR of selected RNAs confirmed these FUS-dependent splicing changes

(**Figure 4C** and **Supplementary Fig. 6F**), including transcripts previously implicated in neurodegenerative diseases such as the N-myc downstream-regulated gene 2 (*Ndrg2*) that is misaccumulated in Alzheimer's disease (Mitchelmore et al, 2004), the microtubule-associated protein tau (*Mapt*) gene mutated in frontotemporal dementia (Hutton et al, 1998), the ataxin 2 (*Atxn2*) gene mutated in ALS (Elden et al, 2010) and spinocerebellar ataxia type 2 (SCA2) (Imbert et al, 1996) and the pro-neurotrophin receptor sortilin 1 (*Sort1*) (Hu et al, 2010). Interestingly, inclusion of sortilin 1 exon 17b (also referred as exon 18 in (Polymenidou et al, 2011)) was previously associated with low levels of TDP-43 (Polymenidou et al, 2011; Prudencio et al, 2012) and found significantly increased in cortex of FTD patients with TDP-43 proteinopathy (Prudencio et al, 2012). Here, we observe that *Fus* mutation and deletion have an opposite effect on sortilin 1 as compared to TDP-43 on sortilin 1 exon17b, with decreased inclusion of exon 17b in embryonic brains from both $Fus^{\Delta NLS/\Delta NLS}$ and $Fus^{-/-}$ mice (**Figure 4C** and **Supplementary Fig. 6F**).

Despite expected developmental differences in the alternative splicing patterns of embryonic and adult brains, 57 splicing events found misregulated by RASL-seq in $Fus^{\Delta NLS/\Delta NLS}$ and $Fus^{-/-}$ mice were also identified by Affymetrix microarrays in striatum from adult wild-type mice with acute depletion of *Fus* by antisense oligonucleotide treatment (Lagier-Tourenne et al, 2012), or in embryonic brains from another *Fus* knock-out model that expresses low levels of truncated FUS protein (Hicks et al, 2000; Lagier-Tourenne et al, 2012). Among FUS-dependent alterations, abnormal splicing of *Mapt* exon 10 (**Figure 4C** and **Supplementary Fig. 6F**) is of particular relevance for disease pathogenesis as mutations enhancing exon 10 inclusion are linked to frontotemporal dementia (Liu & Gong, 2008). While in embryonic mouse brains the predominant mRNA isoforms of *Mapt* do not include exon 10 and encode for tau protein with three microtubule binding repeats (3R-tau) (Dillman et al, 2013; McMillan et al, 2008), we observed increased inclusion of exon 10 encoding for the 4-repeat tau isoform (4R tau) in both $Fus^{\Delta NLS/\Delta NLS}$ and $Fus^{-/-}$ mice. In all, splicing alterations caused by cytoplasmic FUS mislocalization are largely overlapping with those elicited by complete loss of FUS. Nevertheless, a subset of events were uniquely found in $Fus^{\Delta NLS/\Delta NLS}$ **(Supplementary Fig. 6D),** which may be the consequence of functional

disruption of other RNA binding proteins by abnormal accumulation of FUS in the cytoplasm.

Cytoplasmic mislocalization of FUS leads to increased perinatal motor neuron apoptosis

We next asked whether perinatal death of $Fus^{\Delta NLS/\Delta NLS}$ and $Fus^{-/-}$ mice was accompanied by loss of motor neurons in the lumbar spinal cord. Immunostaining for choline acetyltransferase (ChAT), which specifically labels large motor neurons in the spinal cord ventral horn, revealed that the number of motor neurons was reduced by approximately 30% in $Fus^{\Delta NLS/\Delta NLS}$ mice as compared with both $Fus^{+/+}$ and $Fus^{\Delta NLS/+}$ mice (**Figure 5A-B**). To exclude the possibility that this reduced number of ChAT-positive motor neurons reflects downregulation of ChAT expression rather than loss of motor neurons, we also performed Nissl staining, a histochemical stain independent of marker gene expression. Quantification of neurons with an area of $\geq 80\mu m^2$ revealed a 50% reduction of the number of large motor neurons in the ventral horn of $Fus^{\Delta NLS/\Delta NLS}$ newborn mice (**Figure 5C**). Interestingly, $Fus^{\Delta NLS/+}$ mice displayed a smaller but statistically significant loss of large Nissl stained cells, suggesting that motor neurons were also affected in these mice despite showing normal numbers of ChAT positive cells. In striking contrast with the situation in $Fus^{\Delta NLS/\Delta NLS}$ mice, spinal motor neuron counts were similar between $Fus^{-/-}$ mice and their wild type littermates (**Figure 5A, D**), demonstrating that the mutant FUS protein expressed in $Fus^{\Delta NLS/\Delta NLS}$ mice is toxic to motor neurons during development.

At birth, mouse motor neurons are still in the developmental period, and motor neurons that did not efficiently create synaptic contacts with muscles undergo apoptosis until P10 (Kanning et al, 2010). We hypothesized that the reduced number of motor neurons in the lumbar spinal cord of $Fus^{\Delta NLS/\Delta NLS}$ mice could be due to increased perinatal motor neuron apoptosis. Consistently, the number of apoptotic cells detected by terminal deoxynucleotidyl transferase dUTP nick end labeling (TUNEL) was significantly increased in lumbar spinal cord sections of $Fus^{\Delta NLS/\Delta NLS}$ newborn mice (**Figure 6A-B**). Furthermore, double-immunostaining for ChAT and active caspase 3, labeling motor neurons actively undergoing apoptosis, revealed that motor neuron apoptosis was twice more frequent in $Fus^{\Delta NLS/\Delta NLS}$ than in wild type littermates (**Figure 6C-E**). Together, these data indicate that cytoplasmic mislocalization of FUS leads to

reduced numbers of lower motor neurons, at least in part attributable to increased motor neuron death. The absence of motor neuron loss in *Fus*$^{-/-}$ mice indicates that cytoplasmic FUS accumulation leads to motor neuron death through a toxic gain of function mechanism.

Cytoplasmic mislocalization of FUS is not sufficient to induce stress granules or alterations in RBPs

In autopsy material of ALS-FUS patients, FUS-containing cytoplasmic aggregates are found in neurons and glial cells. These aggregates are usually also immunopositive for p62 and for ubiquitin (Baumer et al, 2010; Huang et al, 2010; Kobayashi et al, 2010; Tateishi et al, 2010; Vance et al, 2009). Despite motor neuron loss in *Fus*$^{\Delta NLS/\Delta NLS}$ mice, we did not observe any FUS-positive, p62-positive, ubiquitin-positive or neurofilament-positive aggregates in motor neurons of newborn *Fus*$^{\Delta NLS/\Delta NLS}$ mice (**Supplementary Fig. 7**). Furthermore, as FUS is recruited to stress granules, and since neuropathology revealed that cytoplasmic protein aggregates in ALS-FUS patients stain positive for stress granule markers (Baumer et al, 2010; Dormann et al, 2010; Liu-Yesucevitz et al, 2010), we evaluated the distribution of stress granule markers in the spinal cord ventral horn in *Fus*$^{\Delta NLS/\Delta NLS}$ mice. This analysis revealed that markers for stress granules such as phosphorylated eIF2α or TIAR1 displayed a similar pattern in *Fus*$^{\Delta NLS/\Delta NLS}$ and control mice (**Supplementary Fig. 8**). Finally, we asked whether cytoplasmic mislocalization of FUS in *Fus*$^{\Delta NLS/\Delta NLS}$ mice would affect the subcellular localization of other RBPs. In the ventral horn of the spinal cord, nuclear immunoreactivities of other RBPs, such as TDP43 and TAF15 were unaltered in *Fus*$^{\Delta NLS/\Delta NLS}$ mice (**Supplementary Fig. 9**). Taken together, newborn *Fus*$^{\Delta NLS/\Delta NLS}$ mice displayed cytoplasmic mislocalization of FUS that was accompanied by motor neuron death without detectable protein aggregation, stress granule formation or altered subcellular localization of other RBPs.

Cytoplasmic FUS mislocalization is intrinsically toxic to motor neurons

We subsequently asked whether FUS mislocalization within motor neurons is necessary to induce motor neuron loss in *Fus*$^{\Delta NLS/\Delta NLS}$ mice or whether restricted expression of wild type FUS in motor neurons could rescue their survival despite accumulation of the mutant protein in neighboring cells. We

therefore exploited the presence of loxP sites flanking the STOP cassette (**Figure 1A**) to selectively revert the ΔNLS allele to wild type in motor neurons. For this purpose, *Fus*$^{\Delta NLS/+}$ mice were crossed to mice expressing the CRE recombinase from the *ChAT* locus, which leads to CRE recombinase activity in virtually all cholinergic neurons (Rossi et al, 2011; Saxena et al, 2013). We expected that *Fus*$^{\Delta NLS/\Delta NLS}$/ChAT-CRE mice would express truncated FUS protein ubiquitously, except for cholinergic neurons. Double-immunostaining for FUS and ChAT on spinal cord sections of *Fus*$^{\Delta NLS/\Delta NLS}$/*ChAT*-CRE newborn mice revealed that FUS nuclear localization was indeed restored in cholinergic neurons in the ventral spinal cord, but not in other neighboring cells, consistent with motor neuron selective CRE expression (**Figure 7A**). FUS nuclear localization was either completely restored or partially corrected with a mixed cytoplasmic/nuclear FUS localization (**Figure 7A),** consistent with CRE having successfully at least one of *Fus*$^{\Delta NLS}$ allele to wild type. Neonatal lethality of *Fus*$^{\Delta NLS/\Delta NLS}$ mice was not rescued by the *ChAT*-CRE allele, indicating that expression of mutant FUS in motor neurons is not the main contributor of neonatal lethality in homozygous mice. Last, we evaluated whether restoration of FUS nuclear localization in motor neurons would prevent motor neuron loss in *Fus*$^{\Delta NLS/\Delta NLS}$ mice. This approach revealed that the presence of a *ChAT*-CRE allele was indeed sufficient to fully rescue motor neuron loss (**Figure 7B-D**), as well as restore a normal number of caspase 3-positive motor neurons (**Figure 7E**). These findings establish that cytoplasmic FUS mislocalization within motor neurons is required to induce their loss in *Fus*$^{\Delta NLS/\Delta NLS}$ mice.

Discussion

FUS and other related RBPs form cytoplasmic inclusions associated with nuclear clearance in affected cells from ALS and FTD patients. An outstanding question is whether disease is caused by gain of cytoplasmic toxicity or by loss of the nuclear function of the respective RBP. To gain insight into this conundrum, we targeted the FUS locus to generate two novel mouse models. In the first model, the last exon of *Fus* is no longer transcribed, resulting in the production of a truncated FUS protein that lacks the NLS and localizes almost exclusively to the cytoplasm (**Figure 1**). The second model results in complete loss of FUS expression (**Figure 2**). A thorough comparison of these two models allowed us to distinguish phenotypes induced by loss of FUS function from phenotypes contributed by gain of a toxic cytoplasmic function.

Interestingly, this approach revealed that $Fus^{\Delta NLS/\Delta NLS}$ and $Fus^{-/-}$ mice share several features: both mouse models die shortly after birth due to respiratory insufficiency and exhibit reduced body weight and size. Transcriptomic analysis also revealed overlapping alterations in RNA levels and splicing. However, a reduced number of spinal motor neurons associated with increased perinatal motor neuron apoptosis and a subset of expression and splicing changes were uniquely found in $Fus^{\Delta NLS/\Delta NLS}$ mice (**Figures 3, 4, 5 and 6**). Thus, FUS mislocalization to the cytoplasm with reduced levels of nuclear FUS is associated with phenotypes linked to loss of FUS function, but also with motor neuron death induced by a gain of toxicity mechanism that is not recapitulated in the knock-out mouse model (**Figure 5**). The notion that loss of FUS function may not be sufficient to induce motor neuron degeneration is also supported by two recent reports. First, in an outbred genetic background, homozygous *Fus* gene trap mice reached 2 years of age without manifesting ALS-like phenotypes or motor neuron loss (Kino et al, 2015). Second, selective inactivation of the FUS homolog *cabeza* in neurons of adult *Drosophila* did not affect motor performance or life span, indicating that *cabeza* is not required for maintenance of neuronal function in adults (Frickenhaus et al, 2015). Here, we demonstrate that loss of FUS function is not sufficient and that gain of function by cytoplasmic redistribution of FUS is necessary to elicit motor neuron apoptosis. Notably, RNA-seq and RASL-seq experiments showed that the ΔNLS mutation triggered a partial loss of FUS

function in splicing and gene expression regulation. Loss of function, although not sufficient, may be necessary in *Fus*$^{\Delta NLS/\Delta NLS}$ mice to induce motor neuron death. Indeed, a number of genes involved in synaptogenesis and/or in neurodegenerative diseases show altered expression (*Ahi1, Dmpk, Nefl, Nefm, Tuba4a, Taf15)* or splicing (*Ndrg2, Mapt, Atxn2, Sort1*) in *Fus*$^{\Delta NLS/\Delta NLS}$ and *Fus*$^{-/-}$ mice (**Figure 3** and **Figure 4**), and these alterations linked to loss of FUS nuclear function may weaken the motor neuron and sensitize it to the toxic effects of cytoplasmic FUS accumulation.

Importantly, we showed that motor neuron death in *Fus*$^{\Delta NLS/\Delta NLS}$ mice could be prevented by selectively restoring FUS nuclear import in motor neurons (**Figure 7**), demonstrating that FUS cytoplasmic mislocalization within motor neurons is required to induce motor neuron loss. The observation that cytoplasmic mislocalization of FUS is intrinsically toxic to motor neurons contrasts with the non-cell-autonomous contribution to motor neuron degeneration demonstrated for *SOD1* mutations (Boillee et al, 2006). Indeed, abrogation of mutant SOD1 expression in motor neurons delayed, but did not prevent, motor neuron degeneration, and a contribution of neighboring cells to SOD1 mediated toxicity is well established (Ilieva et al, 2009). Moreover, our data support a degenerative rather than developmental origin of motor neuron loss in newborn *Fus*$^{\Delta NLS/\Delta NLS}$ mice. Indeed, the reduced number of motor neurons could have a developmental origin, either by impaired proliferation of motor neuron progenitors or secondary to defects in acquisition of motor neuron fate. However, this scenario is unlikely since motor neuron loss in *Fus*$^{\Delta NLS/\Delta NLS}$ mice can be prevented by ChAT-CRE induced reversal of the *Fus*$^{\Delta NLS}$ locus to wild type (**Figure 7**). Indeed, expression of the ChAT gene, which encodes choline acetyl transferase, an enzyme essential for the biosynthesis of acetylcholine, is detectable only in postmitotic motor neurons, thus after exit from the cell cycle and acquisition of motor neuron fate (Alaynick et al, 2011; Cho et al, 2014). Therefore, the pathogenic events driving motor neuron loss in *Fus*$^{\Delta NLS/\Delta NLS}$ mice occur after motor neuron specification. An attractive hypothesis is that excessive motor neuron apoptosis in *Fus*$^{\Delta NLS/\Delta NLS}$ mice happens during the so-called 'natural cell death period'. During development, motor neurons are generated in excess and approximately 40% of the initially generated motor neurons are progressively removed. This process ensures the generation of the appropriate number of motor neurons

and guarantees the elimination of aberrant cells. According to the 'neurotrophin hypothesis', developing motor neurons compete for limited amounts of neurotrophic factors produced by the muscle targets. Only motor axons that establish stable and functional neuromuscular junctions receive sufficient survival signals and are maintained (Kanning et al, 2010; Oppenheim, 1991). Importantly, we found that motor neuron loss elicited by cytoplasmic FUS mislocalization is associated with increased apoptosis of spinal motor neurons (**Figure 6**). Several motor neuron intrinsic mechanisms may underlie increased motor neuron apoptosis in *Fus*$^{\Delta NLS/\Delta NLS}$ mice and future studies are needed to investigate these possible mechanisms. For instance, expression of axon guidance receptors may be dysregulated in *Fus*$^{\Delta NLS/\Delta NLS}$ mice, leading to defects in motor axon targeting and failure to receive neurotrophic support. Alternatively, *Fus*$^{\Delta NLS/\Delta NLS}$ motor axons may reach their targets, but reduced expression of receptors for muscle-derived neurotrophic factors may render a fraction of motor neurons insensitive to survival signals.

Previous work suggested various potential toxic mechanisms for cytoplasmic FUS, and our study sheds light on several of these candidate pathways. First, cytoplasmic FUS could generate toxic FUS aggregates in the cytosol, as shown in yeast models of FUSopathies (Ju et al, 2011; Sun et al, 2011). Here, we detected neither FUS-positive nor ubiquitin- or p62-positive aggregates expected to occur in case of strong ubiquitin proteasome system (UPS) or autophagy impairment. Thus, at least in this model and at this perinatal age, FUS aggregation or robust FUS-mediated impairment of protein clearance pathways are dispensable for toxicity towards motor neurons. Cytoplasmic FUS could also alter stress granule (SGs) dynamics through its localization to SGs upon stress and its regulatory properties towards SGs assembly (Li et al, 2013). However, in *Fus*$^{\Delta NLS/\Delta NLS}$ mice, we observed neither altered eIF2α phosphorylation, nor formation of SGs in spinal cord motor neurons, suggesting that major impairment of SGs biology is not required for FUS toxicity *in vivo* in this model. Further studies will be necessary to re-evaluate the presence of FUS-containing cytoplasmic aggregates, stress granule alterations or pathology involving other RBPs in aged heterozygous *Fus*$^{\Delta NLS/+}$ mice and *Fus*$^{+/-}$ mice. Finally, impaired FUS nuclear import could affect nuclear function in a manner distinct from pure loss of function. Indeed, FUS is a binding partner of multiple proteins, including SMN (Tsuiji et al, 2013; Yamazaki et al, 2012),

HDAC1 (Wang et al, 2013), Drosha (Morlando et al, 2012), RNA polymerase II (Schwartz et al, 2012), and PRMT1 (Tibshirani et al, 2014), known to have profound effects on splicing and gene expression. The cytoplasmic retention of one, or several, of these proteins by cytoplasmic FUS could lead to differences in splicing or gene expression. Genomewide RNA analysis showed that splicing and gene expression in $Fus^{\Delta NLS/\Delta NLS}$ mice resembled that of $Fus^{-/-}$ mice, consistent with loss of nuclear FUS function, yet this similarity was only partial. Gene ontology analysis pointed to alterations in mRNA translation and extracellular matrix as potential functions uniquely altered in $Fus^{\Delta NLS/\Delta NLS}$ mice, an interesting example being upregulation of KIS, a kinase involved in dendritic mRNA translation. Importantly, FUS has been involved in local mRNA translation at cell protrusions (de Hoog et al, 2004; Yasuda et al, 2013) and SMN, a major FUS interacting partner, is also important in mRNA transport and translation (Jablonka et al, 2007; Rathod et al, 2012; Rossoll et al, 2003; Sanchez et al, 2013; Zhang et al, 2006). Our work provides additional support to the hypothesis that impairment of local mRNA translation may contribute to neuronal death in FUS-associated diseases.

An interesting observation is that both $Fus^{\Delta NLS/\Delta NLS}$ and $Fus^{-/-}$ mice die shortly after birth of respiratory insufficiency, presumably caused by loss of FUS function. A concerted action of several physiological systems is required for newborn mice to breathe normally, and defects in any of these systems can lead to neonatal lethality (Turgeon & Meloche, 2009). Firstly, the respiratory rhythm is generated in the respiratory center in the brainstem and transmitted through the spinal motor neurons to the respiratory muscles (diaphragm and intercostal muscles). Therefore, structural or functional defects of neurons in the respiratory center, motor neurons, neuromuscular junctions and/or respiratory muscles can lead to respiratory distress. Our observation that neonatal lethality of $Fus^{\Delta NLS/\Delta NLS}$ mice is not rescued by restoration of FUS nuclear import in motor neurons indicates that loss of FUS function in cell types other than motor neurons is sufficient to trigger neonatal lethality. Alternatively, we cannot exclude that the rescued motor neurons, despite being histologically normal, remain functionally abnormal, in a manner analogous to Nova double knock-out animals rescued with neuronal agrin (Ruggiu et al, 2009). Electrophysiological characterization of neuromuscular transmission could help discriminate between

these two possibilities. Apart from neuromuscular alterations, defects in lung morphogenesis or maturation, cardiovascular defects, hematological defects or skeletal defects can all result in poor blood oxygenation and the characteristic cyanosis observed in *Fus*$^{\Delta NLS/\Delta NLS}$ and *Fus*$^{-/-}$ neonates. It will be interesting to investigate these possible causes of neonatal lethality due to loss of FUS function in future studies. In particular, generation of conditional *Fus* knock-out mice would provide a valuable tool to evaluate whether selective FUS inactivation in all neurons, muscle, lung epithelium or the vasculature would result in respiratory insufficiency and neonatal death. Possibly, loss of FUS function in a combination of these tissues is necessary to induce this phenotype.

The recessive pattern of inheritance of *FUS* mutations in a few families (Bertolin et al, 2014; Kwiatkowski et al, 2009) render our studies of *Fus*$^{\Delta NLS/\Delta NLS}$ mice clinically relevant. However, the vast majority of *FUS* mutations are characterized by a dominant inheritance pattern. In this respect, it will be highly interesting to age heterozygous *Fus*$^{\Delta NLS/+}$ mice and *Fus*$^{+/-}$ mice and characterize their phenotype. Indeed, some mechanisms apparently not at play in homozygous *Fus*$^{\Delta NLS/\Delta NLS}$ mice, such as FUS-containing cytoplasmic aggregates, stress granule alterations or pathology involving other RBPs, will have to be re-evaluated in these mice. The very severe phenotype of *Fus*$^{\Delta NLS/\Delta NLS}$ mice resembles spinal muscular atrophy, which is caused by mutations in the *SMN1* gene, whose product SMN interacts directly with FUS and is an integral component of the spliceosome (Gerbino et al, 2013; Groen et al, 2013; Sun et al, 2015; Tsuiji et al, 2013; Yamazaki et al, 2012; Yu et al, 2015). This is further reinforced by the strong splicing defects observed in *Fus*$^{\Delta NLS/\Delta NLS}$ mice and is consistent with juvenile onset in many *FUS*-ALS patients with C-terminal truncation mutations. These similarities strengthen the links between ALS and SMA, and suggest that SMA, ALS and FTD could constitute extremes of the same disease continuum.

In conclusion, this study provides *in vivo* genetic evidence that cytoplasmic mislocalization of FUS triggers apoptotic motor neuron degeneration and demonstrates a crucial role for a gain of toxic function in this process. Motor neuron loss occurs at least partially through a cell autonomous gain of function mechanism, since complete loss of FUS is not associated with motor neuron death, and rescue of nuclear FUS within motor neurons prevents neuronal death.

Materials and Methods:

Generation of conditional knock-in *Fus* $^{\Delta NLS/\Delta NLS}$ and *Fus* $^{-/-}$ mice

Knock-in *Fus* mice with the conditional ablation of exon 15 were generated in the Institut Clinique de la Souris (ICS, Illkirch, Strasbourg) using standard procedures. The *Fus* locus was engineered to include, in between the exons 12 and 13 of the gene, an inserted floxed cDNA encoding exons 13 and 14 of *FUS*, followed by 3 STOP cassettes. We obtained germline transmission of the recombinant allele. Homozygous *Fus* $^{\Delta NLS/\Delta NLS}$ mice were generated by intercrossing *Fus* $^{\Delta NLS/+}$ animals.

For generation of *Fus* $^{-/-}$ mice, the mouse ES cell clone EUCE0131_G08 was obtained from the European Conditional Mouse Mutagenesis Consortium (EUCOMM)(Friedel et al, 2007). Southern blotting and sequencing of PCR-amplified genomic sequences confirmed a single gene trap insertion event in the first intron of *Fus*. Blastocyst injection of ES cells resulted in chimeric mice, which allowed for germline transmission of the mutant *Fus* allele. As the ES cells were generated in a 129P2 background, the resulting offspring was backcrossed at least five times to C57Bl6 mice. The genetic background of all mice used in this study is C57Bl6.

Animal breeding and genotyping

Fus $^{\Delta NLS}$ and *ChAT-CRE* mice were housed in the animal facility of the Faculty of medicine from Strasbourg University, with 12/12 hours of light/dark cycle. The animals had unrestricted access to standard diet and water. *Fus* $^{+/+}$, *Fus* $^{\Delta NLS/+}$ and *Fus* $^{\Delta NLS/\Delta NLS}$ mice were produced by interbreeding *Fus* $^{\Delta NLS/+}$ mice, and littermates were systematically used as controls. *Fus* $^{\Delta NLS/\Delta NLS}$/ChAT-CRE mice were generated by a two-step breeding strategy. First, heterozygous *Fus* $^{\Delta NLS/+}$ mice were crossed with ChAT-CRE mice. *Fus* $^{\Delta NLS/\Delta NLS}$/ChAT-CRE were then crossed with heterozygous *Fus* $^{\Delta NLS/+}$ mice and these F2 litters were used in experiments. *Fus* $^{\Delta NLS}$ mice were genotyped by PCR on tail DNA using following primers: GAT TTG AAG TGG GTA GAT AGA TAG TGC AGG and CCT TTC CAC ACT TTA GGT TAG TCA CAG. *ChAT-CRE* mice were genotyped by PCR on tail DNA using following primers: CCA TCT GCC

ACC AGC CAG and TCG CCA TCT TCC AGC AGG.

Fus$^{-/-}$, *Fus*$^{+/-}$ and *Fus*$^{+/+}$ mice were generated by crossing *Fus*$^{+/-}$ mice and PCR genotyped using a combination of three primers: (i) a common forward primer (CTC TCC TGG CCC GGT CAC) which anneals upstream of the gene trap insertion, (ii) a reverse primer (GCC AGA GGA GCG CGT GC) which anneals downstream of the gene trap insertion and gives rise to a 150 bp band for wild type *Fus*, but no band for the gene trap allele under the cycling conditions used, and (iii) a reverse primer (CTG GAC TAC TGC GCC CTA C) which anneals in the gene trap and gives rise to a 715 bp band when the gene trap allele is present.

All experiments were approved by the local ethical committees of Strasbourg and Muenster universities.

Western blot

For western blotting, tissue powder (brain, spinal cord and gastrocnemius muscle) was homogenized in lysis buffer (250 mM Sucrose solution, 1 mM EDTA, 2% SDT, 1 mM DTT, 10 mM Tris HCl pH 7.4) containing protease inhibitor (Sigma P8340) and phosphatase inhibitor cocktail (Sigma 8345) and centrifuged at 12000 x rpm for 15 minutes at room temperature. Protein concentration was measured using BCA Protein Assay. Equal amounts of protein (20µg) were separated by SDS-PAGE 10% and blotted onto a nitrocellulose membrane. Membranes were saturated with 10% non-fat milk and then incubated with the primary antibodies against the N-terminal part of FUS (Proteintech^{TM}, 18592-1-AP; 1:1000 and Bethyl A303-839A; 1:1000) diluted in 3% non-fat milk , and antibodies against the C-terminal part of FUS (Bethyl A300-294A; 1:10000 and Bethyl A300-302A; 1:10000), followed by anti-rabbit (P.A.R.I.S.; BI2413) or anti-goat (Sigma A5420) secondary antibody diluted 1:5000. Of note, the Bethyl antibody A300-302A is reported by the company as raised against the N-terminal part of the protein, but evidence supports that this antibody recognizes the C-terminal NLS of FUS.. Antibodies against Histone 3 (Cell signaling, #9715; 1:1000) was used as loading control. All blots were analyzed with chemiluminescence (ECL; Luminata Forte Kit, Millipore WBLUF0500) using the Molecular Imager Chemidoc XRS (Biorad) as detection system.

Immunodetection of FUS in mouse embryonic fibroblasts and motor neurons

Localization of FUS protein was analyzed in spinal cord motor neurons on cryosections prepared as described below and double stained for FUS (Proteintech™; 11570-1-AP; 1:100), and ChAT (Millipore, AB144-P; 1:50) or for FUS (Proteintech™; 11570-1-AP; 1:100 and NeuN (Millipore, ABN78; 1:100).

Fus immunoreactivity was visualized with a confocal microscope (LSM 510; Carl Zeiss, Thornwood, NY), within mouse embryonic fibroblasts (MEF) double stained with antibodies against the internal or N-terminal part of FUS (Proteintech™, 11570-1-AP; 1:100 and Bethyl A303-839A; 1:100) and Draq5 (Cell Signaling, 4084; 1:1000) followed by fluorescent secondary antibodies donkey anti-rabbit Alexa 488 (Jackson, A21206) and donkey anti-goat Alexa 594 (Molecular Probes, A11058) diluted 1:500. This experiment was repeated three times; data shown are from one representative experiment.

Quantification of spinal cord motor neurons

Spinal cords were removed and immersed in fixative for 2 h at 4°C. Samples were transferred overnight into 30% sucrose in 0.1 M phosphate buffer (PB) at 4°C for cryoprotection, embedded in medium (Tissue-Tek® O.C.T.Compound, SAKURA#4583) and cut with a cryostat (Leica CM 3050S). P0 spinal cords were cut in serial 25 μm-thick sections and mounted onto 2% gelatin-coated slides to be processed for immunostaining.

For Nissl staining slides were air-dried overnight. Sections were then hydrated through 100% and 95% alcohol to distilled water, immersed in 0.1% Cresyl violet acetate Certistain®, MERCK#5235) and cover-slipped with Roti-histokitt (Roth, 6638.1).

For immunohistochemistry (IHC), unspecific binding sites were blocked with 5% horse serum (HS), 0.5% Triton X-100 for 30 minutes at room temperature (RT), immersed in 3% hydrogen peroxide (H_2O_2) to remove the endogenous peroxidase activity, rinsed in phosphate buffered saline (PBS) and incubated with goat polyclonal anti-Choline Acetyl Transferase (ChAT) antibody (Millipore, AB144-P; diluted 1:50) overnight at RT in a humidified chamber. After rinsing in PBS, sections were incubated with

biotinylated donkey anti-goat IgG (Jackson, 705-066-147; 1:250) for 1.5 h, rinsed in PBS and then incubated with ABC kit (Vektor, PK7200; 1:4000) for 1 h. All antibodies were diluted in 0.01M PBS, 0.1% Triton X-100. Peroxidase staining was obtained by incubating the sections in 0.075% 3,3'-diaminobenzidine tetrahydrochloride (DAB; Sigma Aldrich) and 0.002% H_2O_2 in 50 mM Tris-HCl pH 7.5. Sections were dehydrated, air dried and coverslipped with Roti-histokitt (Roth, 6638.1).

Motor neurons were counted at L1–L5 on both cresyl violet and ChAT stained sections at 20X magnification (for each genotype: exact numbers of animals per group are provided in figure legends). The counting was performed per ventral horn in every tenth section for ten sections in total per animal. In Nissl-stained sections, only neurons with an area $\geq 80\ \mu m^2$ and located in a position congruent with that of motor neuron groups were counted(d'Errico et al, 2013). All $ChAT^+$ profiles located in the ventral horns of immunostained sections clearly displayed on the plane of the section were counted. Total estimated motor neuron numbers were obtained using a computer-assisted microscope (Nicon Eclipse E800) and the software (Nis Elements version 4.0). Cells were counted on the computer screen using a digital camera (Nicon Digital Sight DS-U3) mounted on a microscope. The soma size of Nissl+ motor neurons was also analyzed by measuring cross-sectional areas at 20X magnification using ImageJ software(Schneider et al, 2012).

This experiment was repeated two times for both groups of animals *Fus* $^{\Delta NLS}$ and *ChAT-CRE*; images shown are from one representative experiment.

In situ detection of apoptosis in spinal cord cells by TUNEL assay

For TUNEL staining, the spinal cord cryosections prepared as described above were treated with TUNEL reagent (Trevigen, 4812-30-K) according to the kit instructions. The tissue sections were permeabilized with Cytonnin^{TM}. All TUNEL-positive cells were counted and examined for the typical pathological feature of apoptosis under a fluorescent microscope (Nikon Eclipse E800) at a 20x magnification. The numbers in each set of sections were summed up and divided by number of the sections in a set. The mean number of TUNEL-positive cells for each genotype group was calculated.

Caspase 3 immunostaining and apoptotic events

Apoptotic bodies across the lumbar spinal cord cross-sectional area were determined by fluorescence microscopy. For detection of caspase-positive motor neurons sections were double-stained with goat-anti-ChAT (Millipore, AB144-P; diluted 1:50) and rabbit-anti-cleaved caspase-3 (R&D Systems, AF835; 1:100) and combination of secondary antibodies Alexa 594 anti-goat (Molecular Probes, A11058; 1:500) and Alexa 488 anti-rabbit (Jacson, A21206; 1:500) plus Draq5 (both 1:1000). Total number of apoptotic bodies were counted all over the cross sectional area for every tenth section for 10 sections in total per animal. Apoptotic motoneurons were counted as cells triple positive for ChAT, caspase and condensed chromatin by Draq5. Information on the total numbers of apoptotic counts and further details are presented along with the description of the results. This experiment was repeated two times for both groups of animals *Fus* $^{\Delta NLS}$ and *ChAT-CRE* mice; images shown are from one representative experiment.

Lungs histology

Lungs were harvested and fixed with 4% formaldehyde solution (Sigma 47608) for 24 h and embedded in paraffin; Sections of 6 μm were stained with hematoxylin (Vector H-3401) and eosin (Eosin Y-solution 0.5%; Roth X883.1) for light microscope observation (Nikon Eclipse E800) at a 40x magnification.

Other immunostainings

For detection of protein aggregation spinal cord sections were double immunostained with N-terminal part of FUS (Bethyl A303-839A; 1:100) and either anti-Sqstm1 (p62, Abcam 56416; 1:100) or anti-Neurofilament (Abcam 24574, clone SMI-312; 1:100) or anti-Ubiquitin (Millipore, MAB1510; 1:100) and Draq5 (Cell Signaling, 4084; 1:1000) followed by fluorescent secondary antibodies donkey anti-mouseAlexa 488 (Jackson, 715-545-150) and donkey anti-goat Alexa 594 (Molecular Probes, A11058) diluted 1:500. Peroxidase staining was performed on the spinal cord for analyzing the localization of TARDBP (Proteintech 10782-2-AP; 1:100) and TAF15 (Abcam 134916; 1:100) followed by biotinylated

donkey anti-rabbit IgG (Jackson, 711-165-152; 1:250). For stress granule markers we used following antibodies eIF2a phosphorylated at Ser51 (rabbit monoclonal, Abcam 32157 ; 1 :500), and TIAR (mouse monoclonal, BD Biosciences ; 1 :500) with DAPI (Molecular Probes D1306 ; 1 ug/ml).

Imaging

Single-layer images (except for mouse embryonic fibroblasts (MEF) were acquired using a laser-scanning microscope (confocal Leica SP5 Leica Microsystems CMS GmbH) equipped with 63×oil objective (NA1.4). Excitation rays are sequential argon laser 488nm, diode 561nm, Helium Neon laser 633nm. Emission bandwidths are 500-550nm for Alexa488, 570-620nm for Alexa594, and 650-750nm for Draq5.

Analysis of expression changes by RNA-seq

Total RNA from brains of $Fus^{\Delta NLS/\Delta NLS}$, $Fus^{-/-}$ and their control littermates were extracted with TRIzol (Invitrogen). RNA quality was measured using the Agilent Bioanalyzer system or RNA screen Tape (Agilent technologies) according to the manufacturer's recommendations, and processed using the Illumina TruSeq Stranded mRNA Sample Preparation Kit according to manufacturer's protocol. Generated cDNA libraries were sequenced using an Illumina HiSeq 2000 sequencer with 4-5 biological replicates sequenced per condition using single read, 50 cycle runs. Quality of sequencing reads was assessed using FastQC (Babraham Bioinformatics) and then aligned to a mouse reference genome (mm9, UCSC Genome Browser) using TopHat (version v2.0.10). Sequencing yielded, on average, 15 million non-redundant reads per sample with a 48.4 - 58.7% mapping rate. Cufflinks (version v2.1.1) was used to generate transcript abundance for each annotated protein-coding gene as Fragments Per Kilobase of transcript per Million mapped reads (FPKM), and statistical analysis and comparison of FPKM values was calculated using Cuffdiff (version v2.1.1). Genome-wide unsupervised clustering analysis and heat maps with significant changes between different groups were generated using R (Bioconductor).

Confirmation of expression changes by quantitative RT-PCR

RNA samples from brains of *Fus*$^{\Delta NLS/\Delta NLS}$, *Fus*$^{-/-}$ and their control littermates were treated with DnaseI (Invitrogen) and converted to cDNA using SuperScript III kit (Invitrogen) with random hexamers or the Iscript Reverse Transcriptase (Bio-Rad). qRT-PCR reactions were performed with 3-5 mice for each group and two technical replicates using the iQ SYBR green Supermix (Bio-Rad) on either the IQ5, the CFX96 Touch or the CFX384 Touch Real-Time PCR detection system (Bio-Rad). Analysis was performed using the iQ5 optical system software (Bio-Rad; version 2.1) or the CFX manager system software (Bio-Rad; version 3.1). Expression values were normalized to the control gene Rsp9, and were expressed as a percentage of the average expression of the control samples. Primer sequences were designed using Primer3 software (http://frodo.wi.mit.edu/primer3/) and are available in **Supplementary Table 9**.

Analysis of splicing alterations by RASL-seq

RNA-mediated oligonucleotide Annealing, Selection, and Ligation with Next-Generation sequencing (RASL-seq) analysis of alternative splicing changes was carried out as already described elsewhere(Li et al, 2012; Zhou et al, 2012). In brief, a pool of oligonucleotides was designed to detect 3859 alternative splicing events in mice. One hundred fmol of RASL-seq oligos were annealed to 1 μg of total RNA isolated from brains of *Fus*$^{\Delta NLS/\Delta NLS}$, *Fus*$^{-/-}$ and their control littermates. After ligation, 5 μl eluted ligated oligos was used for 16 ~ 18 cycles of PCR amplification, and the bar-coded PCR products were sequenced using an Illumina HiSeq 2000 sequencer with 24-30 samples per lanes. Sequencing data was decoded allowing no mismatch with each barcode, and target sequences were mapped with RASL-seq oligo pool sequences using the short read alignment software bowtie allowing for 1 mismatch at both the left and right side of the ligated oligos. An average of ~5 million reads from each sample was mapped, with events with less than 4 counts in one of the isoforms removed. Ratios of the counts of shorter to longer isoforms were calculated. The significantly changed events were identified by t-test and average fold change. Unsupervised clustering analysis and heat maps with significant changes between different

groups were generated using R (Bioconductor).

Confirmation of splicing changes by semi-quantitative RT-PCR

Semi-quantitative RT-PCR (25-30 cycles) was used to validate alternative splicing changes. Isoform products were separated on 10% polyacrylamide gels and stained with SYBR gold (Invitrogen) and quantified with ImageJ software to record the intensity of the bands corresponding to different splicing isoforms. Intensity ratios of long and short isoforms were averaged from three biological replicates per group. Primer sequences were designed using Primer3 software (http://frodo.wi.mit.edu/primer3/) in exons flanking the alternatively spliced exon. PCR primer sequences are shown in **Supplementary Table 9**.

Statistics

For the animal experiments, the values from each animal were averaged for each genotype group and analyzed by unpaired Student's t-test, two tailed. Comparison of three or four groups was performed using One-way ANOVA and Tukey *post-hoc* test. Data were analyzed by using the Graphics Prism Program (Graph Pad Software, San Diego, CA) and expressed as mean ± SEM (standard error of the mean) and differences were considered significant when $p \leq 0.05$.

Acknowledgements:

We thank Dr Pico Caroni for providing the ChAT-CRE knock-in mice, and helpful discussions. We thank Marlene Bartos for her help in achieving this project. We are grateful to Dr. Don W. Cleveland and the members of his group for tremendous support and fruitful discussions. This work is supported by an ALS Association Investigator Initiated Award (grants 2235 and 3209; to LD and CLT); the Frick Foundation (award 2013 to LD and CLT, award 2010 to ES); Association Française contre les Myopathies (grant #18280; to LD, CLT and ES); Target ALS (grant 13-0840; to CLT); Virtual Helmholtz Institute "RNA dysmetabolism in ALS and FTD" (WP2, to LD, AW and ACL); Association de recherche sur la SLA (ArSLA; to LD); State North Rhine Westphalia (to ES); Minna-James-Heinemann-Stiftung (to ES). JSZ received a Erasmus Mundus Neurotime fellowship to perform these studies. OS received a fellowship from the German National Academic Foundation. CLT receives salary support from the Ludwig Institute for Cancer Research.

Authors contributions:

JSZ, OS, ES, CLT and LD designed research; JSZ, OS, HEO, MJ, SM, SD, JS, SDG, KD, NM, MCB, JQ, CR, TS and ES performed research; SY, JQ, YZ, HL, XDF, AW, ACL and FK contributed reagents and data analysis; JSZ, OS, MJ, SY, KD, ES, CLT and LD analyzed data and made figures; JSZ, ES, CLT and LD wrote the manuscript.

Conflict of interest:

The authors declare no conflicts of interest.

Figure Legends:

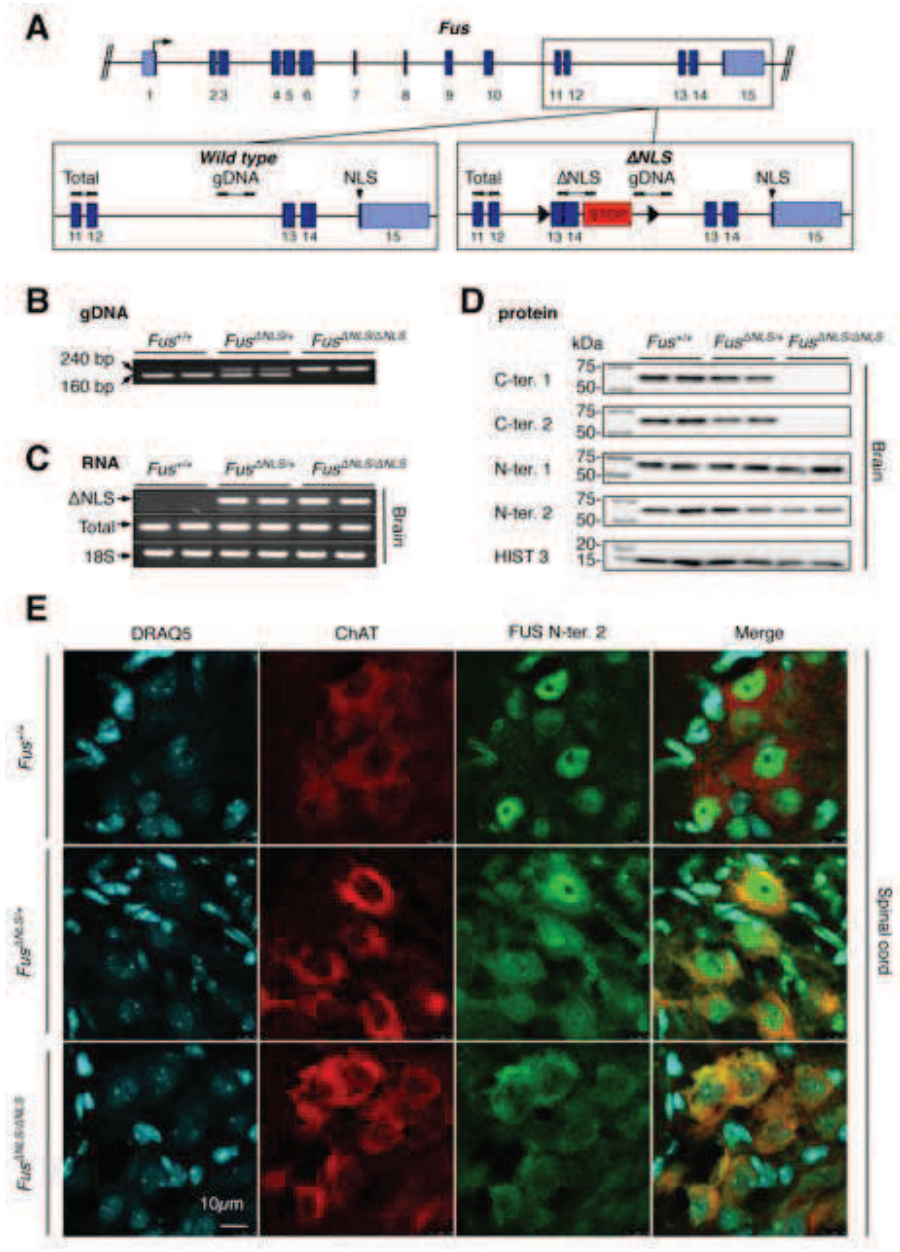

Figure 1: FUS mislocalization in *Fus*$^{\Delta NLS/\Delta NLS}$ mice.
(A) Schematic representation of the *Fus* gene locus (upper panel). Lower panels depict exons 11-15 in the wild type allele (left) and ΔNLS allele (right) with localization of PCR primers used for genotyping (gDNA, used in B) and for RT-PCR (Total and ΔNLS, used in C). Arrow: translational start site. STOP cassettes are indicated in red; loxP sites as black triangles; coding regions are in dark blue and UTRs in light blue. Location of the region encoding the nuclear localization signal (NLS) is indicated in exon 15.
(B) Representative PCR genotyping results from 2 *Fus*$^{+/+}$, 2 *Fus*$^{\Delta NLS/+}$ and 2 *Fus*$^{\Delta NLS/\Delta NLS}$ knock-in mice using primers designed around the distal loxP site of the *Fus*$^{\Delta NLS}$ allele and shown as gDNA in panel A. The expected size of the PCR product of the ΔNLS allele is 240 bp; the size of wild type allele is 160 bp.
(C) RT-PCR analysis of brain from 2 *Fus*$^{+/+}$, 2 *Fus*$^{\Delta NLS/+}$ and 2 *Fus*$^{\Delta NLS/\Delta NLS}$ knock-in P0 mice using

primers located in the STOP cassette, and thus specific to the ΔNLS mRNA (ΔNLS, upper panel), or primers located in exon 11, *i.e.* upstream of the floxed cDNA insertion, and thus amplifying total *Fus*-derived mRNA (Total, middle panel). PCR amplification of 18S rRNA is shown as standard gene (lower panel). Presence of the ΔNLS mRNA is detected in both $Fus^{\Delta NLS/+}$ and $Fus^{\Delta NLS/\Delta NLS}$ while absent in $Fus^{+/+}$ tissues.

(D) Immunoblot analysis of FUS protein in cerebral cortex of 2 $Fus^{+/+}$, 2 $Fus^{\Delta NLS/+}$ and 2 $Fus^{\Delta NLS/\Delta NLS}$ knock-in mice using a combination of two different antibodies targeting either the C-terminal (C-ter. 1 and C-ter. 2) NLS, the N-terminal part (N-ter. 1) or an internal part (N-ter. 2) of FUS. Note that immunoblots with C-terminal antibodies show a complete disappearance of immunoreactive bands in $Fus^{\Delta NLS/\Delta NLS}$ knock-in tissues confirming that FUS protein derived from the ΔNLS allele lacks NLS. Histone 3 (HIST3) was used as a loading control. Molecular weight markers are shown on the left, and apparent MW is indicated.

(E) Double immunostaining for the motor neuronal marker ChAT and the Fus N-terminal part on the ventral horn of spinal cord.

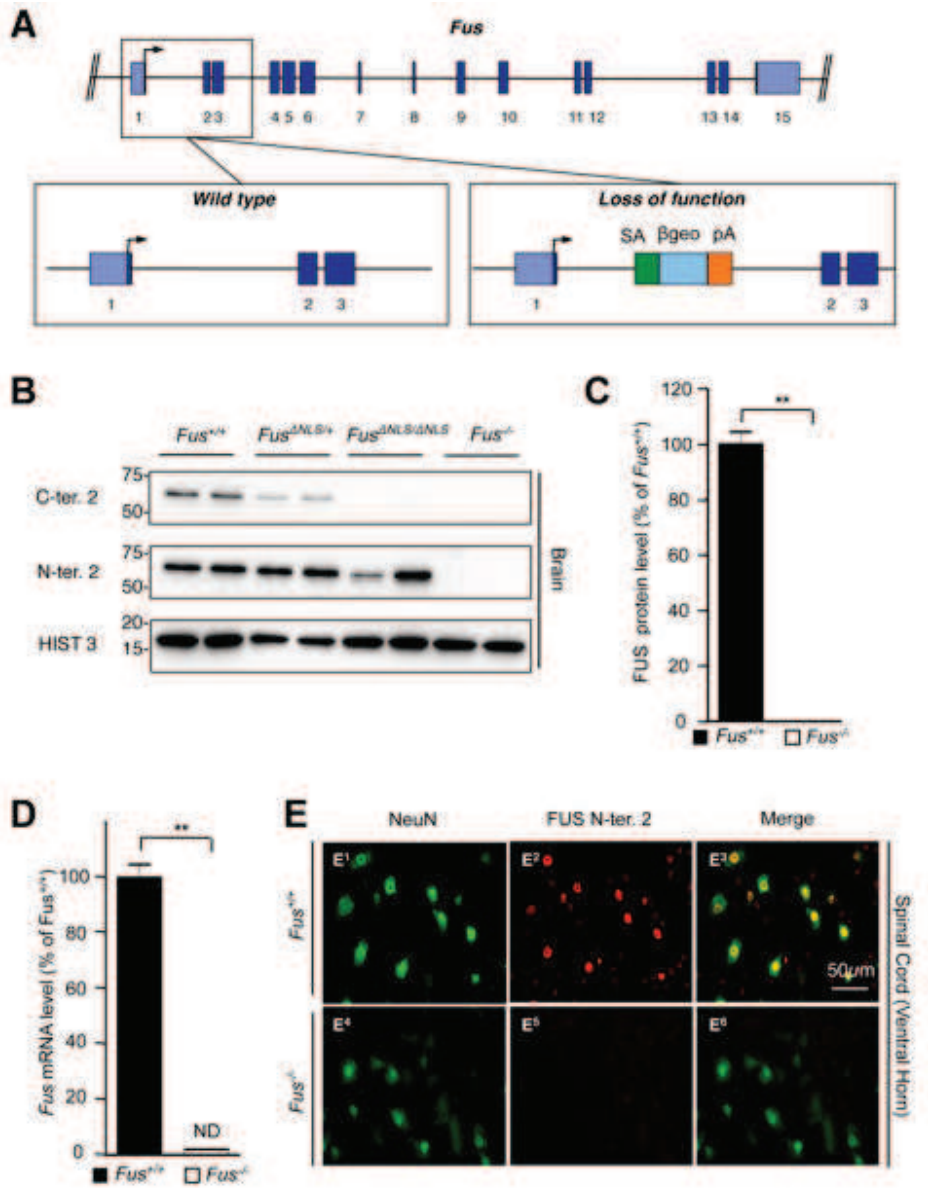

Figure 2: **Generation of a complete *Fus*$^{-/-}$ loss of function mouse model.**
(A) Schematic representation of the *Fus* gene locus (upper panel). Lower panels depict exons 1-3 in the wild type allele (left) and loss of function allele (right). Arrow: translational start site; SA: splice acceptor; βgeo: β-galactosidase/neomycin phosphotransferase fusion gene; pA: polyA.
(B) Representative immunoblot for FUS on protein extracts of E18.5 brain. Histone 3 is used as loading control.
(C) Quantification of FUS protein levels from immunoblots (c) revealed that *Fus*$^{-/-}$ mice do not express FUS protein. (**) p<0.01.
(D) Quantitative real-time PCR showing absence of *Fus* transcript in *Fus*$^{-/-}$ mice. (**) p<0.01.
(E) Immunostaining for the neuronal marker NeuN and FUS on the spinal cord ventral horn of E18.5 *Fus*$^{+/+}$ and *Fus*$^{-/-}$ mice.

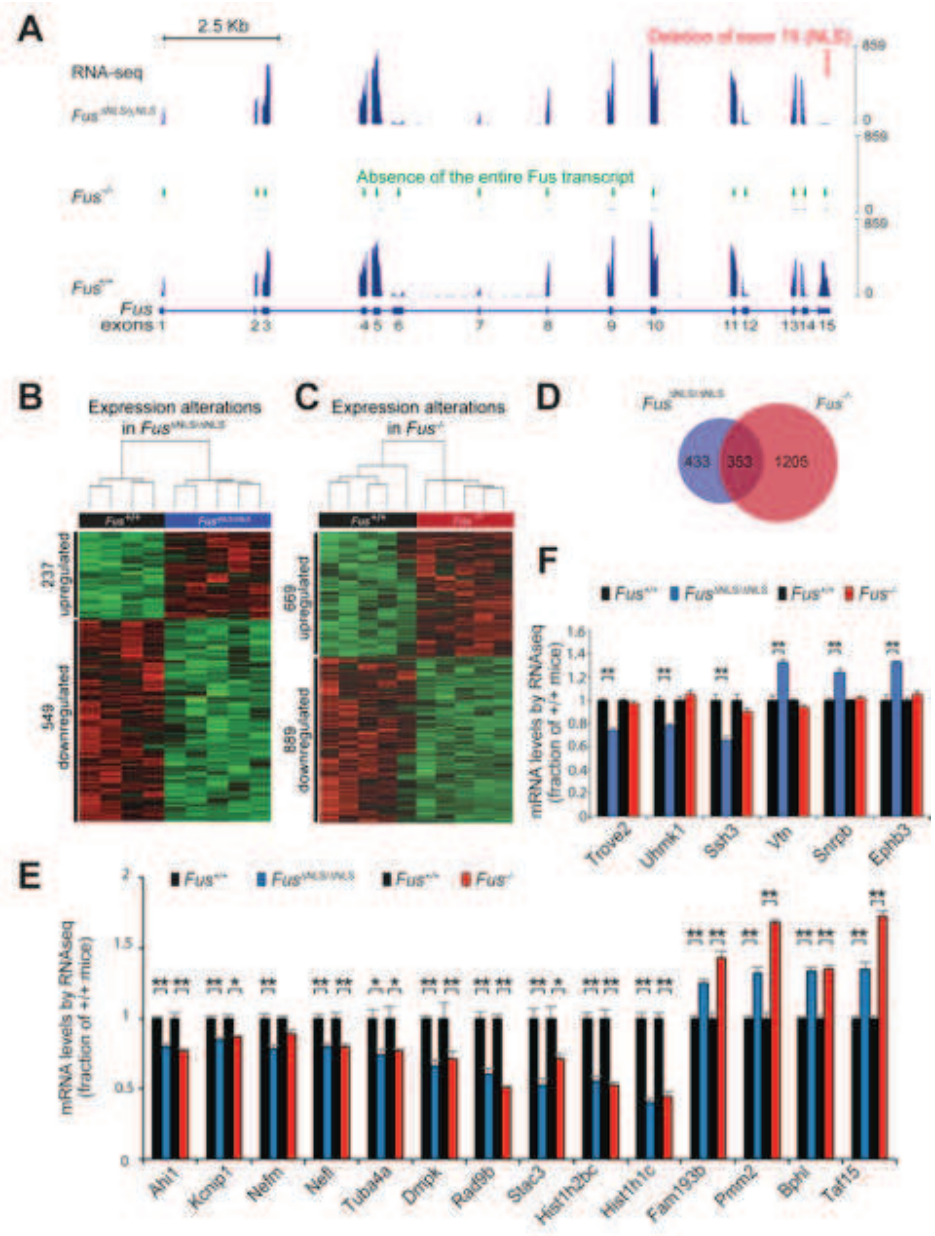

Figure 3: FUS-dependent expression changes in mouse brain

(A) RNA-seq reads from brain of homozygous knock-in (*Fus*$^{\Delta NLS/\Delta NLS}$, upper panel), homozygous knock-out (*Fus*$^{-/-}$, middle panel) and control (*Fus*$^{+/+}$, lower panel) mice showing the absence of exon 15 (red arrow) in *Fus* mRNA in *Fus*$^{\Delta NLS/\Delta NLS}$ mice while the entire *Fus* transcript is absent in *Fus*$^{-/-}$mice (green arrows).

(B) Heatmap with hierarchical clustering of RNA-seq data from biological replicates of *Fus*$^{\Delta NLS/\Delta NLS}$ (N=5) and control littermates (N=4), showing genes differentially regulated between both genotypes among which 237 are upregulated and 549 are downregulated in *Fus*$^{\Delta NLS/\Delta NLS}$ animals.

(C) Heatmap with hierarchical clustering of RNA-seq data from biological replicates of *Fus*$^{-/-}$ (N=5) and control littermates (N=5), showing genes differentially regulated between both genotypes among which 669 are upregulated and 889 are downregulated in *Fus*$^{-/-}$ animals.

(D) Venn diagram showing the number of overlapping genes misregulated in *Fus*$^{\Delta NLS/\Delta NLS}$ (blue circle) and

Fus$^{-/-}$ (red circle) brains with 353 genes similarly downregulated or upregulated upon cytoplasmic mislocalization or complete loss of FUS.
(E) Normalized expression (based on FPKM from RNA-seq) of genes identified by RNA-seq to be significantly downregulated (*Ahi1, Kcnip1, Nefm, Nefl, Tuba4a, Dmpk, Rad9b, Stac3, Hist1h2bc, Hist1h1c)* or upregulated (*Fam193b, Pmm2, Bphl, Taf15*) in both *Fus*$^{\Delta NLS/\Delta NLS}$ and *Fus*$^{-/-}$ compared to their control. RNA-seq results are consistent with expression levels measured by qRT-PCR for these genes (**Supplementary Fig. 5A**). Error bars represent SEM in 4-5 biological replicates.
(F) Normalized expression (based on FPKM from RNA-seq) of genes identified by RNA-seq to be uniquely changed in *Fus*$^{\Delta NLS/\Delta NLS}$ mice (*Trove2, Uhmk1, Ssh3, Vtn, Snrpb, Ephb3).* RNA-seq results are consistent with expression levels measured by qRT-PCR for these genes (**Supplementary Fig. 5D**). Error bars represent SEM in 4-5 biological replicates.

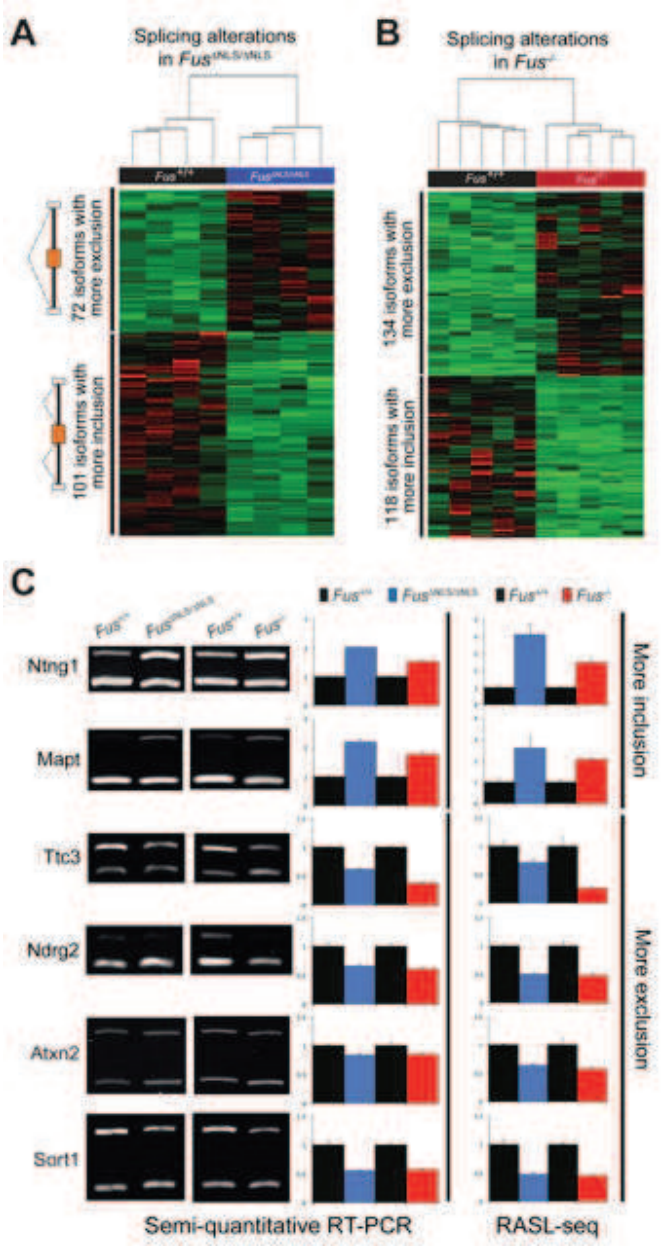

Figure 4: FUS-dependent alternative splicing alterations in mouse brain
(A) Heatmap with hierarchical clustering of RASL-seq data from biological replicates of *Fus*$^{\Delta NLS/\Delta NLS}$ (N=4) and control littermates (N=4), showing 173 alternative splicing alterations associated with expression of cytoplasmic FUS in knock-in animals. **(B)** Heatmap with hierarchical clustering of RASL-seq data from biological replicates of *Fus*$^{-/-}$ (N=5) and control littermates (N=5), showing 252 alternative splicing alterations associated with loss of FUS in knock-out animals. **(C)** Semi-quantitative RT-PCR analyses of selected targets confirmed alternative splicing changes in *Fus*$^{\Delta NLS/\Delta NLS}$ and *Fus*$^{-/-}$ compared to their respective littermate controls. Left panels show representative acrylamide gel pictures of RT-PCR products. Quantification of splicing changes from at least three biological replicates of *Fus*$^{\Delta NLS/\Delta NLS}$ (blue bars) and *Fus*$^{-/-}$ (red bars) compared to their control littermates (*Fus*$^{+/+}$, black bars) by semi-quantitative RT-PCR (middle panel) and RASL-seq (right panel) are shown. Error bars represent SEM.

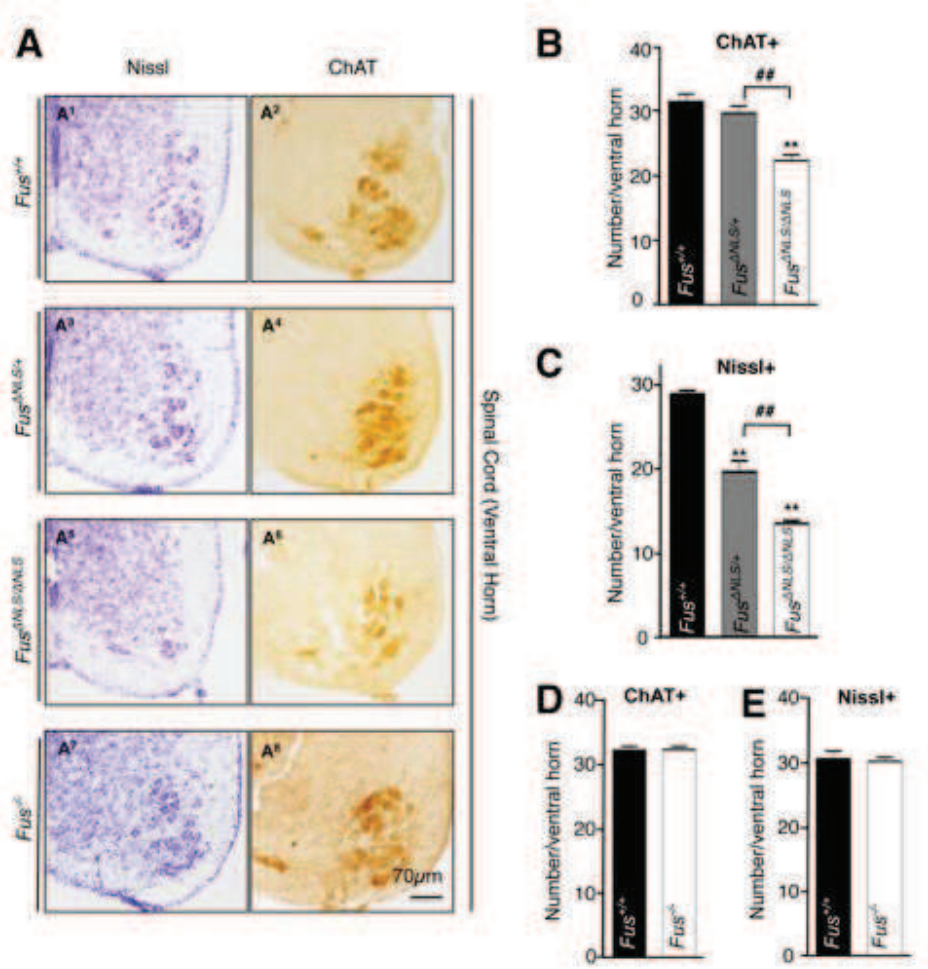

Figure 5: Motor neuron loss in *Fus*$^{\Delta NLS/\Delta NLS}$ mice

(A) Representative light microscopy images of spinal cord sections of *Fus*$^{+/+}$, *Fus*$^{\Delta NLS/+}$, *Fus*$^{\Delta NLS/\Delta NLS}$ and *Fus*$^{-/-}$ mice at birth stained with cresyl violet (Nissl, A^1, A^3 A^5, A^7), or anti-choline acetyl transferase (ChAT, A^2, A^4 A^6, A^8). Note the significantly decreased number of motor neurons in *Fus*$^{\Delta NLS/\Delta NLS}$ mice.

(B-C) Quantification of motor neurons per spinal cord ventral horn in *Fus*$^{\Delta NLS/\Delta NLS}$ mice . The number of ChAT+ motor neurons (B) and Nissl+ motor neurons (defined as Nissl positive cells with a soma area >80μm^2) (C) is significantly lower in *Fus*$^{\Delta NLS/\Delta NLS}$ mice. For Nissl+ N=8-5; and for ChAT+ N=7 per genotype, (**) p<0.01 vs *Fus*$^{+/+}$, (##) p<0.01 vs *Fus*$^{\Delta NLS/+}$; One way ANOVA followed by Tukey *post hoc* test.

(D-E) Quantification of motor neurons per spinal cord ventral horn in *Fus*$^{-/-}$ mice. Number of ChAT+ (D) and Nissl+ (E) motor neurons is not altered in *Fus*$^{-/-}$ mice. N=6 per genotype, (ns) non significant, by Student's unpaired t-test.

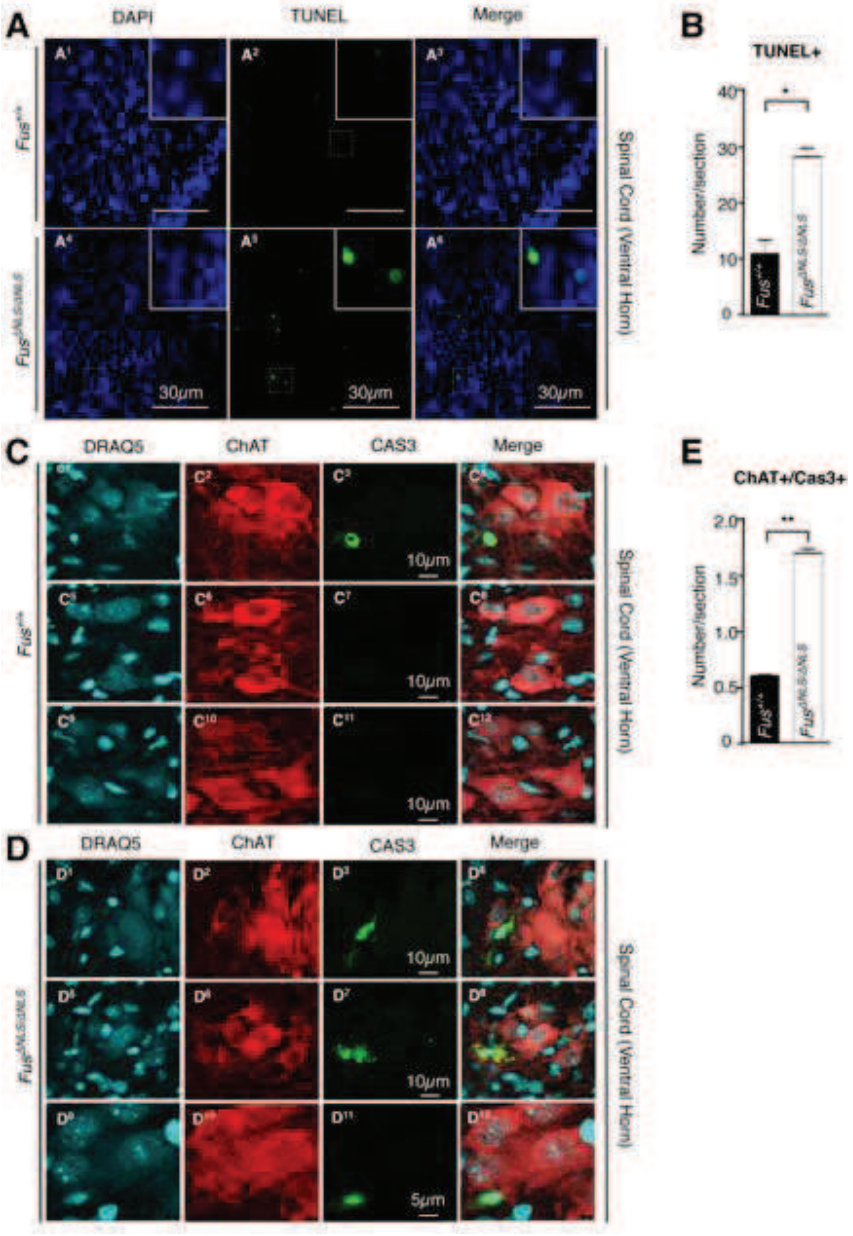

Figure 6: Motor neuron apoptosis in *Fus*$^{\Delta NLS/\Delta NLS}$ mice

(A) *In situ* detection of apoptotic cells in the spinal cord by TUNEL assay. Representative images showing increased DNA fragmentation (TUNEL+ cells in green), a characteristic hallmark of apoptosis, in spinal cord of *Fus*$^{\Delta NLS/\Delta NLS}$ mice (panels A^4-A^6).

(B) Quantification of the total number of TUNEL and DRAQ5 (blue) double-positive cells in *Fus*$^{\Delta NLS/\Delta NLS}$ and *Fus*$^{+/+}$ per spinal cord section. N=3 per genotype, (*) $p<0.05$, by Student's unpaired t-test.

(C-D) Immunofluorescence microscopy of spinal cord of *Fus*$^{+/+}$ (C) and *Fus*$^{\Delta NLS/\Delta NLS}$ (D) mice showing active-caspase 3 (green), ChAT (red) and DNA (cyan, DRAQ5). Note increased co-localization of apoptotic bodies, Cas3-positive with fragmented nuclei, and ChAT-positive motor neurons.

(E) Quantification of *caspase3 (CAS3)*/ChAT/DRAQ5 triple positive cells shows significant increase of apoptotic motor neurons in *Fus*$^{\Delta NLS/\Delta NLS}$ mice. N=7 per genotype, (**) $p<0.01$, by Student's unpaired t-test.

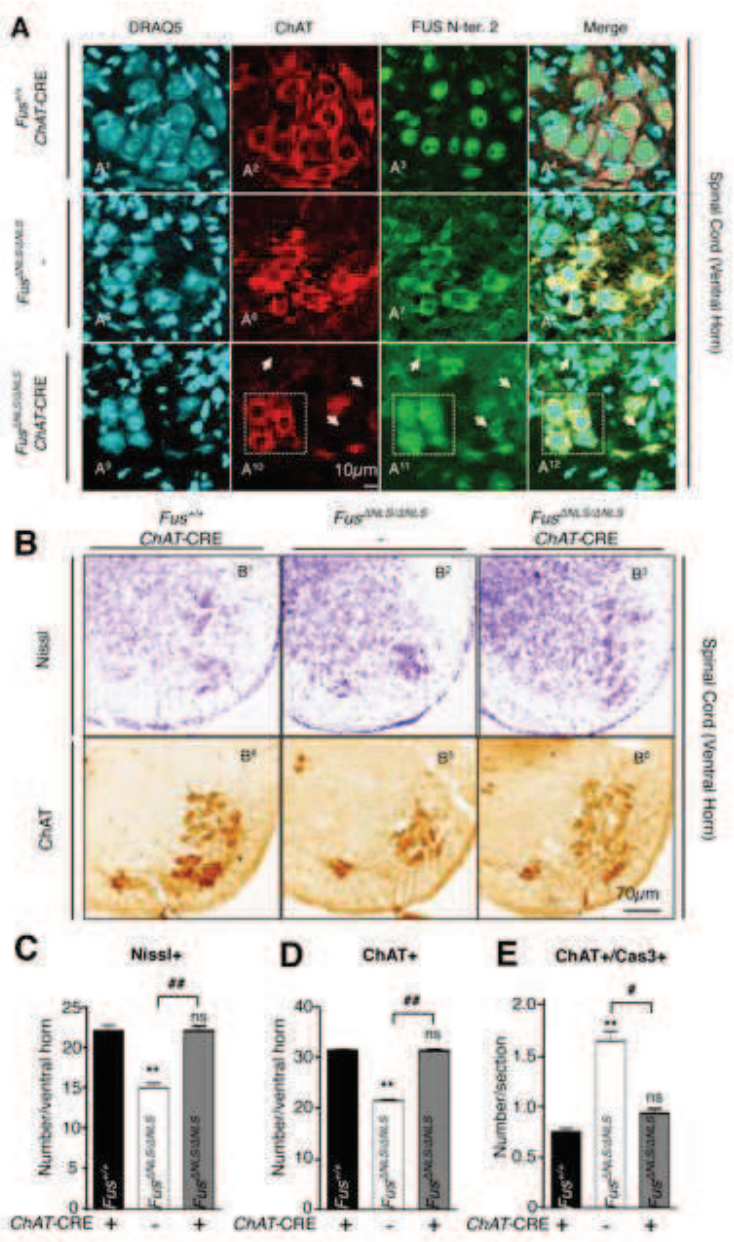

Figure 7: **Selective restoration of FUS nuclear import in motor neurons rescues motor neuron loss**
(A) Double-immunolabeling of spinal cord neurons with ChAT (red) and N-terminal FUS antibody (green). Nuclei were visualized with DRAQ5 (blue). Cellular localization of FUS was analyzed in the ventral spinal cord of *Fus*$^{+/+}$/*ChAT*-CRE (A^{1}-A^{4}), *Fus*$^{\Delta NLS/\Delta NLS}$/- (A^{5}-A^{8}), and *Fus*$^{\Delta NLS/\Delta NLS}$/*ChAT*-CRE (A^{9}-A^{12}).
FUS was completely nuclear in ChAT+ neurons of *Fus*$^{+/+}$/*ChAT*-CRE, while cytoplasmic in *Fus*$^{\Delta NLS/\Delta NLS}$/-, In the ventral horn of *Fus*$^{\Delta NLS/\Delta NLS}$/*ChAT*-CRE mice, ChAT+ neurons (motor neurons, *e.g.* within the dashed square) displayed nuclear FUS immunoreactivity, while ChAT negative cells (arrows) retained cytoplasmic FUS immunoreactivity (A^{9}-A^{12}). Thus, the ChAT-CRE allele induced successful recombination and restoration of FUS nuclear import in motor neurons. **(B)** Representative light microscopy images of spinal cord sections of *Fus*$^{+/+}$/*ChAT*-CRE (B^{1}, B^{4}), *Fus*$^{\Delta NLS/\Delta NLS}$/- (B^{2}, B^{5}) and *Fus*$^{\Delta NLS/\Delta NLS}$/*ChAT*-CRE (B^{3}, B^{6}) mice at birth stained with cresyl violet (Nissl, B^{1}-B^{3}) or anti-choline

acetyl transferase (ChAT, B^4-B^6). Note the fully restored number of motor neurons in *Fus*$^{\Delta NLS/\Delta NLS}$/*ChAT*-CRE mice.

(C-D) Quantification of motor neurons per spinal cord ventral horn. The number of Nissl+ (C) and ChAT+ (D) motoneurons is restored in *Fus*$^{\Delta NLS/\Delta NLS}$/*ChAT*-CRE mice while significantly lower in *Fus*$^{\Delta NLS/\Delta NLS}$ mice. N=11 *Fus*$^{+/+}$/*ChAT*-CRE, N=7 *Fus*$^{\Delta NLS/\Delta NLS}$/- and N=8 *Fus*$^{\Delta NLS/\Delta NLS}$/*ChAT*-CRE; (**) $p<0.01$ vs *Fus*$^{+/+}$, (##) $p<0.01$ vs *Fus*$^{\Delta NLS/+}$; One way ANOVA followed by Tukey *post hoc* test.

(E) Total numbers of *caspase3 (Cas3)*/ChAT/DAPI triple positive cells show a similar number of apoptotic motor neurons in *Fus*$^{\Delta NLS/\Delta NLS}$/*ChAT*-CRE and *Fus*$^{+/+}$/*ChAT*-CRE, but significantly lower numbers than in *Fus*$^{\Delta NLS/\Delta NLS}$/- mice. N=9 *Fus*$^{+/+}$/*ChAT*-CRE, N=7 *Fus*$^{\Delta NLS/\Delta NLS}$/- and N=8 *Fus*$^{\Delta NLS/\Delta NLS}$/*ChAT*-CRE;, (**) $p<0.01$ vs *Fus*$^{+/+}$, (#) $p<0.05$ vs *Fus*$^{\Delta NLS/+}$; (ns) non-significant; One way ANOVA followed by Tukey post hoc test.

References

Alami NH, Smith RB, Carrasco MA, Williams LA, Winborn CS, Han SS, Kiskinis E, Winborn B, Freibaum BD, Kanagaraj A, Clare AJ, Badders NM, Bilican B, Chaum E, Chandran S, Shaw CE, Eggan KC, Maniatis T, Taylor JP (2014) Axonal transport of TDP-43 mRNA granules is impaired by ALS-causing mutations. *Neuron* **81:** 536-543

Alaynick WA, Jessell TM, Pfaff SL (2011) SnapShot: spinal cord development. *Cell* **146:** 178-178 e171

Arnold ES, Ling SC, Huelga SC, Lagier-Tourenne C, Polymenidou M, Ditsworth D, Kordasiewicz HB, McAlonis-Downes M, Platoshyn O, Parone PA, Da Cruz S, Clutario KM, Swing D, Tessarollo L, Marsala M, Shaw CE, Yeo GW, Cleveland DW (2013) ALS-linked TDP-43 mutations produce aberrant RNA splicing and adult-onset motor neuron disease without aggregation or loss of nuclear TDP-43. *Proc Natl Acad Sci U S A*

Ayala YM, De Conti L, Avendano-Vazquez SE, Dhir A, Romano M, D'Ambrogio A, Tollervey J, Ule J, Baralle M, Buratti E, Baralle FE (2011) TDP-43 regulates its mRNA levels through a negative feedback loop. *EMBO J* **30:** 277-288

Baumer D, Hilton D, Paine SM, Turner MR, Lowe J, Talbot K, Ansorge O (2010) Juvenile ALS with basophilic inclusions is a FUS proteinopathy with FUS mutations. *Neurology* **75:** 611-618

Bergeron C, Beric-Maskarel K, Muntasser S, Weyer L, Somerville MJ, Percy ME (1994) Neurofilament light and polyadenylated mRNA levels are decreased in amyotrophic lateral sclerosis motor neurons. *Journal of neuropathology and experimental neurology* **53:** 221-230

Bertolin C, D'Ascenzo C, Querin G, Gaiani A, Boaretto F, Salvoro C, Vazza G, Angelini C, Cagnin A, Pegoraro E, Soraru G, Mostacciuolo ML (2014) Improving the knowledge of amyotrophic lateral sclerosis genetics: novel SOD1 and FUS variants. *Neurobiol Aging* **35:** 1212 e1217-1212 e1210

Boillee S, Vande Velde C, Cleveland DW (2006) ALS: a disease of motor neurons and their nonneuronal neighbors. *Neuron* **52:** 39-59

Calvo A, Moglia C, Canosa A, Brunetti M, Barberis M, Traynor BJ, Carrara G, Valentini C, Restagno G, Chio A (2014) De novo nonsense mutation of the FUS gene in an apparently familial amyotrophic lateral sclerosis case. *Neurobiol Aging* **35:** 1513 e1517-1511

Cambray S, Pedraza N, Rafel M, Gari E, Aldea M, Gallego C (2009) Protein kinase KIS localizes to RNA granules and enhances local translation. *Mol Cell Biol* **29:** 726-735

Cho HH, Cargnin F, Kim Y, Lee B, Kwon RJ, Nam H, Shen R, Barnes AP, Lee JW, Lee S, Lee SK (2014) Isl1 directly controls a cholinergic neuronal identity in the developing forebrain and spinal cord by forming cell type-specific complexes. *PLoS Genet* **10:** e1004280

Couthouis J, Hart MP, Erion R, King OD, Diaz Z, Nakaya T, Ibrahim F, Kim HJ, Mojsilovic-Petrovic J, Panossian S, Kim CE, Frackelton EC, Solski JA, Williams KL, Clay-Falcone D, Elman L, McCluskey L, Greene R, Hakonarson H, Kalb RG, Lee VM, Trojanowski JQ, Nicholson GA, Blair IP, Bonini NM, Van Deerlin VM, Mourelatos Z, Shorter J, Gitler AD (2012) Evaluating the role of the FUS/TLS-related gene EWSR1 in amyotrophic lateral sclerosis. *Hum Mol Genet* **21:** 2899-2911

Couthouis J, Hart MP, Shorter J, DeJesus-Hernandez M, Erion R, Oristano R, Liu AX, Ramos D, Jethava

N, Hosangadi D, Epstein J, Chiang A, Diaz Z, Nakaya T, Ibrahim F, Kim HJ, Solski JA, Williams KL, Mojsilovic-Petrovic J, Ingre C, Boylan K, Graff-Radford NR, Dickson DW, Clay-Falcone D, Elman L, McCluskey L, Greene R, Kalb RG, Lee VM, Trojanowski JQ, Ludolph A, Robberecht W, Andersen PM, Nicholson GA, Blair IP, King OD, Bonini NM, Van Deerlin V, Rademakers R, Mourelatos Z, Gitler AD (2011) A yeast functional screen predicts new candidate ALS disease genes. *Proc Natl Acad Sci U S A* **108:** 20881-20890

D'Alton S, Altshuler M, Lewis J (2015) Studies of alternative isoforms provide insight into TDP-43 autoregulation and pathogenesis. *Rna*

d'Errico P, Boido M, Piras A, Valsecchi V, De Amicis E, Locatelli D, Capra S, Vagni F, Vercelli A, Battaglia G (2013) Selective vulnerability of spinal and cortical motor neuron subpopulations in delta7 SMA mice. *PLoS One* **8:** e82654

de Hoog CL, Foster LJ, Mann M (2004) RNA and RNA binding proteins participate in early stages of cell spreading through spreading initiation centers. *Cell* **117:** 649-662

Deng H, Gao K, Jankovic J (2014) The role of FUS gene variants in neurodegenerative diseases. *Nat Rev Neurol* **10:** 337-348

Dillman AA, Hauser DN, Gibbs JR, Nalls MA, McCoy MK, Rudenko IN, Galter D, Cookson MR (2013) mRNA expression, splicing and editing in the embryonic and adult mouse cerebral cortex. *Nat Neurosci* **16:** 499-506

Dini Modigliani S, Morlando M, Errichelli L, Sabatelli M, Bozzoni I (2014) An ALS-associated mutation in the FUS 3'-UTR disrupts a microRNA-FUS regulatory circuitry. *Nat Commun* **5:** 4335

Dormann D, Rodde R, Edbauer D, Bentmann E, Fischer I, Hruscha A, Than ME, Mackenzie IR, Capell A, Schmid B, Neumann M, Haass C (2010) ALS-associated fused in sarcoma (FUS) mutations disrupt Transportin-mediated nuclear import. *EMBO J* **29:** 2841-2857

Elden AC, Kim HJ, Hart MP, Chen-Plotkin AS, Johnson BS, Fang X, Armakola M, Geser F, Greene R, Lu MM, Padmanabhan A, Clay-Falcone D, McCluskey L, Elman L, Juhr D, Gruber PJ, Rub U, Auburger G, Trojanowski JQ, Lee VM, Van Deerlin VM, Bonini NM, Gitler AD (2010) Ataxin-2 intermediate-length polyglutamine expansions are associated with increased risk for ALS. *Nature* **466:** 1069-1075

Ferland RJ, Eyaid W, Collura RV, Tully LD, Hill RS, Al-Nouri D, Al-Rumayyan A, Topcu M, Gascon G, Bodell A, Shugart YY, Ruvolo M, Walsh CA (2004) Abnormal cerebellar development and axonal decussation due to mutations in AHI1 in Joubert syndrome. *Nat Genet* **36:** 1008-1013

Frickenhaus M, Wagner M, Mallik M, Catinozzi M, Storkebaum E (2015) Highly efficient cell-type-specific gene inactivation reveals a key function for the Drosophila FUS homolog cabeza in neurons. *Sci Rep* **5:** 9107

Friedel RH, Seisenberger C, Kaloff C, Wurst W (2007) EUCOMM--the European conditional mouse mutagenesis program. *Brief Funct Genomic Proteomic* **6:** 180-185

Gerbino V, Carri MT, Cozzolino M, Achsel T (2013) Mislocalised FUS mutants stall spliceosomal snRNPs in the cytoplasm. *Neurobiol Dis* **55:** 120-128

Gitcho MA, Baloh RH, Chakraverty S, Mayo K, Norton JB, Levitch D, Hatanpaa KJ, White CL, 3rd, Bigio EH, Caselli R, Baker M, Al-Lozi MT, Morris JC, Pestronk A, Rademakers R, Goate AM, Cairns NJ (2008) TDP-43 A315T mutation in familial motor neuron disease. *Ann Neurol* **63:** 535-538

Groen EJ, Fumoto K, Blokhuis AM, Engelen-Lee J, Zhou Y, van den Heuvel DM, Koppers M, van Diggelen F, van Heest J, Demmers JA, Kirby J, Shaw PJ, Aronica E, Spliet WG, Veldink JH, van den Berg LH, Pasterkamp RJ (2013) ALS-associated mutations in FUS disrupt the axonal distribution and function of SMN. *Hum Mol Genet* **22:** 3690-3704

Han TW, Kato M, Xie S, Wu LC, Mirzaei H, Pei J, Chen M, Xie Y, Allen J, Xiao G, McKnight SL (2012) Cell-free formation of RNA granules: bound RNAs identify features and components of cellular assemblies. *Cell* **149:** 768-779

Hicks GG, Singh N, Nashabi A, Mai S, Bozek G, Klewes L, Arapovic D, White EK, Koury MJ, Oltz EM, Van Kaer L, Ruley HE (2000) Fus deficiency in mice results in defective B-lymphocyte development and activation, high levels of chromosomal instability and perinatal death. *Nat Genet* **24:** 175-179

Hu F, Padukkavidana T, Vaegter CB, Brady OA, Zheng Y, Mackenzie IR, Feldman HH, Nykjaer A, Strittmatter SM (2010) Sortilin-mediated endocytosis determines levels of the frontotemporal dementia protein, progranulin. *Neuron* **68:** 654-667

Huang C, Zhou H, Tong J, Chen H, Liu YJ, Wang D, Wei X, Xia XG (2011) FUS transgenic rats develop the phenotypes of amyotrophic lateral sclerosis and frontotemporal lobar degeneration. *PLoS Genet* **7:** e1002011

Huang EJ, Zhang J, Geser F, Trojanowski JQ, Strober JB, Dickson DW, Brown Jr RH, Shapiro BE, Lomen-Hoerth C (2010) Extensive FUS-Immunoreactive Pathology in Juvenile Amyotrophic Lateral Sclerosis with Basophilic Inclusions. *Brain Pathol*

Hutton M, Lendon CL, Rizzu P, Baker M, Froelich S, Houlden H, Pickering-Brown S, Chakraverty S, Isaacs A, Grover A, Hackett J, Adamson J, Lincoln S, Dickson D, Davies P, Petersen RC, Stevens M, de Graaff E, Wauters E, van Baren J, Hillebrand M, Joosse M, Kwon JM, Nowotny P, Che LK, Norton J, Morris JC, Reed LA, Trojanowski J, Basun H, Lannfelt L, Neystat M, Fahn S, Dark F, Tannenberg T, Dodd PR, Hayward N, Kwok JB, Schofield PR, Andreadis A, Snowden J, Craufurd D, Neary D, Owen F, Oostra BA, Hardy J, Goate A, van Swieten J, Mann D, Lynch T, Heutink P (1998) Association of missense and 5'-splice-site mutations in tau with the inherited dementia FTDP-17. *Nature* **393:** 702-705

Ilieva H, Polymenidou M, Cleveland DW (2009) Non-cell autonomous toxicity in neurodegenerative disorders: ALS and beyond. *J Cell Biol* **187:** 761-772

Imbert G, Saudou F, Yvert G, Devys D, Trottier Y, Garnier JM, Weber C, Mandel JL, Cancel G, Abbas N, Durr A, Didierjean O, Stevanin G, Agid Y, Brice A (1996) Cloning of the gene for spinocerebellar ataxia 2 reveals a locus with high sensitivity to expanded CAG/glutamine repeats. *Nat Genet* **14:** 285-291

Ishigaki S, Masuda A, Fujioka Y, Iguchi Y, Katsuno M, Shibata A, Urano F, Sobue G, Ohno K (2012) Position-dependent FUS-RNA interactions regulate alternative splicing events and transcriptions. *Sci Rep* **2:** 529

Jablonka S, Beck M, Lechner BD, Mayer C, Sendtner M (2007) Defective Ca2+ channel clustering in axon terminals disturbs excitability in motoneurons in spinal muscular atrophy. *J Cell Biol* **179:** 139-149

Johnson JO, Pioro EP, Boehringer A, Chia R, Feit H, Renton AE, Pliner HA, Abramzon Y, Marangi G, Winborn BJ, Gibbs JR, Nalls MA, Morgan S, Shoai M, Hardy J, Pittman A, Orrell RW, Malaspina A, Sidle KC, Fratta P, Harms MB, Baloh RH, Pestronk A, Weihl CC, Rogaeva E, Zinman L, Drory VE, Borghero G, Mora G, Calvo A, Rothstein JD, Italsgen, Drepper C, Sendtner M, Singleton AB, Taylor JP, Cookson MR, Restagno G, Sabatelli M, Bowser R, Chio A, Traynor BJ (2014) Mutations in the Matrin 3 gene cause familial amyotrophic lateral sclerosis. *Nat Neurosci* **17:** 664-666

Ju S, Tardiff DF, Han H, Divya K, Zhong Q, Maquat LE, Bosco DA, Hayward LJ, Brown RH, Jr., Lindquist S, Ringe D, Petsko GA (2011) A yeast model of FUS/TLS-dependent cytotoxicity. *PLoS biology* **9:** e1001052

Kabashi E, Valdmanis PN, Dion P, Spiegelman D, McConkey BJ, Vande Velde C, Bouchard JP, Lacomblez L, Pochigaeva K, Salachas F, Pradat PF, Camu W, Meininger V, Dupre N, Rouleau GA (2008) TARDBP mutations in individuals with sporadic and familial amyotrophic lateral sclerosis. *Nat Genet* **40:** 572-574

Kanning KC, Kaplan A, Henderson CE (2010) Motor neuron diversity in development and disease. *Annu Rev Neurosci* **33:** 409-440

Kim HJ, Kim NC, Wang YD, Scarborough EA, Moore J, Diaz Z, MacLea KS, Freibaum B, Li S, Molliex A, Kanagaraj AP, Carter R, Boylan KB, Wojtas AM, Rademakers R, Pinkus JL, Greenberg SA, Trojanowski JQ, Traynor BJ, Smith BN, Topp S, Gkazi AS, Miller J, Shaw CE, Kottlors M, Kirschner J, Pestronk A, Li YR, Ford AF, Gitler AD, Benatar M, King OD, Kimonis VE, Ross ED, Weihl CC, Shorter J, Taylor JP (2013) Mutations in prion-like domains in hnRNPA2B1 and hnRNPA1 cause multisystem proteinopathy and ALS. *Nature* **495:** 467-473

Kino Y, Washizu C, Kurosawa M, Yamada M, Miyazaki H, Akagi T, Hashikawa T, Doi H, Takumi T, Hicks GG, Hattori N, Shimogori T, Nukina N (2015) FUS/TLS deficiency causes behavioral and pathological abnormalities distinct from amyotrophic lateral sclerosis. *Acta neuropathologica communications* **3:** 24

Kobayashi Z, Tsuchiya K, Arai T, Aoki M, Hasegawa M, Ishizu H, Akiyama H, Mizusawa H (2010) Occurrence of basophilic inclusions and FUS-immunoreactive neuronal and glial inclusions in a case of familial amyotrophic lateral sclerosis. *Journal of the neurological sciences* **293:** 6-11

Kuroda M, Sok J, Webb L, Baechtold H, Urano F, Yin Y, Chung P, de Rooij DG, Akhmedov A, Ashley T, Ron D (2000) Male sterility and enhanced radiation sensitivity in TLS(-/-) mice. *EMBO J* **19:** 453-462

Kwiatkowski TJ, Jr., Bosco DA, Leclerc AL, Tamrazian E, Vanderburg CR, Russ C, Davis A, Gilchrist J, Kasarskis EJ, Munsat T, Valdmanis P, Rouleau GA, Hosler BA, Cortelli P, de Jong PJ, Yoshinaga Y, Haines JL, Pericak-Vance MA, Yan J, Ticozzi N, Siddique T, McKenna-Yasek D, Sapp PC, Horvitz HR, Landers JE, Brown RH, Jr. (2009) Mutations in the FUS/TLS gene on chromosome 16 cause familial amyotrophic lateral sclerosis. *Science* **323:** 1205-1208

Lagier-Tourenne C, Polymenidou M, Hutt KR, Vu AQ, Baughn M, Huelga SC, Clutario KM, Ling SC,

Liang TY, Mazur C, Wancewicz E, Kim AS, Watt A, Freier S, Hicks GG, Donohue JP, Shiue L, Bennett CF, Ravits J, Cleveland DW, Yeo GW (2012) Divergent roles of ALS-linked proteins FUS/TLS and TDP-43 intersect in processing long pre-mRNAs. *Nat Neurosci* **15:** 1488-1497

Li H, Qiu J, Fu XD (2012) RASL-seq for massively parallel and quantitative analysis of gene expression. *Current protocols in molecular biology / edited by Frederick M Ausubel [et al]* **Chapter 4:** Unit 4 13 11-19

Li YR, King OD, Shorter J, Gitler AD (2013) Stress granules as crucibles of ALS pathogenesis. *J Cell Biol* **201:** 361-372

Ling SC, Polymenidou M, Cleveland DW (2013) Converging mechanisms in ALS and FTD: disrupted RNA and protein homeostasis. *Neuron* **79:** 416-438

Liu F, Gong CX (2008) Tau exon 10 alternative splicing and tauopathies. *Mol Neurodegener* **3:** 8

Liu-Yesucevitz L, Bilgutay A, Zhang YJ, Vanderweyde T, Citro A, Mehta T, Zaarur N, McKee A, Bowser R, Sherman M, Petrucelli L, Wolozin B (2010) Tar DNA binding protein-43 (TDP-43) associates with stress granules: analysis of cultured cells and pathological brain tissue. *PLoS One* **5:** e13250

Mackenzie IR, Rademakers R, Neumann M (2010) TDP-43 and FUS in amyotrophic lateral sclerosis and frontotemporal dementia. *Lancet Neurol* **9:** 995-1007

Manceau V, Kielkopf CL, Sobel A, Maucuer A (2008) Different requirements of the kinase and UHM domains of KIS for its nuclear localization and binding to splicing factors. *J Mol Biol* **381:** 748-762

McMillan P, Korvatska E, Poorkaj P, Evstafjeva Z, Robinson L, Greenup L, Leverenz J, Schellenberg GD, D'Souza I (2008) Tau isoform regulation is region- and cell-specific in mouse brain. *The Journal of comparative neurology* **511:** 788-803

Mitchell JC, McGoldrick P, Vance C, Hortobagyi T, Sreedharan J, Rogelj B, Tudor EL, Smith BN, Klasen C, Miller CC, Cooper JD, Greensmith L, Shaw CE (2013) Overexpression of human wild-type FUS causes progressive motor neuron degeneration in an age- and dose-dependent fashion. *Acta Neuropathol* **125:** 273-288

Mitchelmore C, Buchmann-Moller S, Rask L, West MJ, Troncoso JC, Jensen NA (2004) NDRG2: a novel Alzheimer's disease associated protein. *Neurobiol Dis* **16:** 48-58

Morlando M, Dini Modigliani S, Torrelli G, Rosa A, Di Carlo V, Caffarelli E, Bozzoni I (2012) FUS stimulates microRNA biogenesis by facilitating co-transcriptional Drosha recruitment. *EMBO J* **31:** 4502-4510

Mortazavi A, Williams BA, McCue K, Schaeffer L, Wold B (2008) Mapping and quantifying mammalian transcriptomes by RNA-Seq. *Nature methods* **5:** 621-628

Neumann M, Rademakers R, Roeber S, Baker M, Kretzschmar HA, Mackenzie IR (2009) A new subtype of frontotemporal lobar degeneration with FUS pathology. *Brain* **132:** 2922-2931

Neumann M, Sampathu DM, Kwong LK, Truax AC, Micsenyi MC, Chou TT, Bruce J, Schuck T, Grossman M, Clark CM, McCluskey LF, Miller BL, Masliah E, Mackenzie IR, Feldman H, Feiden

W, Kretzschmar HA, Trojanowski JQ, Lee VM (2006) Ubiquitinated TDP-43 in frontotemporal lobar degeneration and amyotrophic lateral sclerosis. *Science* **314:** 130-133

Oppenheim RW (1991) Cell death during development of the nervous system. *Annu Rev Neurosci* **14:** 453-501

Parkhomchuk D, Borodina T, Amstislavskiy V, Banaru M, Hallen L, Krobitsch S, Lehrach H, Soldatov A (2009) Transcriptome analysis by strand-specific sequencing of complementary DNA. *Nucleic Acids Res* **37:** e123

Pedraza N, Ortiz R, Cornado A, Llobet A, Aldea M, Gallego C (2014) KIS, a kinase associated with microtubule regulators, enhances translation of AMPA receptors and stimulates dendritic spine remodeling. *J Neurosci* **34:** 13988-13997

Polymenidou M, Lagier-Tourenne C, Hutt KR, Huelga SC, Moran J, Liang TY, Ling SC, Sun E, Wancewicz E, Mazur C, Kordasiewicz H, Sedaghat Y, Donohue JP, Shiue L, Bennett CF, Yeo GW, Cleveland DW (2011) Long pre-mRNA depletion and RNA missplicing contribute to neuronal vulnerability from loss of TDP-43. *Nat Neurosci* **14:** 459-468

Prudencio M, Jansen-West KR, Lee WC, Gendron TF, Zhang YJ, Xu YF, Gass J, Stuani C, Stetler C, Rademakers R, Dickson DW, Buratti E, Petrucelli L (2012) Misregulation of human sortilin splicing leads to the generation of a nonfunctional progranulin receptor. *Proc Natl Acad Sci U S A* **109:** 21510-21515

Rathod R, Havlicek S, Frank N, Blum R, Sendtner M (2012) Laminin induced local axonal translation of beta-actin mRNA is impaired in SMN-deficient motoneurons. *Histochem Cell Biol* **138:** 737-748

Rogelj B, Easton LE, Bogu GK, Stanton LW, Rot G, Curk T, Zupan B, Sugimoto Y, Modic M, Haberman N, Tollervey J, Fujii R, Takumi T, Shaw CE, Ule J (2012) Widespread binding of FUS along nascent RNA regulates alternative splicing in the brain. *Sci Rep* **2:** 603

Rossi J, Balthasar N, Olson D, Scott M, Berglund E, Lee CE, Choi MJ, Lauzon D, Lowell BB, Elmquist JK (2011) Melanocortin-4 receptors expressed by cholinergic neurons regulate energy balance and glucose homeostasis. *Cell Metab* **13:** 195-204

Rossoll W, Jablonka S, Andreassi C, Kroning AK, Karle K, Monani UR, Sendtner M (2003) Smn, the spinal muscular atrophy-determining gene product, modulates axon growth and localization of beta-actin mRNA in growth cones of motoneurons. *J Cell Biol* **163:** 801-812

Ruggiu M, Herbst R, Kim N, Jevsek M, Fak JJ, Mann MA, Fischbach G, Burden SJ, Darnell RB (2009) Rescuing Z+ agrin splicing in Nova null mice restores synapse formation and unmasks a physiologic defect in motor neuron firing. *Proc Natl Acad Sci U S A* **106:** 3513-3518

Sanchez G, Dury AY, Murray LM, Biondi O, Tadesse H, El Fatimy R, Kothary R, Charbonnier F, Khandjian EW, Cote J (2013) A novel function for the survival motoneuron protein as a translational regulator. *Hum Mol Genet* **22:** 668-684

Saxena S, Roselli F, Singh K, Leptien K, Julien JP, Gros-Louis F, Caroni P (2013) Neuroprotection through excitability and mTOR required in ALS motoneurons to delay disease and extend survival. *Neuron* **80:** 80-96

Schneider CA, Rasband WS, Eliceiri KW (2012) NIH Image to ImageJ: 25 years of image analysis. *Nature methods* **9:** 671-675

Schwartz JC, Ebmeier CC, Podell ER, Heimiller J, Taatjes DJ, Cech TR (2012) FUS binds the CTD of RNA polymerase II and regulates its phosphorylation at Ser2. *Genes Dev* **26:** 2690-2695

Sephton CF, Tang AA, Kulkarni A, West J, Brooks M, Stubblefield JJ, Liu Y, Zhang MQ, Green CB, Huber KM, Huang EJ, Herz J, Yu G (2014) Activity-dependent FUS dysregulation disrupts synaptic homeostasis. *Proc Natl Acad Sci U S A* **111:** E4769-4778

Sheffler-Collins SI, Dalva MB (2012) EphBs: an integral link between synaptic function and synaptopathies. *Trends Neurosci* **35:** 293-304

Smith BN, Ticozzi N, Fallini C, Gkazi AS, Topp S, Kenna KP, Scotter EL, Kost J, Keagle P, Miller JW, Calini D, Vance C, Danielson EW, Troakes C, Tiloca C, Al-Sarraj S, Lewis EA, King A, Colombrita C, Pensato V, Castellotti B, de Belleroche J, Baas F, ten Asbroek AL, Sapp PC, McKenna-Yasek D, McLaughlin RL, Polak M, Asress S, Esteban-Perez J, Munoz-Blanco JL, Simpson M, Consortium S, van Rheenen W, Diekstra FP, Lauria G, Duga S, Corti S, Cereda C, Corrado L, Soraru G, Morrison KE, Williams KL, Nicholson GA, Blair IP, Dion PA, Leblond CS, Rouleau GA, Hardiman O, Veldink JH, van den Berg LH, Al-Chalabi A, Pall H, Shaw PJ, Turner MR, Talbot K, Taroni F, Garcia-Redondo A, Wu Z, Glass JD, Gellera C, Ratti A, Brown RH, Jr., Silani V, Shaw CE, Landers JE (2014) Exome-wide rare variant analysis identifies TUBA4A mutations associated with familial ALS. *Neuron* **84:** 324-331

Sreedharan J, Blair IP, Tripathi VB, Hu X, Vance C, Rogelj B, Ackerley S, Durnall JC, Williams KL, Buratti E, Baralle F, de Belleroche J, Mitchell JD, Leigh PN, Al-Chalabi A, Miller CC, Nicholson G, Shaw CE (2008) TDP-43 mutations in familial and sporadic amyotrophic lateral sclerosis. *Science* **319:** 1668-1672

Sun S, Ling SC, Qiu J, Albuquerque CP, Zhou Y, Tokunaga S, Li H, Qiu H, Bui A, Yeo GW, Huang EJ, Eggan K, Zhou H, Fu XD, Lagier-Tourenne C, Cleveland DW (2015) ALS-causative mutations in FUS/TLS confer gain- and loss-of-function by altered association with SMN and U1-snRNP. *Nat Commun*

Sun Z, Diaz Z, Fang X, Hart MP, Chesi A, Shorter J, Gitler AD (2011) Molecular determinants and genetic modifiers of aggregation and toxicity for the ALS disease protein FUS/TLS. *PLoS biology* **9:** e1000614

Tateishi T, Hokonohara T, Yamasaki R, Miura S, Kikuchi H, Iwaki A, Tashiro H, Furuya H, Nagara Y, Ohyagi Y, Nukina N, Iwaki T, Fukumaki Y, Kira JI (2010) Multiple system degeneration with basophilic inclusions in Japanese ALS patients with FUS mutation. *Acta Neuropathol* **119:** 355-364

Tibshirani M, Tradewell ML, Mattina KR, Minotti S, Yang W, Zhou H, Strong MJ, Hayward LJ, Durham HD (2014) Cytoplasmic sequestration of FUS/TLS associated with ALS alters histone marks through loss of nuclear protein arginine methyltransferase 1. *Hum Mol Genet*

Tollervey JR, Curk T, Rogelj B, Briese M, Cereda M, Kayikci M, Konig J, Hortobagyi T, Nishimura AL, Zupunski V, Patani R, Chandran S, Rot G, Zupan B, Shaw CE, Ule J (2011) Characterizing the RNA targets and position-dependent splicing regulation by TDP-43. *Nat Neurosci* **14:** 452-458

Trapnell C, Roberts A, Goff L, Pertea G, Kim D, Kelley DR, Pimentel H, Salzberg SL, Rinn JL, Pachter

L (2012) Differential gene and transcript expression analysis of RNA-seq experiments with TopHat and Cufflinks. *Nature protocols* **7:** 562-578

Tsuiji H, Iguchi Y, Furuya A, Kataoka A, Hatsuta H, Atsuta N, Tanaka F, Hashizume Y, Akatsu H, Murayama S, Sobue G, Yamanaka K (2013) Spliceosome integrity is defective in the motor neuron diseases ALS and SMA. *EMBO Mol Med* **5:** 221-234

Turgeon B, Meloche S (2009) Interpreting neonatal lethal phenotypes in mouse mutants: insights into gene function and human diseases. *Physiological reviews* **89:** 1-26

Van Hoecke A, Schoonaert L, Lemmens R, Timmers M, Staats KA, Laird AS, Peeters E, Philips T, Goris A, Dubois B, Andersen PM, Al-Chalabi A, Thijs V, Turnley AM, van Vught PW, Veldink JH, Hardiman O, Van Den Bosch L, Gonzalez-Perez P, Van Damme P, Brown RH, Jr., van den Berg LH, Robberecht W (2012) EPHA4 is a disease modifier of amyotrophic lateral sclerosis in animal models and in humans. *Nat Med* **18:** 1418-1422

Vance C, Rogelj B, Hortobagyi T, De Vos KJ, Nishimura AL, Sreedharan J, Hu X, Smith B, Ruddy D, Wright P, Ganesalingam J, Williams KL, Tripathi V, Al-Saraj S, Al-Chalabi A, Leigh PN, Blair IP, Nicholson G, de Belleroche J, Gallo JM, Miller CC, Shaw CE (2009) Mutations in FUS, an RNA processing protein, cause familial amyotrophic lateral sclerosis type 6. *Science* **323:** 1208-1211

Vance C, Scotter EL, Nishimura AL, Troakes C, Mitchell JC, Kathe C, Urwin H, Manser C, Miller CC, Hortobagyi T, Dragunow M, Rogelj B, Shaw CE (2013) ALS mutant FUS disrupts nuclear localisation and sequesters wild-type FUS within cytoplasmic stress granules. *Hum Mol Genet*

Vandesompele J, De Preter K, Pattyn F, Poppe B, Van Roy N, De Paepe A, Speleman F (2002) Accurate normalization of real-time quantitative RT-PCR data by geometric averaging of multiple internal control genes. *Genome Biol* **3:** research0034.0031–0034.0011

Waibel S, Neumann M, Rabe M, Meyer T, Ludolph AC (2010) Novel missense and truncating mutations in FUS/TLS in familial ALS. *Neurology* **75:** 815-817

Waibel S, Neumann M, Rosenbohm A, Birve A, Volk AE, Weishaupt JH, Meyer T, Muller U, Andersen PM, Ludolph AC (2013) Truncating mutations in FUS/TLS give rise to a more aggressive ALS-phenotype than missense mutations: a clinico-genetic study in Germany. *Eur J Neurol* **20:** 540-546

Wang WY, Pan L, Su SC, Quinn EJ, Sasaki M, Jimenez JC, Mackenzie IR, Huang EJ, Tsai LH (2013) Interaction of FUS and HDAC1 regulates DNA damage response and repair in neurons. *Nat Neurosci* **16:** 1383-1391

Wegorzewska I, Bell S, Cairns NJ, Miller TM, Baloh RH (2009) TDP-43 mutant transgenic mice develop features of ALS and frontotemporal lobar degeneration. *Proc Natl Acad Sci U S A* **106:** 18809-18814

Yamazaki T, Chen S, Yu Y, Yan B, Haertlein TC, Carrasco MA, Tapia JC, Zhai B, Das R, Lalancette-Hebert M, Sharma A, Chandran S, Sullivan G, Nishimura AL, Shaw CE, Gygi SP, Shneider NA, Maniatis T, Reed R (2012) FUS-SMN protein interactions link the motor neuron diseases ALS and SMA. *Cell Rep* **2:** 799-806

Yasuda K, Zhang H, Loiselle D, Haystead T, Macara IG, Mili S (2013) The RNA-binding protein Fus directs translation of localized mRNAs in APC-RNP granules. *J Cell Biol* **203:** 737-746

Yu Y, Chi B, Xia W, Gangopadhyay J, Yamazaki T, Winkelbauer-Hurt ME, Yin S, Eliasse Y, Adams E, Shaw CE, Reed R (2015) U1 snRNP is mislocalized in ALS patient fibroblasts bearing NLS mutations in FUS and is required for motor neuron outgrowth in zebrafish. *Nucleic Acids Res* **43:** 3208-3218

Zhang H, Xing L, Rossoll W, Wichterle H, Singer RH, Bassell GJ (2006) Multiprotein complexes of the survival of motor neuron protein SMN with Gemins traffic to neuronal processes and growth cones of motor neurons. *J Neurosci* **26:** 8622-8632

Zhou Y, Liu S, Liu G, Ozturk A, Hicks GG (2013) ALS-associated FUS mutations result in compromised FUS alternative splicing and autoregulation. *PLoS Genet* **9:** e1003895

Zhou Z, Qiu J, Liu W, Zhou Y, Plocinik RM, Li H, Hu Q, Ghosh G, Adams JA, Rosenfeld MG, Fu XD (2012) The Akt-SRPK-SR axis constitutes a major pathway in transducing EGF signaling to regulate alternative splicing in the nucleus. *Mol Cell* **47:** 422-433

Zou ZY, Cui LY, Sun Q, Li XG, Liu MS, Xu Y, Zhou Y, Yang XZ (2013) De novo FUS gene mutations are associated with juvenile-onset sporadic amyotrophic lateral sclerosis in China. *Neurobiol Aging* **34:** 1312 e1311-1318

Supplementary figures

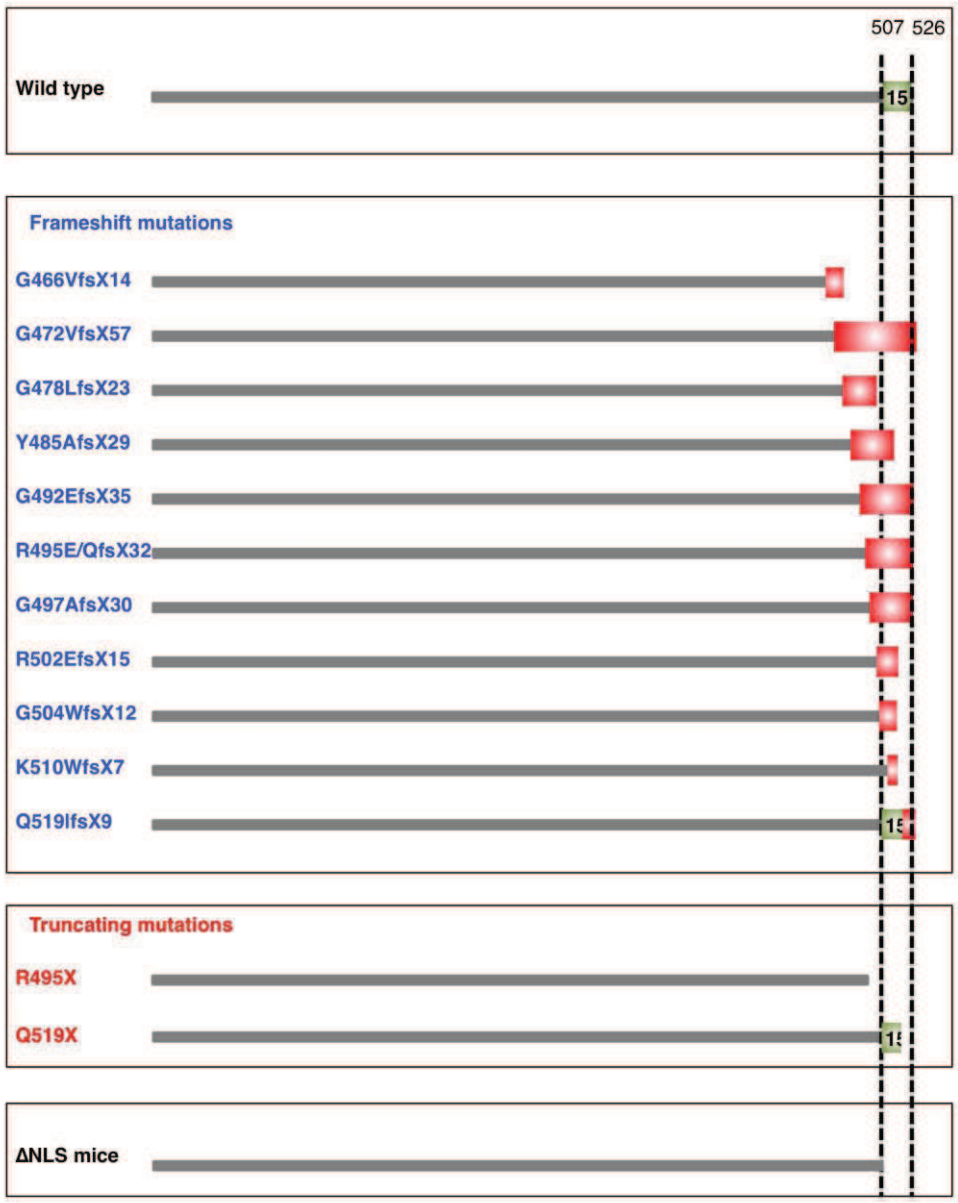

Supplementary Figure 1: Relevance of *Fus*$^{\Delta NLS}$ mice to human ALS
Upper panel: scheme of the wild type FUS protein. The NLS, encoded by exon 15, includes the C-terminal amino-acids (from 507-526, boundaries shown as the two dashed lines).
Middle panels: 11 frameshift mutations (upper middle panel) and 2 truncating mutations (lower middle panel) in the *FUS* gene have been identified in ALS families. The corresponding mutant FUS proteins are shown. Insertions of abnormal polypeptide sequences induced by frameshift mutations are shown as red boxes.
Lower panel: structure of FUS$^{\Delta NLS}$ protein in *Fus*$^{\Delta NLS}$ mice.

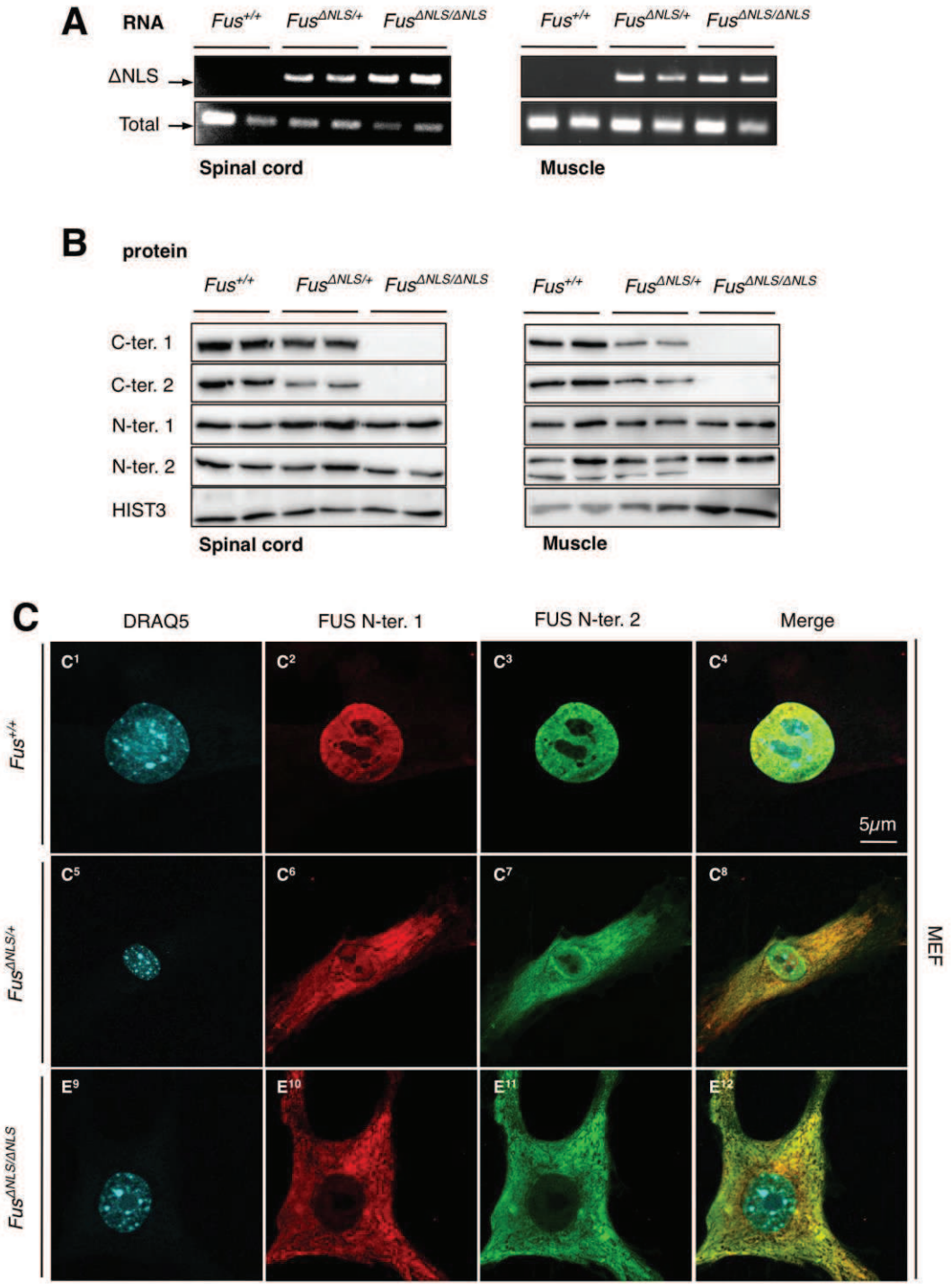

Supplementary Figure 2: Expression of the *Fus* gene in various tissues of *Fus*$^{\Delta NLS}$ mice

(A) RT-PCR analysis of spinal cord and gastrocnemius muscle from 2 *Fus*$^{+/+}$, 2 *Fus*$^{\Delta NLS/+}$ and 2 *Fus*$^{\Delta NLS/\Delta NLS}$ P0 mice using primers located in the STOP cassette, and thus specific to the *Fus* ΔNLS mRNA (ΔNLS, upper panel), or primers located in exon 11, *i.e.* upstream the floxed cDNA insertion, and thus amplifying total *Fus* mRNA (Total, lower panel). Presence of the *Fus* ΔNLS mRNA is observed in both *Fus*$^{\Delta NLS/+}$ and *Fus*$^{\Delta NLS/\Delta NLS}$ while absent in *Fus*$^{+/+}$ tissues.

(B) Immunoblot analysis of FUS protein in spinal cord and gastrocnemius of 2 *Fus*$^{+/+}$, 2 *Fus*$^{\Delta NLS/+}$ and 2 *Fus*$^{\Delta NLS/\Delta NLS}$ mice using two different antibodies targeting the C-terminal (C-ter. 1 and C-ter. 2) nuclear localization signal (NLS), or antibodies targeting the N-terminal (N-ter. 1) and internal parts (N-ter. 2) of FUS. Note the complete absence of immunoreactive bands when using C-terminal antibodies in *Fus*$^{\Delta NLS/\Delta NLS}$ tissues, confirming that the FUS protein derived from the ΔNLS allele lacks NLS.

(C) Representative confocal images for fluorescent immunocytochemical localization of FUS protein in mouse embryonic fibroblasts (MEF). A complete loss of FUS staining from the nucleus (marked in blue, DRAQ5) in *Fus*$^{\Delta NLS/\Delta NLS}$ was demonstrated using the two N-terminal FUS antibodies used in B (red and green). A combination of cytoplasmic and nuclear localization is seen in *Fus*$^{\Delta NLS/+}$ MEFs.

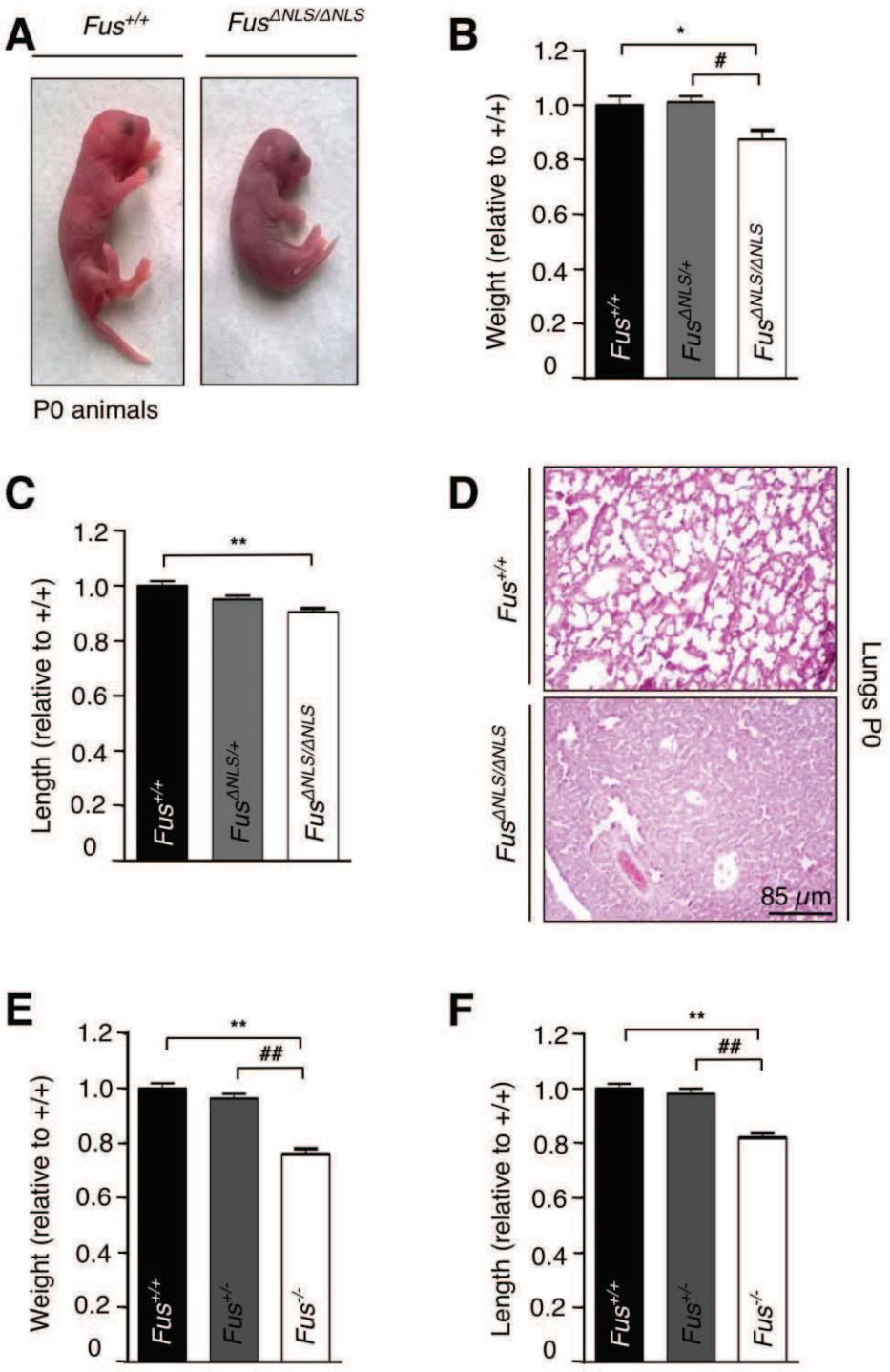

Supplementary Figure 3: Perinatal letality in *Fus*$^{\Delta NLS/\Delta NLS}$ and *Fus*$^{-/-}$ mice

(A) Photographs of *Fus*$^{+/+}$ and *Fus*$^{\Delta NLS/\Delta NLS}$ pups immediately after birth (P0 animals). Note the difference in skin color with cyanotic appearance indicating insufficient blood oxygenation in *Fus*$^{\Delta NLS/\Delta NLS}$ mice.

(B-C) *Fus*$^{\Delta NLS/\Delta NLS}$ mice showed significantly reduced body weight (C) and length (D). Weight and length values normalized to wild type (*Fus*$^{+/+}$) are presented. N=11 *Fus*$^{+/+}$, N=26 *Fus*$^{\Delta NLS/+}$ and N=14 *Fus*$^{\Delta NLS/\Delta NLS}$; (*) p<0.05 (**) p<0.01 vs *Fus*$^{+/+}$, (#) p<0.05 (##) p<0.01 vs *Fus*$^{\Delta NLS/+}$; One way ANOVA followed by Tukey *post hoc* test.

(D) Representative hematoxylin and eosin stainings of lungs of *Fus*$^{+/+}$ and *Fus*$^{\Delta NLS/\Delta NLS}$ at birth.

(E, F) Body weight (E) and length (F) of *Fus*$^{+/+}$, *Fus*$^{+/-}$ and *Fus*$^{-/-}$ pups at birth; N=14 *Fus*$^{+/+}$, N=36 *Fus*$^{+/-}$ and N=13 *Fus*$^{-/-}$ for body weight; N=6 per genotype for body length; (**) p<0.01 vs *Fus*$^{+/+}$, (##) p<0.01 vs *Fus*$^{+/-}$; One way ANOVA followed by Tukey *post hoc* test.

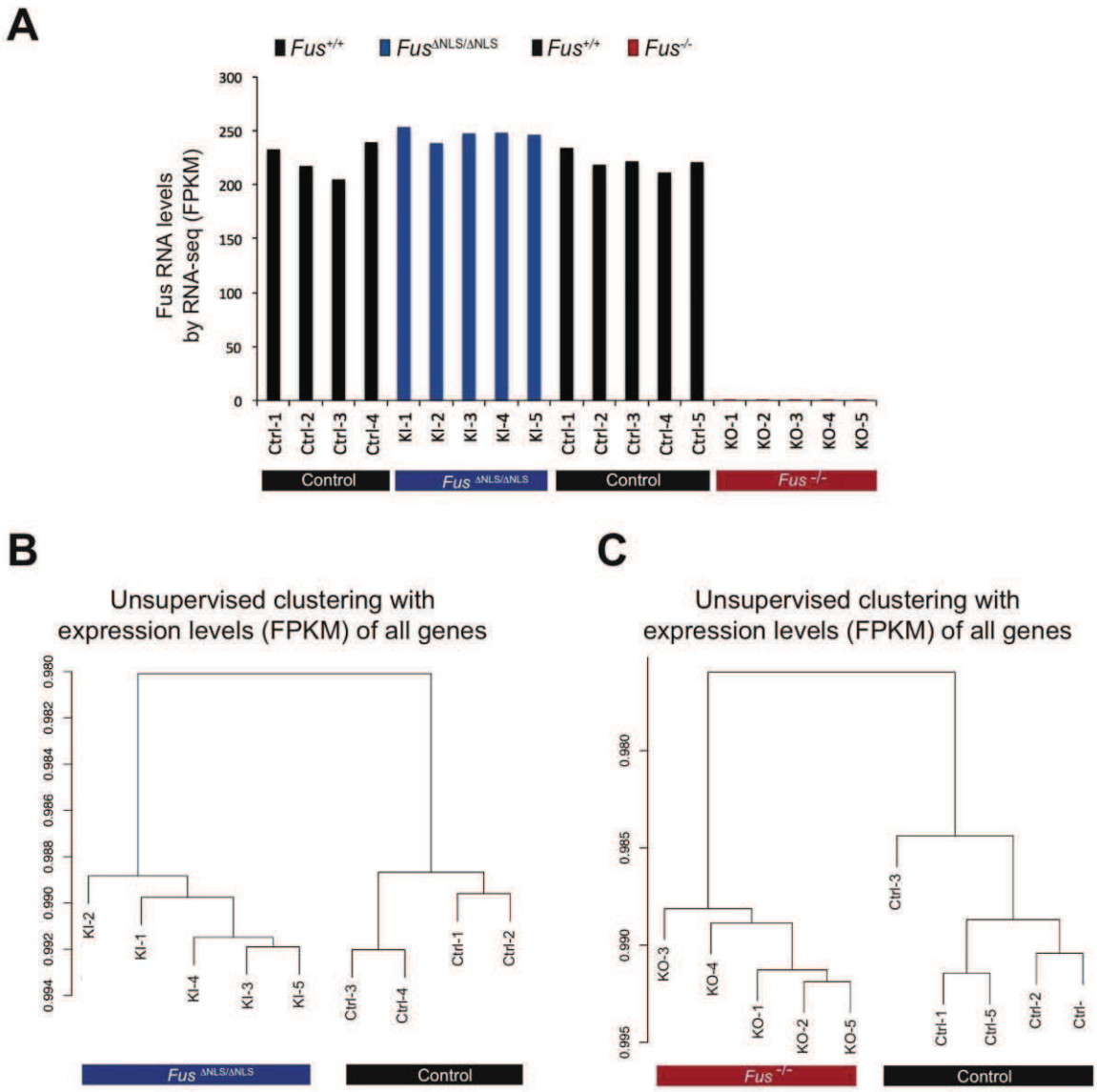

Supplementary Figure 4: Genome-wide expression changes identified by RNA-seq in Fus$^{\Delta NLS/\Delta NLS}$ and Fus$^{-/-}$ brains
(A) Quantification of *Fus* RNA levels by strand-specific RNA sequencing in brains from *Fus*$^{\Delta NLS/\Delta NLS}$ (blue bars), *Fus*$^{-/-}$ (red bars) and control littermates (*Fus*$^{+/+}$, black bars). RNA levels were determined by Fragments Per Kilobase of transcript per Million mapped reads (FPKM) values.
(B) Unsupervised hierarchical cluster analysis using all RNAs expressed in brains of *Fus*$^{\Delta NLS/\Delta NLS}$ mice (KI-1 to KI-5) and their control littermates (Ctrl-1 to Ctrl-4) showing that mice expressing truncated FUS have an expression profile distinct from control mice.
(C) Unsupervised hierarchical cluster analysis using all RNAs expressed in brains of *Fus*$^{-/-}$ mice (KO-1 to KO-5) and their control littermates (Ctrl-1 to Ctrl-5) showing that mice with complete loss of FUS have an expression profile distinct from control mice.

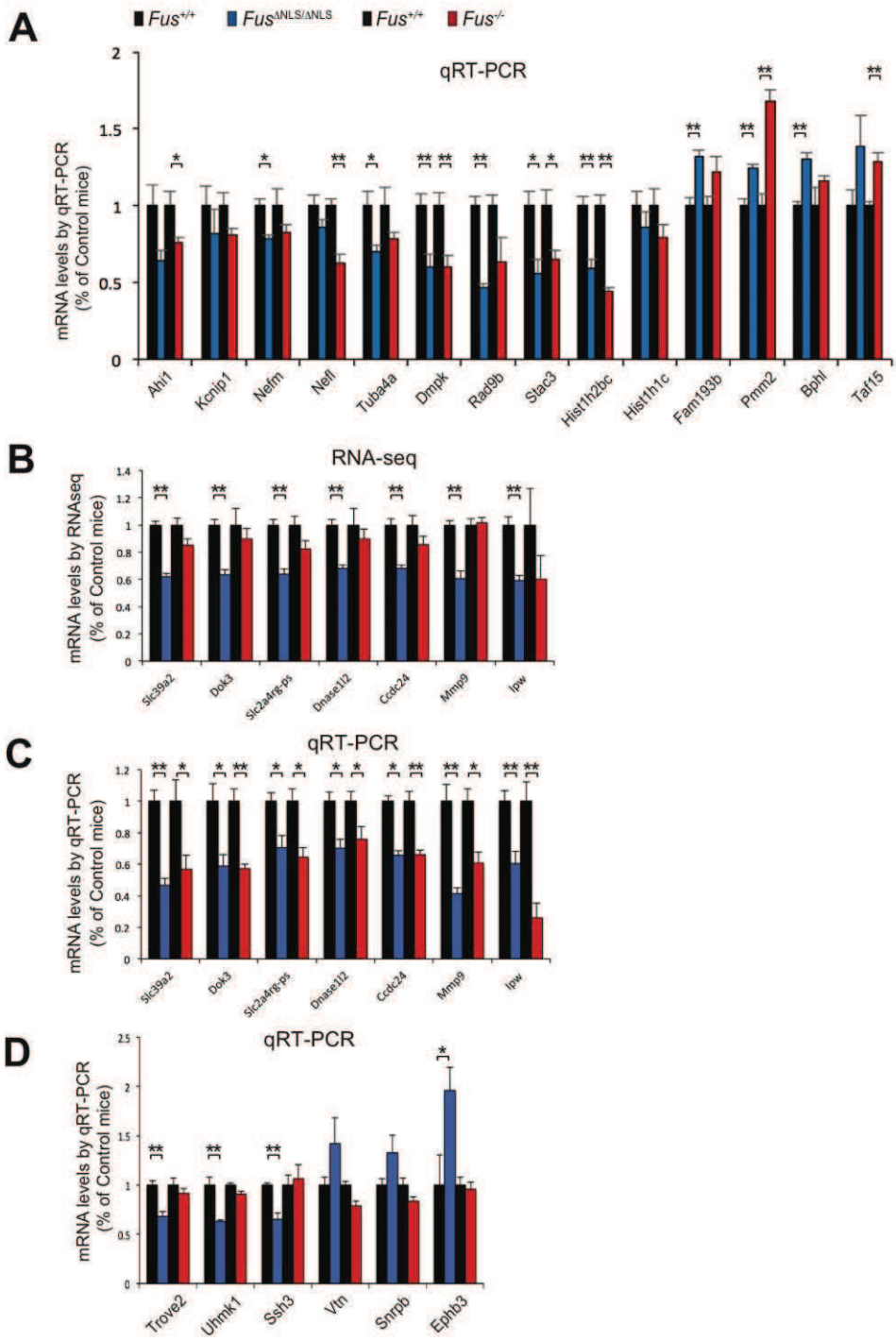

Supplementary Figure 5: Validation of expression changes identified by RNA-seq in *Fus*$^{\Delta NLS/\Delta NLS}$ and *Fus*$^{-/-}$ mouse brain

Expression levels of selected genes in *Fus*$^{\Delta NLS/\Delta NLS}$ (blue bars) and *Fus*$^{-/-}$ (red bars) compared to their control littermates (*Fus*$^{+/+}$, black bars).

(A) Quantitative RT-PCR (qRT-PCR) for genes identified by RNA-seq to be significantly downregulated (*Ahi1, Kcnip1, Nefm, Nefl, Tuba4a, Dmpk, Rad9b, Stac3, Hist1h2bc, Hist1h1c)* or upregulated (*Fam193b, Pmm2, Bphl, Taf15*) in both *Fus*$^{\Delta NLS/\Delta NLS}$ (blue bars) and *Fus*$^{-/-}$ (red bars) compared to their control littermates (*Fus*$^{+/+}$, black bars). Error bars represent SEM in 3-5 biological replicates.

(B) Normalized expression (based on FPKM from RNA-seq) of genes identified by RNA-seq to be significantly downregulated only in *Fus*$^{\Delta NLS/\Delta NLS}$ mice (*Slc39a2, Dok3, Slc2a4rg-ps, Dnase1l2, Ccdc24, Mmp9, Ipw*). Error bars represent SEM in 4-5 biological replicates.

(C) qRT-PCR analysis of the genes shown in (b) found that this set of genes was consistently downregulated in *Fus*$^{\Delta NLS/\Delta NLS}$ brains but also presented a similar trend in *Fus*$^{-/-}$ animals despite not being significantly changed by RNA-seq. Error bars represent SEM in 3-5 biological replicates.

(D) qRT-PCR for *Trove2, Uhmk1, Ssh3, Vtn, Snrpb* and *Ephb3* in brains from $Fus^{\Delta NLS/\Delta NLS}$ (blue bars), $Fus^{-/-}$ (red bars) and control littermates ($Fus^{+/+}$, black bars), showing genes identified by RNA-seq to be associated with the presence of truncated FUS in $Fus^{\Delta NLS/\Delta NLS}$ animals and not modified by loss of FUS in $Fus^{-/-}$ mice. Error bars represent SEM in 3-5 biological replicates.

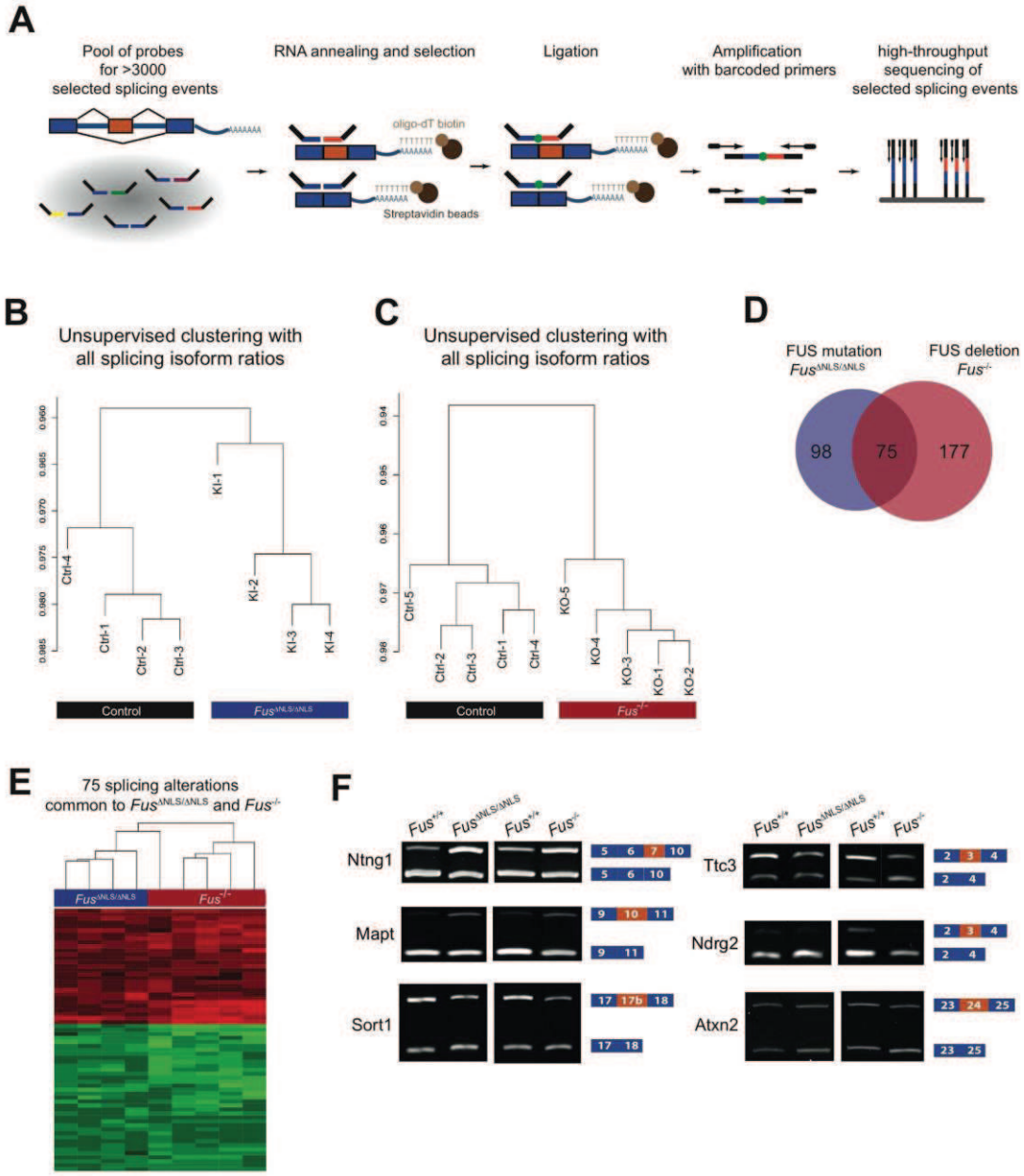

Supplementary figure 6: FUS-dependent splicing alterations identified by RASL-seq

(A) Schematic representation of the RASL-seq strategy to measure ratios of alternative splicing isoforms from thousands of selected splicing events by high-throughput sequencing.

(B) Unsupervised hierarchical cluster analysis using all splicing events sequenced in brains of $Fus^{\Delta NLS/\Delta NLS}$ mice (KI-1 to KI-4) and their control littermates (Ctrl-1 to Ctrl-4) showing that mice expressing truncated FUS have an RNA splicing profile distinct from control mice.

(C) Unsupervised hierarchical cluster analysis using all splicing events in brains of $Fus^{-/-}$ mice (KO-1 to KO-5) and their control littermates (Ctrl-1 to Ctrl-5) showing that mice with complete loss of FUS have an RNA splicing profile distinct from control mice.

(D) Venn diagram showing the number of overlapping splicing events that are misregulated in $Fus^{\Delta NLS/\Delta NLS}$ (blue circle) and $Fus^{-/-}$ (red circle) brains with 75 exons similarly altered upon cytoplasmic mislocalization or complete loss of FUS.

(E) Heatmap using the fold changes of the 75 splicing events commonly regulated in $Fus^{\Delta NLS/\Delta NLS}$ and $Fus^{-/-}$ mice showing that 100% of the events were differentially included or excluded in the same direction.

(F) Semi-quantitative RT-PCR analyses of selected targets shown in **Fig. 4C** with alternatively spliced exons depicted in

orange boxes with their flanking constitutive exons in blue boxes.

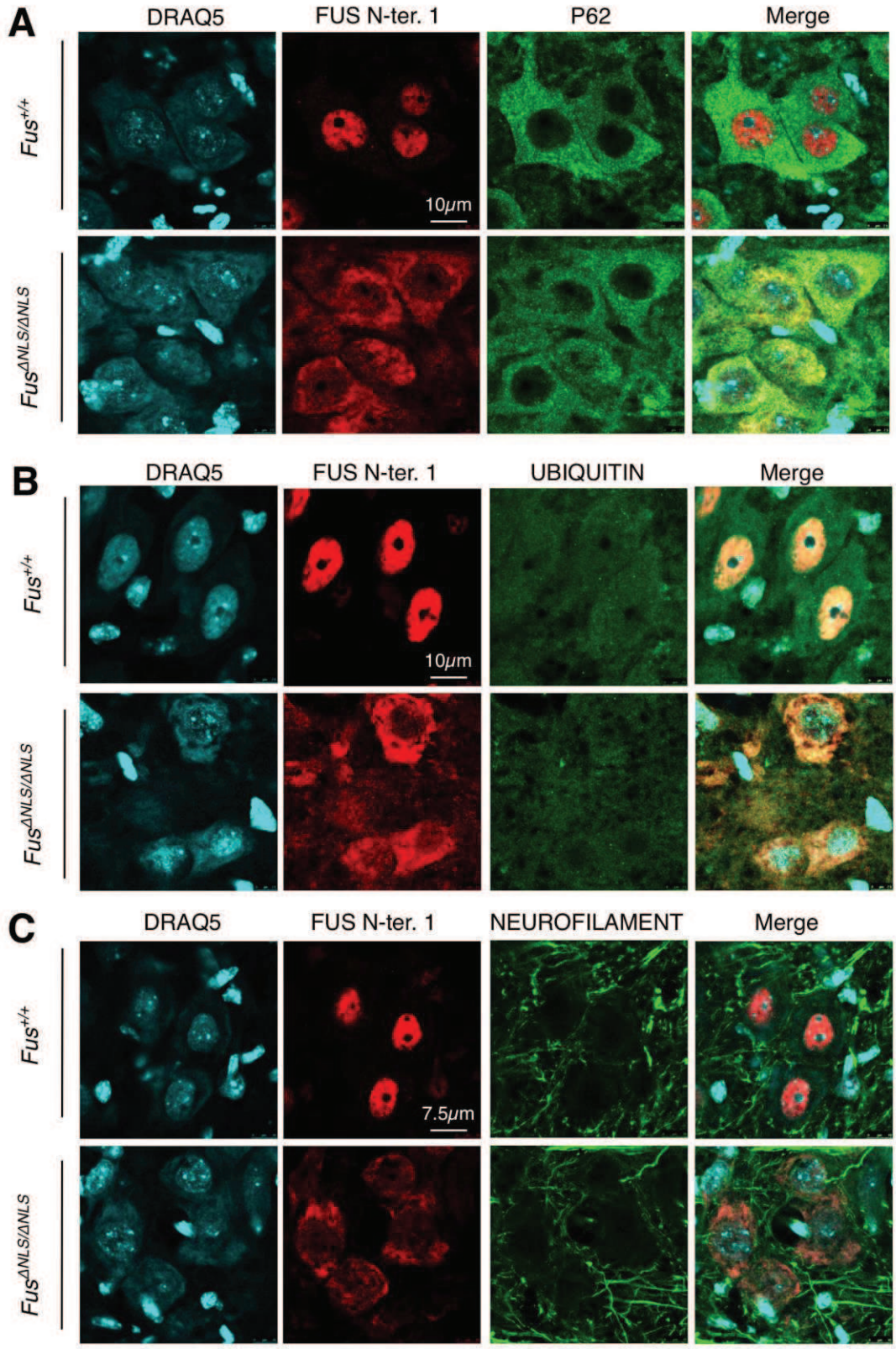

Supplementary Figure 7: Absence of protein aggregates in *Fus*$^{\Delta NLS/\Delta NLS}$ mice
(A-C) Representative images of double immunostaining of spinal cord neurons with N-terminal FUS antibody (red) and p62 (A), ubiquitin (B), or neurofilament (C) (green). DRAQ5 (blue) was used to mark nuclei. Upper panels: *Fus*$^{+/+}$; lower panels: *Fus*$^{\Delta NLS/\Delta NLS}$.
We did not observe FUS-, ubiquitin-, p62- or neurofilament-positive aggregates in *Fus*$^{\Delta NLS/\Delta NLS}$ animals.

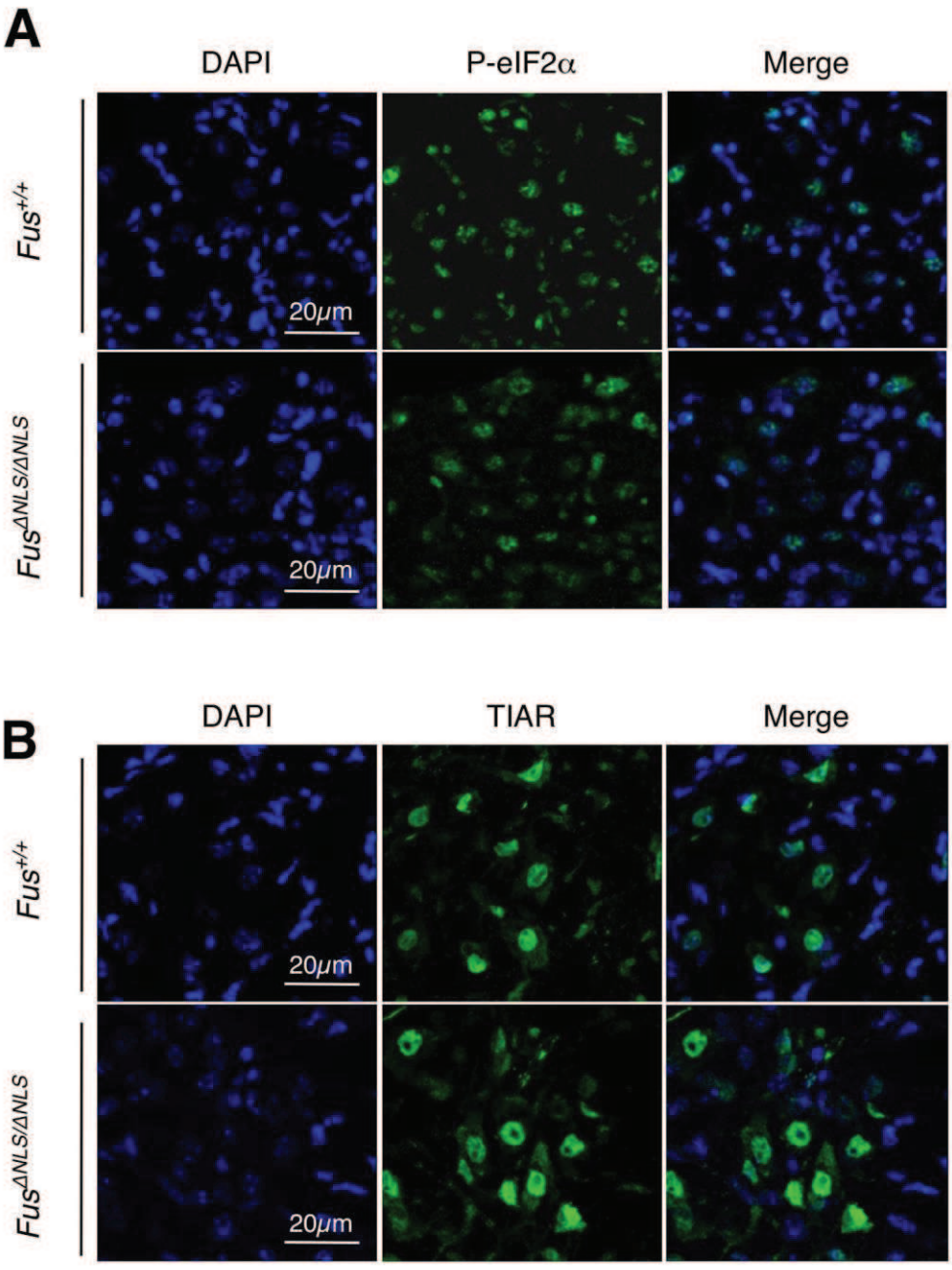

Supplementary Figure 8: Stress granules in *Fus*$^{\Delta NLS/\Delta NLS}$ mice
(A, B) Representative images of immunofluorescent staining of spinal cord neurons with antibodies against phosphorylated eIF2α (A, green), a general stress response marker, or TIAR (B, green), a stress granule marker. DNA is labeled in blue with DAPI. Upper panels: *Fus*$^{+/+}$; lower panels: *Fus*$^{\Delta NLS/\Delta NLS}$.
No difference between *Fus*$^{+/+}$ and *Fus*$^{\Delta NLS/\Delta NLS}$ animals was detected.

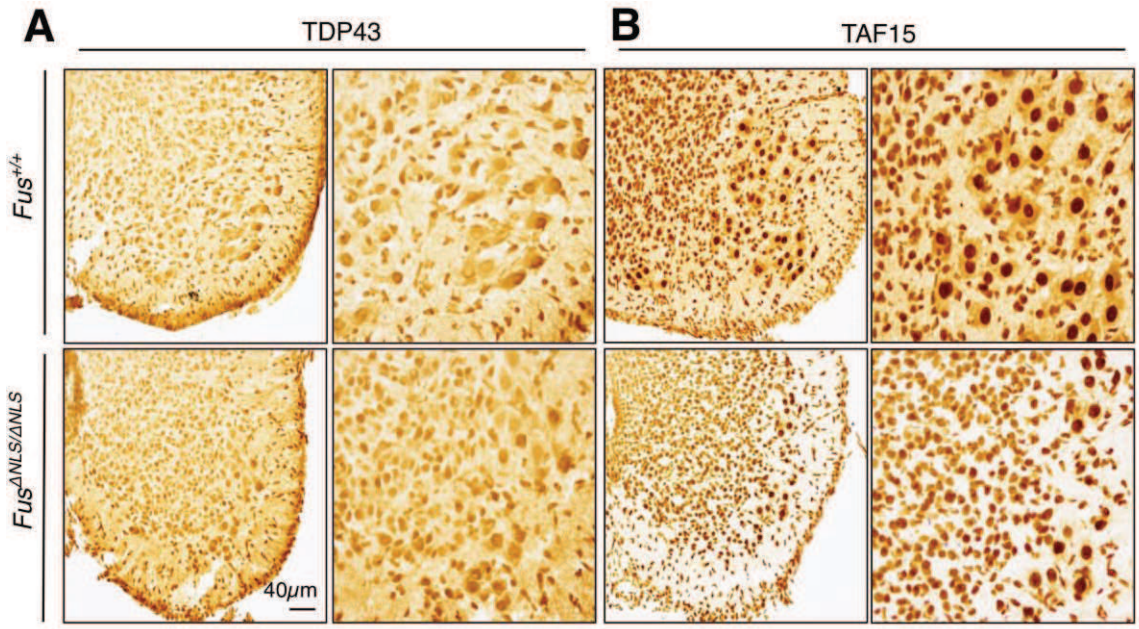

Supplementary Figure 9: Subcellular distribution of TDP-43 and TAF15 proteins in *Fus*$^{\Delta NLS/\Delta NLS}$ mice
(A, B) TDP-43 (A) and TAF-15 (B) immunoreactivities in spinal cord sections of *Fus*$^{+/+}$ (upper panels) and *Fus*$^{\Delta NLS/\Delta NLS}$ (lower panels) mice. Both proteins were mostly nuclear in spinal cord neurons of both genotypes.

II. PUBLICATION Nº2

(Manuscript in preparation)

Partial cytoplasmic mislocalization of FUS leads to motor neuron disease and behavioural symptoms relevant to FTLD

A. Summary – publication nº2

We next sought to investigate if the partial suppression (**Figure 26**) of FUS nuclear import, through heterozygous ΔNLS mutation, with aging could precipitate ALS and/or FTLD phenotype. To test our assumption we followed up two large cohorts of wild type $Fus^{+/+}$and heterozygous $Fus^{\Delta NLS/+}$mice. At different age time points we looked for motor behavioural changes characteristic for ALS, accompanied with pathohistological analysis.

Figure 26. Comparative analysis and follow up of mice during aging

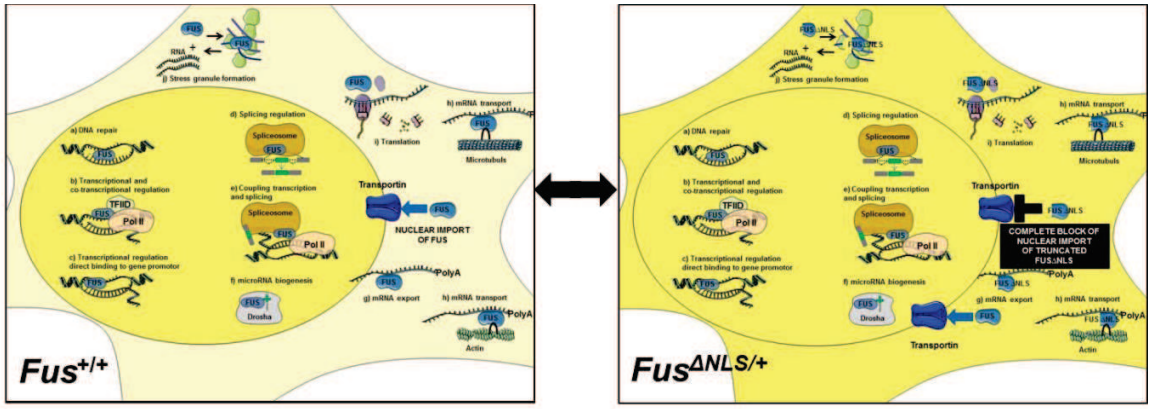

Schematically represented (by yellow color) FUS subcellular localization in $Fus^{+/+}$ with nuclear enrichment $Fus^{+/+}$, and partialy mislocalized to cytoplasm in $Fus^{\Delta NLS/+}$mice

Since FUS pathology is also observed in a subset of FTLD patients, we performed behavioural tests that are relevant for frontal lobe function and for presence of FTLD like symptoms. Although, finding the right test corresponding to human FLTD symptoms is quite challenging and frontal cortex in mice is much less developed, tests are crucial for model validation and therapeutic approaches. We focused on several commonly used in existing FTLD models to evaluate disinibition, anxiety, apathy or social disinterest and memory.

Results

Partial cytoplasmic mislocalization of FUS in *Fus*$^{\Delta NLS/+}$mice

We recently generated a conditional knock-in mouse model (*Fus*$^{\Delta NLS}$ mice) allowing the deletion of the last 19 amino acids of the FUS protein, constituting the atypical nuclear localization signal (PY-NLS) (**Figure 1A**). This part of FUS protein is responsible for importing FUS protein from cytoplasm to nucleus and the complete deletion of the PY-NLS leads to complete mislocalization of FUS (Scekic-Zahirovic et al, 2015). Here, we examine the phenotype of *Fus*$^{\Delta NLS/+}$ mice. *Fus*$^{\Delta NLS/+}$ mice are fertile and able to transmit the ΔNLS allele to their progreny (**Figure 1B**). While absent in wild type *Fus*$^{+/+}$ mice, the ΔNLS mRNA could be detected by RT-PCR in multiple tissues of *Fus*$^{\Delta NLS/+}$ mice (**Figure 1C**). Endogenous *Fus* expression was modestly increased in *Fus*$^{\Delta NLS/+}$ mice at the mRNA level in spinal cord and frontal cortex (**Figure 1D**), yet not at the protein level **(Figure 1E**). Importantly, the expression of *Taf15* and *Ewsr1,* the two other FET family members, was unchanged in *Fus*$^{\Delta NLS/+}$ mice (**Figure1D, 1E**).

To determine whether bearing one ΔNLS allele of the *Fus* gene leads to partial mislocalization of FUS, we first performed subcellular fractionation followed by western blotting. Interestingly, we were able to detect a robust FUS signal from cytoplasmic fractions of *Fus*$^{\Delta NLS/+}$ spinal cord, but not from cytoplasmic fractions of wild type littermates spinal cord (**Figure 2A).** Consistently, we observed generally increased cytoplasmic FUS staining in *Fus*$^{\Delta NLS/+}$ motor neurons using immunohistochemistry (**Figure 2B**). It should be noted however that cytoplasmic redistribution of FUS protein was heterogeneous, at least in spinal cord neurons with large nucleus (**Figure 2B**). Thus, *Fus*$^{\Delta NLS/+}$ mice express a truncated FUS protein that partially localizes to the cytoplasm.

Figure 1

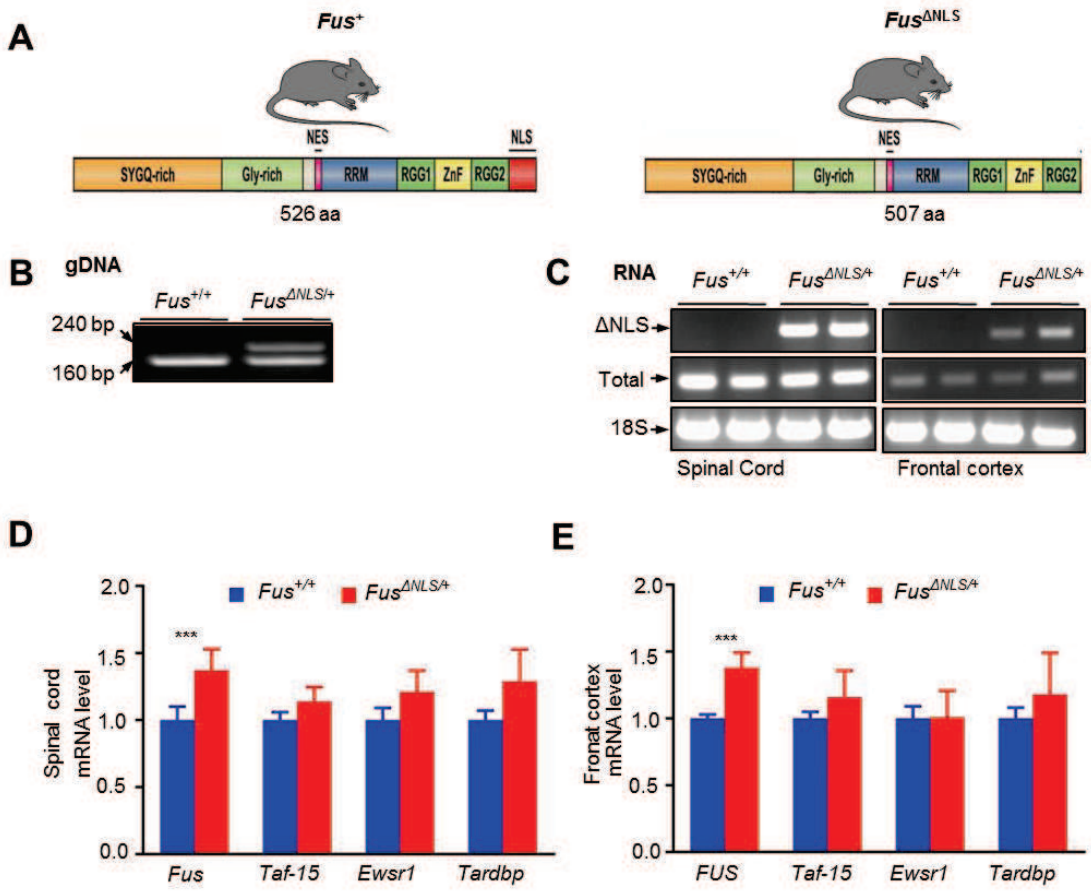

Figure 1: Genetic strategy for *Fus*$^{\Delta NLS/+}$ mice.
(A) Schematic representation of the truncated FUS protein completely devoid of NLS in *Fus*$^{\Delta NLS/+}$ knock-in mice (right panel).
(B) Representative PCR genotyping results from *Fus*$^{+/+}$and *Fus*$^{\Delta NLS/+}$ knock-in mice using primers designed around the distal loxP site of the *Fus*$^{\Delta NLS}$ allele and shown as gDNA. The expected size of the PCR product of the ΔNLS allele is 240 bp; the size of wild type allele is 160 bp.
(C) RT-PCR analysis of spinal cord and frontal cortex from 2 *Fus*$^{+/+}$and 2 *Fus*$^{\Delta NLS/+}$ knock-in 22 months mice using primers located in the STOP cassette, and thus specific to the ΔNLS mRNA (ΔNLS, upper panel), or primers located in exon 11, *i.e.* upstream of the floxed cDNA insertion, and thus amplifying total *Fus*-derived mRNA (Total, middle panel). PCR amplification of 18S rRNA is shown as standard gene (lower panel). Presence of the ΔNLS mRNA is detected in *Fus*$^{\Delta NLS/+}$ while absent in the *Fus*$^{+/+}$ tissues.
(D, E) Expression levels of total *Fus*, *Taf-15*, *Ewsr1* and *Tardbp* mRNA in spinal cord and frontal cortex.Total *Fus* were slightly increased in both tissues of *Fus*$^{\Delta NLS/+}$ knock-in mice as revealed by quantitative real-time PCR analysis. N=7 *Fus*$^{+/+}$, N=8 *Fus*$^{\Delta NLS/+}$. (*) p<0.05, (***) p<0.01; One way ANOVA followed by Tukey *post hoc* test.

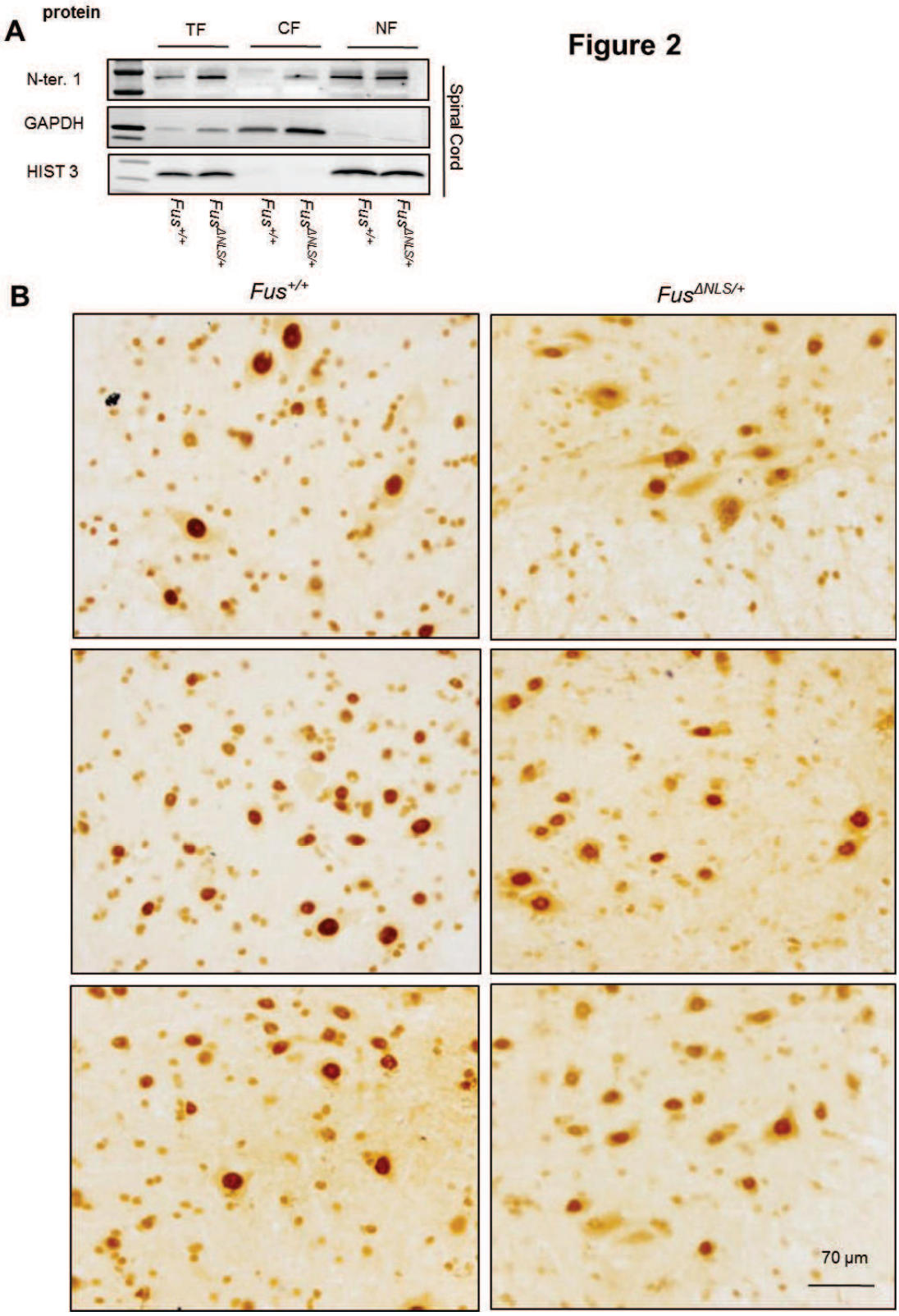

Figure 2

Figure 2: Partial cytoplasmic mislocalization of FUS in *Fus*$^{\Delta NLS/+}$mice

(**A**) Immunoblot analysis of FUS protein in total (TF), cytoplasmic (CF) and nuclear (NF) fractions from spinal cord of *Fus*$^{+/+}$ and *Fus*$^{\Delta NLS/+}$ knock-in mice using an antibody targeting the N-terminal part of FUS. Note that immunoblots show immunoreactive band in cytoplasm of *Fus*$^{\Delta NLS/+}$knock-in tissues confirming the redistribution of FUS truncated protein. Histone 3 (HIST3) was used as a loading control for nuclear fractions and GAPDH for cytoplasmic fractions. Molecular weight markers are shown on the left.

(**B**) Illustrative light microscopy images of peroxidase immunostaining of spinal cord ventral horn using an antibody against the N-terminal part of FUS. FUS redistributes to the cytoplasm in *Fus*$^{\Delta NLS/+}$. Scale bars: 70 µm.

Partial cytoplasmic mislocalization of FUS leads to mild, late onset motor deficit

We next intended to investigate whether *Fus*$^{\Delta NLS/+}$ mice develop ALS like motor symptoms during their lifespan. To this aim, we performed a large breeding effort and obtained 14 *Fus*$^{+/+}$ male mice, and 14 male *Fus*$^{\Delta NLS/+}$mice. Animals were weekly followed up for general health, neurological symptoms, body weight, grip test and accelerating rotarod performance. Until 22 months of age when mice were sacrificed, we did not observe onset of massive paralysis, nor important weight loss related to genotype (**Figure 3A-C**). The absence of robust motor phenotype was further confirmed by similar distance and velocity of *Fus*$^{+/+}$ mice and *Fus*$^{\Delta NLS/+}$ mice during open field test(**Figure 5E, 5F**).

Although, grip test and rotarod are among the most commonly used tests to assess motor function in mice (1), they often lack the sensitivity needed to detect subtle alterations in the motor system. For example, parkin deficient mice with subtle alterations in dopamine function do not display impairments on the rotarod but do display motor impairments on adhesive removal test (2). In addition, mice treated with moderate doses of the neurotoxin 1-methyl-4-phenyl-1,2,3,6-tetrahydropyridine (MPTP) do not show impairments on the rotarod but do have significant alterations in gait and impairments on an inverted grid test (3). Therefore, we turned to additional tests to evaluate motor function in *Fus*$^{\Delta NLS/+}$mice.

In an adhesive removal test we did not observe changes in initiation and completion of movement in *Fus*$^{\Delta NLS/+}$mice compared to *Fus*$^{+/+}$ for both examined ages 10 and 22 months old mice, indicating preserved basal ganglia function (2). (**Figure 4A-B**). However, *Fus*$^{\Delta NLS/+}$mice displayed a significantly shorter hanging time in an inverted grid test (**Figure 4C**) for both ages as well as shorter holding impulse (**Figure 4D**). This result was the first indication of a motor defect in *Fus*$^{\Delta NLS/+}$mice. To further confirm this motor defect, we performed Catwalk analysis to study in detail gait of the mice. We observed a decrease in the stride length in 22 months old, but not in 10 months old (**Figure 4E-H)** *Fus*$^{\Delta NLS/+}$ mice, along with an increase in body speed variation for both ages compared to the control mice (**Figure 4F**). Thus, our results indicate that partial cytoplasmic mislocalization of FUS leads to a mild, late onset progressive motor deficit in mice.

Figure 3

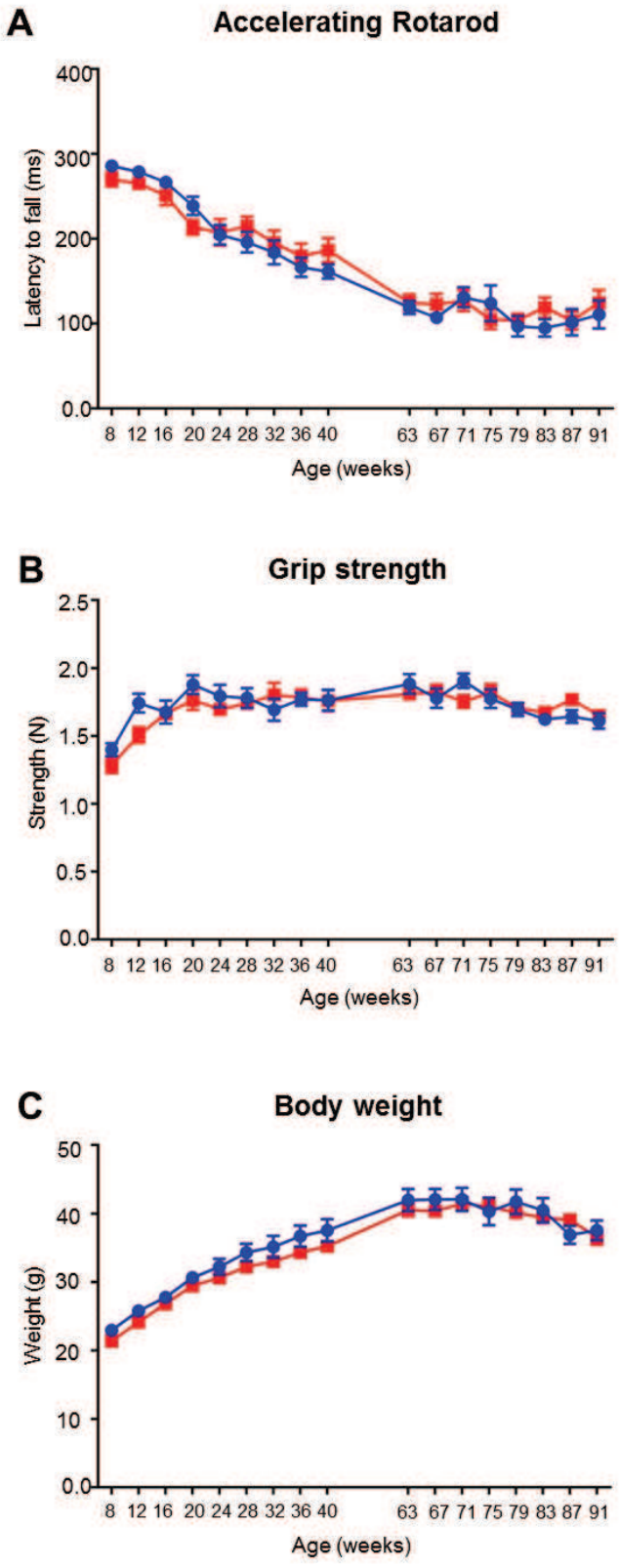

Figure 3: Motor behavioral performances in *Fus*$^{\Delta NLS/+}$ mice.
(**A**) Grip strength, (**B**) accelerating rotarod performance, (**C**) monthly weight follow up for 14 *Fus*$^{+/+}$and 14 *Fus*$^{\Delta NLS/+}$male mice. (*) p<0.05, (***) p<0.01 with respect to *Fus*$^{+/+}$; One way ANOVA followed by Tukey*post hoc* tes.

Figure 4

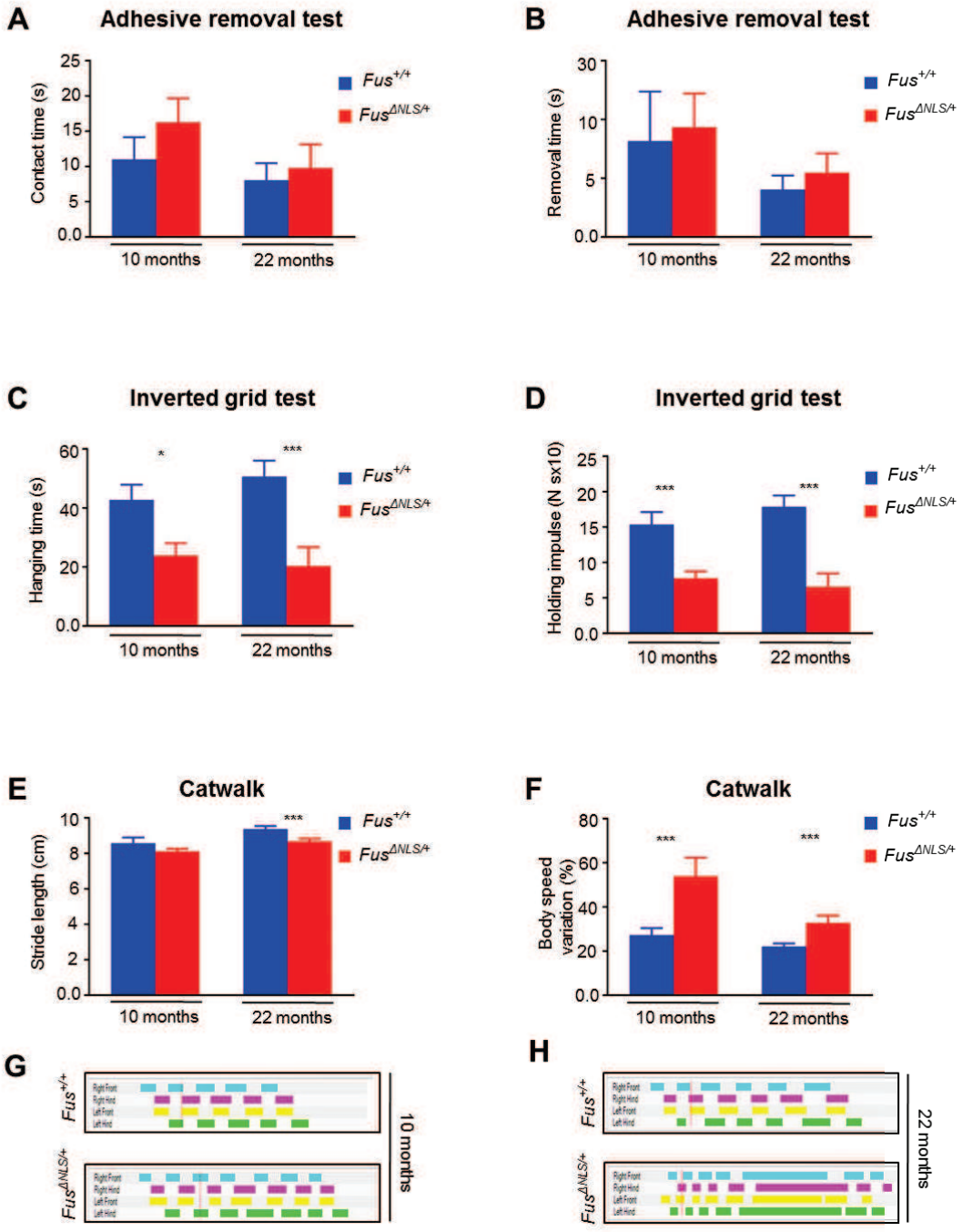

Figure 4: Mild, late motor deficit in *Fus*$^{\Delta NLS/+}$ mice.
(**A, B**) The graphs represent adhesive removal performance - time to contact (**A**) or to remove (**B**) the adhesive tape. N=3 for 10 months; N=6 for 22 months.
(**C, D**) Age-dependent changes in the mean hanging time (**C**) and holding impulse (**D**) of the four limb wire inverted grid test in *Fus*$^{+/+}$ and *Fus*$^{\Delta NLS/+}$mice. N=7 for 10 months; N=5 for 22 months.
(**E, F**)Gait changes and variability in *Fus*$^{\Delta NLS/+}$mice. (**E**) Stride length: distance between successive placements of the same paw.(**F**) Bodyspeed variation: regularity of body speed. N=3 for 10 months; N=5 for 22 months.
(**G, H**) Representative illuminations of footprints.
All graphs show the meansand standard errors at various ages (10 months; 22 months) for *Fus*$^{+/+}$ (blue histobars) and *Fus*$^{\Delta NLS/+}$ (red histobars) mice. (*) p<0.05, (***) p<0.01 with respect to *Fus*$^{+/+}$; One way ANOVA followed by Tukey *post hoc* test.

Partial cytoplasmic mislocalization of FUS induces morphological defects at the neuromuscular junction

To determine whether this mild motor behavioral phenotype could be due to an underlying motor neuron disease, we performed electromyographical analysis (EMG) on *Fus*$^{+/+}$and *Fus*$^{\Delta NLS/+}$ mice at 10 and 22 months of age. We did not observe stereotypical denervation-related electrical activities in *gastrocnemius* (GA) or *tibialis* anterior (TA) muscle of 10 month old *Fus*$^{+/+}$and *Fus*$^{\Delta NLS/+}$ mice (**Figure 5A**). However, 22 month old *Fus*$^{\Delta NLS/+}$ mice analyzed in parallel showed typical fibrillations and fasciculation in both muscles (**Figure 5A**). Consistent with qualitative observations, a quantitative analysis of pathological EMG demonstrated significantly increased frequency of abnormal EMG in 22 month old *Fus*$^{\Delta NLS/+}$ mice, but not at 10 months of age (**Figure 5B**). To determine whether alteration of EMG patter reflect morphological changes of the individual neuromuscular junctions (NMJ) we analyzed TA of 10 months and of 22 months mice for both genotypes (**Figure 6A**). We performed morphometric analysis of the post-synaptic apparatus in these mice and found that the area of the NMJ was smaller in *Fus*$^{\Delta NLS/+}$ at both ages (**Figure 6B**). However, there was no obvious effect of *Fus* genotype on either NMJs fragmentation or complexity (**Figure 6C-D**).

Thus, partial cytoplasmic mislocalization of FUS triggers electrophysiological defects in muscle, associated with morphological defects of the post-synaptic end plates of NMJs.

Figure 5

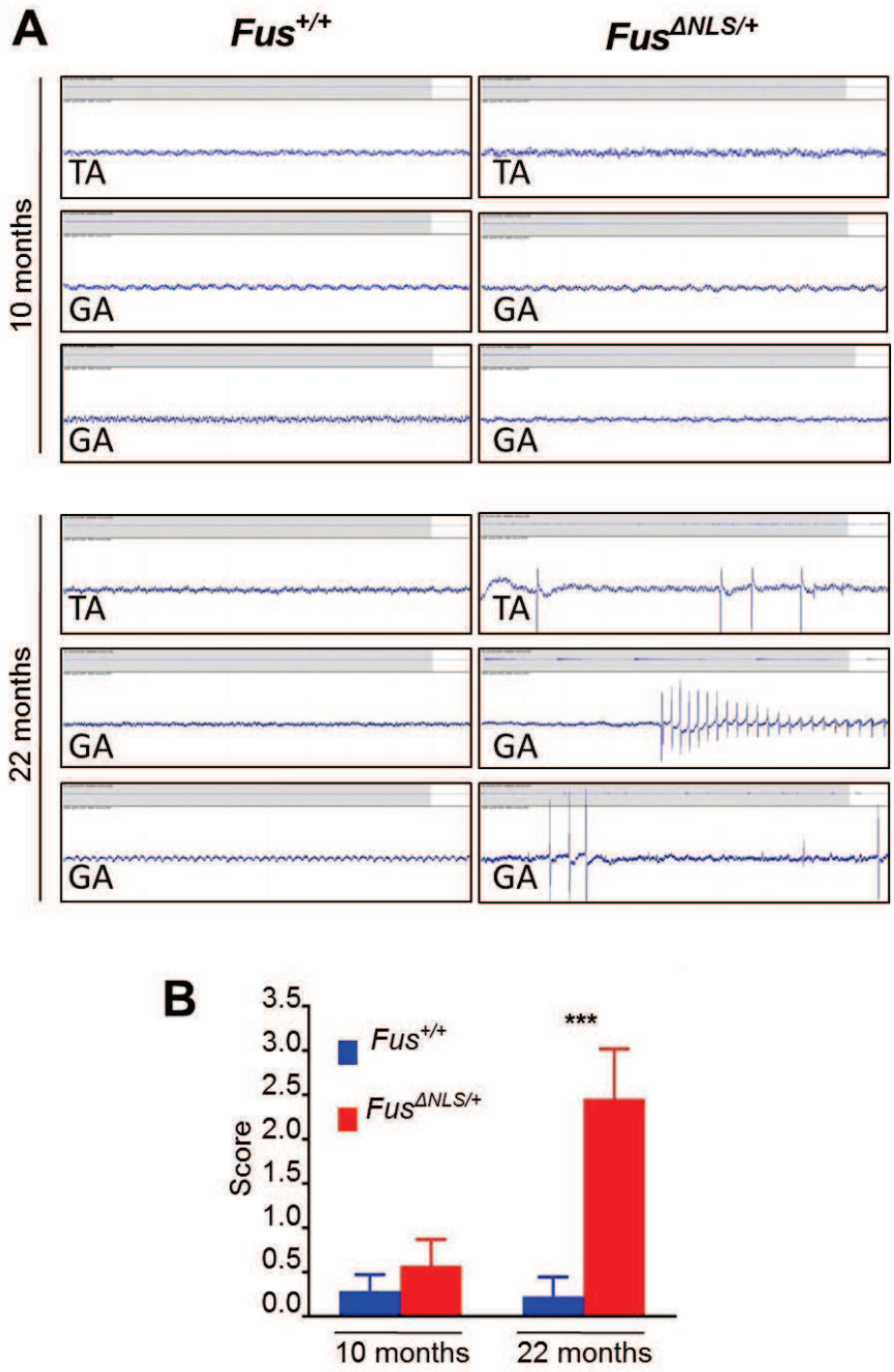

Figure 5: Electromyographical analysis (EMG) on *Fus*$^{+/+}$ and *Fus*$^{\Delta NLS/+}$ mice at 10 and 22 months of age

(**A**) Representative electromyograms of *Fus*$^{+/+}$ and *Fus*$^{\Delta NLS/+}$ mice in two gastrocnemius (GA) and one tibialis anterior (TA) muscles in 10 months (left panels) and 22 months (right panels). Note the presence of typical spontaneous denervation activities in *Fus*$^{\Delta NLS/+}$ mice muscles. Scale bars= 50ms and 50µV per division

(**B**) Graph showing valuse of EMG recording score for *Fus*$^{+/+}$ (blue histobars) and *Fus*$^{\Delta NLS/+}$ (red histobars) mice. Note significant diffrence detected only for 22 months old animals. (*) $p<0.05$, (***) $p<0.01$ with respect to *Fus*$^{+/+}$; N=7 for 10 months; N=9 for 22 months; One way ANOVA followed by Tukey *post hoc* test

Figure 6

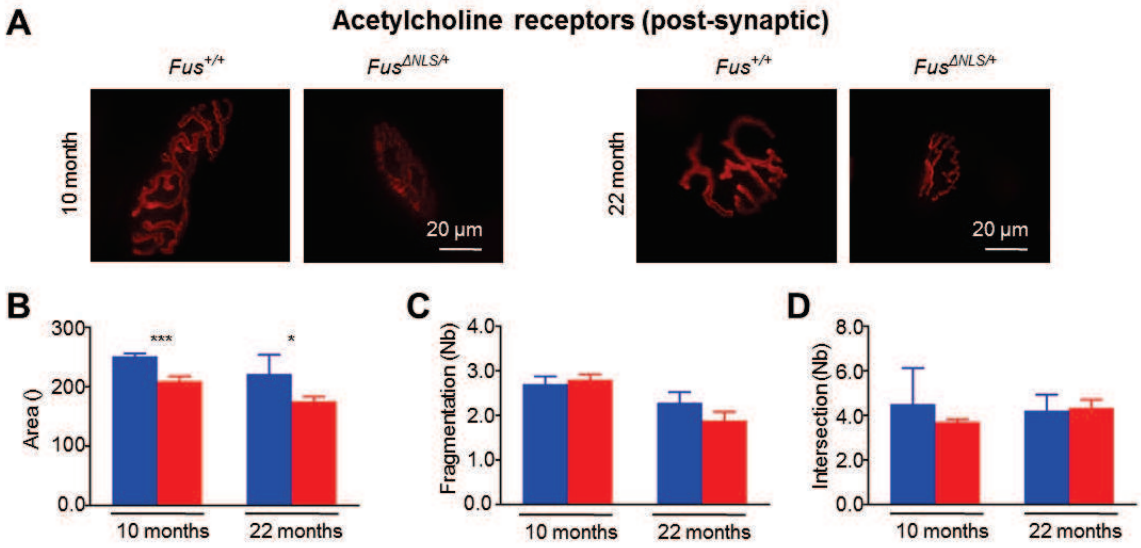

Figure 6: NMJsmorphology in *Fus*$^{\Delta NLS/+}$ mice.
(**A**) Representative epifluorescent microphotographs of NMJ post-synaptic apparatus in tibialis anterior (TA) muscles from *Fus*$^{+/+}$ and *Fus*$^{\Delta NLS/+}$ mice at 10 months of age (left panels) and 22 months of age (right panels). Note the smaller but normally pretzel-shaped morphology of NMJs. Scale bar: 20 µm.
(**B, C, D**) Quantitative morphometry of NMJs in tibialis anterior (TA) from *Fus*$^{+/+}$ and *Fus*$^{\Delta NLS/+}$ mice at 10 and 22 months showed decreased area (**B**) but preserved complexity of post-synaptic apparatus (**C, D**). (*) $p<0.05$, (***) $p<0.01$ with respect to *Fus*$^{+/+}$; N=3 for 10 months; N=3 for 22 months; Oneway ANOVA followed by Tukey *post hoc* test.

Partial cytoplasmic mislocalization of FUS drives age-dependent, progressive motor neuron degeneration

We next asked whether the mild motor deficit in *Fus*$^{\Delta NLS/+}$ mice was accompanied by degeneration of motor neurons in the lumbar spinal cord. We observed loss of lumbar spinal cord motor neurons in 22 months old *Fus*$^{\Delta NLS/+}$ mice, using either Nissl Staining (**Figure 7A-C)** or immunostaining for choline acetyltransferase (ChAT) (**Figure 7 D-F)**. Quantitative analysis using either Nissl or ChaT staining demonstrated that the number of motor neurons was reduced by ≈30% in older *Fus*$^{\Delta NLS/+}$ mice as compared with *Fus*$^{+/+}$ mice (**Figure 7C- 7F**). Importantly, the number of lumbar spinal cord motor neurons was preserved at earlier age, for 10 months old animals indicating that the pathological process is progressive. In addition, some of the remaining neurons appear shrunken and/or chromatolytic (indicated with arrows **Figure 7B)**, and we noted a decresement of synaptic buttons (indicated with arrows **Figure 7E**). Thus, partial cytoplasmic mislocalization of FUS triggers to a late onset progressive motor neuron degeneration consistent with the mild motor deficit observed.

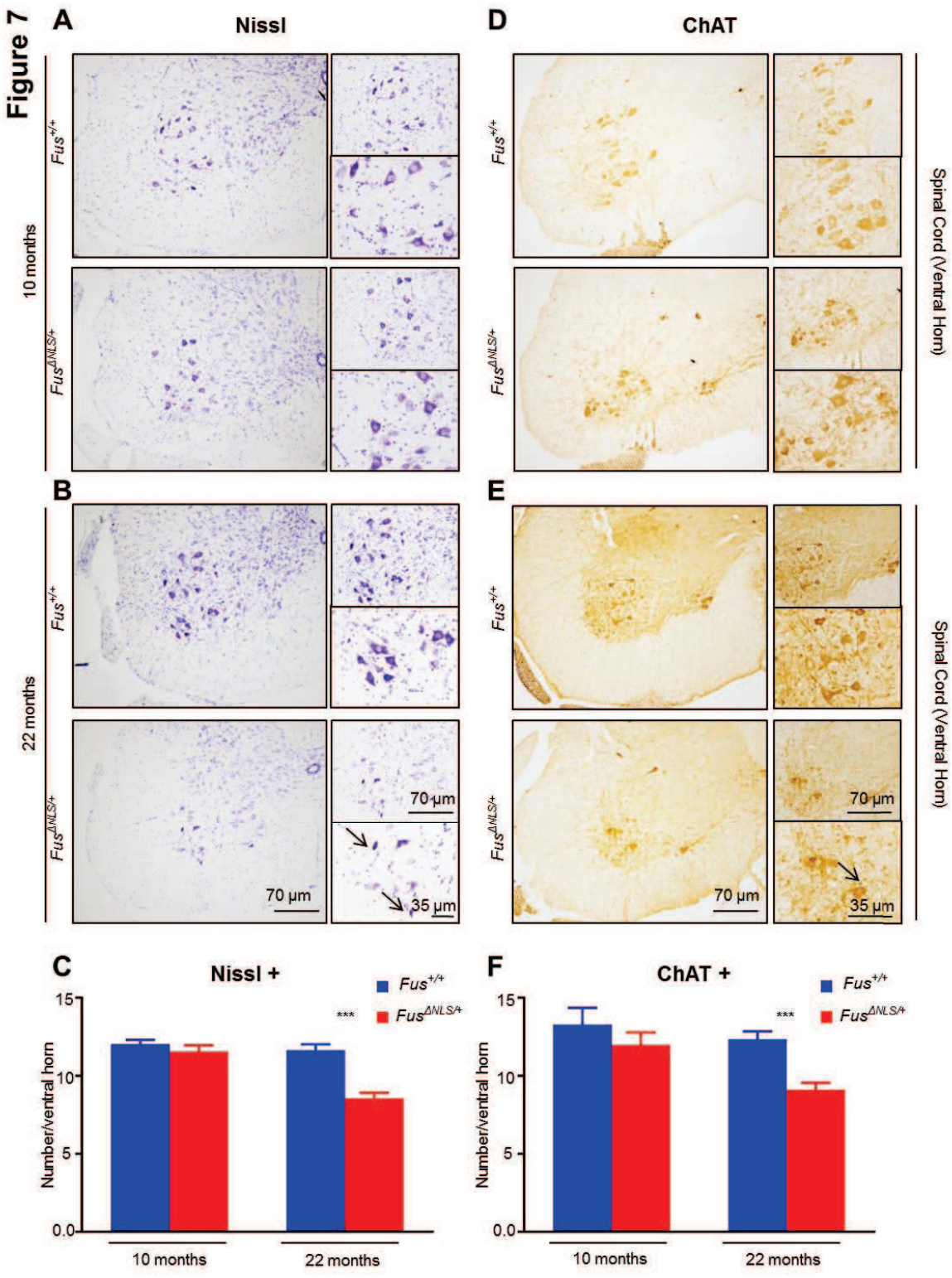

Figure 7: Degeneration and loss of spinal motorneurons in *Fus*$^{\Delta NLS/+}$ mice.
(**A-E**) Representative images of cresyl violet (**A-B**) and ChAT (**D-E**) stained sections through ventral spinal cord horn of 10 months old (**A-D**) and 22 months old (**B-E**) *Fus*$^{+/+}$ and *Fus*$^{\Delta NLS/+}$ animals. Left panels present lower and two panels on the right side higher magnification images. In the lowest panels (**B-E**) arrows show degenerative changes (shrinking, chromatolysis) and loss of synaptic buttons in surviving motor neurons of 22 months old *Fus*$^{\Delta NLS/+}$ animals.
(**C, F**) Bar charts showing means and standard errors for Nissl+ (**C**) and ChAT+(**F**) motor neuron number in the ventral horn of the spinal cord at various ages (10 months; 22 months) for *Fus*$^{+/+}$(blue histobars) and *Fus*$^{\Delta NLS/+}$ (red histobars) mice. (*) $p<0.05$, (***) $p<0.01$ with respect to *Fus*$^{+/+}$; N=3 for 10 months; N=6 for 22 months; Oneway ANOVA followed by Tukey*post hoc* test. Scale bars: lower magnification : 70µm; higher magnification : 70µm and 35µm.

Partial cytoplasmic mislocalization of FUS leads to hyperactivity, in the absence of anxiety like behaviours

Since FUS mislocalization and aggregation is also observed in a subset of FTLD patients, we then asked whether *Fus*$^{\Delta NLS/+}$ mice might develop FTLD-like symptoms. A number of FTLD patients display behavioural disinhibitions, in particular impulsivity and unawareness of consequences of their actions. This type of behavior is measured in mice with anxiety tests. A reduced anxiety in mice is often interpreted as disinhibition. We used an open field and the dark/ light box test to assess the state of disinhibition of *Fus*$^{\Delta NLS/+}$ mice. In an open field, mice tend to show preference for peripheral quadrants over central quadrants, considered as more anxiogenic. *Fus*$^{\Delta NLS/+}$ mice showed identical preference as wild type littermates for the peripheral quadrants, either at 10 months or at 22 months of age (**Figure 8A-F**). To further confirm this initial test, we used the dark/light box, a test more sensitive than open field for evaluating anxiety levels. This test is based on the preference of mice for dark compartments over illuminated places. In this test, *Fus*$^{\Delta NLS/+}$ mice showed a trend towards shorter latency to enter illuminated compartment (**Figure 9A**), as well as tended to explore more the illuminated compartment (**Figure 9B-C**) as well as transitioning more frequently from light to dark compartments (**Figure 9D**). None of these parameters however reached significance, suggesting that the decrease in anxiety of *Fus*$^{\Delta NLS/+}$ mice, if any, is very low. We then recorded spontaneous activity in the homecage during three consecutive days. Interestingly, *Fus*$^{\Delta NLS/+}$ mice displayed significant hyperactivity during early morning, just before the light was turned on, from 5 am to 7 am (**Figure 9E)**. In all, partial cytoplasmic FUS mislocalization leads to barely normal anxiety levels, along with increased spontaneous activity.

Figure 8

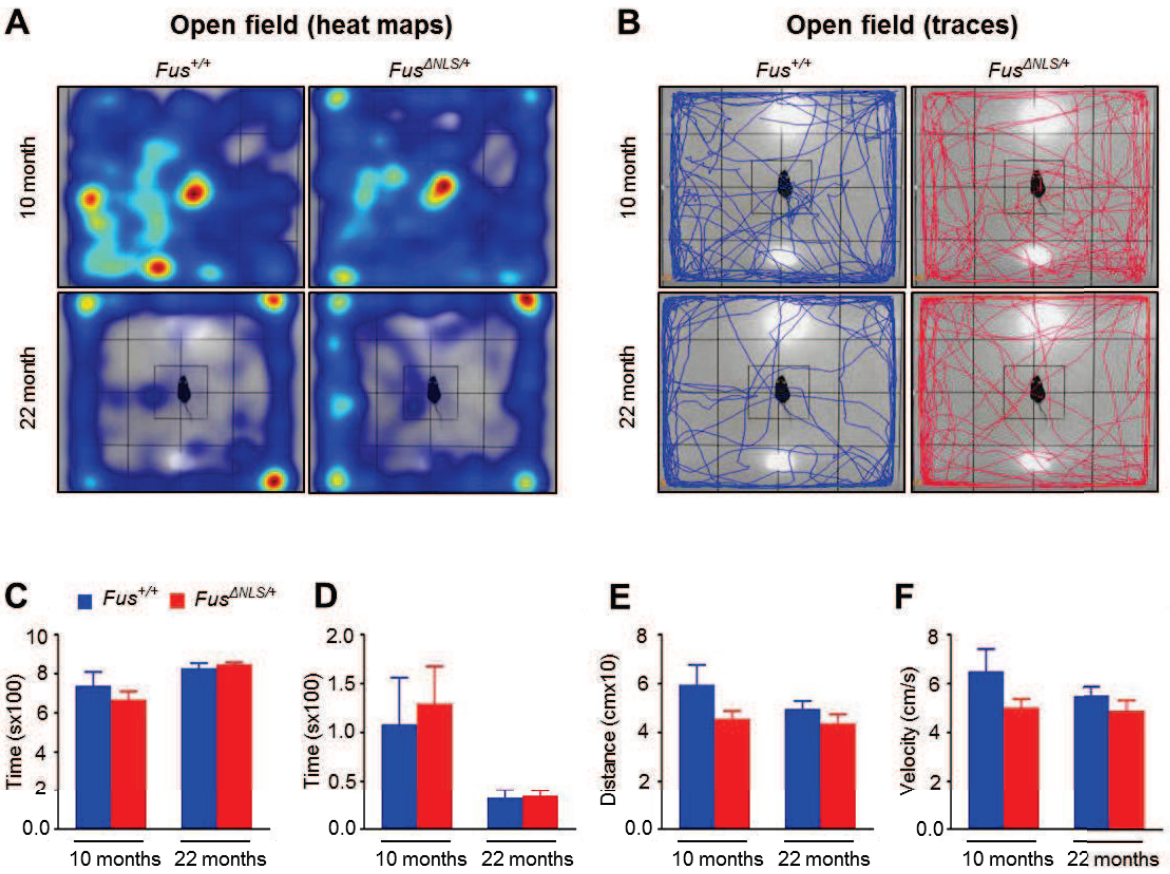

Figure 8: Lack of anxiety in *Fus*$^{\Delta NLS/+}$ mice.
(**A-B**) Representative images of heat maps (**A**) and trajectory trackings (**B**) in the open field of 10 month sold (upper pannels) and 22 monthsold (lower pannels) *Fus*$^{+/+}$ and *Fus*$^{\Delta NLS/+}$ animals.
(**C-E**) Bar chart showing mean sand standard errors of time spent in peripheral quadrants (**C**) and central quadrants (**D**) of the open field at various ages (10 months; 22 months) for *Fus*$^{+/+}$(blue histobars) and *Fus*$^{\Delta NLS/+}$ (red histobars) mice. Total distance traveled is shown (**E**) and avarage speed velocity (**F**). (*) $p<0.05$, (***) $p<0.01$ with respect to *Fus*$^{+/+}$; N=3 for 10 months; N=6 for 22 months; Oneway ANOVA followed by Tukey *post hoc* test.

Figure 9

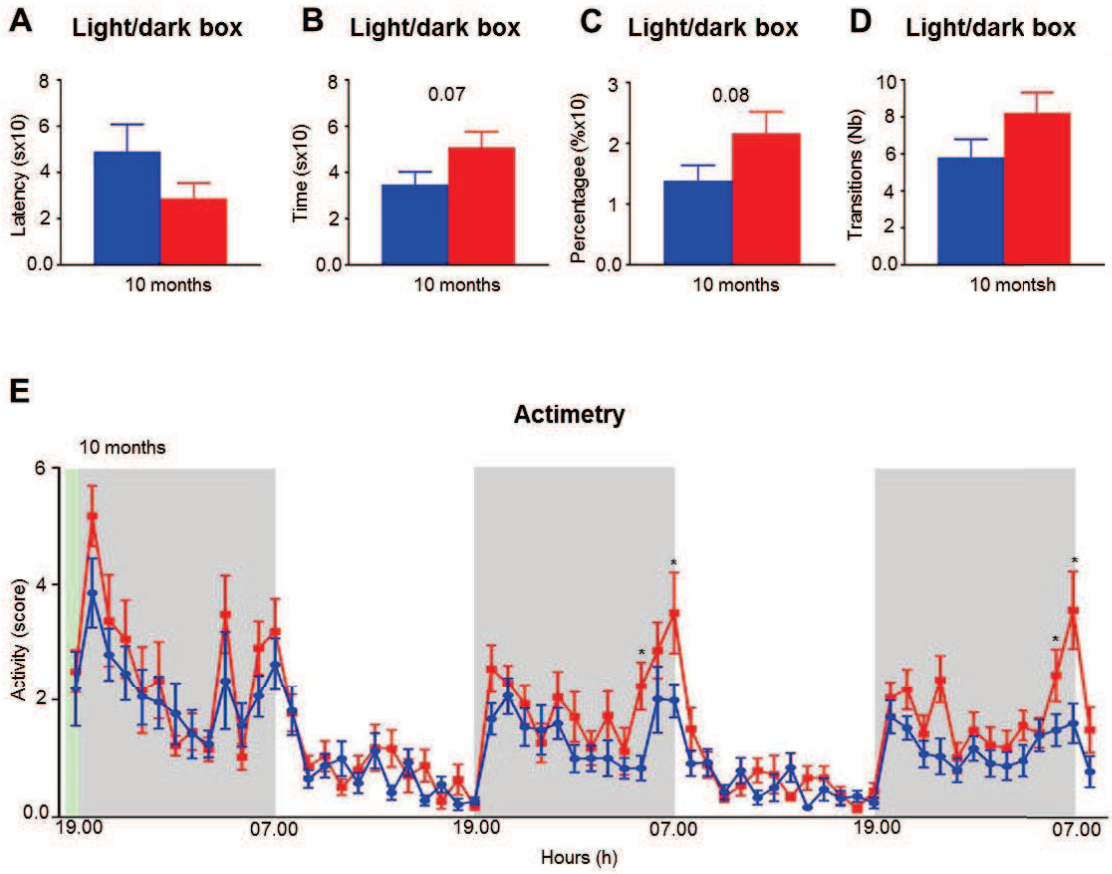

Figure 9: Lack of anxiety in *Fus*$^{\Delta NLS/+}$ mice.
(**A, B**) Bar chart showing means and standard errors of latency time to enter the illuminated compartment (**A**), absolut time spent in the illuminated compartment (**B**), percentage of total exploration time spent in the illuminated compartment (**C**) and number of transitions between dark and the illuminated compartments (**D**) in the dark-light box at 10 monthsfor *Fus*$^{+/+}$(blue histobars) and *Fus*$^{\Delta NLS/+}$ (red histobars) mice. (*) p<0.05, (***) p<0.01 with respect to *Fus*$^{+/+}$; N=14-15 for 10 months; Student t-test.
(**E**) Graph represents mice activity during three consecutive days at 10 months old *Fus*$^{+/+}$ (blue lines) and *Fus*$^{\Delta NLS/+}$ (red lines) mice. (*) p<0.05, (***) p<0.01 with respect to *Fus*$^{+/+}$; N=14-15 for 10 months. Oneway ANOVA followed by Tukey *post hoc* test.

Partial cytoplasmic mislocalization of FUS leads to impairment of social behaviour

Marked changes in social behaviour such as either social withdrawal or social disinhibition, obsessive-compulsive behaviours, euphoria or apathy are common in subjects with bvFTD (4,5). Social deficits were also reported in progranulin haploinsufficient mice, an independent mouse model of FTLD (6). To determine whether our mice have disease-relevant social behavioral deficits we performed tests specific for evaluating sociability in mice. In order to exclude possible olfactory dysfunction that can affect social behavior we first performed olfactory preference test. Results showed no differences between genotypes at 22 months of age in the time spent sniffing filter paper covered with either attractive scent (vanilla) or an aversive scent (2-methyl butyrate) **(Figure 10**) suggesting that the olfactory function of *Fus*$^{\Delta NLS/+}$ mice was preserved.

To evaluate social behaviour of *Fus*$^{\Delta NLS/+}$ mice, we first used the resident-intruder test (**Figure 11A**). Interestingly, two distinct cohorts of 10 months old *Fus*$^{\Delta NLS/+}$ mice displayed higher interaction times with the intruder as compared with *Fus*$^{+/+}$ mice (**Figure 11B**). Such a social disinhibition was no longer observed in 22 months old mice (**Figure 11C**). To further characterize the social behavioral impairement, we used a modified version of the three-chamber social paradigm (**Figure 12A**). In this test, the test mouse is introduced in the middle compartment of a set up composed of 3 communicating chambers. After a first trial of habituation using an empty set up, a stranger mouse is introduced in a second compartment. The interactions initiated by the test mouse with either the stranger mouse or the empty cage are quantified. In Trial 2, both *Fus*$^{+/+}$ and *Fus*$^{\Delta NLS/+}$ mice interacted three to four times more with the stranger mouse than with the empty cage (**Figure 12 B-C**). Across the different trials, we observed that 10 months *Fus*$^{\Delta NLS/+}$ mice consistently interacted more with the stranger mouse than *Fus*$^{+/+}$ mice (**Figure 12 D-E**). This was not observed at 22 months of age. Thus, both resident intruder test and 3 chamber test indicate that *Fus*$^{\Delta NLS/+}$ mice display social disinhibition that disappears with older mice.

The 3 chamber test was also used to evaluate social memory. In a fifth trial, both a familiar mouse (Stranger 1) and an unknown mouse (Stranger 2) were introduced in the two empty compartments (**Figure 13A**). The time spent interacting with either mice is then measured. If the interaction time is higher with the Stranger 2 than with Stranger 1, this suggests that the tested mouse was able to recognize Stranger 1 as familiar. In this test, *Fus*$^{\Delta NLS/+}$ mice and *Fus*$^{+/+}$ mice displayed similarly increased interaction with the novel mouse, suggesting preserved social memory at both ages, independent of the genotype (**Figure 13B-C**). In all, these results indicate that partial cytoplasmic mislocalization of FUS leads to a selective transient impairment in sociability that could recapitulate some of the clinical symptoms of bvFTD, like social disinhibition that already have been reported in patients (5).

Figure 10

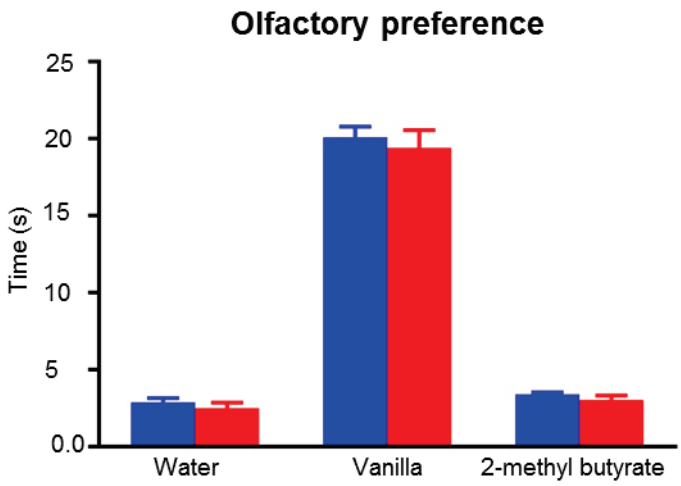

Figure 10: Olfactory preference test in *Fus*$^{\Delta NLS/+}$ mice.
(**A**) Analysis of olfactory preference in *Fus*$^{+/+}$ and *Fus*$^{\Delta NLS/+}$mice at 22 months. All values are means and standard errors. (*) p<0.05, (***) p<0.01 with respect to corresponding *Fus*$^{+/+}$; N=6 for 22 months; Student t-test.

Figure 11

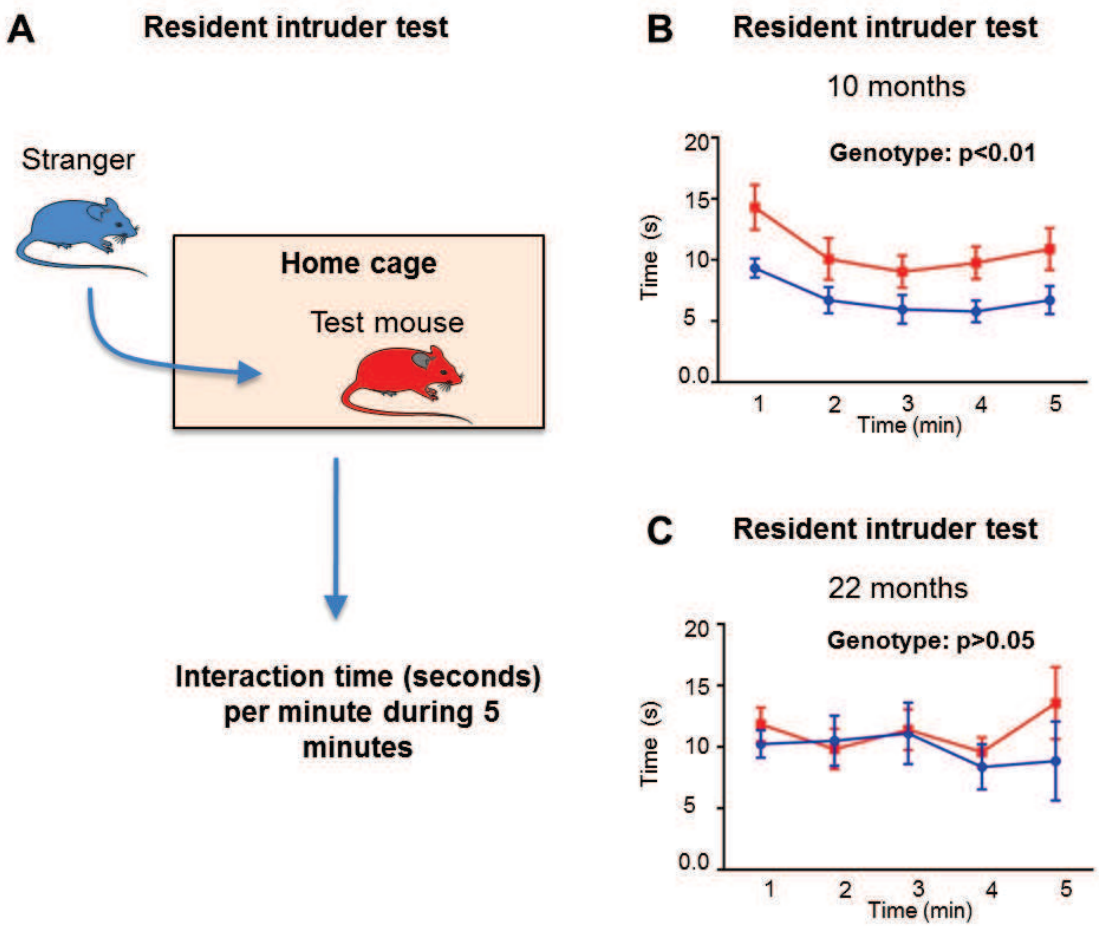

Figure 11: *Fus*$^{\Delta NLS/+}$ mice showed age-dependent impairment of social behaviour – resident intruder test.
(**A**) Schematic representation of resident intruder test
(**B-C**) Interaction in home cage task in 10 (**B**) and 22 (**C**) months old *Fus*$^{+/+}$ (blue lines) and *Fus*$^{\Delta NLS/+}$ (red lines) mice. The difference in interaction time (defined as the time the test mouse explores the intruder mouse in 1-min intervals) is significant at the first and two last points of the task (1, 4 and 5 min time points in 10 months old animals (**B**). (*) p<0.05, (***) p<0.01 with respect to *Fus*$^{+/+}$; N=15 for 10 months; N=10 for 22 months; Student t-test.and Twoway ANOVA.

Figure 12

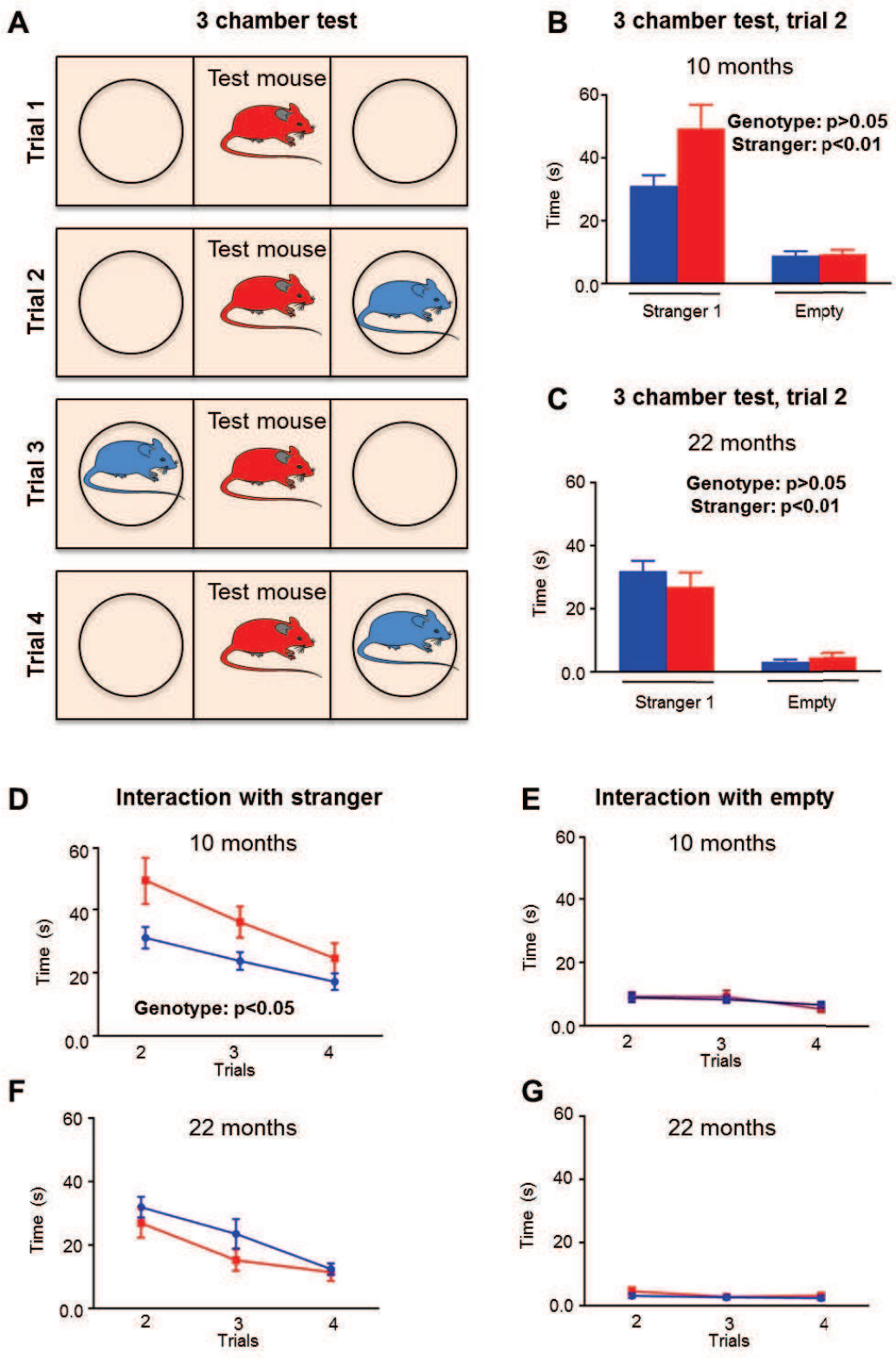

Figure 12: *Fus*$^{\Delta NLS/+}$ mice showed age-dependent impairment of social behavior – three chamber task.
(**A**) Schematic representation of three chamber task across the trials
(**B-C**) Social recognition, namely time spent interacting with Stranger 1 and time exploring empty wired cage (object) in Trial 2 , 10 months (**B**) and 22 months (**C**) for *Fus*$^{+/+}$(blue histobars) and *Fus*$^{\Delta NLS/+}$ (red histobars) mice. (*) p<0.05, (***) p<0.01 with respect to Stranger 1; N=15 for 10 months; N=10 for 22 months; Oneway ANOVA followed by Tukey*post hoc* test
(**D-E**) Sociability of *Fus*$^{+/+}$ (blue lines) and *Fus*$^{\Delta NLS/+}$ (red lines) mice, 10 months (**D**) and 22 months (**E**) are measured based on interaction time with Stranger 1 across trials. N=15 for 10 months; N=10 for 22 months; Twoway ANOVA
(**F-G**)Time exploring empty wired cage (object) across trials of *Fus*$^{+/+}$ (blue lines) and *Fus*$^{\Delta NLS/+}$ (red lines) mice 10 months(**G**) and 22 months(**H**). N=15 for 10 months; N=10 for 22 months; Twoway ANOVA.

Figure 13

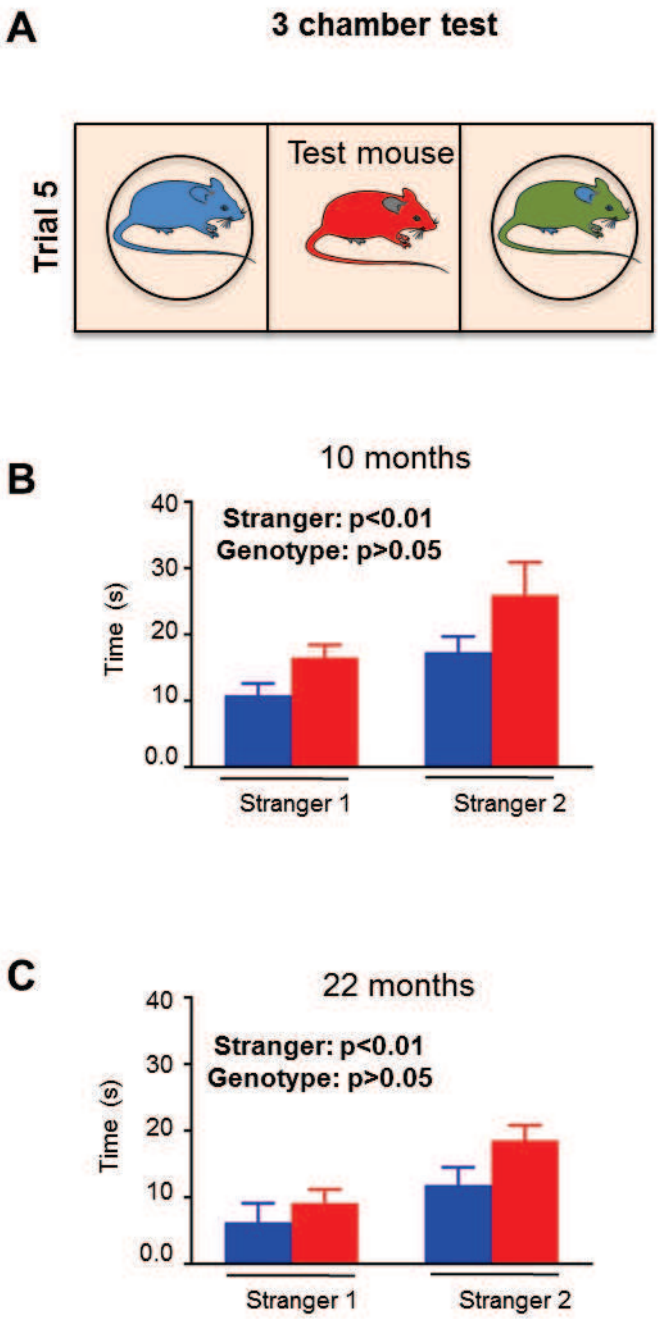

Figure 13: *Fus*$^{\Delta NLS/+}$ mice showed age-dependent impairment of social behavior – three chamber task.
(**A**) Schematic representation of three chamber task in the Trial 5
(**B-C**) Graphs showing interaction time spent with Stranger 2 in Trial 5 that was measured as an indicator for social memory and novelty in *Fus*$^{+/+}$ (blue histobars) and *Fus*$^{\Delta NLS/+}$ (red histobars) for 10 months (**B**) and 22 months (**C**) mice. N=15 for 10 months; N=10 for 22 months; All values are mean and standard errors. Twoway ANOVA.

Partial cytoplasmic mislocalization of FUS leads to cognitive defect and altered memory consolidation.

To further explore the possibility that a subset of phenotypes of *Fus*$^{\Delta NLS/+}$ mice is related with frontal lobe dysfunction, we tested spatial reference memory in the Morris water maze. This task requires the hippocampal function, at least during acquisition and to form a recent memory, but relies on a proper (fronto)cortico-hippocampal dialog for longer retention times or remote memory (7). As shown in **Figure 14A-C**, *Fus*$^{\Delta NLS/+}$ mice displayed a significant acquisition regarding distance travel and latency to find hidden platform over training days similar to their *Fus*$^{+/+}$ littermates. We then performed a probe trial 18 days after the last training followed by two extinction tests and observed that *Fus*$^{\Delta NLS/+}$ mice displayed a significantly decreased performance at this retention time point (**Figure 14D**). Furthermore, *Fus*$^{\Delta NLS/+}$ mice extinguished their previous memory much faster than wild type mice as an extinction test performed 2 hours after the probe trial showed a weaker memory trace in wild type mice, while *Fus*$^{\Delta NLS/+}$ mice did not show a performance superior to chance (**Figure 14E**), and this was maintained in a second extinction test (**Figure 14F**). All together, these data show that *Fus*$^{\Delta NLS/+}$ mice are able to learn, but display alterations in the persistence of memory consolidation in agreement with a dysfunction in the fronto-cortical regions.

Figure 14

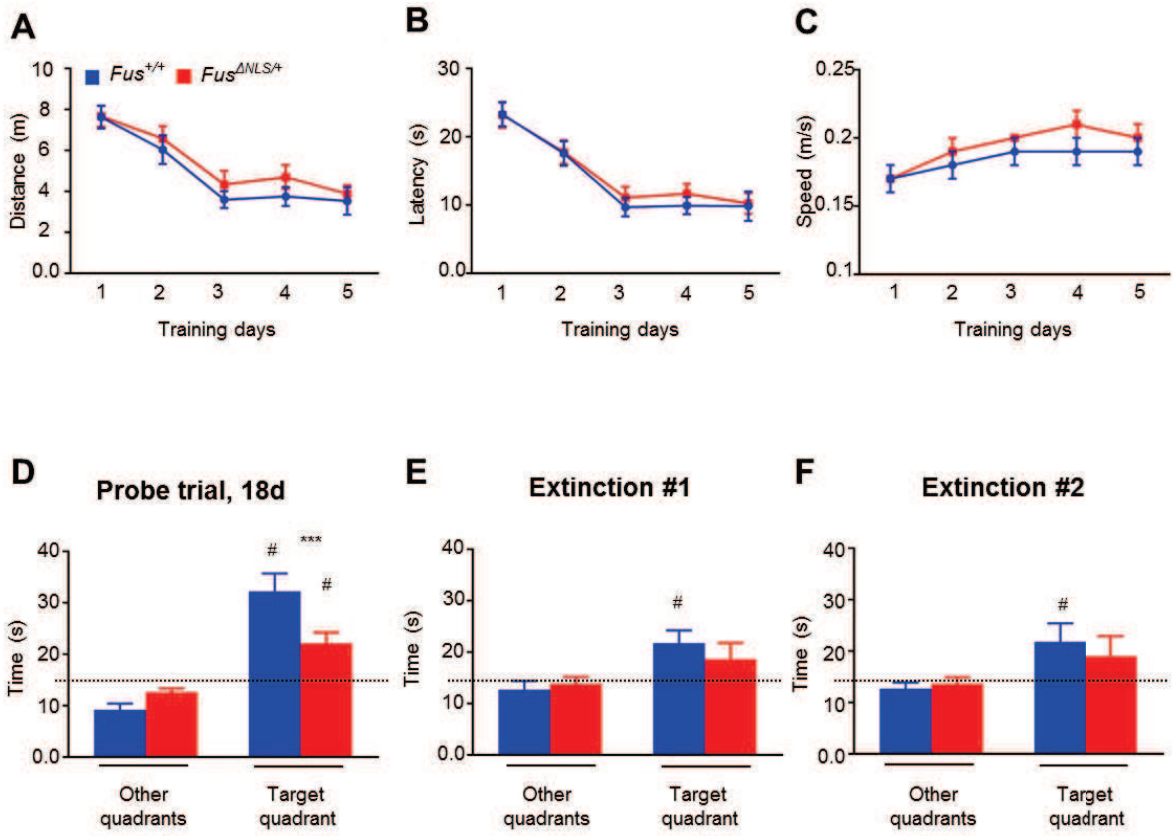

Figure 14: Cognitive defect, altered memory consolidation in *Fus*$^{\Delta NLS/+}$mice.
(**A**) Distance swimed (in meters) (**B**)latency (in seconds) and (**C**) speed velocity (in meters per secons) to find the platform of 10 *Fus*$^{+/+}$ and 11 *Fus*$^{\Delta NLS/+}$male mice tested for spatial reference memory in the Morris water maze. Both genotypes improved similarly their performance between day 1 and 5. *Fus*$^{+/+}$(blue lines) and *Fus*$^{\Delta NLS/+}$ (red lines) mice 10 months. N=10 ; Twoway ANOVA (**A**)« days»: F(4,76)=24,35; p=0,00000 « genotype »: F(1,19)=1,10; p=0,64 (**B**)« days »: F(4,76)=35,62; p=0,00000 « genotype »: F(1,19)=0,21; p=0,64(**C**) « days »: F(4,76)=16,41; p=0,00000 « genotype »: F(1,19)=1,13; p=0,29
(**D**) Mice were tested for retention in a probe trial (60sec) performed 18 days after the last training session as indicated. The time spent in the target quadrant (target) is represented and compared with the average of the time spent in the three other quadrants (others). Chance is shown as a dashed line (15s per quadrant; i.e.25%). *Fus*$^{\Delta NLS/+}$mice performed significantly worse than +/+ littermates. *Fus*$^{+/+}$ (blue histobars) and *Fus*$^{\Delta NLS/+}$ (red histobars) for 10 months N=10. (***) Oneway ANOVA genotype effect F(1,19)=6,33, p=0,02 ; Student t test comparaison to chance level (#) Target quadrant: *Fus*$^{+/+}$=0,0008 Mean 3 others: *Fus*$^{+/+}$=0,0008 Target quadrant: *Fus*$^{\Delta NLS/+}$=0,006 Mean 3 others: *Fus*$^{\Delta NLS/+}$=0,005
(**E-F**) Two extinction test: the first 2 hours after completing probe trial and the second 2 hours after the first.

Partial cytoplasmic mislocalization of FUS triggers fronto-temporal atrophy

Since our results suggested that the partial mislocalization of FUS to the cytoplasm leads to a neurological deficit that could be reminiscent of FTD, we began to study fronto-temporal lobe morphology. Interestingly, we observed significant frontotemporal lobes atrophy in *Fus*$^{\Delta NLS/+}$ mice at both 10 and 22 months of age (**Figure 15A-C**). Interestingly, younger mice showed asymmetrical pattern of atrophy (**Figure 15B**), while in older animals it was presented along whole length of frontal and temporal lobes bilaterally (**Figure 15C**). This shows that *Fus*$^{\Delta NLS/+}$ mice develop progressive fronto-temporal atrophy, and histopathological analysis of these brains is currently ongoing to characterize the neuroanatomical substrate of this atrophy.

In all our current results demonstrate that the partial cytoplasmic mislocalization of FUS is sufficient to trigger a mild and progressive motor deficit associated with motor neuron degeneration, reminiscent of FUS-ALS. Intriguingly, partial cytoplasmic mislocalization of FUS also triggers behavioural and anatomical impairments suggestive of FTLD.

Figure 15

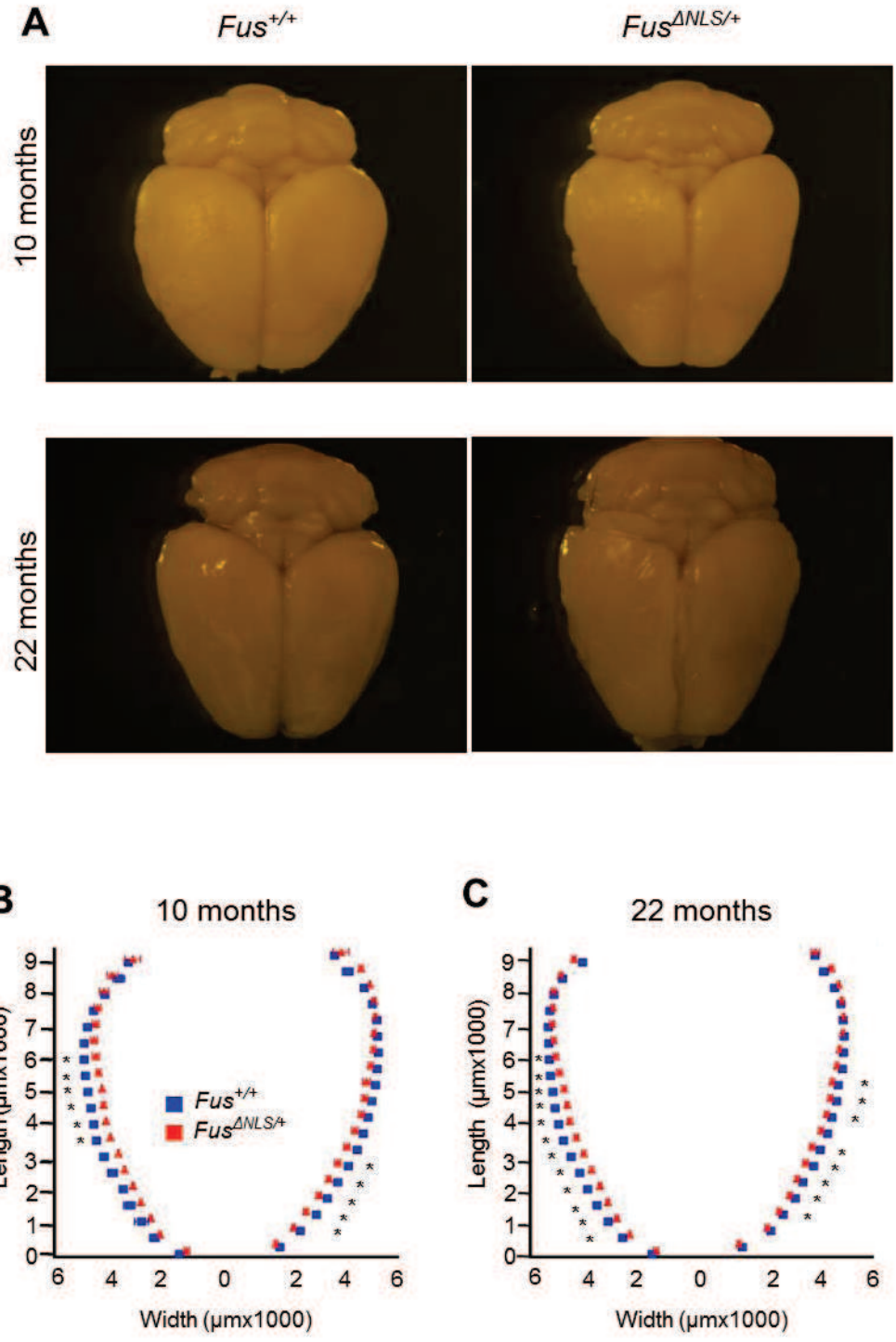

Figure 15: Asymmetrical frontotemporal brain atrophy in *Fus*$^{\Delta NLS/+}$ mice.
(**A**) Representative images of whole brain for *Fus*$^{+/+}$ and *Fus*$^{\Delta NLS/+}$mice in 10 month (upper panels) and 22 months (lower panels).
(**B-C**) Graphs showing level of atrophy in *Fus*$^{+/+}$(blue lines) and *Fus*$^{\Delta NLS/+}$ (red lines) for 10 months (**B**) and 22 months(**C**) mice. N=3 for 10 months; N=6 for 22 months; All values are mean and standard errors. (*) $p<0.05$, (***) $p<0.01$ with respect to*Fus*$^{+/+}$Oneway ANOVA followed by Tukey*post hoc* test.

Material and methods

Animal housing and genotyping

Wild type and heterozygous *Fus*$^{\Delta NLS/+}$mice, generated as described previously (Scekic-Zahirovic et al., 2015), were bred and housed in the central animal facility of the faculty of medecine of Strasbourg, with a regular 12-h light and dark cycle (light on at 7:00 am) under constant conditions (21 ± 1 °C; 60% humidity). Standard laboratory rodent food and water were available ad libitum throughout all experiments. These protocols were approved by the local ethical committee (Cremeas), under reference number AL/27/34/02/13.

Mice were genotyped by PCR of genomic DNA from tail biopsies as described previously (Scekic-Zahirovic et al., 2015).

Ten- to twenty two-months-old male littermates of each genotype (*Fus*$^{+/+}$and *Fus*$^{\Delta NLS/+}$) on a pure genetic background (C57/Bl6) were subjected to behavioral tests and molecular analyses. Behavioral test were done during the light phase of their light/dark cycle except for indicated experiments, in collaboration with JC Cassel and AL Boutillier (Laboratoire de Neurosciences Cognitives et Adaptatives, UMR7364, CNRS, Université de Strasbourg).

RT-PCR analysis

RT-PCR analysis was done in microdissected frontal cortex and spinal cord tissue from *Fus*$^{+/+}$ and 2 *Fus*$^{\Delta NLS/+}$ and *Fus*$^{\Delta NLS/\Delta NLS}$ using primers located in the STOP cassette, and thus specific to the ΔNLS mRNA (ΔNLS), or primers located in exon 11, *i.e.* upstream of the floxed cDNA insertion, and thus amplifying total *Fus*-derived mRNA (Total Fus) and PCR amplification of 18S rRNA as standard gene. The correspondent primer list was published previously (Scekic-Zahirovic et al., 2015).

Frontal cortex and spinal cord were harvested, rapidly frozen in liquid nitrogen and stored at -80°C until the time of analysis. For RT-qPCR, frozen tissues were placed into tubes containing a 5 mm stainless steel bead (Qiagen, Courtaboeuf, France) and 1 ml of Trizol reagent (Invitrogen, Paisley, UK) and homogenized using a TissueLyser (Qiagen). RNA was prepared on tissue homogenates following Trizol manufacturer's instructions. RNA reverse transcription and SYBR Green real-time PCR assays were performed using the Bio-Rad (Biorad, Marnes la Coquette, France) iCycler kits and protocols. PCR conditions were 3 min at 94°C, followed by 40 cycles of 45 s at 94°C and 10 s at 60°C. Three standard genes: 18S (18S Ribosomal RNA), Pol2 (Polr2 polymerase RNA 2 DNA directed polypeptide A) and Tbp (TATA-box binding protein) were used to compute a normalization factor using Genorm software v3.5. Primers sequences are provided in (Scekic-Zahirovic etal., 2015).

Western blot- nuclear-cytosolic fractionation

Fresh spinal cord were homogenized by using a pre-chilled 1 ml Dounce homogenizer in a detergent-free lysis buffer A containing 10 mM Hepes-KOH pH 7.4, 10 mM KCl, 1.5 mM MgCl, 0.5 mM EDTA, 0.5 mM EGTA, 1X protease inhibitors (Roche, Berlin, Germany). A part of lysate was saved as total fraction. The homogenates were centrifuged at 1000G for 5 min at 4 °C. The supernatant was spin down at 1000G for 5 min at 4°C and then saved as the cytosol fraction. The pellet was resuspended in five pellet volumes of buffer B (10 mM Hepes-KOH, pH 7.4, 0.42 M NaCl, 2.5% v/v glycerol, 1.5 mM MgCl, 0.5 mM EDTA, 0.5 mM EGTA, 1 mM dithiothreitol, 1× protease inhibitors) and incubated for 60 min at 4°C while rotating at 60 rpm. The sample was centrifuged at 14,000 rpm for 10 min at 4°C, and the supernatant was saved as the nuclear fraction(8).

Equal amounts of protein (10µg) were separated by electrophoresis on SDS-PAGE 10% and blotted onto a nitrocellulose membrane. Membranes were saturated with 10% non-fat milk and then incubated with the primary antibodies against the N-terminal part of FUS (Bethyl A303-839A; 1:1000) diluted in 3% non-fat milk followed by anti-goat (Sigma A5420) secondary antibody diluted 1:5000. Antibodies against Histone 3 (Cell signaling, #9715; 1:1000) was used as loading control for nuclear fraction and GAPDH (Invitrogen, #398600; 1:1000) was used as loading control for cytoplasmic fraction. All blots were analyzed with chemiluminescence (ECL; Luminata Forte Kit, Millipore WBLUF0500) using the Molecular Imager Chemidoc XRS (Biorad) as detection system.

Motor coordination and muscle strength analysis

Mice were followed weekly for general health, neurological symptoms, body weight, grip test and accelerating rotarod performance starting from weaning (4 weeks of age) until 22 months of age as described previously (9,10). Briefly, mouse motor performance was assessed using rotarod (Ugobasile model 7650). Each session consisted of three tests of 300 s with an acceleration period (4 to 20 rpm during 150 s) followed by 150 s at constant speed. To evaluate muscle strength, we used a gripmeter test (Bioseb, ALG01; France). The muscle force (in Newton) was measured three times per mouse. Results are presented as one measurement point per month.

Adhesive removal test

Adhesive removal test was performed for two different ages 10 and 22 months old mice as described (Bouet V et al., 2009; Fleming SM et al., 2013). Mouse was placed alone in a clean cage with ~3/4 of the bedding. The test mouse was scruffed in order to restrain it and using a pair of small forceps one adhesive label was placed and gently pressed onto the snout of the mouse. After mouse was released in the cage. Time was recorded twice :

when the mouse made an attempt to remove the label with its forepaws as contact time (or initial time) and when mouse succeded to remove the label as removal (or total time). If the mouse did not contact or remove the sticker within 60 sec the trial was ended and the sticker was removed manually by the experimenter (2,11).

Inverted grid test

The four limb hang test uses a wire grid system to non-invasively measure the ability of mice to exhibit sustained limb tension to oppose to their gravitational force. The procedure measures the 4 limb hang time in seconds as well as the minimal holding impulse. Each mouse was placed at the simple cage grid and was allowed to accommodate to this environment for 3–5 s before the grid was inverted and held approximately 35 cm over a mouse cage containing 5–6 cm of bedding (wood chips). Each of these holding periods began with all four paws of the mouse grasping the grid. Typically, the mice lose their grasp of the mesh one or two paws at a time. Shortly before the fall, most mice usually have only one or two paws grasping the screen. The wire grid hanging time (or "hang time") was defined as the amount of time that it takes the mouse to fall from the inverted grid and was measured visually with a stop watch. In each session, the procedure was repeated three times with approximately 10 min between each assessment of holding time. The mouse body weight was obtained shortly before or after the test. The physical impulse (minimal holding impulse) is the hanging time multiplied by the gravitational force of the mouse (body mass (g) ×0.00980665N/g×hanging time (s)) and represents the minimal total sustained force that was exerted to oppose the gravitational force (12,13).

Gait analysis

Gait parameters of freely moving mice were measured using the Catwalk gait analysis system (Noldus Information Technology, The Netherlands) (14–16). CatWalk instrument consists of a hardware system of a long, enclosed glass walkway plate, illuminated with green light, a high-speed video camera, and a software package for quantitative assessment of animal footprints. A green light emitted by a fluorescent lamp positioned underneath the glass plate is reflected within the glass plate except at points being touched where the mouse paws made contact with the glass plate. It scatters and illuminates the contact area. The intensity of the area of illumination, which is proportional to the exerted pressure, is digitally captured by the video camera connected to a computer that runs the CatWalk software 7.1.

The recordings were carried out when the room was completely dark, except for the light from the computer screen. Each mouse was placed individually in the CatWalk walkway and allowed to walk freely, in an unforced manner and traverse from one side to the other

of the walkway glass plate. Mouse tracks that were straight without any interruption or hesitation were treated as successful runs. Runs with any wall climbing, grooming, and staying on the walkway were not analyzed. An average number of 3 replicate crossings made by each mouse was recorded. The CatWalk software was used to analyze crossings that had at least five cycles of complete steps. The software automatically labelled all the areas containing pixels above the set threshold. These areas were identified and assigned to the respective paws. Analysis of the recording generated a wide range of parameters of which only the following gait and co-ordination parameters were analysed:

Stride length: distance between successive placements of the same paw

Body speed variation: regularity of body speed

Spinal cord histology and motor neurons quantifications

Spinal cord were dissected and fixed by immersion in 4% paraformaldehyde in 0.1 M phosphate buffer pH 7.4 overnight. Spinal cords lumbar part (L1-L5) were cryoprotected in 30% sucrose and snap frozen in melting isopropanoland embbeded in TissueTek (O.C.T.Compound, SAKURA#4583). Cryosections (Leica CM 3050S) of 16µm were obtained for histological analysis (10 sections per animal).

To identify localization of FUS protein spinal cord neurons were stained using antibody against FUS N-terminal part (Bethyl A303-839A; 1:100) followed by biotinylated secondary antibody donkey anti-goat IgG (Jackson, 705-066-147; 1:250). To quantify motor neurons spinal cord section were stained with 0.1% Cresyl violet acetate (Certistain®, MERK#5235) and anti-ChaT (Millipore, AB144-P; diluted 1:50) followed by biotinylated secondary antibody donkey anti-goat IgG (Jackson, 705-066-147; 1:250). The staining was revealed using the ABC kit (Vektor, PK7200; 1:4000), by the avidin-botin complex immunoperoxidase technique. Motor neurons counting was performed in L1-L3 ventral horn in every tenth section for ten sections in total per animal. Total number of motor neurons were obtained using ImageJ freeware (http://rsbweb.nih.gov/ij/) after images acquisition at 20X under the same exposition parameters with a digital camera (Nikon Digital Sight DS-U3). The observer was blinded to the genotype of studied mice.

Electromyography

Electromyography was performed as previously described (9,10,17). Mice at 10 and 22 month of age were anaesthetized with a solution of ketamine/xylasine (100 mg/kg; 5 mg/kg) and electrical activity was recorded using a monopolar needle electrode (diameter 0.3 mm; 9013R0312; Medtronic, Minneapolis, MN) inserted into the tail of the mouse. Recordings were made with a concentric needle electrode (diameter 0.3 mm; 9013S0011; Medtronic).

Electrical activity was monitored in both *m.gastrocnemius* (GA) and *m.tibialis* (TA) on both legs for at least 2 min. Spontaneous activity was differentiated from voluntary activity by visual and auditory inspection. Results were scored as described previously (9,10,17).

NMJ histology

Muscle tissues were dissected and fixed by immersion in 4% paraformaldehyde in 0.1 M phosphate buffer pH 7.4 overnight. The whole muscles were dissected into fibers muscle bundles, stained using Alexa Fluor 594-conjugated α-Bungarotoxin (Sigma, T195; 1µg/µl) for post-synaptic apparatus. Images were acquired using a under a fluorescent microscope (Nikon Eclipse E800) at 40x magnification and analyzed *post hoc*.

Behavioral tests

All experiments we conducted between 9 am and 5 pm. We conducted all behavioral studies using male mice and analyzed data blind to genotypes. For all tasks, we tested two cohorts of mice at 10 and 22 months of age. A large cohort of 15 $Fus^{+/+}$ and 15 $Fus^{\Delta NLS/+}$mice was followed for motor behaviour until the end of 22 months of age. When mice were 10 months old they underwent a battery of behavioural tests: water maze, light-dark box test and beam walking tests. When mice were 22 months old as well as two independent group of 10 month old mice one of 7 and other of 8 mice per genotype were used for testing in open field, for resident-intruder and three chamber task.

Open field test

We tested general exploratory locomotion and anxiety in a novel open-field environment in 15 min sessions in a 72 × 72 × 36 cm the open field arena constructed of white plywood. The lines divided the floor into sixteen 18 x 18 cm squares. A central square (18 cm x 18 cm) was drawn in the middle of the open field. The maze was located in a test room and lit by a 600 lux for background lighting. The open field maze was cleaned between each mouse using 70 % ethyl alcohol. The mouse was placed in the center of the arena and allowed to freely move while being recorded by an overhead camera. We analyzed behaviour with an automated tracking system (Ethovision software, Noldus). The time spent in the center (four central quadrants) vs the perimeter (12 peripheral quadrants) were automatically calculated and were used to measure exploration and anxiety.The total distance traversed and velocity were used to evaluate locomotor activity. For each mouse independently a heat map and tracking trajectory map presenting corresponding locomotion activity were made (18).

The light/dark box test

The first cohort of 10 months-old males littermates (*n*=6–9 per group) was tested in the light/dark box test to assess for anxiety level and exploratory behaviour of the mouse. Test was conducted during the morning. The apparatus consists of two PVC compartments of equal size (18.5 x 18.5 x 15cm) one opaque and the other transparent, connected with an opaque PVC tunnel (5 x 5.5 x 5cm). The illumination of the transparent compartment was set at 400 lux. The mice were placed in the dark compartment. A video camcorder located approximately 150 cm above the center of the box recorded the mouse's behaviour. After 5 minutes, mice were removed from the box by the base of their tails and returned to their home cage. The box was then cleaned with a solution of 70% ethyl alcohol and permitted to dry between tests. The latency before the first transition to the light compartment, the number of transitions between the two compartments and the time spent in each compartment were measured (19).

The beam walking test - actimetry

One session lasting for 3 days was performed in order to determine the activity of the subjects. The mice were placed individually in large transparent Makrolon cages (42x26x15 cm) adapted to the shelves of the testing device (eight cages/shelve). Two infrared light beams, passing trough each cage, were targeted on two photocells, 2.5 cm above the cage floor level and 28 cm apart. The number of cage crossing was recorded by a computer. The experiment began at 17.00 pm and after 2 hours of habituation continued for 3 day for a complete 24 h nyctemeral cycle (12h dark and 12h light) (20).

Olfactory preference testing

This test is designed to identify specific detection deficiencies, namely the ability to sense attractive or aversive scents. After habituation to empty cages with no bedding, we tested mice for odor preference. In the task, mice are challenged with a filter paper embedded with two strong scents (vanilla and 2-methyl butyrate) or a neutral scent (water). The total exploratory timeis recorded (upon video viewing) for various scents during a 3 min. The time mouse spent sniffing the filter paperis calculated *post hoc*with one researcher blind to subject genotypes and/or condition. Those scents with total exploratory times greater than water are designated as "attractive" while those with times less than water are termed "aversive". The researcher then considers whether the same scents are "attractive" or "aversive" for different test subjects (21,22).

Social interaction in home cage (resident-intruder test)

We assessed social interaction in the home cage by a standard protocol. Briefly, we housed individual test mouse for 1 week before the task. Then, they were habituated for 30 min to the test room. In this task, a mouse in his home cage is allowed to freely roam in the absence of the cage top for 1 min. A novel male intruder mouse (non-littermate of same background, approximately same age, and similar weight) is then placed in the opposite corner as the resident subject and allowed to roam freely for 5 min. The task is video-recorded, and total physical interaction between the two mice is quantified visually by an examiner blind for genotype. Social interaction is scored separately for each minute during test, as the time during which the resident mouse actively explores the intruder (time spent investigating, grooming, following or sniffing the intruder). We did not observe fighting, biting, or attacking in this task (23).

Three-chamber social task

The task consists of three consecutive parts: habituation, social recognition and sociability, and preference for social novelty (social discrimination or social recognition memory).

The apparatus is made of transparent plexiglass walls (**Figure16**, Noldus Information and Technology BV, Wageningen, The Netherlands). The box measures 59 × 39.5 × 21.5 cm and is divided into three chambers of equal size (18.5 × 39.5 cm) by walls with a 7 × 7 cm square opening that could be closed by a slide door. Each of the two side chambers contains a cylinder. These cylinders (20 × 10 cm diameter) are made out of 18 transparent plexiglass bars placed 6 mm apart; the upper end of the cylinder is closed with a black lid. At the end of the task for each mouse the apparatus is cleaned with tap water and 70% ethyl alcohol and dried.

15 *Fus*$^{+/+}$ and 15 *Fus*$^{\Delta NLS/+}$ that underwent experimental procedure will be referred to as “test” mice and adult male mice of same background, age and weight used as the social stimulus are called “stranger mouse”. Test mice were housed individually for 1 week before the test. We habituated the mice in the testing room for at least 1 min before the start of behavioural tasks. One day before the start of testing, the strangers are placed into the cylinders in the social test apparatus for 5 min. Keeping the stranger mouse in a cylinder prevents aggressive and sexual interactions, also ensuring that all social approach is initiated by the test mouse. Sessions are video-taped and analyzed *post hoc* visually by an examiner blind for genotype. The following parameters were considered: time spent (in seconds and percentage) in middle and side chambers; time spent intereacting with a stranger mouse or an empty cylinder.

The experimental procedure is adapted from (24–27), and was carried out in five trials of 5 min each (after each trial, we returned the mouse to his home cage for 15 min), separated in three consecutive parts.

Trial 1 (habituation): the test mouse is placed to the middle chamber and left to explore the arena containing the empty wire cages (cylinders) for 5 min

Trials 2–4 (sociability, social learning acquisition): the mouse is placed in the middle chamber, but an unfamiliar mouse (Stranger 1) is placed into a wire cage in one of the side-chambers (the wire cage in the other side-chamber remains empty). The test mouse has access to all three chambers. Trials 2 (social recognition) defined as the ability to identify a conspecific (Stranger 1 versus the empty cage). Increased time spent in the chamber and in the perimeter around the cylinder with the stranger indicates preference for the social stimulus compared to the empty cage.

Trial 5 (social novelty,social discrimination,social recognition memory and sociability): a novel stranger mouse (Stranger 2) is placed in the previously empty wire cage, the “old” stranger (Stranger 1) remains in position in its cylinder and chamber, and again the test mouse is left to explore for 5 min. Social novelty, defined as the ability to discriminate between a novel mouse (Stranger 2) and a familiar mouse (Stranger 1) It is expected that the test mouse will spent more time with the new stranger than the old stranger. Increased time spent with the new stranger is a measure for the discriminative ability of the test mouse, also indicative for intact working memory.

Sociability reflects the motivation of the test mouse to spontaneously interact with target mice in Trials 2-5.

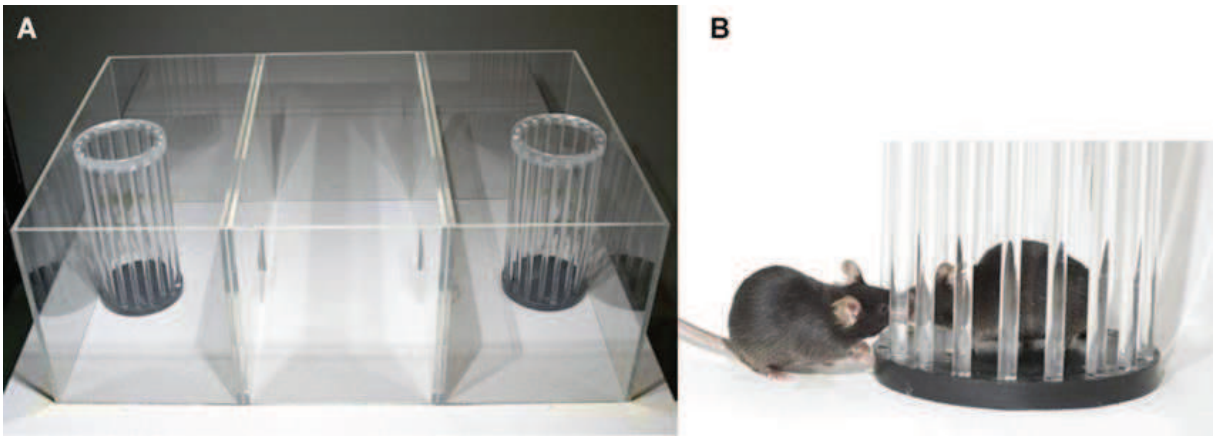

Figure 16. Social apparatus three chamber test. (A) A picture of the apparatus containing the two cylinders; **(B)** Close-up of an interaction between the stranger mouse in the cylinder and the test mouse.

Water maze task

The water maze consisted of a circular pool (diameter 160 cm; height 60 cm) filled with water (21 ± 1°C) made opaque by addition of powdered milk (about 1.5 g/L). The first day consisted in one 4-trial session using a visible platform (diameter 11 cm, painted black, protruding 1 cm above the water surface and located in the South-East quadrant of the pool), starting randomly from each of the four cardinal points at the edge of the pool. During this pre-training day, a blue curtain surrounded the pool to prevent the use of distal cues and thus incidental encoding of spatial information. For the following days, the curtain was removed. Mice were given a 5-day training period (4 consecutive trials/day, maximum duration of a trial = 60 s, inter-trial interval = 10–15 s) with a hidden platform located at a fixed position in the North-West quadrant. Animals were starting randomly from each of the four cardinal points at the edge of the pool and the sequence of the start points was randomized over days. Mice were tested for retention in a 18-days delay probe trial and two extintion tests : first 2 h after probe trial and secon 2 hour after the first. For the probe trial, the platform was removed; the mice were introduced in the pool from the North-East (a start point never used during acquisition) and allowed a 60-s swimming time to explore the pool. Data analyses used (computed by a video-tracking system (SMART; PanLab)) for the visible platform and training trials were : the distance traveled as well as the latency before reaching the platform and avarage speed. For the probe trial and extinction tests the time (in %) spent in the target quadrant (i.e., where the platform was located during acquisition) was analyzed (28).

Statistical analysis

Unless otherwise indicated, the values from each animal were averaged for each genotype group and analyzed by unpaired Student's t-test, two tailed or comparison between groups was performed by Oneway ANOVA followed by Tukey's post-hoc test using the Graphics Prism Program (Graph Pad Software, San Diego, CA). The null hypothesis was rejected at the level of 0.05.

Twoway ANOVA with repeated measure factors was used for resident intruder test and three chamber task using genotype and trial as interaction factors.

Water maze data were analyzed by analysis of variance using a twoway- ANOVA with repeated measure factors to study interactions between genotype and trial, day, quadrant (Statistica 8.0; Statsoft, Inc., Tulsa, OK). The time spent in the target quadrant of the water maze was compared to the 15 s chance value by one-sample Student's *t* test. The 15 s chance value corresponds to the time spent for random search in four quadrants during the 60 s probe test.

All data are expressed as mean ± standard error of the mean (SEM).

Bibliography

1. Sedelis M, Schwarting RKW, Huston JP. Behavioral phenotyping of the MPTP mouse model of Parkinson's disease. Behav Brain Res. 2001;125(1-2):109–25.

2. Fleming SM, Ekhator OR, Ghisays V. Assessment of sensorimotor function in mouse models of Parkinson's disease. J Vis Exp. 2013;(76):1–7.

3. Tillerson JL, Caudle WM, Reverón ME, Miller GW. Detection of behavioral impairments correlated to neurochemical deficits in mice treated with moderate doses of 1-methyl-4-phenyl-1,2,3,6-tetrahydropyridine. Exp Neurol. 2002;178(1):80–90.

4. Neary D, Snowden J, Mann D. Frontotemporal dementia. Lancet Neurol. 2005;4(11):771–80.

5. Piguet O, Hornberger M, Mioshi E, Hodges JR. Behavioural-variant frontotemporal dementia: Diagnosis, clinical staging, and management. Lancet Neurol 2011;10(2):162–72.

6. Roberson ED, Filiano AJ, Martens LH, Young AH, Warmus B a., Zhou P, et al. Dissociation of frontotemporal dementia-related deficits and neuroinflammation in progranulin haploinsufficient mice. Ann Intern Med. 2013;158(6):5352–62.

7. Frankland PW, Bontempi B. The organization of recent and remote memories. Nat Rev Neurosci. 2005;6(2):119–30.

8. Dara Ditsworth, Wei-Xing Zong 1 and Craig B. Thompson2. Activation of Poly(ADP)-ribose Polymerase (PARP-1) Induces Release of the Pro-inflammatory Mediator HMGB1 from the Nucleus. J Biol Chem. 2007;282(24):17845–54.

9. Dupuis L, Fergani A, Braunstein KE, Eschbach J, Holl N, Rene F, et al. Mice with a mutation in the dynein heavy chain 1 gene display sensory neuropathy but lack motor neuron disease. Exp Neurol. 2009;215(1):146–52.

10. Dupuis L, Gonzalez de Aguilar JL, Echaniz-Laguna A, Eschbach J, Rene F, Oudart H, et al. Muscle mitochondrial uncoupling dismantles neuromuscular junction and triggers distal degeneration of motor neurons. PLoS One. 2009;4(4).

11. Bouet V, Boulouard M, Toutain J, Divoux D, Bernaudin M, Schumann-Bard P, et al. The adhesive removal test: a sensitive method to assess sensorimotor deficits in mice. Nat Protoc. 2009;4(10):1560–4.

12. Carlson CG, Rutter J, Bledsoe C, Singh R, Hoff H, Bruemmer K, et al. A simple protocol for assessing inter-trial and inter-examiner reliability for two noninvasive measures of limb muscle strength. J Neurosci Methods. 2010;186(2):226–30

13. Carlson G, Carlson G. The use of four limb hanging tests to monitor muscle strength and condition over time Official reviewer. 2014;(Id):1–11.

14. Parvathy SS, Masocha W. Gait analysis of C57BL/6 mice with complete Freund's adjuvant-induced arthritis using the CatWalk system. BMC Musculoskelet Disord 2013;14(1):14.

15. Wang XH, Lu G, Hu X, Tsang KS, Kwong WH, Wu FX, et al. Quantitative assessment of gait and neurochemical correlation in a classical murine model of Parkinson's disease. BMC Neurosci. 2012;13:142.

16. Möller K a., Berge OG, Hamers FPT. Using the CatWalk method to assess weight-bearing and pain behaviour in walking rats with ankle joint monoarthritis induced by carrageenan: Effects of morphine and rofecoxib. J Neurosci Methods. 2008;174(1):1–9.

17. Rouaux C, Panteleeva I, René F, Gonzalez de Aguilar J-L, Echaniz-Laguna A, Dupuis L, et al. Sodium valproate exerts neuroprotective effects in vivo through CREB-binding protein-dependent mechanisms but does not improve survival in an amyotrophic lateral sclerosis mouse model. J Neurosci. 2007;27(21):5535–45.

18. Gould T, Dao D, Kovacsics C. The open field test. Mood Anxiety Relat Phenotypes … [Internet]. 2009;(July):1–9.

19. Hascoët M, Bourin M. The mouse light-dark box test. Neuromethods. 2009;42:197–223.

20. Moreau PH, Cosquer B, Jeltsch H, Cassel JC, Mathis C. Neuroanatomical and behavioral effects of a novel version of the cholinergic immunotoxin mu p75-saporin in mice. Hippocampus. 2008;18(6):610–22.

21. Kobayakawa K, Kobayakawa R, Matsumoto H, Oka Y, Imai T, Ikawa M, et al. Innate versus learned odour processing in the mouse olfactory bulb. Nature. 2007;450(7169):503–8.

22. Witt RM, Galligan MM, Despinoy JR, Segal R. Olfactory behavioral testing in the adult mouse. J Vis Exp. 2009;(23):1–5.

23. Winslow JT. Mouse social recognition and preference. Curr Protoc Neurosci. 2003;Chapter 8:Unit 8.16.

24. Gascon E, Lynch K, Ruan H, Almeida S, Verheyden JM, Seeley WW, et al. Alterations in microRNA-124 and AMPA receptors contribute to social behavioral deficits in frontotemporal dementia. Nat Med. 2014;20(12):1444–51.

25. Moy SS, Nadler JJ, Young NB, Perez A, Holloway LP, Barbaro RP, et al. Mouse behavioral tasks relevant to autism: Phenotypes of 10 inbred strains. Behav Brain Res. 2007;176(1):4–20.

26. Page DT, Kuti OJ, Sur M. Computerized assessment of social approach behavior in mouse. Front Behav Neurosci. 2009;3(November):48.

27. Ter Horst JP, van der Mark M, Kentrop J, Arp M, van der Veen R, de Kloet ER, et al. Deletion of the forebrain mineralocorticoid receptor impairs social discrimination and decision-making in male, but not in female mice. Front Behav Neurosci. 2014;8(February):26.

28. Cholvin T, Loureiro M, Cassel R, Cosquer B, Herbeaux K, de Vasconcelos AP, et al. Dorsal hippocampus and medial prefrontal cortex each contribute to the retrieval of a recent spatial memory in rats. Brain Struct Funct. 2014;

DISCUSSION

DISCUSSION

This section will be mostly dedicated to the discussion of the current results obtained in adult heterozygous $Fus^{\Delta NLS/+}$ mice. I will first discuss the points that are currently missing in this study and that will need to be completed before submission. I will then compare our $Fus^{\Delta NLS/+}$ mice with the currently existing FUS-based mouse models, discuss the relevance of our model for ALS and FTLD, and draw mechanistic and clinical perspectives.

I. A STUDY TO BE COMPLETED

We observe a number of behavioural phenotypes in our $Fus^{\Delta NLS/+}$ mice, and began to characterize the anatomical substrate of these behavioural deficits in the spinal cord. We also obtained preliminary evidence of fronto-temporal atrophy. A number of key anatomical pathology studies are however missing. First, we did not directly show motor neuron degeneration, and markers of apoptosis, necroptosis or dysfunctional autophagy should be studied. It would be particularly interesting to determine whether $Fus^{\Delta NLS/+}$ motor neurons develop ubiquitin positive and/or p62 positive aggregates. In the same line, it would be of importance to reevaluate the appearance of stress granules in our old $Fus^{\Delta NLS/+}$ mice. In the frontal cortex, we currently have no evidence of actual neurodegeneration, and neuronal counts, as well as microgliosis and astrocytosis should be evaluated as a function of age and correlated with behavioural deficit.

A second important series of studies that need to be completed is to determine the exact fate of the FUS protein in $Fus^{\Delta NLS/+}$ mice with age. First, a quantitative analysis of nuclear vs cytoplasmic FUS remains to be done. This is critical to determine whether $Fus^{\Delta NLS/+}$ mice are indeed haplo-insufficient mice, or whether the phenotypes observed could be entirely ascribed to gain of function. Indeed, nuclear clearing of FUS is not as evident as observed for TDP-43 (83), suggesting that loss of function might not be key to the pathogenesis of FUSopathies. Consistently, complete FUS knock out mice outbred to favour survival show several traits also observed in our $Fus^{\Delta NLS/+}$ mice, in particular hyperactivity (221), yet these mice do not develop motor neuron degeneration as our $Fus^{\Delta NLS/+}$ mice. Second, we did not observe large, FUS positive inclusions in $Fus^{\Delta NLS/+}$ mice, yet smaller punctate inclusions could be occasionnally observed, and it is currently unknown whether this truncated FUS protein becomes hyper-methylated, or not. This would be of importance to understand the relevance of our findings to ALS and FTLD since methylation of FUS appears differentially involved in FUS-ALS and FUS-FTLD (151,262). Third, it is critical to determine whether FUS itself becomes ubiquitinated in $Fus^{\Delta NLS/+}$ mice. Indeed, ubiquitinated cytoplasmic inclusions of brains and spinal cords from TDP-43 negative ALS and FTLD patients identified FUS as the major ubiquitinated protein

component (128,256). However some studies demonstrated that mutant FUS protein itself is not ubiquitinated, hyperphosphorylated or cleaved, yet insoluble (29). Our $Fus^{\Delta NLS/+}$ mice could help to shed light on the biochemical modifications of mutant FUS when expressed from the endogenous locus, and whether this could be relevant for disease pathogenesis. Last, it will be critical to determine whether the truncated FUS modifies the nuclear localization and/or aggregation of other FET proteins or related proteins. Indeed, ALS-FUS is characterized by the selective deposition of FUS, while FTLD-FUS shows co-accumulation together with TAF15 and EWSR1 and their nuclear import receptor Transportin (149). In contrast, in cases of ALS-FUS, TAF15 and EWSR1 remained localized to the nucleus and did not label FUS-positive inclusions (149). It is of utmost importance to determine which of these proteins display alterations in localization and/or levels in our $Fus^{\Delta NLS/+}$ mice.

II. $FUS^{\Delta NLS/+}$ MICE AS A GENETICALLY RELEVANT MODEL OF FUS-ALS

Our study in homozygous $Fus^{\Delta NLS/\Delta NLS}$ mice provided in vivo genetic evidence that cytoplasmic mislocalization of FUS triggers apoptotic motor neuron degeneration and demonstrated a crucial role for a gain of toxic function in this process. Motor neuron loss occured at least partially through a cell autonomous gain of function mechanism, since complete loss of FUS was not associated with motor neuron death, and rescue of nuclear FUS within motor neurons prevented neuronal death (Scekic-Zahirovic et al., 2015). However, we did not detect the presence of FUS-containing cytoplasmic aggregates, ubiquitin or p62 positive, stress granule alterations or pathology involving other proteins. This could be due to early perinatal lethality of both $Fus^{\Delta NLS/\Delta NLS}$ and $Fus^{-/-}$ mice, which prevented us to examine in detail potential toxic mechanisms for cytoplasmic FUS, and our study only shed light on several posible candidate pathways. Interstingly, a number of genes involved in synaptogenesis and/or in neurodegenerative diseases show altered expression (*Ahi1, Dmpk, Nefl, Nefm, Tuba4a, Taf15*) or splicing (*Ndrg2, Mapt, Atxn2, Sort1*) in $Fus^{\Delta NLS/\Delta NLS}$ mice. The most important an upregulation of KIS, a kinase involved in dendritic mRNA translation supporting finding (286) that impairment of local mRNA translation may contribute to neuronal death in FUS-mediated diseases. Despite the potential interest of homozygous $Fus^{\Delta NLS/\Delta NLS}$ mice, only two families have been shown to display homozygous mutations in the FUS gene, suggesting a recessive pattern of inheritance (50,251). The vast majority of FUS mutations are dominantly inherited, suggesting that $Fus^{\Delta NLS/+}$ mice are a much better model of FUS-ALS from a genetic point of view.

How do $Fus^{\Delta NLS/+}$ mice compare with other FUS-based mouse models ? Previous in vivo studies using transgenic FUS rodent models (194–197,283) have established that elevated

levels of both wild-type and mutant FUS, can be inherently toxic to neurons. This suggests that transgenic based overexpression will be limited in the possibility to differentiate between neurotoxicity due to overexpression from disease relevant toxicity due to mutation. A major advantage of our model is that it is a knock-in, and, as such that $Fus^{\Delta NLS/+}$ mice bear one copy of ALS-linked truncated mutation of FUS expressed from the endogenous promoter. A minor drawback is that this exact truncating mutation (leading to a R506X truncation) has not been observed in human patients. However R495X, G497AFs, R502EFs G504WFs and K510Wfs (249,257) and rewieved in (230) mutations have been linked to ALS, and truncation mutations spanning the exact amino acid mutant in our mice thus exist in ALS families. The heterozygous ΔNLS mutation leads to a moderate overexpression of FUS at the mRNA level (1–1.3x). This increased expression is expected since two mechanisms of autoregulation of FUS have been documented, exon 7 exclusion (238) and microRNA autoregulatory loop (287). Both of these mechanisms could in principle account for the observed overexpression. However, this mild overexpression is unlikely to be the cause of the observed phenotypes. First, it is not observed at the protein level, suggesting either decreased translation of FUS mRNA or decreased stability of FUS protein. Second, the overexpression is mostly observed in peripheral tissues (muscle>liver>>brain and spinal cord), suggesting it has little relevance to the CNS phenotype. In all, our $Fus^{\Delta NLS/+}$ mice display a quasi-identical genetic situation as many FUS-ALS patients, suggesting that they represent a good model of FUS-ALS, likely more relevant than classical transgenic overexpressors. A comparative summary of pros and cons of existing FUS models with our $Fus^{\Delta NLS/+}$ mice is provided in Annex (Table 4-5).

III. ARE $FUS^{\Delta NLS/+}$ MICE A MODEL OF ALS USEFUL FOR PRECLINICAL STUDIES?

Analysis of $Fus^{\Delta NLS/+}$ mice revealed that truncated FUS, partially mislocalized to cytoplasm and led to late, mild, adult-onset, lower motor neuron deficits in a mutant-dependent, age-dependent manner. $Fus^{\Delta NLS/+}$ mice developed subtle motor deficits by the age of 10 months, characterized by subtle reduction of muscle strength, whereas $Fus^{+/+}$ mice remained phenotypically normal (Figure 3, 4). Importantly, this motor phenotype was progressing with age, since 22 months old animals showed further deterioration in muscle strength, developped more severe motor deficits leading to gait abnormalities. Indeed, the 22 months old animals fulfilled two major criteria of ALS, with abnormal EMGs, defective neuromuscular junctions and motor neuron loss. Motor phenotype was histologically caracterized by defective NMJ and loss of spinal cord motor neurons up to ~30%. These defects are thus adult onset, and progressive, and this is analogous to ALS in humans that appears with a median age 65 years. It is intriguing

that truncation of FUS, that leads to very severe disease, with sometimes juvenile onset in humans, does lead to a mild and late onset disease in mice. This could be due to a species difference, and can be influenced by the genetic background of the mice. Indeed, the C57Bl6 background of $Fus^{\Delta NLS/+}$ mice is known to be resistant to ALS induced by SOD1 mutations (288). Backcrossing in a more sensitive genetic background might unveil a more pronounced phenotype.

Importantly, ALS-like defects observed in $Fus^{\Delta NLS/+}$ mice are similar, yet milder, to those observed in other commonly used ALS models, in particular those based on SOD1 mutations (64,289,290) or TDP-43 (82,83). However, these defects are not sufficient to trigger paralysis of the mice and shortened survival, and this would be a major drawback for the use of $Fus^{\Delta NLS/+}$ mice for preclinical studies. In all, $Fus^{\Delta NLS/+}$ mice constitute a relevant model of FUS-ALS, but will be difficult to use, at least in their current C57Bl6 background, for preclinical studies.

IV. ARE $FUS^{\Delta NLS/+}$ MICE A MODEL OF FTLD?

Analysis of $Fus^{\Delta NLS/+}$ mice revealed that these mice developed behavioural deficits that could be similar to those observed in FTLD patients, as well as prominent fronto-temporal atrophy. Bearing in mind that we currently lack anatomical pathology of these mice, thus precluding us to definitely conclude on a potential FTLD phenotype in these mice, it would be tempting to speculate that $Fus^{\Delta NLS/+}$ mice could constitute a mouse model of FTLD-FUS.

Several notes of caution should however be raised. First, we surprisingly observed hyperactivity and increased social behaviour in $Fus^{\Delta NLS/+}$ mice, while most studies to date in FTLD mouse models rather described apathetic behaviours and decresed social interests (190–193,291–298) as well in a model recently characterized in our laboratory bearing CHMP2Bintron5 (A. Verney & F. Rene, in preparation). Our findings could be relevant for FTLD since a number of FTLD patients initially develop social disinhibitions, that could be translated in our experiments as increased social interest. It is thus possible that the lifespan of a mouse is not long enough so that $Fus^{\Delta NLS/+}$ mice then develop a secondary apathy and decreased social behaviour. Here again, backcrossing in another genetic background might accelerate these age-dependent processes. Second, it is important to consider that FUS mutations, in particular truncating mutations, are very rare in FTLD patients, and that FUS-ALS patients develop in general pure ALS, in the absence of FTLD. The difference between clinical observations and our mouse models could be due to either a lack of sensitivity in the neuropsychological tests in clinical settings, or to an intrinsic difference of sensitivity between mice and humans. It is critical to characterize the biochemical alterations of FUS in our $Fus^{\Delta NLS/+}$ mice to determine whether

$Fus^{\Delta NLS/+}$ mice develop FTLD-like alterations (hypomethylation) rather than ALS-like (hypermethylation) of FUS protein. This might provide a mechanistic explanation to our results.

V. GAIN VS. LOSS OF FUNCTION

It is interesting to observe that $Fus^{\Delta NLS/+}$ mice develop motor neuron disease without massive loss of endogenous nuclear FUS, with modest redistribution, partial mislocalization of truncated FUS to cytoplasm and without massive aggregation of truncated FUS within the nucleus or cytoplasm, contrary to what has been reported in human ALS (50,51,143,256,299) or FTLD (29,106,128,145,147) patients. In this respect, findings in $Fus^{\Delta NLS/+}$ mice are consistent with our prior study, wherein motor neuron degeneration occured only with cytoplasmic accumulation of truncated FUS and not in case of complete absnce of FUS (Scekic-Zahirovic et al., 2015). Despite there is no complete nuclear clearance of FUS in $Fus^{\Delta NLS/+}$ mice, there could nevertheless be haploinsufficiency. To answer this question, we are currently performing parallel transcriptomic analysis of spinal cord and frontal cortex of 10 and 22 months old $Fus^{\Delta NLS/+}$ mice and compare to $Fus^{+/+}$ mice. The contribution of loss of function will also be investigated by crossing our $Fus^{\Delta NLS/+}$ mice with BAC transgenic mice expressing either wild type or mutant FUS protein. If loss of function is required for the development of perinatal death and motor neuron degeneration, it would be expected that the BAC transgenic expressing wild type FUS protein would rescue at least partially the $Fus^{\Delta NLS/\Delta NLS}$ and $Fus^{\Delta NLS/+}$ mice phenotypes.

VI. WHY IS $FUS^{\Delta NLS/+}$ MICE PHENOTYPE SO MILD? THE SECOND HIT THEORY

Despite the genetic situation in $Fus^{\Delta NLS/+}$ mice is identical to human FUS-ALS patients, these mice develop only mild motor neuron disease while FUS-ALS in humans is extremely severe. A potential explantation to this dyscrepancy is that a second hit is necessary to trigger the full blown phenotype. In this last paragraph, I would like to speculate on several potential second hits.

First, the second hit could be a genetic modifier. Indeed, ALS is now considered as an oligogenic disease (3,87), and multiple examples arose in the litterature of ALS and FTLD patients with more than one disease-linked mutation. For example, the *C9orf72* expansion has been described in association with *TARDBP*, *FUS*, and *SOD1* mutations in patients with ALS, with *PGRN*, *MAPT*, *PSEN*-2, and *SQSTM1* mutations in FTD patients. Patients harboring mutations in *TARDBP* and *FUS* have been found to carry variants in angiogenin (*ANG*), a gene associated with ALS but considered as low-risk as well as with *SETX* mutations (rewieved in

(3)). In this respect, the backcrossing in a more sensitive genetic background could be considered as a second genetic hit.

Second, the second hit could be environmental. Brain trauma (300), electric shocks, increased physical activity and dietary alterations (301) are all considered to be potential modifiers of ALS pathogenesis. In this respect, the involvement of FUS in stress granules could be key in the understanding of its pathogenic function. It is possible that the full blown toxicity of ΔNLS FUS will only uncover in situations of stress, either traumatic or energetic. A tempting speculation would be that mutant FUS aggregates in response to stress, in a discrete number of neurones, and that this initial nucleus of aggregation then spreads through pathological seeding of aggregated FUS. Such a scenario would be entirely consistent with the general spreading pattern of proteinopathy in ALS (302) as well as with the global spreading of symptoms from one region to another. This hypothesis should be further tested using our $Fus^{\Delta NLS/+}$ mice, subjected to either stress situations or seeding of pathological proteins.

VII. GENERAL CONCLUSION

The work presented in this thesis shows that the cytoplasmic mislocalization of FUS triggers a gain of toxic function, leading to a dose-dependent death of motor neurons. Complete cytoplasmic mislocalization leads to global loss of FUS function but also to important motor neuron apoptosis not observed in full knock-out animals. Partial FUS cytoplasmic mislocalization leads to a milder, adult onset, progressive motor neuron disease phenotype, associated with a number of behavioural abnormalities relevant to frontal lobe dysfunction.

Importantly, the toxicity of FUS mislocalization appears, at least in homozygous mice, to be cell autonomous, and the rescue of mislocalization in motor neurons is sufficient to counteract motor neuron apoptosis.

These novel animal models of FUS-ALS will allow to gain deeper understanding of the pathogenic mechanisms and hopefully help in the design of therapeutic strategies.

BIBLIOGRAPHY

BIBLIOGRAPHY

1. Chiò A, Mora G, Calvo A, Mazzini L, Bottacchi E MRP. Epidemiology of ALS in Italy: a 10-year prospective population-based study. Neurology. 2009;72(8):725–31.

2. Nelson LM. Epidemiology of ALS. Clin Neurosci. 1996;3:327–31.

3. Lattante S, Ciura S, Rouleau G a., Kabashi E. Defining the genetic connection linking amyotrophic lateral sclerosis (ALS) with frontotemporal dementia (FTD). Trends Genet. 2015;31(5):263–73.

4. Ling S-C, Polymenidou M, Cleveland DW. Converging mechanisms in ALS and FTD: disrupted RNA and protein homeostasis. Neuron. 2013;79(3):416–38.

5. Agosta F, Al-Chalabi A, Filippi M, Hardiman O, Kaji R, Meininger V, et al. The El Escorial criteria: Strengths and weaknesses. Amyotroph Lateral Scler Front Degener. 2015;16(1-2):1–7.

6. Swinnen B, Robberecht W. The phenotypic variability of amyotrophic lateral sclerosis. Nat Rev Neurol. 2014;10(11):661–70.

7. Chiò A, Calvo A, Moglia C, Mazzini L, Mora G. Phenotypic heterogeneity of amyotrophic lateral sclerosis: a population based study. J Neurol Neurosurg Psychiatry. 2011;82(7):740–6.

8. Pupillo E, Messina P, Logroscino G, Beghi E. Long-term survival in amyotrophic lateral sclerosis: A population-based study. Ann Neurol. 2014;75(2):287–97.

9. Amendola J, Verrier B, Roubertoux P, Durand J. Altered sensorimotor development in a transgenic mouse model of amyotrophic lateral sclerosis. Eur J Neurosci. 2004;20(10):2822–6.

10. Williamson TL, Cleveland DW. Slowing of axonal transport is a very early event in the toxicity of ALS-linked SOD1 mutants to motor neurons. Nat Neurosci. 1999;2(1):50–6.

11. Van Zundert B, Peuscher MH, Hynynen M, Chen A, Neve RL, Brown RH, et al. Neonatal neuronal circuitry shows hyperexcitable disturbance in a mouse model of the adult-onset neurodegenerative disease amyotrophic lateral sclerosis. J Neurosci. 2008;28(43):10864–74.

12. Régal L1, Vanopdenbosch L, Tilkin P, Van den Bosch L, Thijs V, Sciot R RW. The G93C Mutation in Superoxide Dismutase Clinicopathologic Phenotype and Prognosis. Arch Neurol. 2006;63(2):262–7.

13. Van Damme P, Robberecht W. Clinical implications of recent breakthroughs in amyotrophic lateral sclerosis. Current opinion in neurology. 2013;26(5):466–72.

14. Dadon-Nachum M, Melamed E, Offen D. The “dying-back” phenomenon of motor neurons in ALS. J Mol Neurosci. 2011;43(3):470–7.

15. Turner MR, Hardiman O, Benatar M, Brooks BR, Chio A, De Carvalho M, et al. Controversies and priorities in amyotrophic lateral sclerosis. Lancet Neurol. 2013;12(3):310–22.

16. Strong MJ, Yang W. The frontotemporal syndromes of ALS. Clinicopathological correlates. J Mol Neurosci. 2011;45(3):648–55.

17. Lillo P, Hodges JR. Frontotemporal dementia and motor neurone disease: Overlapping clinic-pathological disorders. J Clin Neurosci. 2009;16(9):1131–5.

18. Ashworth NL, Satkunam LE, Deforge D. Treatment for spasticity in amyotrophic lateral sclerosis/motor neuron disease. Cochrane Database Syst Rev. 2006;(1):CD004156.

19. Swash M. Why are upper motor neuron signs difficult to elicit in amyotrophic lateral sclerosis? J Neurol Neurosurg Psychiatry. 2012;83(6):659–62.

20. Dentel C, Palamiuc L, Henriques A, Lannes B, Spreux-Varoquaux O, Gutknecht L, et al. Degeneration of serotonergic neurons in amyotrophic lateral sclerosis: A link to spasticity. Brain. 2013;136(2):483–93.

21. Ng AS, Rademakers R, Miller BL. Frontotemporal dementia: a bridge between dementia and neuromuscular disease. Ann N Y Acad Sci. 2015;1338:71-93.

22. Van Langenhove T, van der Zee J, van Broeckhoven C. The molecular basis of the frontotemporal lobar degeneration–amyotrophic lateral sclerosis spectrum. Ann Med. 2012;44(8):817–28.

23. Harvey RJ, Skelton-Robinson M, Rossor MN. The prevalence and causes of dementia in people under the age of 65 years. J Neurol Neurosurg Psychiatry. 2003;74(9):1206–9.

24. Snowden JS, Neary D, Mann DM a. Frontotemporal dementia. Br J Psychiatry. 2002;180:140–3.

25. Statement C. Clinical and neuropathological criteria for frontotemporal dementia. The Lund and Manchester Groups. J Neurol Neurosurg Psychiatry. 1994;57(4):416–8.

26. Neary D, et al.. Frontotemporal lobar degeneration: a consensus on clinical diagnostic criteria. Neurology.1998;51(6):1546–54.

27. Hodges JR, Davies R, Xuereb J, Kril J, Halliday G. Survival in frontotemporal dementia. Neurology. 2003;12(61(3)):349–54.

28. Neumann M, Sampathu DM, Kwong LK, Truax AC, Micsenyi MC, Chou TT, et al. Ubiquitinated TDP-43 in Frontotemporal Lobar Degeneration and Amyotrophic Lateral Sclerosis. Science. 2006;130(2006).

29. Neumann M, Rademakers R, Roeber S, Baker M, Kretzschmar H a., MacKenzie IR a. A new subtype of frontotemporal lobar degeneration with FUS pathology. Brain. 2009;132(11):2922–31.

30. Sieben A, Van Langenhove T, Engelborghs S, Martin JJ, Boon P, Cras P, et al. The genetics and neuropathology of frontotemporal lobar degeneration. Acta Neuropathol. 2012;124(3):353–72.

31. MacKenzie IR a, Neumann M, Bigio EH, Cairns NJ, Alafuzoff I, Kril J, et al. Nomenclature and nosology for neuropathologic subtypes of frontotemporal lobar degeneration: An update. Acta Neuropathol. 2010;119(1):1–4.

32. Burrell JR, Kiernan MC, Vucic S, Hodges JR. Motor Neuron dysfunction in frontotemporal dementia. Brain. 2011;134(9):2582–94.

33. Cardarelli R, Kertesz A, Knebl J a. Frontotemporal dementia: A review for primary care physicians. Am Fam Physician. 2010;82(11):1372–7.

34. Josephs K a., Hodges JR, Snowden JS, MacKenzie IR, Neumann M, Mann DM, et al. Neuropathological background of phenotypical variability in frontotemporal dementia. Acta Neuropathol. 2011;122(2):137–53.

35. Piguet O. Eating disturbance in behavioural-variant frontotemporal dementia. J Mol Neurosci. 2011;45(3):589–93.

36. Rascovsky K, Hodges JR, Knopman D, Mendez MF, Kramer JH, Neuhaus J, et al. Sensitivity of revised diagnostic criteria for the behavioural variant of frontotemporal dementia. Brain. 2011;134(9):2456–77.

37. Johnson J. Frontotemporal Lobar Degeneration. Arch Neurol. 2005;62(6):925–30.

38. Phukan J, Pender NP, Hardiman O. Cognitive impairment in amyotrophic lateral sclerosis. Lancet Neurol. 2007;6(11):994–1003.

39. Steele JC The ALSPDC syndrome of Guam and the cycad hypothesis. Neurology. 2008;70(21):1684–90.

40. Renton AE, Chiò A, Traynor BJ. State of play in amyotrophic lateral sclerosis genetics. Nat Neurosci.2014;17(1):17–23.

41. Deng H-X, Chen W, Hong S-T, Boycott KM, Gorrie GH, Siddique N, et al. Mutations in UBQLN2 cause dominant X-linked juvenile and adult-onset ALS and ALS/dementia. Nature. 2011;477(7363):211–5.

42. Okamoto K, Kihira T, Kondo T, Kobashi G, Washio M, Sasaki S, et al. Nutritional status and risk of amyotrophic lateral sclerosis in Japan. Amyotroph Lateral Scler. 2007 ;8(5):300–4.

43. Nelson LM, Matkin C, Longstreth WT, McGuire V. Population-based case-control study of amyotrophic lateral sclerosis in western Washington State. II. Diet. Am J Epidemiol. 2000;151(2):164–73.

44. LC K. Association between blood lead and the risk of amyotrophic lateral sclerosis. J Neurol Sci.2010;291(1-2):22–9.

45. Scarmeas N, Shih T, Stern Y, Ottman R, Rowland LP. Premorbid weight, body mass, and varsity athletics in ALS. Neurology. 2002;59(5):773–5.

46. Chiò A, Benzi G, Dossena M, Mutani R, Mora G. Severely increased risk of amyotrophic lateral sclerosis among Italian professional football players. Brain. 2005 Mar;128(Pt 3):472–6.

47. Al-Chalabi A, Hardiman O. The epidemiology of ALS: a conspiracy of genes, environment and time. Nat Rev Neurol. 2013;9(11):617–28.

48. Peters OM, Ghasemi M, Jr RHB. Emerging mechanisms of molecular pathology in ALS. 2015;125(5):1767–79.

49. Rosen DR, Siddique T, Patterson D, Figlewicz D a, Sapp P, Hentati a, et al. Mutations in Cu/Zn superoxide dismutase gene are associated with familial amyotrophic lateral sclerosis. Nature. 1993;362(6415):59–62.

50. Kwiatkowski T, Bosco DA, L LA, E T, Hosler BA, Cortelli P, et al. Mutations in the FUS/TLS Gene on Chromosome 16 Cause Familial Amyotrophic Lateral Sclerosis. Science. 2009;323(5918):1205–9.

51. Vance C, Rogelj B, Nishimura AL, Sreedharan J, Hu X, Smith B, et al. Mutations in FUs, an RNA Processing Protein, Cause Familial Amyotrophic Lateral Scelrosis Type. Science. 2009;323(5918):1208–11.

52. Sreedharan J, Blair IP, Tripathi VB, Hu X, Vance C, Rogelj B, et al. TDP-43 mutations in familial and sporadic amyotrophic lateral sclerosis.Science 2008;319 (5870):1668-72.

53. DeJesus-Hernandez M, Mackenzie IR, Boeve BF, Boxer AL, Baker M, Rutherford NJ, et al. Expanded GGGGCC Hexanucleotide Repeat in Noncoding Region of C9ORF72 Causes Chromosome 9p-Linked FTD and ALS. Neuron . 2011;72(2):245–56.

54. Renton AE, Majounie E, Waite A, Simón-Sánchez J, Rollinson S, Gibbs JR, et al. A hexanucleotide repeat expansion in C9ORF72 is the cause of chromosome 9p21-linked ALS-FTD. Neuron. 2011;72(2):257–68.

55. Maruyama H, Morino H, Ito H, Izumi Y, Kato H, Watanabe Y, et al. Mutations of optineurin in amyotrophic lateral sclerosis. Nature. 2010;465(7295):223–6.

56. Cirulli ET, Lasseigne BN, Petrovski S, Sapp PC, Dion PA, Leblond CS, et al. Exome sequencing in amyotrophic lateral sclerosis identifies risk genes and pathways. Science. 2015;347(6229):1436–41.

57. Freischmidt A, Wieland T, Richter B, Ruf W, Schaeffer V, Müller K, et al. Haploinsufficiency of TBK1 causes familial ALS and fronto-temporal dementia. Nat Neurosci. 2015;18(5):631-6

58. Goldman JS1, Farmer JM, Wood EM, Johnson JK BA. Comparison of family histories in FTLD subtypes and related tauopathies. Neurology. 2005;13(65(11)):1817–9.

59. Hutton M. Association of missense and 5[prime]-splice-site mutations in tau with the inherited dementia FTDP-17 . Nature. 1998;393(6686):702–5.

60. Baker M, Mackenzie IR, Pickering-Brown SM, Gass J, Rademakers R, Lindholm C, et al. Mutations in progranulin cause tau-negative frontotemporal dementia linked to chromosome 17. Nature. 2006;442(7105):916–9.

61. Rademakers R, Neumann M, Mackenzie IR. Advances in understanding the molecular basis of frontotemporal dementia. Nat Rev Neurol. 2012;8(8):423-34.

62. Millecamps S, Salachas F, Cazeneuve C, Gordon P, Bricka B, Camuzat A, et al. SOD1, ANG, VAPB, TARDBP, and FUS mutations in familial amyotrophic lateral sclerosis: genotype-phenotype correlations. J Med Genet. 2010;47(8):554–60.

63. Turner MR, Hammers a., Al-Chalabi a., Shaw CE, Andersen PM, Brooks DJ, et al. Distinct cerebral lesions in sporadic and “D90A” SOD1 ALS: Studies with [11C]flumazenil PET. Brain. 2005;128(6):1323–9.

64. Gurney ME, Pu H, Chiu a Y, Dal Canto MC, Polchow CY, Alexander DD, et al. Motor neuron degeneration in mice that express a human Cu,Zn superoxide dismutase mutation. Science. 1994;264(5166):1772–5.

65. Beckam J, Carson M, Smith CD, Koppenol WH. ALS, SOD and peroxynitrite (1side), Beckman & Carson, Nature 1993;364(6438):584.

66. B, van Zundreta, Izaurieta P, Fritz E AF. Early pathogenesis in the adult-onset neurodegenerative disease amyotrophic lateral sclerosis. J Cell Biochem. 2012;29(6):997–1003.

67. Vande Velde C, McDonald KK, Boukhedimi Y, McAlonis-Downes M, Lobsiger CS, Hadj SB, et al. Misfolded SOD1 associated with motor neuron mitochondria alters mitochondrial shape and distribution prior to clinical onset. PLoS One. 2011;6(7):1–11.

68. Hetz C, Thielen P, Matus S, Nassif M, Court F, Kiffin R, et al. XBP-1 deficiency in the nervous system protects against amyotrophic lateral sclerosis by increasing autophagy. Genes Dev. 2009;23(19):2294–306.

69. Morfini G a., Bosco D a., Brown H, Gatto R, Kaminska A, Song Y, et al. Inhibition of Fast Axonal Transport by Pathogenic SOD1 Involves Activation of p38 MAP Kinase. PLoS One. 2013;8(6).

70. Kanning KC, Kaplan A, Henderson CE. Motor neuron diversity in development and disease. Annu Rev Neurosci. 2010;33:409–40.

71. Bendotti C, Marino M, Cheroni C, Fontana E, Crippa V, Poletti A, et al. Dysfunction of constitutive and inducible ubiquitin-proteasome system in amyotrophic lateral sclerosis: Implication for protein aggregation and immune response. Prog Neurobiol. 2012;97(2):101–26.

72. Caughey B, Lansbury PT. Protofibrils, pores, fibrils, and neurodegeneration: separating the responsible protein aggregates from the innocent bystanders. Annu Rev Neurosci. 2003;26:267–98.

73. Ray SS, Nowak RJ, Strokovich K, Brown RH, Walz T, Lansbury PT. An Intersubunit Disulfide Bond Prevents in Vitro Aggregation of a Superoxide Dismutase-1 Mutant Linked to Familial Amytrophic Lateral Sclerosis. Biochemistry. 2004;43(17):4899–905.

74. Tan CF, Eguchi H, Tagawa A, Onodera O, Iwasaki T, Tsujino A, et al. TDP-43 immunoreactivity in neuronal inclusions in familial amyotrophic lateral sclerosis with or without SOD1 gene mutation. Acta Neuropathol. 2007;113(5):535–42.

75. Bruijn LI, Beal MF, Becher MW, Schulz JB, Wong PC, Price DL, et al. Elevated free nitrotyrosine levels, but not protein-bound nitrotyrosine or hydroxyl radicals, throughout amyotrophic lateral sclerosis (ALS)-like disease implicate tyrosine nitration as an aberrant in vivo property of one familial ALS-linked superoxide di. Proc Natl Acad Sci U S A. 1997;94(14):7606–11.

76. Turner BJ, Talbot K. Transgenics, toxicity and therapeutics in rodent models of mutant SOD1-mediated familial ALS. Prog Neurobiol. 2008;85(1):94–134.

77. Ludolph AC, Bendotti C, Blaugrund E, Hengerer B, Löffler J-P, Martin J, et al. Guidelines for the preclinical in vivo evaluation of pharmacological active drugs for ALS/MND: report on the 142nd ENMC international workshop. Amyotroph Lateral Scler. 2007;8(4):217–23.

78. Chio A, Calvo A, Mazzini L, Cantello R, Mora G, Moglia C, et al. Extensive genetics of ALS : A population-based study in Italy. Neurology. 2012;79(19):1983–9.

79. Lee EB, Lee VM-Y, Trojanowski JQ. Gains or losses: molecular mechanisms of TDP43-mediated neurodegeneration. Nat Rev Neurosci. 2011;13(1):38-50.

80. Lagier-Tourenne C, Polymenidou M, Cleveland DW. TDP-43 and FUS/TLS: Emerging roles in RNA processing and neurodegeneration. Hum Mol Genet. 2010;19(R1):46–64.

81. Johnson BS, Snead D, Lee JJ, McCaffery JM, Shorter J, Gitler AD. TDP-43 is intrinsically aggregation-prone, and amyotrophic lateral sclerosis-linked mutations accelerate aggregation and increase toxicity. J Biol Chem. 2009;284(30):20329–39.

82. Arnold ES, Ling S-C, Huelga SC, Lagier-Tourenne C, Polymenidou M, Ditsworth D, et al. ALS-linked TDP-43 mutations produce aberrant RNA splicing and adult-onset motor neuron disease without aggregation or loss of nuclear TDP-43. Proc Natl Acad Sci. 2013;110(8):E736–45.

83. Mitchell JC, Constable R, So E, Vance C, Scotter E, Glover L, et al. Wild type human TDP-43 potentiates ALS-linked mutant TDP-43 driven progressive motor and cortical neuron degeneration with pathological features of ALS. Acta Neuropathol Commun. Acta Neuropathologica Communications; 2015;3(1):36.

84. Van Deerlin VM, Leverenz JB, Bekris LM, Bird TD, Yuan W, Elman LB, et al. TARDBP mutations in amyotrophic lateral sclerosis with TDP-43 neuropathology: a genetic and histopathological analysis. Lancet Neurol. 2008;7(5):409–16.

85. M van B. How do C9ORF72 repeat expansions cause amyotrophic lateral sclerosis and frontotemporal dementia can we learn from other noncoding repeat expansion disorders. Changes. 2012;29(6):997–1003.

86. Van Blitterswijk M, DeJesus-Hernandez M, Niemantsverdriet E, Murray ME, Heckman MG, Diehl NN, et al. Association between repeat sizes and clinical and pathological characteristics in carriers of C9ORF72 repeat expansions (Xpansize-72): A cross-sectional cohort study. Lancet Neurol. 2013;12(10):978–88.

87. Van Blitterswijk M, Van Es M a., Hennekam E a M, Dooijes D, Van Rheenen W, Medic J, et al. Evidence for an oligogenic basis of amyotrophic lateral sclerosis. Hum Mol Genet. 2012;21(17):3776–84.

88. Majounie E, Renton AE, Mok K, Dopper EGP, Waite A, Rollinson S, et al. Frequency of the C9orf72 hexanucleotide repeat expansion in patients with amyotrophic lateral sclerosis and frontotemporal dementia: A cross-sectional study. Lancet Neurol. 2012;11(4):323–30.

89. Chiò A, Borghero G, Restagno G, Mora G, Drepper C, Traynor BJ, et al. Clinical characteristics of patients with familial amyotrophic lateral sclerosis carrying the pathogenic GGGGCC hexanucleotide repeat expansion of C9ORF72. Brain. 2012;135(3):784–93.

90. Millecamps S, Boillee S, Le Ber I, Seilhean D, Teyssou E, Giraudeau M, et al. Phenotype difference between ALS patients with expanded repeats in C9ORF72 and patients with mutations in other ALS-related genes. J Med Genet. 2012;49(4):258–63.

91. Brettschneider J, Van Deerlin VM, Robinson JL, Kwong L, Lee EB, Ali YO, et al. Pattern of ubiquilin pathology in ALS and FTLD indicates presence of C9ORF72 hexanucleotide expansion. Acta Neuropathol. 2012;123(6):825–39.

92. Byrne S, Elamin M, Bede P, Shatunov A, Walsh C, Corr B, et al. Cognitive and clinical characteristics of patients with amyotrophic lateral sclerosis carrying a C9orf72 repeat expansion: A population-based cohort study. Lancet Neurol. 2012;11(3):232–40.

93. Farg M a., Sundaramoorthy V, Sultana JM, Yang S, Atkinson R a K, Levina V, et al. C9ORF72, implicated in amytrophic lateral sclerosis and frontotemporal dementia, regulates endosomal trafficking. Hum Mol Genet. 2014;23(13):3579–95.

94. Ash PE a, Bieniek KF, Gendron TF, Caulfield T, Lin WL, DeJesus-Hernandez M, et al. Unconventional Translation of C9ORF72 GGGGCC Expansion Generates Insoluble Polypeptides Specific to c9FTD/ALS. Neuron.2013;77(4):639–46.

95. Mori K, Weng S, Arzberger T, May S, Rentzsch K, Broeckhoven C Van, et al. The C9orf72 GGGGCC repeat is translated into aggregating dipeptide-repeat proteins in FTLD/ALS. 2013;339:1335–8.

96. Mizielinska S, Grönke S, Niccoli T, Ridler CE, Clayton EL, Devoy A, et al. C9orf72 repeat expansions cause neurodegeneration in Drosophila through arginine-rich proteins. 2014;345(6201):1192–4.

97. Johnson JO, Mandrioli J, Benatar M, Abramzon Y, Van Deerlin VM, Trojanowski JQ, et al. Exome Sequencing Reveals VCP Mutations as a Cause of Familial ALS. Neuron. 2010;68(5):857–64.

98. Weihl CC. Valosin containing protein associated fronto-temporal lobar degeneration: clinical presentation, pathologic features and pathogenesis. Curr Alzheimer Res. 2011;8(3):252–60.

99. Watts GDJ, Wymer J, Kovach MJ, Mehta SG, Mumm S, Darvish D, et al. Inclusion body myopathy associated with Paget disease of bone and frontotemporal dementia is caused by mutant valosin-containing protein. Nat Genet. 2004;36(4):377–81.

100. Ju JS, Fuentealba R a., Miller SE, Jackson E, Piwnica-Worms D, Baloh RH, et al. Valosin-containing protein (VCP) is required for autophagy and is disrupted in VCP disease. J Cell Biol. 2009;187(6):875–88.

101. Ju JS, Weihl CC. Inclusion body myopathy, Paget's disease of the bone and fronto-temporal dementia: A disorder of autophagy. Hum Mol Genet. 2010;19(R1):38–45.

102. Williams KL, Warraich ST, Yang S, Solski J a., Fernando R, Rouleau G a., et al. UBQLN2/ubiquilin 2 mutation and pathology in familial amyotrophic lateral sclerosis. Neurobiol Aging. 2012;33(10):2527.e3–2527.e10.

103. Skibinski G, Parkinson NJ, Brown JM, Chakrabarti L, Lloyd SL, Hummerich H, et al. Mutations in the endosomal ESCRTIII-complex subunit CHMP2B in frontotemporal dementia. Nat Genet. 2005;37(8):806–8.

104. Parkinson N, Ince PG, Smith MO, Highley R, Skibinski G, Andersen PM, et al. ALS phenotypes with mutations in CHMP2B (charged multivesicular body protein 2B). Neurology. 2006;67(6):1074–7.

105. Holm IE, Isaacs AM, MacKenzie IR a. Absence of FUS-immunoreactive pathology in frontotemporal dementia linked to chromosome 3 (FTD-3) caused by mutation in the CHMP2B gene. Acta Neuropathol. 2009;118(5):719–20.

106. MacKenzie IR a, Neumann M, Cairns NJ, Munoz DG, Isaacs AM. Novel types of frontotemporal lobar degeneration: Beyond Tau and TDP-43. J Mol Neurosci. 2011;45(3):402–8.

107. Albagha OME, Visconti MR, Alonso N, Langston AL, Cundy T, Dargie R, et al. Genome-wide association study identifies variants at CSF1, OPTN and TNFRSF11A as genetic risk factors for Paget's disease of bone. Nat Genet. 2010;42(6):520–4.

108. Zhu G, Wu CJ, Zhao Y, Ashwell JD. Optineurin Negatively Regulates TNF??- Induced NF-??B Activation by Competing with NEMO for Ubiquitinated RIP. Curr Biol. 2007;17(16):1438–43.

109. Ying H, Yue BY. Optineurin: The autophagy connection. Exp Eye Res. 2015;4835(15):00217-1.

110. Sahlender D a., Roberts RC, Arden SD, Spudich G, Taylor MJ, Luzio JP, et al. Optineurin links myosin VI to the Golgi complex and is involved in Golgi organization and exocytosis. J Cell Biol. 2005;169(2):285–95.

111. Deng H-X, Bigio EH, Zhai H et al. Differential Involvement of Optineurin in Amyotrophic Lateral Sclerosis With or Without SOD1 Mutations. Arch Neurol. 2012;68(8):1057–61.

112. Ito H, Fujita K, Nakamura M, Wate R, Kaneko S, Sasaki S, et al. Optineurin is co-localized with FUS in basophilic inclusions of ALS with FUS mutation and in basophilic inclusion body disease. Acta Neuropathol. 2011;121(4):555–7.

113. Keller B a, Volkening K, Droppelmann C a, Ang LC, Rademakers R, Strong MJ. Co-aggregation of RNA binding proteins in ALS spinal motor neurons: evidence of a common pathogenic mechanism. Acta Neuropathol . 2012;124(5):733–47.

114. Laurin N, Brown JP, Morissette J, Raymond V. Recurrent mutation of the gene encoding sequestosome 1 (SQSTM1/p62) in Paget disease of bone. Am J Hum Genet. 2002;70(6):1582–8.

115. Faisal Fecto, MD; Jianhua Yan, MD, PhD; S. Pavan Vemula; Erdong Liu, MD; Yi Yang, MS; Wenjie Chen, MD; Jian Guo Zheng, MD; Yong Shi, MD, PhD; Nailah Siddique, RN, MSN; Hasan Arrat, MD; Sandra Donkervoort, MS; Senda Ajroud-Driss, MD; Robert L. Sufit, MD; S M. SQSTM1 Mutations in Familial and Sporadic Amyotrophic Lateral Sclerosis. Neurology. 2011;68(11):1440–6.

116. Rubino E, Rainero I, Chio a., Rogaeva E, Galimberti D, Fenoglio P, et al. SQSTM1 mutations in frontotemporal lobar degeneration and amyotrophic lateral sclerosis. Neurology. 2012;79(15):1556–62.

117. Teyssou E, Takeda T, Lebon V, Boillée S, Doukouré B, Bataillon G, et al. Mutations in SQSTM1 encoding p62 in amyotrophic lateral sclerosis: Genetics and neuropathology. Acta Neuropathol. 2013;125(4):511–22.

118. Moscat J, Diaz-Meco MT. P62: A versatile multitasker takes on cancer. Trends Biochem Sci. 2012;37(6):230–6.

119. Bannwarth S, Ait-El-Mkadem S, Chaussenot A, Genin EC, Lacas-Gervais S, Fragaki K, et al. A mitochondrial origin for frontotemporal dementia and amyotrophic lateral sclerosis through CHCHD10 involvement. Brain. 2014;137(8):2329–45.

120. Rademakers R, Cruts M, Van Broeckhoven C. The role of tau (MAPT) in frontotemporal dementia and related tauopathies. Hum Mutat. 2004;24(4):277–95.

121. Rohrer JD WJ. Phenotypic signatures of genetic frontotemporal dementia. Curr Opin Neurol. 2011;26(6):542–9.

122. Cruts M, Theuns J, Van Broeckhoven C. Locus-specific mutation databases for neurodegenerative brain diseases. Hum Mutat. 2012;33(9):1340–4.

123. Gijselinck I, Van Broeckhoven C, Cruts M. Granulin mutations associated with frontotemporal lobar degeneration and related disorders: An update. Hum Mutat. 2008;29(12):1373–86.

124. Le Ber I, Camuzat A, Hannequin D, Pasquier F, Guedj E, Rovelet-Lecrux A, et al. Phenotype variability in progranulin mutation carriers: A clinical, neuropsychological, imaging and genetic study. Brain. 2008;131(3):732–46.

125. Chen-Plotkin AAS, Martinez-Lage M, Sleiman PM a, Hu W, Greene R, Wood EM, et al. Genetic and clinical features of progranulin-associated frontotemporal lobar degeneration. Arch Neurol [Internet]. 2011;68(4):488–97.

126. Gijselinck I, Van Langenhove T, van der Zee J, Sleegers K, Philtjens S, Kleinberger G, et al. A C9orf72 promoter repeat expansion in a Flanders-Belgian cohort with disorders of the frontotemporal lobar degeneration-amyotrophic lateral sclerosis spectrum: A gene identification study. Lancet Neurol. 2012;11(1):54–65.

127. Nishimura AL, Mitne-Neto M, Silva HC a, Richieri-Costa A, Middleton S, Cascio D, et al. A mutation in the vesicle-trafficking protein VAPB causes late-onset spinal muscular atrophy and amyotrophic lateral sclerosis. Am J Hum Genet. 2004;75(5):822–31.

128. Seelaar H, Klijnsma KY, De Koning I, Van Der Lugt A, Chiu WZ, Azmani A, et al. Frequency of ubiquitin and FUS-positive, TDP-43-negative frontotemporal lobar degeneration. J Neurol. 2010;257(5):747–53.

129. Arai T, Nonaka T, Hasegawa M, Akiyama H, Yoshida M, Hashizume Y, et al. Neuronal and glial inclusions in frontotemporal dementia with or without motor neuron disease are immunopositive for p62. Neurosci Lett. 2003;342(1-2):41–4.

130. Al-Chalabi A, Jones A, Troakes C, King A, Al-Sarraj S, Van Den Berg LH. The genetics and neuropathology of amyotrophic lateral sclerosis. Acta Neuropathol. 2012;124(3):339–52.

131. Paviour DC, Lees a. J, Josephs K a., Ozawa T, Ganguly M, Strand C, et al. Frontotemporal lobar degeneration with ubiquitin-only-immunoreactive neuronal changes: Broadening the clinical picture to include progressive supranuclear palsy. Brain. 2004;127(11):2441–51.

132. Benajiba L, Ber I Le, Camuzat A, Lacoste M, Thomas-Anterion C, Couratier P, et al. TARDBP mutations in motoneuron disease with frontotemporal lobar degeneration. Ann Neurol. 2009;65(4):470–4.

133. Borghero G, Floris G, Cannas A, Marrosu MG, Murru MR, Costantino E, et al. A patient carrying a homozygous p.A382T TARDBP missense mutation shows a syndrome including ALS, extrapyramidal symptoms, and FTD. Neurobiol Aging. 2011;32(12):1–8.

134. Borroni B, Bonvicini C, Alberici a., Buratti E, Agosti C, Archetti S, et al. Mutation within TARDBP leads to frontotemporal dementia without motor neuron disease. Hum Mutat. 2009;30(11).

135. Chiò A, Calvo A, Moglia C, Restagno G, Ossola I, Brunetti M, et al. Amyotrophic Lateral Sclerosis-Frontotemporal Lobar Dementia in 3 Families With p.Ala382Thr TARDBP Mutation. Arch Neurol. 2010;67(8):1002–9.

136. Mosca L, Lunetta C, Tarlarini C, Avemaria F, Maestri E, Melazzini M, et al. Wide phenotypic spectrum of the TARDBP gene: Homozygosity of A382T mutation in a patient presenting with amyotrophic lateral sclerosis, Parkinson's disease, and frontotemporal lobar degeneration, and in neurologically healthy subject. Neurobiol Aging . 2012;33(8):1846.e1–1846.e4.

137. Štochl J, Hagtvet K a., Brožová H, Klempíř J, Roth J, Růžička E. Handedness does not predict side of onset of motor symptoms in Parkinson's disease. Mov Disord. 2009;24(12):1836–9.

138. Mackenzie IR a, Bigio EH, Ince PG, Geser F, Neumann M, Cairns NJ, et al. Pathological TDP-43 distinguishes sporadic amyotrophic lateral sclerosis from amyotrophic lateral sclerosis with SOD1 mutations. Ann Neurol. 2007;61(5):427–34.

139. Rohrer, Jonathan D.; Warren JD. Phenotypic signatures of genetic frontotemporal dementia. Curr Opin Neurol. 2011;24(6):542–9.

140. Neumann, Manuela MD; Mackenzie, Ian R. MD; Cairns, Nigel J. PhD; Boyer, Philip J. MD, PhD; Markesbery, William R. MD; Smith, Charles D. MD; Taylor, J. Paul MD, PhD; Kretzschmar, Hans A. MD; Kimonis, Virginia E. MD; Forman, Mark S. MD P. TDP-43 in the Ubiquitin Pathology of Frontotemporal Dementia With VCP Gene Mutations. J Neuropathol Exp Neurol. 2007;66(2):152–7.

141. RH B. TDP-43: the relationship between protein aggregation and neurodegeneration in amyotrophic lateral sclerosis and frontotemporal lobar degeneration. FEBS J. 2011;278:3539–49.

142. Mackenzie IR a. A harmonized classification system for FTLD-TDP pathology. Acta Neuropathol. 2012;122(1):111–3.

143. Eric J. Huang1, 2, Jiasheng Zhang1, 2, Felix Geser3, John Q. Trojanowski3 JB, Strober4, Dennis W. Dickson5, Robert H. Brown Jr6, Barbara E. Shapiro7 and C, Lomen-Hoerth8. Extensive FUS-immunoreactive Pathology in Juvenile Amyotrophic Lateral Sclerosis with Basophilic Inclusions. 2011;20(6):1069–76.

144. Deng H, Zhai H, Bigio EH, Yan J, Fecto F, Ajroud K, et al. FUS-immunooreactive inclusions are a common feature in sporadic and non-SOD1 familial lateral sclerosis. Ann Neurol. 2010;67(6):739–48.

145. Neumann M, Roeber S, Kretzschmar H a., Rademakers R, Baker M, MacKenzie IR a. Abundant FUS-immunoreactive pathology in neuronal intermediate filament inclusion disease. Acta Neuropathol. 2009;118(5):605–16.

146. Munoz DG, Neumann M, Kusaka H, Yokota O, Ishihara K, Terada S, et al. FUS pathology in basophilic inclusion body disease. Acta Neuropathol. 2009;118(5):617–27.

147. MacKenzie IR a, Munoz DG, Kusaka H, Yokota O, Ishihara K, Roeber S, et al. Distinct pathological subtypes of FTLD-FUS. Acta Neuropathol. 2011;121(2):207–18.

148. Langenhove V. Genetic contribution of FUS to frontotemporal lobar degeneration. Neurology. 2010;74(5):366–71.

149. Neumann M, Valori CF, Ansorge O, Kretzschmar H a., Munoz DG, Kusaka H, et al. Transportin 1 accumulates specifically with FET proteins but no other transportin cargos in FTLD-FUS and is absent in FUS inclusions in ALS with FUS mutations. Acta Neuropathol. 2012;124(5):705–16.

150. Neumann M, Bentmann E, Dormann D, Jawaid A, Dejesus-Hernandez M, Ansorge O, et al. FET proteins TAF15 and EWS are selective markers that distinguish FTLD with FUS pathology from amyotrophic lateral sclerosis with FUS mutations. Brain. 2011;134(9):2595–609.

151. Dormann D, Madl T, Valori CF, Bentmann E, Tahirovic S, Abou-Ajram C, et al. Arginine methylation next to the PY-NLS modulates Transportin binding and nuclear import of FUS. EMBO J. 2012;31(22):4258–75.

152. Kulathu Y, Komander D. Atypical ubiquitylation — the unexplored world of polyubiquitin beyond Lys48 and Lys63 linkages. Nat Rev Mol Cell Biol. 2012;13(8):508–23.

153. Chesi A, Staahl BT, Jovičić A, Couthouis J, Fasolino M, Raphael AR, et al. Exome sequencing to identify de novo mutations in sporadic ALS trios. Nat Neurosci . 2013 Jul [cited 2014 Jul 17];16(7):851–5.

154. Couthouis J, Hart MP, Erion R, King OD, Diaz Z, Nakaya T, et al. Evaluating the role of the FUS/TLS-related gene EWSR1 in amyotrophic lateral sclerosis. Hum Mol Genet. 2012;21(13):2899–911.

155. Kim HJ, Kim NC, Wang Y, Scarborough E a, Diaz Z, Maclea KS, et al. Prion-like domain mutations in hnRNPs cause multisystem proteinopathy and ALS. NIH public access. 2013;495(7442):467–73.

156. Conforti FL1, Spataro R, Sproviero W, Mazzei R, Cavalcanti F, Condino F, Simone IL, Logroscino G, Patitucci A, Magariello A, Muglia M, Rodolico C, Valentino P, Bono F, Colletti T, Monsurrò MR, Gambardella A LB V. Ataxin-1 and ataxin-2 intermediate-length PolyQ expansions in amyotrophic lateral sclerosis. Neurology. 2012;79(24):2315–20.

157. Kukharsky MS, Quintiero A, Matsumoto T, Matsukawa K, An H, Hashimoto T, et al. Calcium-responsive transactivator (CREST) protein shares a set of structural and functional traits with other proteins associated with amyotrophic lateral sclerosis. Mol Neurodegener. 2015;10(1):1–18.

158. Johnson JO, Pioro EP, Boehringer A, Chia R, Feit H, Renton AE, et al. Mutations in the Matrin 3 gene cause familial amyotrophic lateral sclerosis. Nat Neurosci.2014;17(5):664–6.

159. Elden AC, Kim H-J, Hart MP, Chen-Plotkin AS, Johnson BS, Fang X, et al. Ataxin-2 intermediate-length polyglutamine expansions are associated with increased risk for ALS. Nature. 2010;466(7310):1069–75.

160. Lemmens R, Moore MJ, Al-Chalabi A, Brown RH, Robberecht W. RNA metabolism and the pathogenesis of motor neuron diseases. Trends Neurosci. 2010;33(5):249–58.

161. Vance C, Scotter EL, Nishimura AL, Troakes C, Mitchell JC, Kathe C, et al. ALS mutant FUS disrupts nuclear localization and sequesters wild-type FUS within cytoplasmic stress granules. Hum Mol Genet. 2013;22(13):2676–88.

162. Robberecht W, Philips T. The changing scene of amyotrophic lateral sclerosis. Nat Rev Neurosci. 2013;14(4):248–64.

163. Colombrita C, Onesto E, Megiorni F, Pizzuti A, Baralle FE, Buratti E, et al. TDP-43 and FUS RNA-binding proteins bind distinct sets of cytoplasmic messenger RNAs and differently regulate their post-transcriptional fate in motoneuron-like cells. J Biol Chem. 2012;287(19):15635–47.

164. Lagier-Tourenne C, Polymenidou M, Hutt KR, Vu AQ, Baughn M, Huelga SC, et al. Divergent roles of ALS-linked proteins FUS/TLS and TDP-43 intersect in processing long pre-mRNAs. Nat Neurosci. 2012;15(11):1488–97.

165. Hoell JI, Larsson E, Runge S, Nusbaum JD, Duggimpudi S, Farazi T a, et al. RNA targets of wild-type and mutant FET family proteins. Nat Struct Mol Biol. 2011;18(12):1428–31.

166. Polymenidou M, Lagier-tourenne C, Hutt KR, Stephanie C, Moran J, Liang TY, et al. Long pre-mRNA depletion and RNA missplicing contribute to neuronal vulnerability from loss of TDP-43. Nat Neurosci. 2011;14(4):459–68.

167. Nagai M, Re DB, Nagata T, Chalazonitis A, Jessell TM, Wichterle H, et al. Astrocytes expressing ALS-linked mutated SOD1 release factors selectively toxic to motor neurons. Nat Neurosci. 2007;10(5):615–22.

168. Marchetto MCN, Muotri AR, Mu Y, Smith AM, Cezar GG, Gage FH. Non-cell-autonomous effect of human SOD1 G37R astrocytes on motor neurons derived from human embryonic stem cells. Cell Stem Cell. 2008;3(6):649–57.

169. Dupuis L, Echaniz-Laguna A. Skeletal muscle in motor neuron diseases: therapeutic target and delivery route for potential treatments. Curr Drug Targets. 2010;11(10):1250–61.

170. Chakkalakal J V, Nishimune H, Ruas JL, Spiegelman BM, Sanes JR. Retrograde influence of muscle fibers on their innervation revealed by a novel marker for slow motoneurons. Development. 2010;137(20):3489–99.

171. Dupuis L, Gonzalez de Aguilar JL, Echaniz-Laguna A, Eschbach J, Rene F, Oudart H, et al. Muscle mitochondrial uncoupling dismantles neuromuscular junction and triggers distal degeneration of motor neurons. PLoS One. 2009;4(4).

172. Wong M, Martin LJ. Skeletal muscle-restricted expression of human SOD1 causes motor neuron degeneration in transgenic mice. Hum Mol Genet. 2010;19(11):2284–302.

173. Nimchinsky E a, Vogt B a, Morrison JH, Hof PR. Spindle neurons of the human anterior cingulate cortex. J Comp Neurol. 1995;355(1):27–37.

174. Seeley WW, Carlin D a., Allman JM, Macedo MN, Bush C, Miller BL, et al. Early frontotemporal dementia targets neurons unique to apes and humans. Ann Neurol. 2006;60(6):660–7.

175. Santillo a. F, Nilsson C, Englund E. von Economo neurones are selectively targeted in frontotemporal dementia. Neuropathol Appl Neurobiol. 2013;39(5):572–9.

176. Santillo AF, Englund E. Greater loss of von Economo neurons than loss of layer II and III neurons in behavioral variant frontotemporal dementia. 2014;3(2):64–71.

177. Krabbe G, Matyash V, Pannasch U, Mamer L, Boddeke HWGM, Kettenmann H. Activation of serotonin receptors promotes microglial injury-induced motility but attenuates phagocytic activity. Brain Behav Immun. 2012;26(3):419–28.

178. Valori CF, Brambilla L, Martorana F, Rossi D. The multifaceted role of glial cells in amyotrophic lateral sclerosis. Cell Mol Life Sci. 2014;71(2):287–97.

179. Murayama S, Inoue K, Kawakami H, Bouldin TW, Suzuki K. A unique pattern of astrocytosis in the primary motor area in amyotrophic lateral sclerosis. Acta Neuropathol. 1991;82(6):456–61.

180. Kawamata T, Akiyama H, Yamada T, McGeer PL. Immunologic reactions in amyotrophic lateral sclerosis brain and spinal cord tissue. Am J Pathol. 1992;140(3):691–707.

181. Yoshihara T, Ishigaki S, Yamamoto M, Liang Y, Niwa JI, Takeuchi H, et al. Differential expression of inflammation- and apoptosis-related genes in spinal cords of a mutant SOD1 transgenic mouse model of familial amyotrophic lateral sclerosis. J Neurochem. 2002;80(1):158–67.

182. Boillée S, Yamanaka K, Lobsiger CS, Copeland NG, Jenkins N a, Kassiotis G, et al. Onset and progression in inherited ALS determined by motor neurons and microglia. Science. 2006;312(5778):1389–92.

183. Yamanaka K, Chun SJ, Boillee S, Fujimori-Tonou N, Yamashita H, Gutmann DH, et al. Astrocytes as determinants of disease progression in inherited amyotrophic lateral sclerosis. Nat Neurosci. 2008;11(3):251–3.

184. Brun a, Liu X, Erikson C. Synapse loss and gliosis in the molecular layer of the cerebral cortex in Alzheimer's disease and in frontal lobe degeneration. Neurodegeneration. 1995;4(2):171–7.

185. Mann DM, South PW, Snowden JS, Neary D. Dementia of frontal lobe type: neuropathology and immunohistochemistry. J Neurol Neurosurg Psychiatry. 1993;56(6):605–14.

186. Schofield E, Kersaitis C, Shepherd CE, Kril JJ, Halliday GM. Severity of gliosis in Pick's disease and frontotemporal lobar degeneration: Tau-positive glia differentiate these disorders. Brain. 2003;126(4):827–40.

187. Kersaitis C, Halliday GM, Kril JJ. Regional and cellular pathology in frontotemporal dementia: Relationship to stage of disease in cases with and without Pick bodies. Acta Neuropathol. 2004;108(6):515–23.

188. Sjögren M, Folkesson S, Blennow K, Tarkowski E. Increased intrathecal inflammatory activity in frontotemporal dementia: pathophysiological implications. J Neurol Neurosurg Psychiatry. 2004;75(8):1107–11.

189. Martinac J a., Craft DK, Su JH, Kim RC, Cotman CW. Astrocytes degenerate in frontotemporal dementia: Possible relation to hypoperfusion. Neurobiol Aging. 2001;22(2):195–207.

190. Swarup V, Phaneuf D, Bareil C, Robertson J, Rouleau G a., Kriz J, et al. Pathological hallmarks of amyotrophic lateral sclerosis/frontotemporal lobar degeneration in transgenic mice produced with TDP-43 genomic fragments. Brain. 2011;134(9):2610–26.

191. Yoshiyama Y, Higuchi M, Zhang B, Huang SM, Iwata N, Saido TC, et al. Synapse Loss and Microglial Activation Precede Tangles in a P301S Tauopathy Mouse Model. Neuron. 2007;53(3):337–51.

192. Ghazi-Noori S, Froud KE, Mizielinska S, Powell C, Smidak M, Fernandez De Marco M, et al. Progressive neuronal inclusion formation and axonal degeneration in CHMP2B mutant transgenic mice. Brain. 2012;135(3):819–32.

193. Yin F, Banerjee R, Thomas B, Zhou P, Qian L, Jia T, et al. Exaggerated inflammation, impaired host defense, and neuropathology in progranulin-deficient mice. J Exp Med. 2010;207(1):117–28.

194. Huang C, Tong J, Bi F, Wu Q, Huang B, Zhou H, et al. Entorhinal cortical neurons are the primary targets of FUS mislocalization and ubiquitin aggregation in FUS transgenic rats. Hum Mol Genet. 2012;21(21):4602–14.

195. Huang C, Zhou H, Tong J, Chen H, Liu YJ, Wang D, et al. FUS transgenic rats develop the phenotypes of amyotrophic lateral sclerosis and frontotemporal lobar degeneration. PLoS Genet. 2011;7(3).

196. Mitchell JC, McGoldrick P, Vance C, Hortobagyi T, Sreedharan J, Rogelj B, et al. Overexpression of human wild-type FUS causes progressive motor neuron degeneration in an age- and dose-dependent fashion. Acta Neuropathol. 2013;125(2):273–88.

197. Qiu H, Lee S, Shang Y, Wang W-Y, Au KF, Kamiya S, et al. ALS-associated mutation FUS-R521C causes DNA damage and RNA splicing defects. J Clin Invest [Internet]. 2014 Mar 3;124(3):981–99.

198. Shelkovnikova T a., Peters OM, Deykin A V., Connor-Robson N, Robinson H, Ustyugov A a., et al. Fused in sarcoma (FUS) protein lacking nuclear localization signal (NLS) and major RNA binding motifs triggers proteinopathy and severe motor phenotype in transgenic mice. J Biol Chem. 2013;288(35):25266–74.

199. Forman MS, Lal D, Zhang B, Dabir D V, Swanson E, Lee VM-Y, et al. Transgenic mouse model of tau pathology in astrocytes leading to nervous system degeneration. J Neurosci. 2005;25(14):3539–50.

200. Roberson ED, Filiano AJ, Martens LH, Young AH, Warmus B a., Zhou P, et al. Dissociation of frontotemporal dementia-related deficits and neuroinflammation in progranulin haploinsufficient mice. Ann Intern Med. 2013;158(6):5352–62.

201. Crozat a, Aman P, Mandahl N, Ron D. Fusion of CHOP to a novel RNA-binding protein in human myxoid liposarcoma. Nature. 1993;363(6430): 640–4.

202. Kretzschmar H a, Rademakers R, Mackenzie IR a. Abundant FUS-immunoreactive pathology in neuronal intermediate filament inclusion disease. Acta Neuropathol. 2010;118(5):605–16.

203. Dormann D, Rodde R, Edbauer D, Bentmann E, Fischer I, Hruscha A, et al. ALS-associated fused in sarcoma (FUS) mutations disrupt Transportin-mediated nuclear import. EMBO J. 2010;29(16):2841–57.

204. Lee BJ, Cansizoglu AE, Süel KE, Louis TH, Zhang Z, Chook YM. Rules for Nuclear Localization Sequence Recognition by Karyopherinβ2. Cell. 2006;126(3):543–58.

205. Prasad DD, Ouchida M, Lee L, Rao VN, Reddy ES. TLS/FUS fusion domain of TLS/FUS-erg chimeric protein resulting from the t(16;21) chromosomal translocation in human myeloid leukemia functions as a transcriptional activation domain. Oncogene. 1994. p. 3717–29.

206. Zinszner H, Albalat R, Ron D. A novel effector domain from the RNA-binding protein TLS or EWS is required for oncogenic transformation by CHOP. Genes Dev. 1994;8(21):2513–26.

207. Kato M, Han TW, Xie S, Shi K, Du X, Wu LC, et al. Cell-free formation of RNA granules: Low complexity sequence domains form dynamic fibers within hydrogels. Cell. 2012;149(4):753–67.

208. Sun Z, Diaz Z, Fang X, Hart MP, Chesi A, Shorter J, et al. Molecular determinants and genetic modifiers of aggregation and toxicity for the ALS disease protein FUS/TLS. PLoS Biol . 2011;9(4):e1000614.

209. Gitler AD, Shorter J. RNA-binding proteins with prion-like domains in ALS and FTLD-U. Prion. 2011;5(3):179–87.

210. Burd CG, Dreyfuss G. Conserved structures and diversity of functions of RNA-binding proteins. Science. 1994;265(5172):615–21.

211. Zinszner H, Sok J, Immanuel D, Yin Y, Ron D. TLS (FUS) binds RNA in vivo and engages in nucleo-cytoplasmic shuttling. J Cell Sci. 1997;110(Pt 15):1741–50.

212. Bentmann E, Neumann M, Tahirovic S, Rodde R, Dormann D, Haass C. Requirements for stress granule recruitment of fused in sarcoma (FUS) and TAR DNA-binding protein of 43 kDa (TDP-43). J Biol Chem. 2012;287(27):23079–94.

213. Iko Y, Kodama TS, Kasai N, Oyama T, Morita EH, Muto T, et al. Domain architectures and characterization of an RNA-binding protein, TLS. J Biol Chem. 2004;279(43):44834–40.

214. Huang C, Xia PY, Zhou H. Sustained Expression of TDP-43 and FUS in Motor Neurons in Rodent's Lifetime. Int J Biol Sci. 2010;6(4):396–406.

215. Browner WS, Kahn AJ, Ziv E, Reiner AP, Oshima J, Cawthon RM, et al. The genetics of human longevity. Am J Med. 2004;117(11):851–60.

216. Baechtold H, Kuroda M, Sok J, Ron D, Lopez BS, Akhmedov AT. Human 75-kDa DNA-pairing protein is identical to the pro-oncoprotein TLS/FUS and is able to promote D-loop formation. J Biol Chem. 1999;274(48):34337–42.

217. Gardiner M, Toth R, Vandermoere F, Morrice N a, Rouse J. Identification and characterization of FUS/TLS as a new target of ATM. The Biochemical journal. 2008;415(2):297–307.

218. Wang W-Y, Pan L, Su SC, Quinn EJ, Sasaki M, Jimenez JC, et al. Interaction of FUS and HDAC1 regulates DNA damage response and repair in neurons. Nat Neurosci. 2013;16(10):1383–91.

219. Hicks GG, Singh N, Nashabi a, Mai S, Bozek G, Klewes L, et al. Fus deficiency in mice results in defective B-lymphocyte development and activation, high levels of chromosomal instability and perinatal death. Nat Genet. 2000;24(2):175–9.

220. Kuroda M, Sok J, Webb L, Baechtold H, Urano F, Yin Y, et al. Male sterility and enhanced radiation sensitivity in TLS(-/-) mice. EMBO J. 2000;19(3):453–62.

221. Kino Y, Washizu C, Kurosawa M, Yamada M, Miyazaki H, Akagi T, et al. FUS/TLS deficiency causes behavioral and pathological abnormalities distinct from amyotrophic lateral sclerosis. Acta Neuropathol Commun. 2015;3(1):1–11.

222. Das R, Yu J, Zhang Z, Gygi MP, Krainer AR, Gygi SP, et al. SR Proteins Function in Coupling RNAP II Transcription to Pre-mRNA Splicing. Mol Cell. 2007;26(6):867–81.

223. Yang L, Embree LJ, Hickstein DD. TLS-ERG leukemia fusion protein inhibits RNA splicing mediated by serine-arginine proteins. Mol Cell Biol. 2000;20(10):3345–54.

224. Li X, Decker M, Westendorf JJ. TEThered to Runx: Novel binding partners for runx factors. Blood Cells, Mol Dis. 2010;45(1):82–5.

225. Powers C a, Mathur M, Raaka BM, Ron D, Samuels HH. TLS (translocated-in-liposarcoma) is a high-affinity interactor for steroid, thyroid hormone, and retinoid receptors. Mol Endocrinol. 1998;12(1):4–18.

226. Uranishi H, Tetsuka T, Yamashita M, Asamitsu K, Shimizu M, Itoh M, et al. Involvement of the Pro-oncoprotein TLS (Translocated in Liposarcoma) in Nuclear Factor-??B p65-mediated Transcription as a Coactivator. J Biol Chem. 2001;276(16):13395–401.

227. Tan AY, Manley JL. TLS inhibits RNA polymerase III transcription. Mol Cell Biol. 2010;30(1):186–96.

228. Wang X, Arai S, Song X, Reichart D, Du K, Pascual G, et al. Induced ncRNAs allosterically modify RNA-binding proteins in cis to inhibit transcription. Nature. 2008;454(7200):126–30.

229. Tan AY, Riley TR, Coady T, Bussemaker HJ, Manley JL. TLS / FUS (translocated in liposarcoma / fused in sarcoma) regulates target gene transcription via single-stranded DNA response elements. Proc Natl Acad Sci U S A. 2012;109(16):6030-5.

230. Lanson N a., Pandey UB. FUS-related proteinopathies: Lessons from animal models. Brain Res. 2012;1462:44–60.

231. Carvalho T, Almeida F, Calapez A, Lafarga M, Berciano MT, Carmo-Fonseca M. The Spinal Muscular Atrophy Disease Gene Product, Smn. J Cell Biol. 1999;147(4):715–28.

232. Hartmuth K, Urlaub H, Vornlocher H-P, Will CL, Gentzel M, Wilm M, et al. Protein composition of human prespliceosomes isolated by a tobramycin affinity-selection method. Proc Natl Acad Sci U S A. 2002;99(26):16719–24.

233. Zhou Z, Licklider LJ, Gygi SP, Reed R. Comprehensive proteomic analysis of the human spliceosome. Nature. 2002;419(6903):182–5.

234. Tsuiji H, Iguchi Y, Furuya A, Kataoka A, Hatsuta H, Atsuta N, et al. Spliceosome integrity is defective in the motor neuron diseases ALS and SMA. EMBO Mol Med. 2013;5(2):221–34.

235. Yamazaki T, Chen S, Yu Y, Yan B, Haertlein TC, Carrasco M a., et al. FUS-SMN Protein Interactions Link the Motor Neuron Diseases ALS and SMA. Cell Rep. The Authors; 2012;2(4):799–806.

236. Ishigaki S, Masuda A, Fujioka Y, Iguchi Y, Katsuno M, Shibata A, et al. Position-dependent FUS-RNA interactions regulate alternative splicing events and transcriptions. Sci Rep. 2012;2:529.

237. Rogelj B, Easton LE, Bogu GK, Stanton LW, Rot G, Curk T, et al. Widespread binding of FUS along nascent RNA regulates alternative splicing in the brain. Sci Rep. 2012;2:1–10.

238. Zhou Y, Liu S, Liu G, Öztürk A, Hicks GG. ALS-Associated FUS Mutations Result in Compromised FUS Alternative Splicing and Autoregulation. PLoS Genet. 2013;9(10).

239. Gregory RI, Yan K-P, Amuthan G, Chendrimada T, Doratotaj B, Cooch N, et al. The Microprocessor complex mediates the genesis of microRNAs. Nature. 2004;432(7014):235–40.

240. Newman M a., Hammond SM. Emerging paradigms of regulated microRNA processing. Genes Dev. 2010;24(11):1086–92.

241. Morlando M, Dini Modigliani S, Torrelli G, Rosa A, Di Carlo V, Caffarelli E, et al. FUS stimulates microRNA biogenesis by facilitating co-transcriptional Drosha recruitment. EMBO J. 2012;31(24):4502–10.

242. Fujii R, Okabe S, Urushido T, Inoue K, Yoshimura A, Tachibana T, et al. The RNA binding protein TLS is translocated to dendritic spines by mGluR5 activation and regulates spine morphology. Curr Biol. 2005;15(6):587–93.

243. Tolino M, Köhrmann M, Kiebler M a. RNA-binding proteins involved in RNA localization and their implications in neuronal diseases. European Journal of Neuroscience. 2012;35(12):1818–36.

244. Tibshirani M, Tradewell ML, Mattina KR, Minotti S, Yang W, Zhou H, et al. Cytoplasmic sequestration of FUS/TLS associated with ALS alters histone marks through loss of nuclear protein arginine methyltransferase 1. Hum Mol Genet . 2014;24(3):773–86.

245. Doi H, Okamura K, Bauer PO, Furukawa Y, Shimizu H, Kurosawa M, et al. RNA-binding protein TLS is a major nuclear aggregate-interacting protein in Huntingtin exon 1 with expanded polyglutamine-expressing cells. J Biol Chem. 2008;283(10):6489–500.

246. Mori F, Tanji K, Kon T, Odagiri S, Hattori M, Hoshikawa Y, et al. FUS immunoreactivity of neuronal and glial intranuclear inclusions in intranuclear inclusion body disease. Neuropathol Appl Neurobiol. 2012;38(4):322–8.

247. Woulfe J, Gray D a., MacKenzie IR a. FUS-Immunoreactive intranuclear inclusions in neurodegenerative disease. Brain Pathol. 2010;20(3):589–97.

248. Dormann D, Haass C. TDP-43 and FUS: a nuclear affair. Trends Neurosci. 2011; 34(7):339–48.

249. Bosco D a., Lemay N, Ko HK, Zhou H, Burke C, Kwiatkowski TJ, et al. Mutant FUS proteins that cause amyotrophic lateral sclerosis incorporate into stress granules. Hum Mol Genet. 2010;19(21):4160–75.

250. Deng H, Gao K, Jankovic J. The role of FUS gene variants in neurodegenerative diseases. Nat Rev Neurol. 2014;10(6):337–48.

251. Bertolin C, D'Ascenzo C, Querin G, Gaiani A, Boaretto F, Salvoro C, et al. Improving the knowledge of amyotrophic lateral sclerosis genetics: Novel SOD1 and FUS variants. Neurobiol Aging . 2014;35(5):1212.e7–1212.e10.

252. O B. FUS mutations in frontotemporal lobar degeneration with amyotrophic lateral sclerosis. J Alzheimer's Dis. 2010;vol. 22,(no. 3):56–61.

253. Ticozzi N, Silani V, Leclerc a. L, Keagle P, Gellera C, Ratti a., et al. Analysis of FUS gene mutation in familial amyotrophic lateral sclerosis within an Italian cohort. Neurology. 2009;73(15):1180–5.

254. Yan J, Deng HX, Siddique N, Fecto F, Chen W, Yang Y, et al. Frameshift and novel mutations in FUS in familial amyotrophic lateral sclerosis and ALS/dementia. Neurology. 2010;75(9):807–14.

255. Langenhove T Van, Zee J Van Der, Sleegers K, Van Langenhove T, van der Zee J, Engelborghs S, et al. Genetic contribution of FUS to frontotemporal lobar degeneration. Neurology. 2010;74(5):366–71.

256. Bäumer D, Hilton D, Paine SML, Turner MR, Lowe J, Talbot K, et al. Juvenile ALS with basophilic inclusions is a FUS proteinopathy with FUS mutations. Neurology. 2010;75(7):611–8.

257. Waibel S, Neumann M, Rosenbohm a., Birve a., Volk a. E, Weishaupt JH, et al. Truncating mutations in FUS/TLS give rise to a more aggressive ALS-phenotype than missense mutations: A clinico-genetic study in Germany. Eur J Neurol. 2013;20(3):540–6.

258. Lashley T, Rohrer JD, Bandopadhyay R, Fry C, Ahmed Z, Isaacs AM, et al. A comparative clinical, pathological, biochemical and genetic study of fused in sarcoma proteinopathies. Brain. 2011;134(Pt 9):2548–64.

259. Urwin H, Josephs K a., Rohrer JD, MacKenzie IR, Neumann M, Authier A, et al. FUS pathology defines the majority of tau-and TDP-43-negative frontotemporal lobar degeneration. Acta Neuropathol. 2010;120(1):33–41.

260. Snowden JS, Hu Q, Rollinson S, Halliwell N, Robinson A, Davidson YS, et al. The most common type of FTLD-FUS (aFTLD-U) is associated with a distinct clinical form of frontotemporal dementia but is not related to mutations in the FUS gene. Acta Neuropathol. 2011;122(1):99–110.

261. Neumann M. Frontotemporal lobar degeneration and amyotrophic lateral sclerosis: Molecular similarities and differences. Rev Neurol. 2013;169(10):793–8.

262. Dormann D, Haass C. Fused in sarcoma (FUS): An oncogene goes awry in neurodegeneration. Mol Cell Neurosci. 2013;56:475–86.

263. Orozco D, Tahirovic S, Rentzsch K, Schwenk BM, Haass C, Edbauer D. Loss of fused in sarcoma (FUS) promotes pathological Tau splicing. EMBO Rep . 2012;13(8):759–64.

264. Nover L, Scharf KD, Neumann D. Cytoplasmic heat shock granules are formed from precursor particles and are associated with a specific set of mRNAs. Mol Cell Biol. 1989;9(3):1298–308.

265. Gal J, Zhang J, Kwinter DM, Zhai J, Jia H, 2 Jia J, Zhu H. Nuclear localization sequence of FUS and induction of stress granules by ALS mutants. Neurobiol Aging. 2011;32(126):27–40.

266. Li YR, King OD, Shorter J, Gitler AD. Stress granules as crucibles of ALS pathogenesis. J Cell Biol. 2013;201(3):361–72.

267. Takanashi K, Yamaguchi A. Aggregation of ALS-linked FUS mutant sequesters RNA binding proteins and impairs RNA granules formation. Biochem Biophys Res Commun. 2014;452(3):600–7.

268. Andersson MK, Ståhlberg A, Arvidsson Y, Olofsson A, Semb H, Stenman G, et al. The multifunctional FUS, EWS and TAF15 proto-oncoproteins show cell type-specific expression patterns and involvement in cell spreading and stress response. BMC Cell Biol. 2008;9:37.

269. Frost B, Diamond MI. Prion-like mechanisms in neurodegenerative diseases. Nat Rev Neurosci. 2010;11(3):155–9.

270. King ODE Al. The tip of the iceberg: RNA-binding proteins with prion-like domains in neurodegenerative disease. Brain Res. 2012;(1462):61–80.

271. Polymenidou M, Cleveland DW. The seeds of neurodegeneration: Prion-like spreading in ALS. Cell. 2011;147(3):498–508.

272. Tradewell ML, Yu Z, Tibshirani M, Boulanger MC, Durham HD, Richard S. Arginine methylation by prmt1 regulates nuclear-cytoplasmic localization and toxicity of FUS/TLS harbouring ALS-linked mutations. Hum Mol Genet. 2012;21(1):136–49.

273. Ju S, Tardiff DF, Han H, Divya K, Zhong Q, Maquat LE, et al. A Yeast Model of FUS/TLS-Dependent Cytotoxicity. PLoS Biol. 2011;9(4).

274. Fushimi K, Long C, Jayaram N, Chen X, Li L, Wu JY. Expression of human FUS/TLS in yeast leads to protein aggregation and cytotoxicity, recapitulating key features of FUS proteinopathy. Protein Cell. 2011;2(2):141–9.

275. Lanson N a., Maltare A, King H, Smith R, Kim JH, Taylor JP, et al. A Drosophila model of FUS-related neurodegeneration reveals genetic interaction between FUS and TDP-43. Hum Mol Genet. 2011;20(13):2510–23.

276. Miguel L, Avequin T, Delarue M, Feuillette S, Frébourg T, Campion D, et al. Accumulation of insoluble forms of FUS protein correlates with toxicity in Drosophila. Neurobiol Aging. Elsevier Inc.; 2012;33(5):1008.e1–1008.e15.

277. Chen Y, Yang M, Deng J, Chen X, Ye Y, Zhu L, et al. Expression of human FUS protein in Drosophila leads to progressive neurodegeneration. Protein Cell. 2011;2(6):477–86.

278. Xia R, Liu Y, Yang L, Gal J, Zhu H, Jia J. Motor neuron apoptosis and neuromuscular junction perturbation are prominent features in a Drosophila model of Fus-mediated ALS. Mol Neurodegener. 2012;7:10.

279. Frickenhaus M, Wagner M, Mallik M, Catinozzi M, Storkebaum E. Highly efficient cell-type-specific gene inactivation reveals a key function for the Drosophila FUS homolog cabeza in neurons. Sci Rep. 2015;5:9107.

280. Murakami T, Yang SP, Xie L, Kawano T, Fu D, Mukai A, et al. Als mutations in FUS cause neuronal dysfunction and death in caenorhabditis elegans by a dominant gain-of-function mechanism. Hum Mol Genet. 2012;21(1):1–9.

281. Vaccaro A, Tauffenberger A, Aggad D, Rouleau G, Drapeau P, Parker JA. Mutant TDP-43 and FUS cause age-dependent paralysis and neurodegeneration in C. elegans. PLoS One. 2012;7(2):1–10.

282. Udagawa T, Fujioka Y, Tanaka M, Honda D, Yokoi S, Riku Y, et al. FUS regulates AMPA receptor function and FTLD/ALS-associated behaviour via GluA1 mRNA stabilization. Nat Commun. 2015;6:7098.

283. Verbeeck C, Deng Q, Dejesus-Hernandez M, Taylor G, Ceballos-Diaz C, Kocerha J, et al. Expression of Fused in sarcoma mutations in mice recapitulates the neuropathology of FUS proteinopathies and provides insight into disease pathogenesis. Mol Neurodegener. 2012;7(1):53.

284. Parkhomchuk D, Borodina T, Amstislavskiy V, Banaru M, Hallen L, Krobitsch S, et al. Transcriptome analysis by strand-specific sequencing of complementary DNA. Nucleic Acids Res. 2009;37(18).

285. Zhou Z, Qiu J, Liu W, Zhou Y, Plocinik RM, Li H, et al. The Akt-SRPK-SR Axis Constitutes a Major Pathway in Transducing EGF Signaling to Regulate Alternative Splicing in the Nucleus. Mol Cell. 2012;47(3):422–33.

286. Brudvig XJ, Cain J. Journal Club KIS: Synaptic Plasticity's Missing Molecular Link? 2015;35(7):2839–41.

287. Dini Modigliani S, Morlando M, Errichelli L, Sabatelli M, Bozzoni I. An ALS-associated mutation in the FUS 3'-UTR disrupts a microRNA-FUS regulatory circuitry. Nat Commun. 2014;5:4335.

288. Jokic N, Gonzalez de Aguilar J-L, Dimou L, Lin S, Fergani A, Ruegg M a, et al. The neurite outgrowth inhibitor Nogo-A promotes denervation in an amyotrophic lateral sclerosis model. EMBO Rep. 2006;7(11):1162–7.

289. Wong PC, Pardo C a, Borchelt DR, Lee MK, Copeland NG, Jenkins N a, et al. An adverse property of a familial ALS-linked SOD1 mutation causes motor neuron disease characterized by vacuolar degeneration of mitochondria. Neuron. 1995;14(6):1105–16.

290. Bruijn LI, Becher MW, Lee MK, Anderson KL, Jenkins N a., Copeland NG, et al. ALS-linked SOD1 mutant G85R mediates damage to astrocytes and promotes rapidly progressive disease with SOD1-containing inclusions. Neuron. 1997;18(2):327–38.

291. Alfieri J a., Pino NS, Igaz LM. Reversible Behavioral Phenotypes in a Conditional Mouse Model of TDP-43 Proteinopathies. J Neurosci. 2014;34(46):15244–59.

292. Chew J, Gendron TF, Prudencio M, Sasaguri H, Zhang Y, Castanedes-casey M, et al. C9ORF72 repeat expansions in mice cause TDP-43 pathology, neuronal loss, and behavioral deficits. 2015;348(6239):1151–4.

293. Gascon E, Lynch K, Ruan H, Almeida S, Verheyden JM, Seeley WW, et al. Alterations in microRNA-124 and AMPA receptors contribute to social behavioral deficits in frontotemporal dementia. Nat Med. 2014;20(12):1444–51.

294. Badadani M, Nalbandian A, Watts GD, Vesa J, Kitazawa M, Su H, et al. VCP associated inclusion body myopathy and paget disease of bone knock-in mouse model exhibits tissue pathology typical of human disease. PLoS One. 2010;5(10).

295. Custer SK, Neumann M, Lu H, Wright AC, Taylor JP. Transgenic mice expressing mutant forms VCP/p97 recapitulate the full spectrum of IBMPFD including degeneration in muscle, brain and bone. Hum Mol Genet. 2010;19(9):1741–55.

296. Igaz LM, Kwong LK, Lee EB, Chen-Plotkin A, Swanson E, Unger T, et al. Dysregulation of the ALS-associated gene TDP-43 leads to neuronal death and degeneration in mice. J Clin Invest. 2011;121(2):726–38.

297. Kayasuga Y, Chiba S, Suzuki M, Kikusui T, Matsuwaki T, Yamanouchi K, et al. Alteration of behavioural phenotype in mice by targeted disruption of the progranulin gene. Behav Brain Res. 2007;185(2):110–8.

298. Tsai K-J, Yang C-H, Fang Y-H, Cho K-H, Chien W-L, Wang W-T, et al. Elevated expression of TDP-43 in the forebrain of mice is sufficient to cause neurological and pathological phenotypes mimicking FTLD-U. J Exp Med. 2010;207(8):1661–73.

299. Lashley T, Rohrer JD, Bandopadhyay R, Fry C, Ahmed Z, Isaacs AM, et al. A comparative clinical, pathological, biochemical and genetic study of fused in sarcoma proteinopathies. Brain. 2011;134(9):2548–64.

300. Gardner RC, Yaffe K. Epidemiology of mild traumatic brain injury and neurodegenerative disease. Mol Cell Neurosci. 2015;66:75–80.

301. Dupuis L, Pradat P-F, Ludolph AC, Loeffler J-P. Energy metabolism in amyotrophic lateral sclerosis. Lancet Neurol. 2011;10(1):75–82.

302. Brettschneider J, Del Tredici K, Toledo JB, Robinson JL, Irwin DJ, Grossman M, et al. Stages of pTDP-43 pathology in amyotrophic lateral sclerosis. Ann Neurol. 2013;74(1):20–38.

ANNEX

I. PUBLICATION Nº3

OPEN ACCESS Freely available online

PLOS | GENETICS

VAPB/ALS8 MSP Ligands Regulate Striated Muscle Energy Metabolism Critical for Adult Survival in *Caenorhabditis elegans*

Sung Min Han[1], Hajer El Oussini[2,3], Jelena Scekic-Zahirovic[2,3], Jack Vibbert[1], Pauline Cottee[1], Jeevan K. Prasain[4], Hugo J. Bellen[5,6,7], Luc Dupuis[2,3], Michael A. Miller[1]*

1 Department of Cell, Developmental, and Integrative Biology, University of Alabama School of Medicine, Birmingham, Alabama, United States of America, **2** INSERM, U1118, Mécanismes centraux et périphériques de la neurodégénérescence, Strasbourg, France, **3** Faculté de Médecine, Fédération de Médecine Translationnelle de Strasbourg, Université de Strasbourg, UMRS1118, Strasbourg, France, **4** Department of Pharmacology and Toxicology, University of Alabama School of Medicine, Birmingham, Alabama, United States of America, **5** Howard Hughes Medical Institute, Chevy Chase, Maryland, United States of America, **6** Department of Molecular and Human Genetics, Baylor College of Medicine, Houston, Texas, United States of America, **7** Program in Developmental Biology, Baylor College of Medicine, Houston, Texas, United States of America

Abstract

Mutations in VAPB/ALS8 are associated with amyotrophic lateral sclerosis (ALS) and spinal muscular atrophy (SMA), two motor neuron diseases that often include alterations in energy metabolism. We have shown that *C. elegans* and Drosophila neurons secrete a cleavage product of VAPB, the N-terminal major sperm protein domain (vMSP). Secreted vMSPs signal through Roundabout and Lar-like receptors expressed on striated muscle. The muscle signaling pathway localizes mitochondria to myofilaments, alters their fission/fusion balance, and promotes energy production. Here, we show that neuronal loss of the *C. elegans* VAPB homolog triggers metabolic alterations that appear to compensate for muscle mitochondrial dysfunction. When vMSP levels drop, cytoskeletal or mitochondrial abnormalities in muscle induce elevated DAF-16, the Forkhead Box O (FoxO) homolog, transcription factor activity. DAF-16 promotes muscle triacylglycerol accumulation, increases ATP levels in adults, and extends lifespan, despite reduced muscle mitochondria electron transport chain activity. Finally, *Vapb* knock-out mice exhibit abnormal muscular triacylglycerol levels and FoxO target gene transcriptional responses to fasting and refeeding. Our data indicate that impaired vMSP signaling to striated muscle alters FoxO activity, which affects energy metabolism. Abnormalities in energy metabolism of ALS patients may thus constitute a compensatory mechanism counterbalancing skeletal muscle mitochondrial dysfunction.

Citation: Han SM, El Oussini H, Scekic-Zahirovic J, Vibbert J, Cottee P, et al. (2013) VAPB/ALS8 MSP Ligands Regulate Striated Muscle Energy Metabolism Critical for Adult Survival in *Caenorhabditis elegans*. PLoS Genet 9(9): e1003738. doi:10.1371/journal.pgen.1003738

Editor: Kaveh Ashrafi, University of California San Francisco, United States of America

Received April 5, 2013; **Accepted** July 8, 2013; **Published** September 5, 2013

Funding: This project was funded by the Muscular Dystrophy Association (MDA186119, to MAM), UAB Clinical Nutrition Center Nutrition or Obesity-Related Pilot Feasibility Studies grant (UAB NORC grant P30DK056336, to MAM), Amyotrophic Lateral Sclerosis Association (grant #1698, to LD), Agence Nationale de la Recherche (ANR JCJC Dynemit, to LD), Association pour la recherche sur la SLA et les autres maladies du motoneurone (to LD), Thierry Latran Foundation (SpastALS, to LD), and Association Pour La Recherche Et le Développement de Moyens de Lutte Contre les Maladies Neurodégénératives (to LD). JSZ is supported by the ERASMUS Neurotime project. The UAB Targeted Metabolomics and Proteomics Laboratory has been supported in part by the UAB Skin Disease Research Center (P30 AR050948), the UAB-UCSD O'Brien Acute Kidney Injury Center (P30 DK079337), and the UAB Lung Health Center (R01 HL114439, R01 HL110950). Support for the mass spectrometer was from a NCRR Shared Instrumentation grant (S10 RR19261). The Caenorhabditis Genetics Center is supported by the NIH Office of Research Infrastructure Programs (P40 OD010440) and the Japanese National Bioresource Project is supported by the Ministry of Education, Culture, Science, Sports and Technology. HJB is an investigator of the HHMI. The funders had no role in study design, data collection and analysis, decision to publish, or preparation of the manuscript.

Competing Interests: The authors HJB and MAM declare a potential conflict of interest. A patent application has been filed and HJB is part of HEALS Biopharma.

* E-mail: mamiller@uab.edu

Introduction

ALS is a lethal neurodegenerative disease characterized by the combined degeneration of lower and upper motor neurons [1]. Most ALS cases occur sporadically, but about 10% are familial. These genetic cases are caused by mutations in multiple genes, including in the *Vapb* (VAMP/synaptobrevin-associated protein B) gene. Mutations in *Vapb* lead to ALS8 that manifests as ALS or late-onset SMA, a motor neuron disease restricted to lower motor neurons [2–4]. While *Vapb* mutations are rare, reduced VAPB mRNA or protein levels have been reported in sporadic ALS patients, a mSOD1 ALS mouse model, and *ALS8* patient motor neurons derived from induced pluripotent stem cells [5–7]. Hence, a loss of VAPB might be relevant in non-*ALS8* patients.

VAPB, and its paralog VAPA, are broadly expressed type II membrane proteins that are evolutionarily conserved. These VAPs have been implicated in regulating lipid transport and homeostasis at intracellular organelle contact sites, endoplasmic reticulum (ER) dynamics, and membrane trafficking [8–12]. In addition to these cell autonomous functions, the VAP vMSP is cleaved from the transmembrane domain in the cytoplasm and secreted in a cell-type specific fashion [13–15]. Secreted vMSPs antagonize Eph receptor signaling through a direct interaction with the extracellular domain [13]. More recently, we have shown in *C. elegans* and Drosophila that neurons secrete vMSPs to regulate mitochondrial

Author Summary

ALS patients often present with systemic alterations in energy metabolism, such as dyslipidemia and hypermetabolism of unknown origin. Reduction of *Vapb* function is thought to cause motor neuron disease in *ALS8* patients and may predispose individuals to ALS, in general. We have shown that neurons secrete the N-terminal VAPB vMSP into the extracellular environment. The secreted vMSPs signal through Roundabout and Lar-like receptors on striated muscles. This neuron to muscle signaling pathway localizes mitochondria to myofilament I-bands and promotes mitochondrial function. Here we show that loss of VAPB in *C. elegans* neurons causes metabolic changes in muscles, including altered fat metabolism and elevated DAF-16 FoxO transcription factor activity. DAF-16 promotes muscle triacylglycerol accumulation, increases ATP levels, and prolongs survival in *Vapb* mutants. However, it does not influence muscle mitochondrial localization nor does it affect oxygen consumption. We also show that *Vapb* knockout mice exhibit disrupted muscular triacylglycerol and FoxO target gene transcriptional responses to fasting and refeeding. These data indicate that impaired vMSP signaling to muscle triggers an energy deficiency, which induces a protective metabolic response involving FoxO. Hence, some energy metabolism alterations observed in ALS patients might be a consequence of striated muscle mitochondrial dysfunction.

localization and function in striated muscle [15]. vMSPs interact with muscle SAX-3 Roundabout and CLR-1 Lar-like protein-tyrosine phosphatase receptors to down-regulate CLR-1 signaling. VAP loss causes uncontrolled CLR-1 Lar-like receptor activation in body wall muscle. CLR-1 stimulates actin filament assembly in the muscle belly that requires the actin-related protein 2/3 (Arp2/3) complex. These ectopic actin filaments displace mitochondria from I-bands, cause aberrant fission and fusion balance, and impair respiratory chain activity. Hence, vMSPs secreted by neurons promote muscle mitochondrial localization and function, perhaps in an effort to modulate energy homeostasis.

vMSP signaling to muscle mitochondria might be relevant for the energy balance in *ALS8* disease. Out of five *ALS8* patients studied, five had increased cholesterol levels, four had reduced HDL, three had elevated triacylglycerol levels, and one was diabetic [16]. More generally, ALS is associated with a spectrum of abnormalities in energy metabolism, including mitochondrial defects in neurons and skeletal muscle, insulin resistance, dyslipidemia, and hypermetabolism [17]. These metabolic abnormalities are positively correlated with survival. For instance, increased prediagnostic body fat is associated with decreased risk of ALS mortality [18] and in some patient populations, higher LDL/HDL ratios correlate with increased survival time [19,20]. However, the cause(s) of the metabolic defects and their relationship to each other are not well understood.

Here we show in *C. elegans* that loss of the VAP homolog VPR-1 causes triacylglycerol (TAG) accumulation in striated body wall muscle. Mosaic analysis and tissue-specific expression studies provide compelling evidence that VPR-1 acts in neurons, not muscles to regulate fat levels. Multiple lines of evidence support the model that impaired vMSP signaling from neurons to muscle increases TAG levels in muscle. We propose that this fat metabolism alteration is part of a compensatory response mediated by the DAF-16/FoxO transcription factor. FoxO promotes muscle fat accumulation, maintains ATP levels during aging, and extends lifespan without influencing muscle mitochondrial morphology, localization, or function. Finally, we provide evidence that skeletal muscle metabolism is abnormal in *Vapb* mutant mice. Our results support the model that disrupting vMSP signaling to muscle triggers a compensatory response involving FoxO transcription factors.

Results

vpr-1/vap loss increases fat levels in adult body wall muscle

In our studies of *vpr-1(tm1411)* null mutant hermaphrodites, we noticed that body wall muscles often contain large lipid-like droplets not observed in wild-type controls. These apparent lipid-like droplets were visible in young adults (1–3 days post L4 stage) by differential interference contrast (DIC) microscopy (Figure 1A). In transgenic *vpr-1* mutants expressing mitochondrial matrix-targeted GFP (mitoGFP) in muscle, droplets are observed in the muscle belly surrounded by mitochondria (Figure S1). The vast majority of visible droplets in peripheral tissues are found in muscle. Transmission electron microscopy (TEM) of *vpr-1(tm1411)* mutant muscle shows an expanded muscle belly filled with mitochondria, as previously reported [15], and large droplets (Figures 1B and S2). The droplets are often found in close proximity to mitochondria and ER. Large muscle droplets were not observed in young adult wild-type muscle (Figures 1B and S2). However, muscle lipid droplets and abnormal mitochondria are observed in very old (18 day) wild-type adults [21,22]. In these old worms, large lipid droplets accumulate in the muscle, intestine, and epidermis. We did not detect abnormally large droplets in young *vpr-1* mutant intestinal and epidermal tissues by TEM. Instead, intestinal and epidermal tissues looked similar to wild-type controls, although it is difficult to assess minor differences (Figure S2). Hence, muscle droplets accumulate in aging *vpr-1* mutant worms.

To directly test whether these droplets contain lipid, we fed *vpr-1* mutant worms *E. coli* incubated with Bodipy-conjugated fatty acids (Bodipy-FAs). These fluorescent compounds can be used to directly visualize fat stores in live tissue [23,24]. In wild-type hermaphrodite controls, dietary Bodipy-FAs were observed primarily in the intestine with a few small droplets present in muscle. In contrast, muscles of *vpr-1(tm1411)* null mutants contained numerous large Bodipy-FA-stained droplets (Figure 1C). The fluorescent droplets fully overlapped with those observed in muscle by DIC microscopy (Figure 1D). Similar results are observed with Sudan Black B, which darkly stains neutral TAGs in fixed opaque worms (Figure S3). Bodipy-FAs are continuously transported from the diet, to the worm's intestinal cells, and then to the muscle, where they are tightly packed in membrane-bound vesicles. Bodipy-FAs are also incorporated into yolk lipoprotein complexes [23], which are specifically endocytosed by oocytes [25]. Although yolk accumulates in the pseudocoelom of *vpr-1* mutants (due to defective oogenesis), it is not up-taken by muscle (Figure S4). Both Bodipy-FA and Sudan Black staining show a mild increase in intestinal fat content in *vpr-1* mutants. Whether this apparent increase is due to fat accumulation or increased fat synthesis is not clear.

We also performed mass spectrometry of lipid extracts to determine the lipid composition of wild-type and *vpr-1* mutant adult hermaphrodites. Lipids were analyzed by electrospray ionization tandem mass spectrometry (ESI-MS/MS). ESI-MS/MS analysis of the extracts detected a robust increase in TAGs in *vpr-1* mutant extracts, but not in the membrane phospholipids phosphatidylethanolamine and phosphatidylcholine (Figure 1E and data not shown). These data indicate that loss of *vpr-1* causes TAG accumulation in muscle of adult hermaphrodite worms.

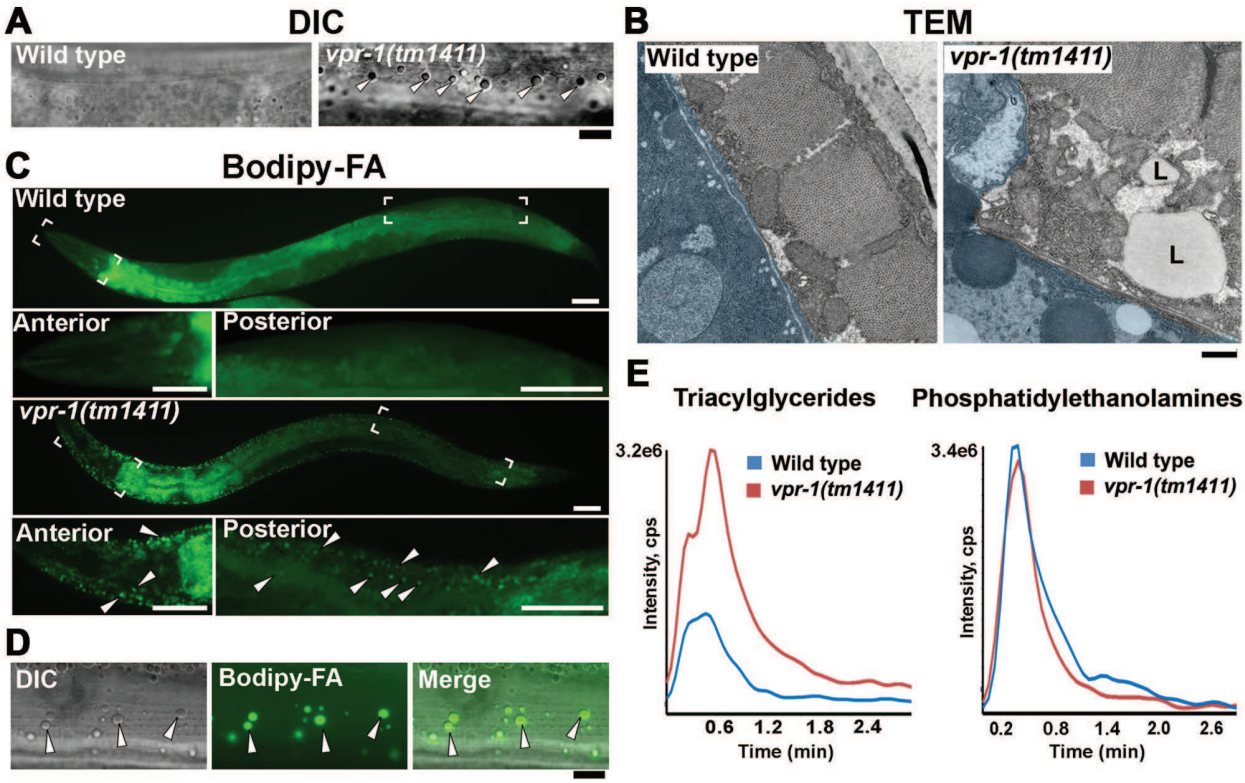

Figure 1. Fat levels in body wall muscle of wild-type and *vpr-1* mutant worms. (A) DIC images of muscle in live adult hermaphrodites. Arrowheads indicate lipid-like droplets. Bar, 5 μm. (B) Transmission electron micrographs of body wall muscle cytoplasm in wild-type and *vpr-1(tm1411)* mutant hermaphrodites. Light blue color demarcates muscle boundary. L, Lipid-like droplet. Bar, 0.5 μm. (C) Fluorescent images of muscle in live adult hermaphrodites fed Bodipy-FAs. Close-up images of boxed areas are shown below. Arrowheads indicate examples of Bodipy-FA-stained droplets. Anterior is to the left in all panels. Bars, 50 μm. (D) High magnification images of muscle showing Bodipy-FA-stained fluorescent droplets and droplets observed by DIC microscopy. Bar, 5 μm. (E) Comparison of total ion chromatograms of wild-type and *vpr-1(tm1411)* mutant adults extracts for 18:0 TAG (Neutral Loss 284) and phosphatidylethanolamine (Neutral Loss 141).
doi:10.1371/journal.pgen.1003738.g001

Increased ER stress does not cause muscle TAG accumulation in *vpr-1/vap* mutants

VAP homologs have been implicated in ER stress pathways [13,26,27], which can modulate lipid metabolism and homeostasis [28]. Furthermore, mitochondrial dysfunction is sometimes associated with ER stress. We considered the possibility that increased ER stress might cause the high muscle fat levels in *vpr-1* mutants. Three lines of evidence argue against this possibility. First, an integrated *hsp-4/BiPp::gfp* ER stress reporter [29] did not show elevated stress levels in *vpr-1* mutants (Figure S5A). Second, *vpr-1* mutants are not more sensitive than wild type to tunicamycin treatment, which induces ER stress (Figure S5B). Third, RNA-mediated interference (RNAi) of *xbp-1*, an ER stress-responsive transcription factor, in *vpr-1* mutants had no effect on muscle fat levels in 3-day old adults (18.0 ± 3.6 droplets/mm^2 for *vpr-1(tm1411)* [n = 12] versus 17.3 ± 3.6 droplets/mm^2 for *vpr-1(tm1411) xbp-1 RNAi* [n = 10]; $P = 0.28$). These data indicate that increased ER stress does not cause the muscle TAG defect in *vpr-1* mutants.

vpr-1/vap acts cell nonautonomously to regulate fat accumulation

vpr-1 is ubiquitously expressed and its homologs have been implicated in regulating lipid dynamics via a cell autonomous mechanism [10,30–32]. To determine in which cell type(s) VPR-1 functions to regulate muscle fat, we first used genetic mosaic analysis. Transgenic *vpr-1(tm1411)* mutant hermaphrodites were generated containing the *vpr-1* genomic locus and the lineage marker *sur-5::GFP* expressed from an extrachromosomal array [33]. In *C. elegans*, extrachromosomal arrays are spontaneously lost at low frequency during cell division, thereby generating mosaic worms. When these events occur early in development, mosaic worms can be generated with losses in neurons, body wall muscles, intestinal cells, and the germ line.

Expressing the *vpr-1* genomic locus in *vpr-1(tm1411)* null worms rescued the fat metabolism defect in muscle (Figure 2), as well as the muscle mitochondrial defects, sterility, slow growth, and other phenotypes. Body wall muscles are generated from multiple cell lineages, including the EMS lineage. Transgene array loss in the EMS lineage generates mosaic worms that have a subset of muscles lacking *vpr-1* expression. These muscle cells exhibited low fat levels, identical to muscle cells that express *vpr-1* (Figure 2). Therefore, VPR-1 is not required in body wall muscle for fat accumulation. Mosaic worms lacking *vpr-1* in the E lineage, which generates the intestine, also did not exhibit elevated muscle fat droplets, indicating that *vpr-1* is not required in the intestine. In contrast to muscle and intestine loss, *vpr-1* loss in the AB lineage, which generates the neurons, did cause increased fat droplets in muscles (Figure 2). Unexpectedly, we also found that *vpr-1* loss in the germ cell lineage causes muscle fat accumulation (Figure 2). These results indicate that VPR-1 acts cell nonautonomously in

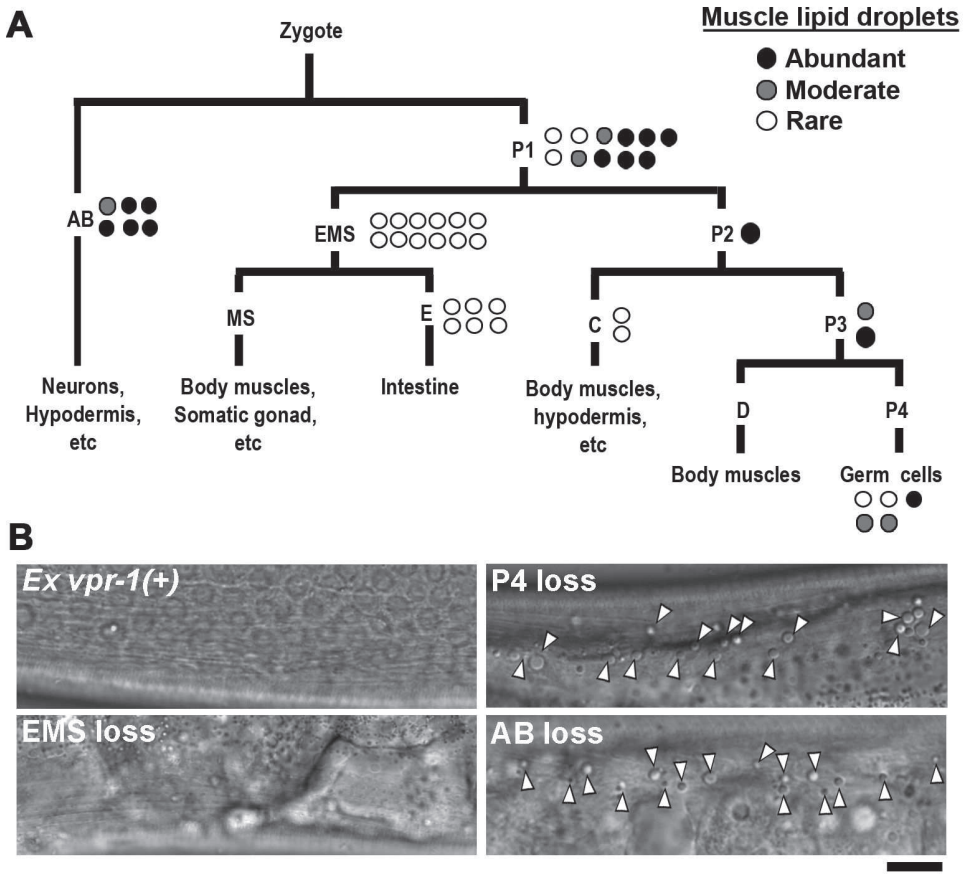

Figure 2. *vpr-1* mosaic analysis. (A) Analysis of vpr-1 genetic mosaics showing the lineages of major tissues. Each circle indicates one genetic mosaic worm. Points at which the genomic copy of *vpr-1(+)* was lost and the resulting phenotype are shown. (B) Representative DIC images of muscle in *vpr-1(tm1411)* mutant mosaic worms. *Ex vpr-1(+)* indicates expression of the vpr-1 genomic locus via an extrachromosomal array. Arrowheads indicate fat droplets. Bar, 5 μm.
doi:10.1371/journal.pgen.1003738.g002

neurons and germ cells (or their differentiation products) to modulate fat levels in muscle.

vpr-1 null mutants are sterile, due to a failure of germ cells to differentiate into sperm and oocytes. Sperm secrete signaling molecules, such as MSPs that may influence fat metabolism [14]. To test whether sperm affect fat levels, we mated sterile 1-day-old adult *vpr-1(tm1411)* hermaphrodites to wild-type males. Supplying sperm to the reproductive tract reduces muscle fat levels in *vpr-1(tm1411)* mutants, as visualized with Bodipy-FAs (Figure S6A). Sperm did not rescue the sterility or muscle mitochondrial defects of *vpr-1* mutants (data not shown). However, preventing spermatogenesis in wild-type hermaphrodites using the *fog-3(q443)* null mutation causes mild muscle fat accumulation, as well as mild mitochondrial morphology defects (Figure S6B), without affecting oxygen consumption [34]. These data indicate that the spermatogenesis defects in *vpr-1* mutants contribute to muscle fat levels and perhaps mitochondrial defects. Two mechanisms appear to affect muscle fat levels, one mechanism involving neuronal *vpr-1* and a second mechanism involving sperm, which can modify specific *vpr-1*-dependent pathways. Here, we focus on the neuronal mechanism.

Genetic mosaics assess the effect of *vpr-1* loss from cells within an otherwise *vpr-1(+)* background. To test whether VPR-1 expression is sufficient in neurons, we expressed VPR-1 under the control of tissue-specific promoters in *vpr-1* null mutants. Consistent with genetic mosaic analysis, VPR-1 expression using the *myo-3* muscle-specific promoter or the *ges-1* intestine-specific promoter did not influence muscle fat levels. In contrast, overexpressing the *vpr-1* cDNA with the *unc-119* pan-neuronal promoter completely rescued the muscle fat levels in approximately 30–40% of transgenic mutant worms (Figures 3A and 3B). These rescued transgenic mutants were still sterile. The incomplete rescue appears to be due to the germ line defects (i.e. lack of sperm) and missing *vpr-1* introns or 3′UTR in the transgene (P. Cottee and M. Miller, unpublished). Consistent with these observations, driving neuronal expression of the *vpr-1* genomic locus instead of the cDNA rescued several *vpr-1* mutant phenotypes with increased efficiency. These results indicate that VPR-1 acts cell nonautonomously in neurons to regulate muscle fat levels.

vMSP signaling to muscle regulates muscle fat levels

The VAPB P56S mutation acts as a dominant negative by inhibiting secretion of the wild-type and mutant vMSPs [13,15]. To test whether neuronal vMSP secretion affects muscle fat levels, we generated transgenic worms expressing P56S VPR-1 under the *unc-119* neuronal promoter. P56S VPR-1 overexpression in wild-type worms causes increased muscle lipid droplets in most worms (Figure 3A), suggesting that vMSP secretion from neurons influences muscle fat accumulation.

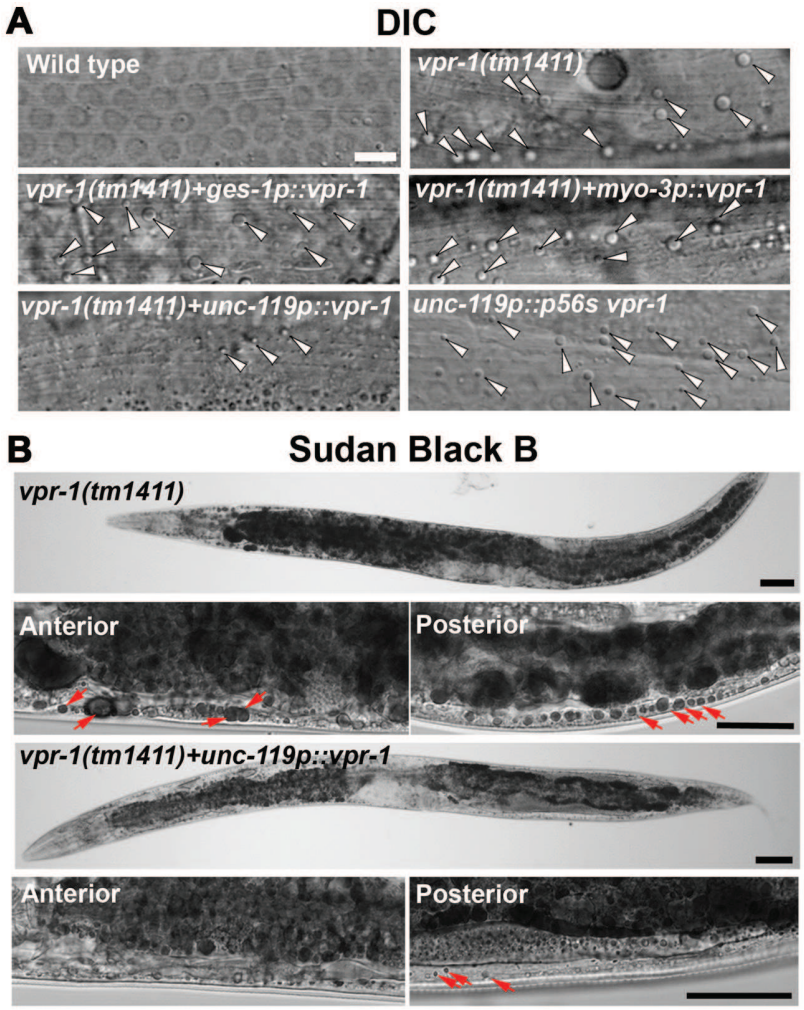

Figure 3. Effect of tissue-specific *vpr-1* expression on fat levels. (A) DIC images of muscle in live wild-type and *vpr-1(tm1411)* mutant hermaphrodites expressing wild-type VPR-1 or VPR-1(P56S) under indicated tissue-specific promoters. Arrowheads indicate lipid-like droplets. Bar, 5 μm. (B) Sudan Black B staining images of *vpr-1* mutants expressing *vpr-1* under the *unc-119* pan-neuronal promoter. Arrows indicate muscle fat droplets. Anterior is to the left in all panels. Wild-type controls (Figure S3) are similar to transgenic *vpr-1(tm1411)* mutants expressing *unc119p::vpr-1*. Low magnification bars, 50 μm; high magnification bars, 25 μm.
doi:10.1371/journal.pgen.1003738.g003

vMSP signaling to muscle is transduced via muscle SAX-3 Robo and CLR-1 Lar-like receptors [15]. *sax-3* mutations cause incompletely penetrant and variably expressed defects in muscle mitochondrial morphology [15]. Similarly, we observed incompletely penetrant defects in muscle fat accumulation by TEM and DIC microscopy (Figure S2; 11.1±13.2 fat droplets/mm^2 for *sax-3(ky123)* [n = 13] versus 0.9±1.8 droplets/mm^2 for wild type [n = 8]). Impaired vMSP signaling causes uncontrolled CLR-1 Lar receptor activity and ectopic Arp2/3-dependent actin filaments in muscle. A reduction of *clr-1* or *arx-2*, which encodes Arp2, rescues the muscle mitochondrial defects, but not the sterility in *vpr-1* mutants [15]. To test whether excess CLR-1 Lar and Arp2/3 activities cause muscle lipid accumulation, we used RNAi to down-regulate their functions in *vpr-1* mutants. *clr-1* or *arx-2* RNAi restored mitochondria to I-bands, as previously reported [15], and reduced muscle fat droplets in *vpr-1(tm1411)* mutants when compared to the mutant control (Figure 4; 18.0±3.6 droplets/mm^2 for *vpr-1(tm1411)* [n = 12] versus 0.6±1.3 droplets/mm^2 for *vpr-1(tm1411) clr-1 RNAi* [n = 9, P<0.001] and 3.1±2.0 droplets/mm^2 for *vpr-1(tm1411) arx-2 RNAi* [n = 6, P<0.001]). Similar results were observed using TEM [15]. We also found that overexpressing *arx-2/arp2* specifically in wild-type muscle causes mild mitochondrial morphology and fat accumulation defects (Figure S7). Taken together, the data strongly support the hypothesis that impaired vMSP signaling from neurons to muscle causes elevated fat levels in muscle.

DAF-16/FoxO is required for fat accumulation in *vpr-1/vap* mutants

The elevated TAGs in *vpr-1* mutants and continuous accumulation of dietary Bodipy-FAs in muscle suggested that fat metabolism and transport pathways are altered. Reduced energy production triggers enhanced activity of the DAF-16/FoxO transcription factor, which controls expression of genes involved in fat synthesis, fat transport, β-oxidation, and stress resistance [35–39]. We hypothesized that the muscle cytoskeletal or mitochondrial defects trigger elevated FoxO activity. To investi-

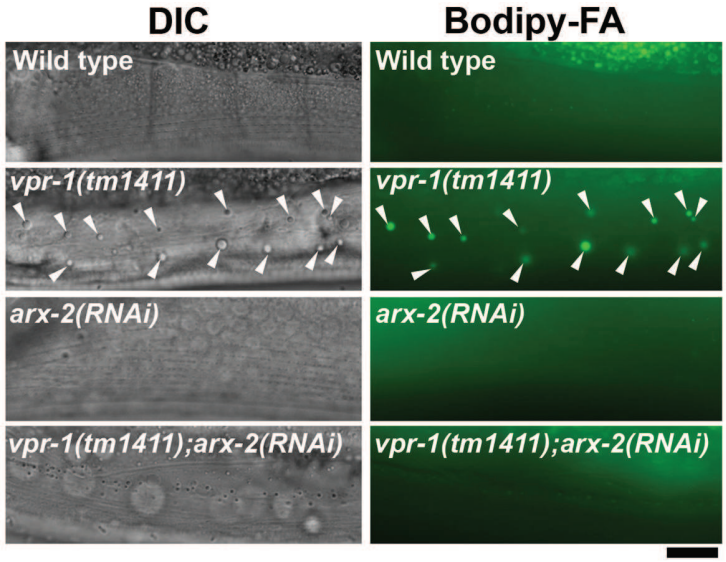

Figure 4. Effect of Arp2/3 inactivation on muscle fat levels. DIC and fluorescent images of muscle in live 3-day-old hermaphrodite worms fed Bodipy-FAs. *arx-2* encodes the Arp2 component of the Arp2/3 complex. Arrowheads indicate Bodipy-FA-stained fat droplets. Bar, 5 μm.
doi:10.1371/journal.pgen.1003738.g004

gate if DAF-16 affects fat metabolism in *vpr-1* mutants, we generated *vpr-1(tm1411) daf-16(mu86)* double mutants. Muscles of *daf-16(mu86)* null mutants contain few Bodipy-FA-stained droplets, similar to muscles of wild-type controls. However, muscle fat levels in the double mutants are also low, and strongly reduced when compared to those in *vpr-1(tm1411)* mutants alone (Figure 5A). *daf-16* loss did not affect food intake, assessed by measuring pharyngeal pumping rates (Figure 5B; $P>0.05$), muscle mitochondria (see below), or sterility of *vpr-1(tm1411)* mutants. We conclude that the elevated fat levels in *vpr-1* null mutants require DAF-16/FoxO activity.

We next examined DAF-16/FoxO transcriptional activity using an integrated transgenic line that expresses GFP under the *sod-3* promoter (*sod-3p::GFP*), a direct DAF-16 target [35,40]. When worms were cultured under normal growth conditions, about 40–50% of 1-day-old adult *vpr-1(tm1411)* transgenic worms showed increased GFP expression relative to control transgenic animals (Figure 5C). By day three of adulthood, most *vpr-1(tm1411)* mutants show broad GFP expression throughout the body, including the intestine, neurons, vulva muscles, and body wall muscles. The elevated GFP expression is due to DAF-16 because GFP expression is suppressed in transgenic *vpr-1(tm1411) daf-16(mu86)* double mutants (Figure 5C). These data indicate that *vpr-1* loss causes elevated DAF-16 activity in muscles and other cell types.

To investigate the mechanism(s) by which VPR-1 controls DAF-16/FoxO, we analyzed DAF-16 subcellular localization in *vpr-1(tm1411)* mutants. An integrated and rescuing transgenic line was used to express DAF-16::GFP under its endogenous promoter. DAF-16::GFP translocates from cytoplasm to nucleus upon loss of insulin signaling, although other mechanisms exist that regulate nuclear DAF-16 activity independent of translocation [41,42]. Under normal growth conditions at 20°C, DAF-16::GFP in *vpr-1* mutant and control transgenic strains was distributed throughout the cytoplasm and nucleus with no significant difference between the two strains (Figures 6A and 6B). However, *vpr-1* mutants appear more sensitive to higher temperatures that require increased metabolic activity (Figures 6A and 6B). We conclude that VPR-1 does not have a strong effect on DAF-16 nuclear translocation under standard conditions.

DAF-16/FoxO likely acts downstream of the Arp2/3 complex

The results thus far strongly support the model that impaired vMSP signaling to muscle triggers DAF-16-dependent muscle fat accumulation. We hypothesized that cytoskeletal or mitochondrial abnormalities in *vpr-1* mutant muscles induce elevated DAF-16 transcriptional activity. If this idea is correct, then inactivating the Arp2/3 complex in *vpr-1* mutants should attenuate DAF-16 activity. To assess DAF-16 transcriptional activity, we used the integrated *sod-3p::GFP* transgenic reporter. *arx-2/arp2* RNAi in *vpr-1(tm1411)* mutants causes a strong reduction in *sod-3p::GFP* expression in body wall muscle, the intestine, and other cells (Figure 6C). *arx-2* RNAi in wild-type worms has little effect on GFP expression. Therefore, the elevated DAF-16 activity in *vpr-1* mutants is at least partially dependent on the Arp2/3 complex.

One possibility is that DAF-16 causes the mitochondrial abnormalities in *vpr-1* mutants. To test this model, we first evaluated mitochondria using the mitoGFP transgene expressed in body wall muscle. As previously documented [15], wild-type muscles contain linear mitochondrial tubules positioned along I-bands. In contrast, *vpr-1(tm1411)* mutants contain disorganized and interconnected mitochondrial networks in the muscle belly (Figure 7A). Loss of *daf-16* in *vpr-1(tm1411)* mutants did not affect muscle mitochondrial morphology or localization (Figure 7A). Next, we examined mitochondrial functional status using MitoTracker CMXRos, which accumulates in the mitochondrial matrix depending on membrane potential, and oxygen consumption of whole worms. DAF-16 loss did not affect the reduced MitoTracker CMXRos accumulation (Figure 7B) or the low oxygen consumption rates of *vpr-1* mutants (Figures 7C and 7D). We conclude that DAF-16 does not affect the muscle mitochondrial defects in *vpr-1* mutants and likely acts downstream of Arp2/3.

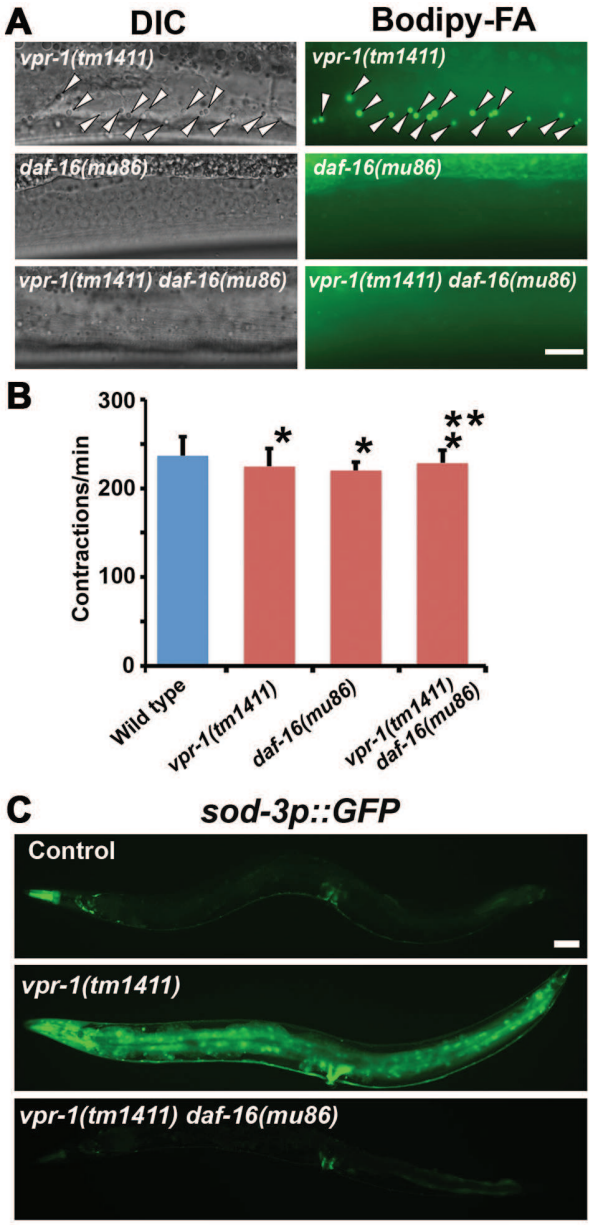

Figure 5. DAF-16 activity in *vpr-1* mutants. (A) DIC and fluorescent images of muscle in live 3-day-old hermaphrodite worms fed Bodipy-FAs. Arrowheads indicate Bodipy-FA-stained droplets. Wild-type controls (not shown) are similar to *daf-16(mu86)* mutants (See figures 1C and 4). Bar, 5 µm. (B) Pharyngeal pumping rates of 1-day-old adult hermaphrodites. Wild type (236.7±21.1 [n = 11]) and *vpr-1(tm1411)* mutants (220.1±9.6 [n = 11]) have similar pharyngeal pumping rate. Error bars represent SD. *$P>0.05$ compared to wild type. **$P>0.05$ compared to *vpr-1(tm1411)* mutant. (C) Transgenic worms expressing GFP under control of the *sod-3* promoter, a direct DAF-16/FoxO target. Anterior is to the left in all panels. Bar, 50 µm.
doi:10.1371/journal.pgen.1003738.g005

DAF-16/FoxO increases ATP levels and extends lifespan of *vpr-1/vap* mutants

As the intestine and epidermis are fat storage sites in *C. elegans*, we hypothesized that the increase in muscle fat is an attempt to provide fuel for energy production. Our previous studies showed that 1-day-old adult *vpr-1(tm1411)* mutants have reduced ATP levels when compared to controls [15]. However, the ATP levels in *vpr-1* mutants did not decrease over the next two days, as observed in the wild type (Figure 8A). 3-day-old adult *vpr-1(tm1411)* mutants had higher ATP levels than wild-type controls at the same age (Figure 8A). Similar ATP dynamics have been observed in aging worms with mutations in the *daf-2* insulin receptor or *clk-1*, a mitochondrial protein involved in ubiquinone biosynthesis [43,44]. Hence, DAF-16 may help maintain ATP levels in these aging worms. To test whether DAF-16 affects the energy balance of *vpr-1* mutants, we measured ATP levels in single and double mutant extracts. *daf-16* loss did not influence ATP levels in 1-day-old adult *vpr-1(tm1411)* mutants (Figure 8A). However, *daf-16* is required for the high ATP concentration in 3-day old mutant adults (Figure 8A; $P<0.001$). ATP levels in *daf-16* mutants are similar to wild-type controls (data not shown), as previously shown [43,44]. These data indicate that DAF-16/FoxO helps *vpr-1* mutants maintain ATP levels during aging.

Based on the abnormalities in energy metabolism, we tested whether DAF-16 influences lifespan in *vpr-1* mutants. Similar to other worm mutants with mild or tissue-specific reduction in mitochondrial function, *vpr-1(tm1411)* mutants have slightly extended adult lifespan compared to wild-type worms (Figure 8B; mean adult lifespan ± SD of 12.9±4.4 days [n = 154] for *vpr-1(tm1411)* versus 10.5±2.1 days [n = 159] for wild type, $P<0.001$). *daf-16* loss in *vpr-1(tm1411)* mutants causes a strong reduction in lifespan relative to *vpr-1* mutants and wild-type controls (Figure 8B; 6.9±2.5 days for *vpr-1(tm1411) daf-16(mu86)* [n = 250]; $P<0.001$). The lifespan of *daf-16* single mutants was similar to wild type (data not shown), as previously shown [38,45]. These data indicate that DAF-16/FoxO activity extends survival of *vpr-1* mutants.

Vapb knockout mice exhibit signs of abnormal skeletal muscle energy metabolism

The data thus far indicate that VPR-1 loss causes profound defects in muscle energy metabolism. We hypothesized that the regulatory function of vMSPs on energy metabolism was conserved in mammals, and studied energy metabolism of *Vapb* −/− mice [4]. In basal conditions, *Vapb* −/− mice do not exhibit overt defects in energy metabolism. In particular, body weight and glycemia appear normal with age (L. Dupuis, unpublished results). However, an energy metabolism defect of *Vapb* deficient mice might be unmasked by modifying insulin supply through feeding and fasting paradigms. In worms and mice, fasting reduces insulin signaling and increases FoxO activity, resulting in altered metabolic gene expression. We used *Vapb* −/− mice of 2–6 months of age to avoid any confounding effect of the motor dysfunction observed at 18 months [4]. Mice were either fasted for 24 hours (fasted group) or fasted for 16 hours and refed for 8 hours to synchronize meals (fed group). In +/+ mice, fasting decreased the TAG levels in the gastrocnemius (GA) muscle (Figure 9A; $P<0.05$). In contrast, TAG levels remained unchanged upon fasting in *Vapb* −/− GA and tibialis anterior (TA) muscles (Figure 9A and data not shown). In liver, TAG levels were unchanged upon fasting and feeding in either +/+ or −/− mice (Figure 9A). Thus, *Vapb* ablation increases the resistance of muscle lipid stores to fasting induced mobilization.

We next looked at mRNA levels of metabolic genes by quantitative RT-PCR. In liver, *Vapb* ablation potentiated induction of the direct FoxO1 target gene phosphoenolpyruvate carboxykinase (PEPCK) in response to fasting, but had no effect on fasting induction of other FoxO1 targets such as glucose 6-phosphatase (G6Pase) and pyruvate dehydrogenase kinase (PDK4) (Figure 9B). FoxO1 and FoxO3 mRNA and proteins were similar

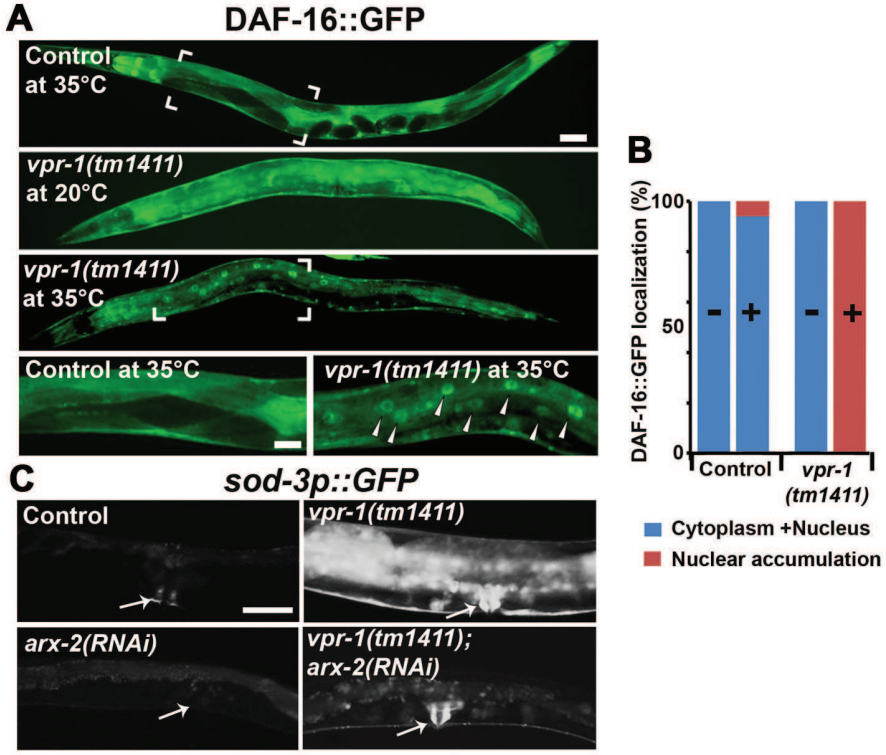

Figure 6. DAF-16 localization and activity in wild-type and mutant worms. (A) Transgenic strains expressing DAF-16::GFP under its endogenous promoter. Transgenic controls raised at 20°C are similar to those raised at 20°C then shifted to 35°C for 30 minutes (see panel B for quantification). Close up images of boxed areas are shown. Anterior is to the left in all panels. Low magnification bar, 50 μm; high magnification bar, 25 μm. (B) Quantification of DAF-16::GFP localization in control (n = 157) and *vpr-1(tm1411)* mutants (n = 49). (−), incubation under normal growth condition; (+), incubation at 35°C for 30 minutes. (C) Magnified images showing transgenic lines expressing GFP under the *sod-3* promoter. *arx-2* encodes Arp2. Arrows indicate vulva muscle region. Anterior is to the left in all panels. Bar, 50 μm.
doi:10.1371/journal.pgen.1003738.g006

in +/+ and −/− livers, and FoxO1 up-regulation by fasting appeared normal in −/− liver (Figure 9B).

We also examined putative FoxO1 and FoxO3 target genes in +/+ and mutant TA muscle. Feeding decreased expression of PEPCK, G6Pase, and lipoprotein lipase (LPL), and increased expression of the lipogenic transcription factor SREBP1c (Figure 9C). This regulation was lost in *Vapb* −/− muscles, as feeding did not modify expression of these four genes. *Vapb* genotype did not affect levels of PDK4 mRNA. FoxO1 and FoxO3 expression was down-regulated upon feeding in control TA muscles, but FoxO3 regulation was lost in −/− muscles (Figure 9C). The expression of muscle FoxO3 targets LC3 and Atrogin1 was up-regulated in fed −/− mice, while another FoxO3 target, ATG12, was unchanged. These results indicate that muscles of *Vapb* −/− mice are partially insensitive to fasting/feeding alterations in lipid mobilization and FoxO target gene expression. Hence, *Vapb* mutant worms and mice appear to have muscle energy metabolism alterations, at least in part involving FoxO targets. Whether the putative metabolic changes in mouse muscle are due to secreted vMSPs is not yet clear.

Discussion

Results from Drosophila and *C. elegans* support the model that VAP MSP domains are secreted neurogenic factors that promote striated muscle oxidative metabolism [15]. In *C. elegans*, neurons cleave the vMSP and secrete it into the surrounding environment. Secreted vMSPs signal through SAX-3 Roundabout and CLR-1 Lar-like receptors expressed in muscle, down-regulating Lar signaling to the Arp2/3 complex. This signaling pathway restricts actin filament formation to I-bands of the myofilaments, thereby localizing mitochondria to I-bands and promoting mitochondrial function [13,15]. Here we show that impaired vMSP signaling to muscle triggers increased DAF-16/FoxO transcription factor activity. FoxO promotes TAG accumulation in muscle, helps maintain ATP levels during aging, and extends lifespan. We propose that reduced vMSP signaling puts animals in an energy deficit, which triggers an altered metabolic response involving FoxO. Evidence for this model and implications for ALS are discussed below.

A VAPB cell nonautonomous mechanism for regulating muscle TAGs

VAPs physically interact with multiple proteins involved in lipid binding and transport, such as oxysterol binding protein and ceramide-transfer protein [10,11,30,46]. Although the biological role of these interactions is not well understood, VAPs have been proposed to act in macromolecular complexes for transporting lipids between organelles at membrane contact sites. This mechanism depends on VAP function in the same cell in which lipid dynamics occur (i.e. a cell autonomous function). Here we show in *C. elegans* that *vpr-1/vap* loss triggers a robust increase in striated muscle TAG levels. Unexpectedly, this function does not require VPR-1 in muscle. Genetic mosaic and cell-type specific expression studies demonstrate that VPR-1 acts in neurons,

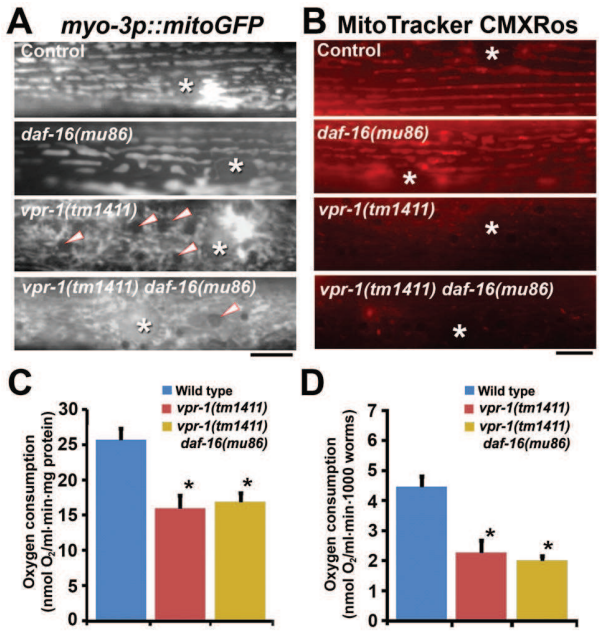

Figure 7. Effect of DAF-16 inactivation on muscle mitochondria. (A) Muscle mitochondrial tubules in indicated genotypes visualized using mitoGFP. Arrowheads indicate fat droplets. Asterisks indicate nucleus. Bar, 5 μm. (B) MitoTracker CMXRos staining of wild-type and mutant muscle. Asterisks indicate nucleus. Bar, 5 μm. (C and D) Oxygen consumption rates of wild-type and mutant hermaphrodites. Measured consumption rates were normalized by protein content (C) or number of worms (D). Error bars represent SD. *, $P<0.001$ compared to wild type. Oxygen consumption rate of wild-type and *vpr-1(tm1411)* mutants includes published data [15] measured together with *vpr-1(tm1411) daf-16(mu86)* mutants.
doi:10.1371/journal.pgen.1003738.g007

consistent with the signaling function. Indeed, muscle vMSP receptors and the downstream Arp2/3 complex mediate this lipid metabolism response. We also found that sperm presence can modulate striated muscle TAG metabolism. Neurons and sperm are two cell types capable of secreting MSP domains [15,47]. Our data do not exclude cell autonomous roles for VPR-1 in regulating lipid dynamics. Nevertheless, they highlight the importance of testing VAP autonomy when evaluating biological mechanism.

The connection between VAPB and FoxO

We show that *vpr-1/vap* loss triggers elevated DAF-16/FoxO activity, resulting in muscle TAG accumulation. Inactivating the Arp2/3 complex largely suppresses these metabolic alterations, as well as the muscle mitochondrial defects. These data support the model that impaired vMSP signaling to muscle triggers elevated FoxO activity. Consistent with this model, over-expressing Arp2 specifically in wild-type muscle causes TAG accumulation and mitochondrial defects. Although we cannot eliminate the possibility that Arp2/3 acts in other tissues, it appears to be a muscle-specific suppressor of *vpr-1* mutants. How might the Arp2/3 complex regulate FoxO? One possibility is that *vpr-1* mutants go into energy deficit as they age, as mitochondrial dysfunction is thought to increase FoxO activity [48–51]. An alternative possibility is that FoxO acts downstream of Arp2/3, but in parallel to mitochondria. In either case, reduced insulin signaling could be involved. A strong reduction in insulin causes increased FoxO nuclear translocation, which is not observed in *vpr-1* mutants under standard conditions. However, subtle changes can be more difficult to detect.

Additional mechanisms could also modulate FoxO in *vpr-1* mutants. The vMSP/ephrin receptor VAB-1 directly interacts with DAF-18/PTEN (phosphatase and tensin homolog deleted on chromosome ten), which regulates FoxO activity [52]. VAB-1 is expressed throughout the adult nervous system and in the gonad [53,54]. Previous studies have shown that sperm presence can modulate DAF-16/FoxO translocation and transcriptional activity [55], perhaps through secreted MSPs. Whether sperm act via the Arp2/3 complex is not clear. An interesting possibility is that global MSP signals from neurons and sperm are sensed through distinct mechanisms. These mechanisms might converge on muscle metabolic output to meet changes in energy requirements.

In mammals, FoxO transcription factors are critical regulators of energy metabolism, particularly under fasting conditions. We show that *Vapb* ablation in mice renders muscle lipid stores resistant to fasting, a situation analogous to lipid accumulation in *vpr-1* mutant worm muscles. Dysregulated lipid stores in mutant mice is associated with alterations in muscle gene expression consistent with abnormal FoxO1 and FoxO3 activity [56]. For instance, FoxO1 target gene mRNAs for PEPCK and G6Pase are clearly up-regulated in muscle of young *Vapb* −/− mice in the fed state (*i.e.* in the presence of insulin that decreases FoxO1 activity). Similar results are observed for FoxO3 target genes LC3 and Atrogin-1. These data suggest that FoxO1/3 are less sensitive to insulin inhibition in *Vapb* −/− mice.

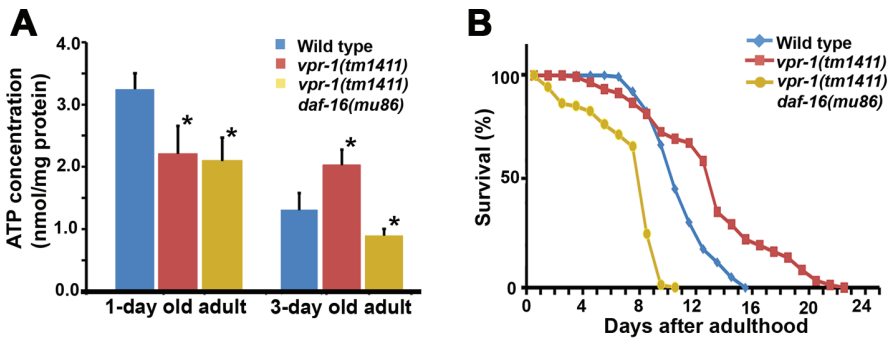

Figure 8. Effect of DAF-16 inactivation on ATP level and lifespan. (A) ATP concentration in wild-type and *vpr-1(tm1411)* mutant adult extracts. *, $P<0.001$ compared to wild type. Error bars represent SD. ATP concentration of wild-type and *vpr-1(tm1411)* mutants at 1-day-old adults include published data [15] measured together with *vpr-1(tm1411) daf-16(mu86)* mutants. (B) Lifespan measurements of indicated genotypes. The lifespan of *daf-16(mu86)* mutants (not shown) was similar to the wild type, as previously shown.
doi:10.1371/journal.pgen.1003738.g008

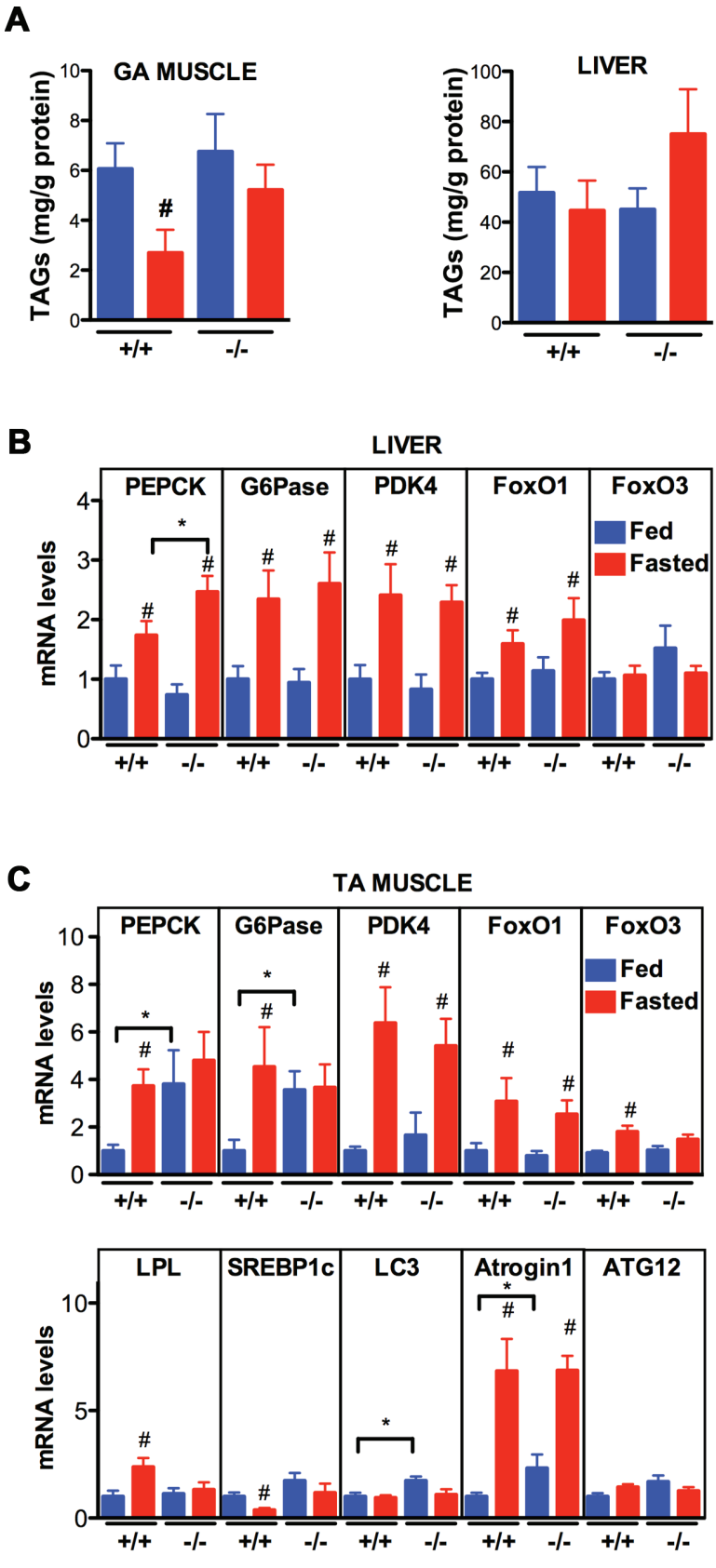
A
GA MUSCLE
TAGs (mg/g protein)
LIVER
+/+
-/-
B
LIVER
PEPCK
G6Pase
PDK4
FoxO1
FoxO3
Fed
Fasted
mRNA levels
C
TA MUSCLE
LPL
SREBP1c
LC3
Atrogin1
ATG12

Figure 9. Effect of *Vapb* ablation on fasting/refeeding energy metabolism in mice. (A) TAG concentration in GA muscle and liver of wild-type (+/+) and *Vapb* knock-out (−/−) mice after 24-hour fasting (red) or 24 hours fasting followed by 6 hours of refeeding (blue). (B and C) Quantitative RT-PCR of indicated genes in liver (B) and TA muscle (C) of wild-type (+/+) and *Vapb* knock-out (−/−) mice after 24-hour fasting (red) or 24 hours fasting followed by 6 hours of refeeding (blue). Relative mRNA levels are shown on the Y-axis. #, $P<0.05$ compared to fed mice of the same genotype. *, $P<0.05$ compared to +/+ under the same condition.
doi:10.1371/journal.pgen.1003738.g009

Not all FoxO target genes studied are sensitive to *Vapb* ablation. For instance, VAPB does not appear to influence PDK4 and ATG12 mRNAs. Additionally, some of the mRNAs studied showed uncoupling from circulating insulin levels, consistent with an insensitivity of FoxO1 to insulin. SREBP1c mRNA, which is negatively regulated by FoxO1 [57], was increased by feeding in +/+ mice, but not in −/− mice. A similar, albeit mirror situation was observed for LPL, a gene positively regulated by FoxO1 [58]. Hence, FoxO1/3 might participate in the abnormal lipid mobilization in *Vapb* −/− mice, but other mechanisms are likely at work to avoid the major consequences of chronic muscle FoxO activation, such as muscle atrophy [59]. In summary, our findings show that VAPB is involved in modulating mouse muscle energy metabolism upon fasting and refeeding, possibly via altered FoxO activity. Whether this occurs through a cell autonomous or a cell nonautonomous mechanism, like in *C. elegans* and Drosophila, remains to be determined.

FoxO is protective in *vap* mutants

A key finding in worms is that DAF-16/FoxO activity prolongs the adult lifespan of *vpr-1* mutants from 6.9±2.5 to 12.9±4.4 days. This lifespan increase may be due to metabolic alterations that compensate for mitochondrial dysfunction. Consistent with this idea, FoxO extends the lifespan of *C. elegans* with reduced mitochondrial function [48,49,60]. The FoxO-dependent fat accumulation in *vpr-1* mutant muscle may reflect an effort to increase energy production. We show that DAF-16 helps *vpr-1* mutants maintain ATP levels in 3-day old adults. Among the numerous DAF-16 metabolic genes are those involved in fat synthesis and transport, β-oxidation, the glyoxylate cycle, and gluconeogenesis [37]. However, additional DAF-16 targets may also be involved, such as stress resistance enzymes [37,38,61]. *vpr-1* mutants are more resistant than the wild type to reactive oxygen species and ER stress. Based on identified DAF-16 targets and *vpr-1* mutant phenotypes, DAF-16 might increase energy substrate availability in muscle, stimulate anaerobic metabolism, increase oxidative metabolism in non-muscle cells, or decrease ATP consumption. Further studies are necessary to distinguish among these possibilities, as well as other models.

Implications for ALS

Metabolic alterations in ALS patients and mouse models are hypothesized to compensate for mitochondrial dysfunction, particularly in skeletal muscle [17,19,62,63]. Differentially expressed gene networks involved in oxidative metabolism and the cytoskeleton, including up-regulated FoxO1 and FoxO3 mRNAs have been found in ALS patient skeletal muscles [64,65]. Our studies of VAPB in worms, flies, and mice are consistent with impaired vMSP signaling to muscle causing some of these alterations. Importantly, *vpr-1* loss in worms, *Vapb* depletion in zebrafish, or *Vapb* loss in mice does not cause motor neuron degeneration [4,15], providing strong evidence that mitochondrial and metabolic defects are not secondary consequences of neurodegeneration. These data contrast with a recent Drosophila study suggesting that *Vapb* loss causes neurodegeneration via increased phosphoinositides [66]. In humans, metabolic alterations caused by reduced VAPB function may not be sufficient to induce motor neuron degeneration, although they could strongly predispose to ALS. Redundancy could be an important consideration in the different models. The worm genome encodes a single *vap* homolog, but many genes with MSP domains. Vertebrate genomes typically encode VAPA and VAPB, which are approximately 60% identical. *Vap* mutant flies have the most severe developmental defects and the fewest MSP genes in the genome.

In summary, our results support the model that striated muscle mitochondrial dysfunction alters FoxO activity, which in turn affects energy metabolism and promotes survival. It is possible that reduced vMSP signaling causes some of the mitochondrial and metabolic alterations in ALS patients. Perhaps vMSPs might protect against ALS via effects on skeletal muscle energy metabolism.

Materials and Methods

C. elegans genetics, strains, and RNA-mediated interference

C. elegans Bristol N2 is the wild-type strain. Worms were grown on NGM plates with NA22 bacteria as the food source [67]. Strain construction and marker scoring were done as previously described [15,54]. The strains and genetic markers used or generated were as follows: CF1553 muIs84[pAD76(*sod-3::GFP*)], CF1038 *daf-16(mu86)* I, *vpr-1(tm1411)*/hT2[*bli-4(e937)* let-?(*q782*) qIs48] I;III, SJ4005 zcIs4[*hsp-4::GFP*], TJ356 zIs356[*daf-16p::daf-16::GFP; rol-6*] IV, *fog-3(q443) I*/hT2[*bli-4(e937)* let-?(*q782*) qIs48] I;III, CX3198 *sax-3(ky123) X*, and XM1004 *vpr-1(tm1411) daf-16(mu86)*/hT2[*bli-4(e937)* let-?(*q782*) qIs48] I;III. Transgenics expressing *vit-2p::vit-2::gfp* were generated by crossing into the pwIs23 integrated line. RNAi was performed using the feeding method starting at the L1 stage, as previously described [15]. *arx-2*, *clr-1*, and *xbp-1* RNAi clones are from the genome-wide library [68]. Each clone was sequenced for confirmation.

Transgenics

To generate transgenic *C. elegans*, the marker plasmids pRF4 [*rol-6*] (60 ng/µl) or *myo-3p::mito::GFP* (30–60 ng/µl) were mixed with *myo-3p::vpr-1* (60 ng/µl), *ges-1p::vpr-1*(60 ng/µl), *unc-119p::vpr-1*(60 ng/µl), *unc-119p::vpr-1* P56S (60 ng/µl), or *myo-3p::arx-2::mCherry* (60 ng/µl) and microinjected into the gonads of young adult hermaphrodites. Injected worms were incubated for 24 hours, transferred to new NGM plates, and screened for transgenic progeny. Transgenic lines were selected based on the roller phenotype or GFP expression. Multiple independent transgenic lines were generated for all strains. To conduct genetic mosaic analysis, 10 ng/µl WRM06B28 fosmid DNA containing the *vpr-1* genomic locus was mixed with 10 ng/µl pTG96 (*sur-5p::GFP*) plasmid and microinjected into the gonads of *vpr-1(tm1411)*/hT2 hermaphrodites. Transgenic lines were selected based on GFP expression. Transgenic lines were maintained as *vpr-1(tm1411)* homozygotes, as the fosmid rescued the sterility, mitochondria, fat metabolism, slow growth, and embryonic defects. For lineage scoring, approximately 15,000 worms were screened. Transgene loss in the AB lineage was scored by GFP loss in head and tail neurons, the nerve cords, and the excretory gland.

Transgene loss in the P1 lineage was scored by GFP loss in the intestine, muscle, somatic gonad, and hyp11. The P2 lineage was scored by GFP loss in numerous body wall muscle cells and hyp11, the P3 lineage was scored by GFP loss in body wall muscle, and the P4 lineage was inferred by a sterile phenotype without GFP loss. Transgene loss in the EMS lineage was scored by GFP loss in the intestine and somatic gonad, while loss in the E lineage was score by exclusive GFP loss in the intestine.

Transmission electron microscopy

TEM was performed as previously described [15].

Bodipy-FA and Sudan Black B staining

For the Bodipy-FA experiments, a 5 mM Bodipy-FA (Molecular probe, U.S.A) stock solution was prepared in DMSO and kept at −20°C. A 200 µM working solution diluted in distilled water was dropped onto seeded plates and allowed to dry. L4 stage worms were placed on the plates and incubated in the dark for 24 hours at 20°C. Bodipy-FAs can get trapped in intestinal gut granules that are not present in muscle.

Sudan Black B staining was conducted as described in previous studies [15]. Briefly, synchronized 1-day-old adult worms were collected into microfuge tubes containing M9 solution. Worms were washed five times, incubated for 40 minutes at 20°C to remove intestinal bacteria, and fixed in 1% paraformaldehyde. The fixed worms were washed three times in cold M9 solution and dehydrated through a 25%, 50%, and 70% ethanol series. Sudan Black B solution was added to the worms and incubated for 1 hour. To remove excess stain, worms were washed five times with 70% ethanol. To normalize for staining variability among experiments, wild type and *vpr-1(tm1411)* mutants were processed in the same tube and identified based on gonad morphology.

Lipid analysis by ESI-MS/MS

For the lipid analysis by ESI-MS/MS, lipids from equal masses of wild type and *vpr-1(tm1411)* mutant adults were extracted by chloroform-methanol following a modified Bligh/Dyer extraction [69]. A mixture of internal standards including T17:1 TAG was added to the chloroform-methanol phase before extraction. The extracted samples were concentrated to dryness under a nitrogen stream, reconstituted with methanol:chloroform (1:1 v/v) and transferred to HPLC auto samplers. Lipids were analyzed by ESI-MS/MS using an API 4000 (Applied Biosystems/MDS Sciex, Concord, Ontario, Canada) triple quadrupole mass spectrometer. Extracted lipid samples (5 ml) were infused into the mass spectrometer with a solvent mixture of chloroform-methanol (1:2, v/v) containing 0.1% formic acid using a Shimadzu Prominence HPLC with a refrigerated auto sampler (Shimadzu Scientific Instruments, Inc. Columbia, MD). Lipids were analyzed in positive ion mode using an API 4000 (Applied Biosystems/MDS Sciex, Concord, Ontario, Canada) triple quadruple mass spectrometer. Samples (5 µl) were directly infused into the electrospray source using a Shimadzu Prominence HPLC with a refrigerated auto sampler (Shimadzu Scientific Instruments, Inc. Columbia, MD). Neutral loss (NL) scanning (228, 254, 256, 268, 278, 280, 284, and 304) of naturally occurring aliphatic chains (i.e. building block of TAG molecular species) were utilized to determine the identities of each molecular species. NL scanning of 141 was used for profiling phosphatidylethanolamine. The following analysis parameters were used: ion spray voltage 5000 V, de-clustering potential 40 V, temperature 300°C (for TAG), collision energy 35 V, and collisionally activated dissociation 5.

Mitochondrial staining

To assess mitochondrial transmembrane potential, worms were stained using the MitoTracker CMXRos dye (Molecular Probes, U.S.A), as previously described [15]. This lipophilic cationic fluorescent dye accumulates in mitochondria in a membrane potential-dependent manner [70]. L4 larval stage worms were placed on dried plates containing a 100 µM MitoTracker CMXRos dye solution (dropped on bacteria). After 24 hours incubation in the dark, worms were transferred to a new NGM plate and incubated in the dark for 20 minutes to remove intestinal background. Worms were mounted on dried 2% agarose pads without anesthetic. Wild-type and *vpr-1(tm1411)* mutant hermaphrodites were cultured on the same plates.

ATP concentration measurement

ATP concentration was measured as described previously, with slight modification [15]. Briefly, 150 worms were individually picked and placed into tubes containing M9 buffer, washed four times, and incubated at 20°C for 40 minutes to remove intestinal bacteria. These worms were then washed four times with TE solution (100 mM Tris–Cl, pH 7.6, 4 mM EDTA) and placed into microfuge tubes containing 300 µl TE solution. Worm extracts were prepared by a series of cycles including freezing, thawing, and sonicating. These extracts were boiled for 10 minutes to release ATP and block ATPase activity. Carcasses and insoluble material were pelleted in a microcentrifuge at 20,000×g for 10 minutes. The soluble extracts were diluted in a 1:10 ratio using TE solution. ATP concentration in 60 µl of diluted extracts was measured using the ENLITEN ATP Assay System (Promega, U.S.A), according to the manufacturer's instructions. A luminometer (Berthold, Germany) was used for quantification. Protein concentration was determined using the BCA protein assay (Pierce, U.S.A). ATP measurements were repeated at least three times for each strain.

Oxygen consumption

Oxygen consumption rates were measured as previously described using the oxygraph system (Hansatech, UK) with minor modifications [15]. Worms were cultured at 20°C and synchronized to the 1-day-old adult stage. For each test, 1000 worms were individually picked and placed into a glass tube with 1 ml M9 buffer at 20°C. Collected worms were incubated for 40 min at 20°C to remove intestinal bacteria, carefully washed five times, and placed into 1 ml M9 buffer. The worm solution was loaded into the chamber equipped with a S1 Clark type polarographic oxygen electrode disc maintained at 20°C. Oxygen concentration was measured for 10 minutes. For normalization, worms were carefully collected from the chamber and protein content was measured using the BCA test kit (Pierce, U.S.A.). Rates were normalized to either total protein content or number of worms. We performed at least three independent measurements per strain.

Feeding rate and lifespan assays

To measure feeding rates, worms were cultured at 20°C and 1-day-old adult worms were placed on new NGM plates. Feeding behavior was recorded using a Zeiss Lumar stereomicroscope with AxioCam MRM digital camera. Measurements were conducted during a 30 second period at room temperature (22°C). The rhythmic contractions of the pharyngeal bulb were counted. For each strain, over 20 worms were counted. To determine lifespan of worms, L4 larval stage worms were placed on new NGM plates

seeded with NA22 bacteria and cultured at 20°C. The L4 stage was used because a small percentage of *vpr-1* mutants die during L1–L4 stages and *vpr-1* mutants develop slowly. Worms were monitored every day and transferred to flesh NGM plates. Death was scored by failure to respond to touching with a platinum wire. Wild-type worms fed NA22 bacteria have slightly shorter lifespan than worms fed OP50 bacteria.

Tunicamycin resistance

To analyze ER homeostasis, worms were cultured on plates with tunicamycin (Sigma, U.S.A) from the embryonic stage to adulthood. NGM plates with 0.1% DMSO and 0 or 5.0 µg/ml tunicamycin were prepared. About 30 adult worms were placed on each tunicamycin plate and allowed to lay embryos for 30 minutes. Adult worms were then removed. Twelve hours later the number of hatched embryos was counted and compared with the number of worms that reached the adult stage within 96 hours. We performed at least three independent measurements for each strain.

Mouse experiments

Mouse experiments were performed using the Institutional European Guidelines, under the supervision of an authorized investigator (LD), and approved by the local ethical committee for animal experiments (CREMEAS, agreement N° AL/01/08/02/13). *Vapb* −/− mice were used and genotyped as described [4]. Mice (8–10 per group) were either fasted for 24 hours from 5PM (fasted group), or fasted from 5PM to 9AM and refed until sacrifice at 5PM. GA and TA muscle and liver tissues were collected, and rapidly frozen in liquid nitrogen for subsequent analyses of gene expression and TAG levels. The tissues were stored at −80°C until the time of analysis.

For RT-qPCR, frozen liver and muscle tissues were placed into tubes containing 5 mm stainless steel beads (Qiagen, Courtaboeuf, France) and 1 ml of Trizol reagent (Invitrogen, Paisley, UK) and homogenized using a TissueLyser (Qiagen). RNA was prepared from tissue homogenates following Trizol manufacturer's instructions. RNA reverse transcription and SYBR Green real-time PCR assays were performed using the Bio-Rad (Biorad, Marnes la Coquette, France) iCycler kits and protocols. PCR conditions were 3 min at 94°C, followed by 40 cycles of 45 s at 94°C and 10 s at 60°C. Primers are shown in Table S1. For western blotting, liver and TA muscles were incubated in Lysis buffer containing complete protease and phosphatase inhibitor cocktails. Protein concentration was measured using BCA Protein Assay. Equal amount of protein (50 µg) were separated by SDS-PAGE 10% and blotted onto nitrocellulose membrane. Membranes were saturated with 10% milk and then incubated with the primary antibodies FoxO1 (Proteintech; 18592-1-AP), FoxO3a (Cell signaling; #2497), VAPB [4] and Histone H3 (Cell signaling; #9715), all diluted (1:1000) followed by anti-rabbit secondary antibody, diluted 1:5000.

For TAG analysis, tissue powder was homogenized in lysis buffer (250 mM Sucrose solution, 1 mM EDTA, 2% SDT, 1 mM DTT, 10 mM Tris HCl pH 7.4) containing protease inhibitors (Sigma P8340) and phosphatase inhibitors (Sigma 8345), centrifuged at 12000×rpm for 15 minutes at room temperature. TAG concentration was determined in duplicate for each sample in 5 µl of supernatant, using the enzymatic method of analysis (Randox *Triglyceride* Colorimetric Assay *Kit*, *Randox Laboratories Limited*, *UK*) as described by the manufacturer. Lipid values were normalized to protein concentration.

Supporting Information

Figure S1 Lipid-like droplets and mitochondria in *vpr-1* mutant striated muscle. (A) Close-up image of a live transgenic *vpr-1(tm1441)* mutant hermaphrodite expressing mitoGFP in body wall muscle. mitoGFP labels muscle mitochondrial tubules. (B) Image of a single body wall muscle in a transgenic *vpr-1(tm1441)* mutant hermaphrodite expressing mitoGFP. (C) Close-up image of the boxed region from panel B showing horizontal and vertical cross-sections. Arrowheads indicate lipid-like droplets. Asterisks indicate nucleus. Bar in A, 1 µm; Bars in B and C, 10 µm.
(TIF)

Figure S2 Transmission electron micrographs of wild-type and mutant adults. Micrographs are transverse sections showing the cuticle (C) and body wall muscle sarcomeres (S) with hypodermis sandwiched in between. A lipid droplet within the hypodermis (HL) is seen in the wild-type panel. The intestine is filled with electron dense and opaque lipid droplets (IL). Yolk lipoprotein complexes (Y) are found between muscle and intestinal tissues (also see Figure S4). Notice that yolk is electron dense, whereas muscle lipid droplets (ML) are opaque. N, muscle nucleus. Bars, 1 µm.
(TIF)

Figure S3 Sudan Black B staining in wild type and *vpr-1* mutants. 1-day-old adult wild-type and *vpr-1(tm1411)* hermaphrodites were stained using Sudan Black B. Arrowheads indicate fat droplets in body wall muscle. Anterior is to the left in all panels. Boxed regions are magnified 5× below. Low magnification bars, 50 µm; high magnification bars, 10 µm.
(TIF)

Figure S4 Yolk lipoprotein complex distribution in wild-type and *vpr-1* mutants. (A) Yolk distribution visualized with the *vit-2p::vit-2::gfp* transgene. *vpr-1* mutants accumulate yolk in the pseudocoelom due to failure of oocyte differentiation. GFP uptake is not observed in peripheral tissues. (B) Close-up image showing muscle fat droplets (arrows) in *vpr-1* mutants. Bar, 5 µm.
(TIF)

Figure S5 ER stress assays in wild-type and *vpr-1* mutant worms. (A) Integrated transgenic lines expressing GFP under the *hsp-4* promoter *(hsp-4p::GFP)* with and without tunicamycin treatment, which induces ER stress. Anterior is to the left in all panels. Bar, 5 mm. (B) Tunicamycin sensitivity in wild-type and *vpr-1(tm1411)* mutants hermaphrodites. Y-axis indicates the percentage of worms that developed to the adult stage in the presence of 5 µg/ml tunicamycin. Error bars represent SD. Three independent measurements were performed.
(TIF)

Figure S6 Effect of sperm presence on muscle fat droplets and mitochondria. (A) DIC and fluorescent images of muscle in live 3-day-old *vpr-1* mutant hermaphrodite worms fed Bodipy-FAs. Mating with wild type (WT) males provides sperm into the uterus. Sperm presence did not affect the sterility or muscle mitochondrial morphology of *vpr-1* mutants (data not shown). Anterior is to the left in all panels. Arrowheads indicate lipid-like droplets. Bar, 5 µm. (B) DIC and fluorescent images of muscle in live transgenic *fog-3(q443)/hT2* hermaphrodites containing sperm and unmated *fog-3(q443)* mutants without sperm. Muscle mitochondrial tubules were visualized using mitoGFP. Arrowheads indicate lipid-like droplets. Asterisks indicate nucleus. Bar, 5 µm.
(TIF)

Figure S7 Effect of ARX-2/Arp2 overexpression on muscle fat droplets and mitochondria. DIC and fluorescent images of muscle in live transgenic wild-type hermaphrodites expressing *arx-2* under

control of the muscle specific *myo-3* promoter. Muscle mitochondrial tubules were visualized using mitoGFP. Notice that muscle mitochondrial morphology closely resembles the morphology seen in *vpr-1* mutants [15]. See Figures 7A, S6B and [15] for controls. Arrows indicate lipid-like droplets. Asterisks indicate nucleus. Bar, 5 μm.
(TIF)

Table S1 Primers used for RT-qPCR in mice.
(TIF)

Acknowledgments

We thank Se-Jin Lee and three anonymous reviewers for comments on the manuscript. We also thank the UAB Targeted Metabolomics and Proteomics Laboratory, the *Caenorhabditis* Genetics Center, and the Japanese National Bioresource Project.

Author Contributions

Conceived and designed the experiments: MAM LD HJB JKP SMH. Performed the experiments: SMH HEO JSZ JV PC JKP. Analyzed the data: SMH MAM HJB JKP LD. Wrote the paper: SMH MAM LD.

References

1. Kiernan MC, Vucic S, Cheah BC, Turner MR, Eisen A, et al. (2011) Amyotrophic lateral sclerosis. Lancet 377: 942–955.
2. Nishimura AL, Mitne-Neto M, Silva HC, Richieri-Costa A, Middleton S, et al. (2004) A mutation in the vesicle-trafficking protein VAPB causes late-onset spinal muscular atrophy and amyotrophic lateral sclerosis. Am J Hum Genet 75: 822–831.
3. Chen HJ, Anagnostou G, Chai A, Withers J, Morris A, et al. (2010) Characterization of the properties of a novel mutation in VAPB in familial amyotrophic lateral sclerosis. J Biol Chem 285: 40266–40281.
4. Kabashi E, El Oussini H, Bercier V, Gros-Louis F, Valdmanis PN, et al. (2013) Investigating the contribution of VAPB/ALS8 loss of function in amyotrophic lateral sclerosis. Hum Mol Genet 22: 2350–2360.
5. Anagnostou G, Akbar MT, Paul P, Angelinetta C, Steiner TJ, et al. (2010) Vesicle associated membrane protein B (VAPB) is decreased in ALS spinal cord. Neurobiol Aging 31: 969–985.
6. Teuling E, Ahmed S, Haasdijk E, Demmers J, Steinmetz MO, et al. (2007) Motor neuron disease-associated mutant vesicle-associated membrane protein-associated protein (VAP) B recruits wild-type VAPs into endoplasmic reticulum-derived tubular aggregates. J Neurosci 27: 9801–9815.
7. Mitne-Neto M, Machado-Costa M, Marchetto MC, Bengtson MH, Joazeiro CA, et al. (2011) Downregulation of VAPB expression in motor neurons derived from induced pluripotent stem cells of ALS8 patients. Hum Mol Genet 20: 3642–3652.
8. Loewen CJ, Levine TP (2005) A highly conserved binding site in vesicle-associated membrane protein-associated protein (VAP) for the FFAT motif of lipid-binding proteins. J Biol Chem 280: 14097–14104.
9. Amarilio R, Ramachandran S, Sabanay H, Lev S (2005) Differential regulation of endoplasmic reticulum structure through VAP-Nir protein interaction. J Biol Chem 280: 5934–5944.
10. Lev S, Ben Halevy D, Peretti D, Dahan N (2008) The VAP protein family: from cellular functions to motor neuron disease. Trends Cell Biol 18: 282–290.
11. Peretti D, Dahan N, Shimoni E, Hirschberg K, Lev S (2008) Coordinated lipid transfer between the endoplasmic reticulum and the Golgi complex requires the VAP proteins and is essential for Golgi-mediated transport. Mol Biol Cell 19: 3871–3884.
12. De Vos KJ, Morotz GM, Stoica R, Tudor EL, Lau KF, et al. (2012) VAPB interacts with the mitochondrial protein PTPIP51 to regulate calcium homeostasis. Hum Mol Genet 21: 1299–1311.
13. Tsuda H, Han SM, Yang Y, Tong C, Lin YQ, et al. (2008) The amyotrophic lateral sclerosis 8 protein VAPB is cleaved, secreted, and acts as a ligand for Eph receptors. Cell 133: 963–977.
14. Han SM, Cottee PA, Miller MA (2010) Sperm and oocyte communication mechanisms controlling C. elegans fertility. Dev Dyn 239: 1265–1281.
15. Han SM, Tsuda H, Yang Y, Vibbert J, Cottee P, et al. (2012) Secreted VAPB/ALS8 Major Sperm Protein Domains Modulate Mitochondrial Localization and Morphology via Growth Cone Guidance Receptors. Dev Cell 22: 348–362.
16. Marques VD, Barreira AA, Davis MB, Abou-Sleiman PM, Silva WA, Jr., et al. (2006) Expanding the phenotypes of the Pro56Ser VAPB mutation: proximal SMA with dysautonomia. Muscle Nerve 34: 731–739.
17. Dupuis L, Pradat PF, Ludolph AC, Loeffler JP (2011) Energy metabolism in amyotrophic lateral sclerosis. Lancet Neurol 10: 75–82.
18. Gallo V, Wark PA, Jenab M, Pearce N, Brayne C, et al. (2013) Prediagnostic body fat and risk of death from amyotrophic lateral sclerosis: The EPIC cohort. Neurology 80: 829–838.
19. Dupuis L, Corcia P, Fergani A, Gonzalez De Aguilar JL, Bonnefont-Rousselot D, et al. (2008) Dyslipidemia is a protective factor in amyotrophic lateral sclerosis. Neurology 70: 1004–1009.
20. Dorst J, Kuhnlein P, Hendrich C, Kassubek J, Sperfeld AD, et al. (2011) Patients with elevated triglyceride and cholesterol serum levels have a prolonged survival in amyotrophic lateral sclerosis. J Neurol 258: 613–617.
21. Herndon LA, Schmeissner PJ, Dudaronek JM, Brown PA, Listner KM, et al. (2002) Stochastic and genetic factors influence tissue-specific decline in ageing C. elegans. Nature 419: 808–814.
22. McGee MD, Weber D, Day N, Vitelli C, Crippen D, et al. (2011) Loss of intestinal nuclei and intestinal integrity in aging C. elegans. Aging cell 10: 699–710.
23. Kubagawa HM, Watts JL, Corrigan C, Edmonds JW, Sztul E, et al. (2006) Oocyte signals derived from polyunsaturated fatty acids control sperm recruitment in vivo. Nat Cell Biol 8: 1143–1148.
24. Klapper M, Ehmke M, Palgunow D, Bohme M, Matthaus C, et al. (2011) Fluorescence-based fixative and vital staining of lipid droplets in Caenorhabditis elegans reveal fat stores using microscopy and flow cytometry approaches. J Lipid Res 52: 1281–1293.
25. Grant B, Hirsh D (1999) Receptor-mediated endocytosis in the Caenorhabditis elegans oocyte. Mol Biol Cell 10: 4311–4326.
26. Moumen A, Virard I, Raoul C (2011) Accumulation of wildtype and ALS-linked mutated VAPB impairs activity of the proteasome. PloS One 6: e26066.
27. Gkogkas C, Middleton S, Kremer AM, Wardrope C, Hannah M, et al. (2008) VAPB interacts with and modulates the activity of ATF6. Hum Mol Genet 17: 1517–1526.
28. Basseri S, Austin RC (2012) Endoplasmic reticulum stress and lipid metabolism: mechanisms and therapeutic potential. Biochem Res Int 2012: 841362.
29. Urano F, Calfon M, Yoneda T, Yun C, Kiraly M, et al. (2002) A survival pathway for Caenorhabditis elegans with a blocked unfolded protein response. J Cell Biol 158: 639–646.
30. Wyles JP, McMaster CR, Ridgway ND (2002) VAMP-associated protein-A (VAP-A) interacts with the oxysterol binding protein (OSBP) to modify export from the endoplasmic reticulum. J Biol Chem 277: 29908–29918.
31. Jansen M, Ohsaki Y, Rita Rega L, Bittman R, Olkkonen VM, et al. (2011) Role of ORPs in sterol transport from plasma membrane to ER and lipid droplets in mammalian cells. Traffic 12: 218–231.
32. Peretti D, Dahan N, Shimoni E, Hirschberg K, Lev S (2008) Coordinated lipid transfer between the endoplasmic reticulum and the Golgi complex requires the VAP proteins and is essential for Golgi-mediated transport. Mol Biol Cell 19: 3871–3884.
33. Yochem J, Herman RK (2003) Investigating C. elegans development through mosaic analysis. Development 130: 4761–4768.
34. Yang Y, Han SM, Miller MA (2010) MSP hormonal control of the oocyte MAP kinase cascade and reactive oxygen species signaling. Dev Biol 342: 96–107.
35. Oh SW, Mukhopadhyay A, Dixit BL, Raha T, Green MR, et al. (2006) Identification of direct DAF-16 targets controlling longevity, metabolism and diapause by chromatin immunoprecipitation. Nat Genet 38: 251–257.
36. Halaschek-Wiener J, Khattra JS, McKay S, Pouzyrev A, Stott JM, et al. (2005) Analysis of long-lived C. elegans daf-2 mutants using serial analysis of gene expression. Genome Res 15: 603–615.
37. Murphy CT (2006) The search for DAF-16/FOXO transcriptional targets: approaches and discoveries. Exp Gerontol 41: 910–921.
38. Murphy CT, McCarroll SA, Bargmann CI, Fraser A, Kamath RS, et al. (2003) Genes that act downstream of DAF-16 to influence the lifespan of Caenorhabditis elegans. Nature 424: 277–283.
39. McElwee J, Bubb K, Thomas JH (2003) Transcriptional outputs of the Caenorhabditis elegans forkhead protein DAF-16. Aging Cell 2: 111–121.
40. Henderson ST, Bonafe M, Johnson TE (2006) daf-16 protects the nematode Caenorhabditis elegans during food deprivation. J Gerontol A Biol Sci Med Sci 61: 444–460.
41. Landis JN, Murphy CT (2010) Integration of diverse inputs in the regulation of Caenorhabditis elegans DAF-16/FOXO. Dev Dyn 239: 1405–1412.
42. Williams TW, Dumas KJ, Hu PJ (2010) EAK proteins: novel conserved regulators of C. elegans lifespan. Aging 2: 742–747.
43. Houthoofd K, Braeckman BP, Lenaerts I, Brys K, Matthijssens F, et al. (2005) DAF-2 pathway mutations and food restriction in aging Caenorhabditis elegans differentially affect metabolism. Neurobiol Aging 26: 689–696.
44. Braeckman BP, Houthoofd K, De Vreese A, Vanfleteren JR (2002) Assaying metabolic activity in ageing Caenorhabditis elegans. Mech Ageing Dev 123: 105–119.
45. Lin K, Hsin H, Libina N, Kenyon C (2001) Regulation of the Caenorhabditis elegans longevity protein DAF-16 by insulin/IGF-1 and germline signaling. Nat Genet 28: 139–145.
46. Stefan CJ, Manford AG, Baird D, Yamada-Hanff J, Mao Y, et al. (2011) Osh proteins regulate phosphoinositide metabolism at ER-plasma membrane contact sites. Cell 144: 389–401.

47. Kosinski M, McDonald K, Schwartz J, Yamamoto I, Greenstein D (2005) C. elegans sperm bud vesicles to deliver a meiotic maturation signal to distant oocytes. Development 132: 3357–3369.
48. Dillin A, Hsu AL, Arantes-Oliveira N, Lehrer-Graiwer J, Hsin H, et al. (2002) Rates of behavior and aging specified by mitochondrial function during development. Science 298: 2398–2401.
49. Lee SS, Lee RY, Fraser AG, Kamath RS, Ahringer J, et al. (2003) A systematic RNAi screen identifies a critical role for mitochondria in C. elegans longevity. Nat Genet 33: 40–48.
50. Billing O, Kao G, Naredi P (2011) Mitochondrial function is required for secretion of DAF-28/insulin in C. elegans. PloS One 6: e14507.
51. Greer EL, Banko MR, Brunet A (2009) AMP-activated protein kinase and FoxO transcription factors in dietary restriction-induced longevity. Ann N Y Acad Sci 1170: 688–692.
52. Brisbin S, Liu J, Boudreau J, Peng J, Evangelista M, et al. (2009) A role for C. elegans Eph RTK signaling in PTEN regulation. Dev Cell 17: 459–469.
53. George SE, Simokat K, Hardin J, Chisholm AD (1998) The VAB-1 Eph receptor tyrosine kinase functions in neural and epithelial morphogenesis in C. elegans. Cell 92: 633–643.
54. Miller MA, Ruest PJ, Kosinski M, Hanks SK, Greenstein D (2003) An Eph receptor sperm-sensing control mechanism for oocyte meiotic maturation in Caenorhabditis elegans. Genes Dev 17: 187–200.
55. Miyata S, Begun J, Troemel ER, Ausubel FM (2008) DAF-16-dependent suppression of immunity during reproduction in Caenorhabditis elegans. Genetics 178: 903–918.
56. Cheng Z, White MF (2011) Targeting Forkhead box O1 from the concept to metabolic diseases: lessons from mouse models. Antioxid Redox Signal 14: 649–661.
57. Kamei Y, Miura S, Suganami T, Akaike F, Kanai S, et al. (2008) Regulation of SREBP1c gene expression in skeletal muscle: role of retinoid X receptor/liver X receptor and forkhead-O1 transcription factor. Endocrinology 149: 2293–2305.
58. Kamei Y, Ohizumi H, Fujitani Y, Nemoto T, Tanaka T, et al. (2003) PPARgamma coactivator 1beta/ERR ligand 1 is an ERR protein ligand, whose expression induces a high-energy expenditure and antagonizes obesity. Proc Natl Acad Sci U S A 100: 12378–12383.
59. Kamei Y, Miura S, Suzuki M, Kai Y, Mizukami J, et al. (2004) Skeletal muscle FOXO1 (FKHR) transgenic mice have less skeletal muscle mass, down-regulated Type I (slow twitch/red muscle) fiber genes, and impaired glycemic control. J Biol Chem 279: 41114–41123.
60. Rea SL, Ventura N, Johnson TE (2007) Relationship between mitochondrial electron transport chain dysfunction, development, and life extension in Caenorhabditis elegans. PLoS Biol 5: e259.
61. Honda Y, Honda S (1999) The daf-2 gene network for longevity regulates oxidative stress resistance and Mn-superoxide dismutase gene expression in Caenorhabditis elegans. FASEB J 13: 1385–1393.
62. Crugnola V, Lamperti C, Lucchini V, Ronchi D, Peverelli L, et al. (2010) Mitochondrial respiratory chain dysfunction in muscle from patients with amyotrophic lateral sclerosis. Arch Neurol 67: 849–854.
63. Zhou J, Yi J, Fu R, Liu E, Siddique T, et al. (2010) Hyperactive intracellular calcium signaling associated with localized mitochondrial defects in skeletal muscle of an animal model of amyotrophic lateral sclerosis. J Biol Chem 285: 705–712.
64. Bernardini C, Censi F, Lattanzi W, Barba M, Calcagnini G, et al. (2013) Mitochondrial network genes in the skeletal muscle of amyotrophic lateral sclerosis patients. PloS One 8: e57739.
65. Leger B, Vergani L, Soraru G, Hespel P, Derave W, et al. (2006) Human skeletal muscle atrophy in amyotrophic lateral sclerosis reveals a reduction in Akt and an increase in atrogin-1. FASEB J 20: 583–585.
66. Forrest S, Chai A, Sanhueza M, Marescotti M, Parry K, et al. (2013) Increased levels of phosphoinositides cause neurodegeneration in a Drosophila model of amyotrophic lateral sclerosis. Hum Mol Genet 22: 2689–2704.
67. Brenner S (1974) The genetics of Caenorhabditis elegans. Genetics 77: 71–94.
68. Kamath RS, Ahringer J (2003) Genome-wide RNAi screening in Caenorhabditis elegans. Methods 30: 313–321.
69. Bligh EG, Dyer WJ (1959) A rapid method of total lipid extraction and purification. Can J Biochem Physiol 37: 911–917.
70. Gilmore K, Wilson M (1999) The use of chloromethyl-X-rosamine (Mitotracker red) to measure loss of mitochondrial membrane potential in apoptotic cells is incompatible with cell fixation. Cytometry 36: 355–358.

II. PUBLICATION Nº4

(Manuscript submitted)

OXFORD UNIVERSITY PRESS | Brain

Alterations in the hypothalamic melanocortin pathway in amyotrophic lateral sclerosis

Journal:	*Brain*
Manuscript ID:	Draft
Manuscript Type:	Original Article
Date Submitted by the Author:	n/a
Complete List of Authors:	Vercruysse, Pauline; Inserm, INSERM U1118; Ulm university, department of Neurology Sinniger, Jerome; Inserm, INSERM U1118 El Oussini, Hajer; Inserm, INSERM U1118 Scekic-Zahirovic, Jelena; Inserm, INSERM U1118 Dieterlé, Stéphane; Inserm, INSERM U1118 Dengler, Reinhard; MHH, Neurology Meyer, Thomas; Charite Hospital - Humboldt University, Department of Neurology Zierz, Stephan; University of Halle, Neurology Kassubek, Jan; University of Ulm, Department of Neurology Fischer, Wilhelm; Ulm university, department of Neurology Dreyhaupt, Jens; Ulm university, Institute of Epidemiology and Medical Biometry Grehl, Torsten; Ruhr-Universität, department of Neurology Hermann, Andreas; Technische Universität, department of Neurology Grosskreutz, Julian; University Hospital Jena, Hans-Berger Department of Neurology Witting, Anke; Ulm university, department of Neurology Van Den Bosch, Ludo; KU, department of Neurology Spreux Varoquaux, Odile; Universite de Versailles, Ludolph, Albert; University and Rehabilitation Clinics Ulm , Dupuis, L.; Strasbourg, France, INSERM U692
Subject category:	Neuromuscular diseases
To search keyword list, use whole or part words followed by an *:	Amyotrophic lateral sclerosis < NEURODEGENERATION: CELLULAR AND MOLECULAR, Neurodegeneration: experimental models < NEURODEGENERATION: CELLULAR AND MOLECULAR, Neuroendocrine system < SYSTEMS/DEVELOPMENT/PHYSIOLOGY, Transgenic model < GENETICS, Anterior horn cell < NEUROMUSCULAR DISEASES

Alterations in the hypothalamic melanocortin pathway in amyotrophic lateral sclerosis

Pauline Vercruysse[1,2,3], Jérôme Sinniger[1,2], Hajer El Oussini[1,2], Jelena Scekic-Zahirovic[1,2], Stéphane Dieterlé[1,2], Reinhard Dengler[4], Thomas Meyer[5], Stephan Zierz[6], Jan Kassubek[3], Wilhelm Fischer[3], Jens Dreyhaupt[7], Torsten Grehl[8], Andreas Hermann[9], Julian Grosskreutz[10] Anke Witting[3], Ludo Van den Bosch[11], Odile Spreux-Varoquaux[12,13,14] , the GERP ALS Study Group , Albert C. Ludolph[3]* & Luc Dupuis[1,2]*

1. Inserm U1118, Mécanismes centraux et périphétiques de la neurodégénérescence, Strasbourg, F-67085 France
2. Université de Strasbourg, Faculté de Médecine, UMRS1118, Strasbourg, F-67085 France
3. Department of Neurology, University of Ulm, Germany
4. Department of Neurology, Hannover Medical School, Hannover, Germany
5. Department of Neurology, Charité University Hospital, Berlin, Germany
6. Department of Neurology, University of Halle-Wittenberg, Germany
7. Institute of Epidemiology and Medical Biometry, University of Ulm, Germany
8. Department of Neurology, Ruhr-Universität, Bochum, Germany
9. Department of Neurology, Technische Universität Dresden, and German Center for Neurodegenerative Disease (DZNE), Dresden, Germany
10. Department of Neurology, University Hospital, Jena, Germany
11. KU Leuven, Leuven, Belgium
12. Faculté de Médecine Paris-Ile de France-Ouest, France
13. Université de Versailles Saint-Quentin-en-Yvelines, France
14. Centre Hospitalier Versailles, Le Chesnay, France

Corresponding authors :
Luc DUPUIS,
INSERM U1118, Faculté de médecine, bat 3, 8e etage, 11 rue Humann, 67085 Strasbourg, Cedex, FRANCE
e-mail : ldupuis@unistra.fr

Albert C. LUDOLPH
RKU, Universitatsklinik Ulm, Oberer Eselsberg 45, 89081 Ulm, Germany
e-mail :albert-c.ludolph@uni-ulm.de

Running title : hypothalamic dysfunction in ALS

Word count : 5112 words
Abstract : 302 words

Collaborators : GERP ALS study group

All centres were located in Germany. Investigators are listed by alphabetical order of centre and investigator:

Berlin (Department of Neurology, Charité University Hospital)
Nadja Borisow; Theresa Holm; Andre Maier; Thomas Meyer

Bochum (Department of Neurology, University Hospital Bergmannsheil)
Paula Budde; Torsten Grehl; Anne-Katrin Guettsches

Bonn (Department of Neurology, University Hospital of Bonn)
Malte Bewersdorff; Michael Heneka

Dresden (Department of Neurology, University Hospital Carl Gustav Carus, Technische Universität Dresden)
Andreas Hermann; Alexander Storch

Göttingen (Department of Neurology, University Hospital of Göttingen)
Tobias Frank; Bettina Göricke; Jochen Weishaupt

Halle (Department of Neurology, University Hospital of Halle/Saale)
Katharina Eger; Frank Hanisch; Stephan Zierz

Hannover (Department of Neurology and Clinical Neurophysiology, Hannover Medical School (MHH), University Clinic)
Anna-Lena Boeck; Reinhard Dengler; Sonja Koerner; Katja Kollewe ; Susanne Petri

Jena (Department of Neurology, University Hospital Jena)
Julian Grosskreutz; Albrecht Kunze; Tino Prell; Thomas Ringer; Jan Zinke

Munich (Department of Neurology, University of Munich)
Johanna Anneser; Gian Domenico Borasio ; Christine Chahli; Andrea S. Winkler

Muenster (Department of Neurology, University of Muenster)
Matthias Boentert; Bianca Stubbe-Draeger; Peter Young

Regensburg (Department of Neurology, University of Regensburg)
Ulrich Bogdahn; Steffen Franz; Verena Haringer; Norbert Weidner

Rostock (Department of Neurology, University of Rostock)
Reiner Benecke ; Stefanie Meister; Johannes Prudlo; Matthias Wittstock

Ulm (Department of Neurology, University of Ulm)
Johannes Dorst ; Corinna Hendrich; Albert C. Ludolph; Anne-Dorte Sperfeld; Ulrike Weiland

Wiesbaden (Department of Neurology, Neurological clinic, DKD)
Sabine Neidhardt; Berthold Schrank

Wurzburg (Department of Neurology, University of Wurzburg)
Marcus Beck ; Peter Kraft; Klaus Toyka ; Jochen Ulzheimer; Carsten Wessig

Abstract

Amyotrophic Lateral Sclerosis (ALS), the most common adult-onset motor neuron disease, leads to death within 3 to 5 years after onset. Beyond progressive motor impairment, ALS patients suffer from major defects in energy metabolism, such as weight loss, which are well correlated with survival. Indeed, nutritional intervention targeting weight loss might be improving survival of patients. However, the neural mechanisms underlying metabolic impairment in ALS patients remain elusive, in particular due to the lack of longitudinal studies. Here we took advantage of samples collected during the clinical trial of pioglitazone (GERP-ALS), and characterized longitudinally energy metabolism of ALS patients in response to pioglitazone, a drug with well characterized metabolic effects. As expected, pioglitazone decreased glycemia, decreased liver enzymes and increased circulating adiponectin in ALS patients, showing its efficacy in the periphery. However, pioglitazone did not increase body weight of ALS patients independently of bulbar involvement. Since pioglitazone increases body weight through a direct inhibition of hypothalamic neurons producing pro-opiomelanocortin (POMC), we studied POMC neurons in mice expressing ALS-linked mutant SOD1(G86R). We observed presymptomatically decreased hypothalamic levels of POMC mRNA, decreased numbers of POMC positive neurons in the hypothalamic arcuate nucleus of SOD1(G86R) mice, and increased food intake after short term fasting, consistent with a defect in the hypothalamic melanocortin system. Importantly, these findings were replicated in two other ALS mouse models based on TDP-43 and FUS mutations. Last, we demonstrate that the melanocortin defect is primarily caused by serotonin loss in mutant SOD1(G86R) mice. In all, the current study combined clinical evidence and experimental studies in rodents to provide a mechanistic explanation for abnormalities in food intake and weight control observed in ALS patients. Importantly, these results also show that ALS progression impairs responsiveness to classical drugs leading to weight gain. This has important implications for pharmacological management of weight loss in ALS.

Keywords: amyotrophic lateral sclerosis, calorie intake, hypothalamus, thiazolinediones, weight loss

Introduction

Amyotrophic Lateral Sclerosis (ALS), the most common adult-onset motor neuron disease, is characterized by the simultaneous degeneration of upper and lower motor neurons, leading to muscle atrophy and paralysis, and death within 3 to 5 years after onset. A subset of ALS cases are of familial origin and five major genes are currently associated with familial ALS (*C9ORF72, SOD1, FUS, TARDBP* and *TBK1*) (Leblond *et al.*, 2014, Cirulli *et al.*, 2015, Freischmidt *et al.*, 2015, Lattante *et al.*, 2015). The *SOD1* gene was the first associated with ALS and most ALS mouse models currently used are based upon overexpression of mutant forms of *SOD1* (Gurney *et al.*, 1994, Ripps *et al.*, 1995).

Beyond progressive motor impairment, ALS patients suffer from major, yet incompletely characterized, defects in energy metabolism (Dupuis *et al.*, 2011). First, ALS is more likely to occur with lower premorbid body fat (Gallo *et al.*, 2013, O'Reilly *et al.*, 2013) or better cardiovascular or physical fitness (Turner *et al.*, 2012, Huisman *et al.*, 2013). Second, weight loss is negatively correlated with survival (Desport *et al.*, 1999, Marin *et al.*, 2011, Paganoni *et al.*, 2011). This weight loss is associated with, and likely caused by, intrinsic hypermetabolism (Desport *et al.*, 2001, Bouteloup *et al.*, 2009), and is exacerbated by dysphagia occuring with bulbar involvement. Third, ALS patients develop abnormalities in lipid (Dupuis *et al.*, 2008, Dorst *et al.*, 2011, Lindauer *et al.*, 2013) and glucose (Pradat *et al.*, 2010) metabolisms. Interestingly, these metabolic alterations are largely replicated in transgenic mice expressing mutant SOD1 (Dupuis *et al.*, 2004, Fergani *et al.*, 2007, Palamiuc *et al.*, 2015). Not much is known on the underlying mechanisms of energy metabolism impairment despite the elucidation of such mechanisms would offer therapeutic strategies to treat weight loss pharmacologically. Furthermore, deciphering the mechanisms of energy metabolism impairment could identify disease-modifying interventions since hypercaloric diet was recently found to increase survival of ALS patients under gastrostomy (Wills *et al.*, 2014, Dorst *et al.*, 2015).

Most of the studies to date have characterized energy metabolism in ALS patients in steady state, at one single time point. The dynamic nature of energy metabolism and its homeostatic regulation thus severely limit the interpretation of these studies. Interventions performed during randomized clinical trials often have metabolic effects, and such studies include long term follow up of patients for many months. These clinical studies thus provide high-quality information useful to understand the metabolic defects of ALS patients.

Here, we performed a *post hoc* analysis of samples obtained during the clinical trial of pioglitazone (Dupuis *et al.*, 2012) to characterize energy metabolism of ALS patients upon a metabolic challenge. Indeed, pioglitazone, like other thiazolinediones (TZDs), has pleiotropic effects on energy metabolism that have been extremely well characterized in both mouse models,

and human patients. In the periphery, pioglitazone sensitizes to insulin, leading to decreased glycaemia, and decreases circulating levels of liver enzymes (Promrat *et al.*, 2004, Belfort *et al.*, 2006, Sanyal *et al.*, 2010, DeFronzo *et al.*, 2011). In the central nervous system, pioglitazone inhibits the hypothalamic melanocortin system to increase food intake (Diano *et al.*, 2011, Lu *et al.*, 2011, Ryan *et al.*, 2011, Long *et al.*, 2014). Specifically, pioglitazone decreases activity of the hypothalamic neurons producing pro-opiomelanocortin (POMC), the precursor of a number of anorexigenic peptides such as α-MSH (melanocyte stimulating hormone) (Diano *et al.*, 2011, Lu *et al.*, 2011, Ryan *et al.*, 2011, Long *et al.*, 2014). In humans, this leads to a robust (3-5 kg) weight gain that was repeatedly observed in multiple clinical trials (Promrat *et al.*, 2004, Belfort *et al.*, 2006, Sanyal *et al.*, 2010, DeFronzo *et al.*, 2011). Here, we show that ALS patients display normal peripheral action of pioglitazone, while they lack weight gain. In transgenic mice expressing mutant SOD1, pioglitazone failed to increase food intake. This was associated with prominent involvement of the hypothalamic melanocortin system, also observed in other mouse models of ALS, independent of mutant SOD1 overexpression. Last, we show that the melanocortin defect occurs downstream of the previously documented serotonin loss (Dentel *et al.*, 2013). Altogether, our analysis of the data from the pioglitazone trial disclosed a previously unanticipated defect in ALS patients that could account for a subset of ALS-related metabolic defects.

Materials and methods

Patients and treatments

All the biological materials from human ALS patients were sampled as part of the GERP-ALS trial (clinicaltrials.gov reference: NCT00690118) (Dupuis *et al.*, 2012). Briefly, patients with possible, probable (clinically or laboratory-supported) or definite ALS according to the revised version of the El Escorial criteria were considered for enrolment into the study. Included patients displayed onset of progressive weakness within 36 months prior to study and had a disease duration of more than six months and less than three years (inclusive) with disease onset defined as date of first muscle weakness, excluding fasciculation and cramps. They reached a best-sitting slow vital capacity between 50 % and 95 % of predicted normal. They were capable of thoroughly understanding the information provided and giving full informed consent. All included patients had been treated with 100 mg riluzole daily for at least three months prior to inclusion. Detailed exclusion and inclusion criteria have been described earlier (Dupuis *et al.*, 2012). All patients gave written informed consent. The study protocol was approved by the ethics committee of the university of Ulm and all other participating centres.

The two treatment groups were 100 mg riluzole plus 45 mg pioglitazone (pioglitazone group) and 100 mg riluzole plus placebo (placebo group). Patients were randomly assigned to one of the two treatment groups and both groups were matched for age, gender and site of onset (Dupuis *et al.*, 2012).

Procedures and biochemical analysis of human samples

After inclusion, patients underwent a screening phase and a treatment phase (18 months), with stepwise increase in dosage (Dupuis *et al.*, 2012). Clinical and physical examinations, blood sampling, and drug compliance were recorded at on-site visits (1, 2, 6, 12 and 18 months after baseline visit). Body weight was also recorded at 9 and 15 months after baseline visit through telephone contacts. Routine clinical laboratory tests were performed at each on-site visit (baseline and 1, 2, 6, 12 and 18months after baseline). All tests were carried out according to standard laboratory procedures at each study centre's locally accredited laboratory, which defined the normal reference range for each analyte. The following laboratory tests were performed using standard methods: Alanine Aminotransferase (ALAT), Aspartate Aminotransferase (ASAT), fasting blood glucose. Adiponectin measurements were done in the neurochemical laboratory in Ulm (MSD assay).

Animals

Transgenic mice were housed in the animal facility of the medicine faculty of Strasbourg University, with 12 h/12 h of light/dark and unrestricted access to food and water. In all experiments, littermates were used for comparison. Transgenic SOD1(G86R) were maintained in their initial FVB/N genetic background according to previous studies (Dentel et al, 2013). Transgenic mice expressing TDP43(A315T) were previously described and were maintained as heterozygous in their initial C57Bl6/J background (Wegorzewska et al, 2009). Heterozygous $Fus^{\Delta NLS/+}$ are knock-in mice expressing FUS protein deleted from its C-terminal NLS from one of the endogenous *Fus* gene. These mice were generated and maintained in C57Bl6/J background. The motor phenotype of these mice will be described elsewhere (Scekic-Zahirovic, submitted). Tph2-YFP mice were purchased from Jackson laboratories (Bar Harbor, ME, USA; strain 014555) and maintained in their initial genetic background. Female Tph2-YFP mice were crossed with male SOD1(G86R) to generate compound transgenic mice.

For biochemical analysis, animals were sacrificed at the ages indicated at 2PM, and tissues were quickly dissected, frozen in liquid nitrogen, and stored at −80 °C until use. For histological analysis, animals were anesthetized by intraperitoneal injection of ketamine (Imalgène 1000®, Merial, Lyon France; 90 mg/kg body weight) and xylazine (Rompun 2% ®, Bayer, Leverkusen, Germany; 10 mg/kg body weight) at the ages indicated at 2PM. After perfusion of 4% paraformaldehyde (PFA, Sigma, St Louis, MO, USA), brains were removed, stored in the same fixative overnight at 4°C and stored in phosphate buffered saline (PBS) until used. These experiments were authorized by the local ethical committee of Strasbourg University (CREMEAS).

Drugs and treatments

Pioglitazone (Actos®, Takeda, London, UK) was dissolved in 10% dimethyl sulfoxide (DMSO, Fisher Scientific, Illkirch, France) and a single oral administration was given by gavage at a dose of 40 mg/kg body weight. Fluoxetine (Sigma, St Louis, MO, USA) was dissolved in 0,9% sodium chloride (NaCl, Sigma, St Louis, MO, USA) and administrated intraperitoneally (i.p.) at a dose of 20 mg/kg body weight.

Measurements of food intake

For the pioglitazone experiment, mice were fasted from 9AM to 3PM, and pioglitazone was administrated at 3PM. Food was reintroduced 1 hour after gavage and food intake was recorded during 24h.

For short term fasting experiments, mice were fasted from 8AM to 3PM (7 hours fasting conditions) or from 2PM to 3PM (1 hour fasting conditions) and food was reintroduced after 7 hours or 1 hour of fasting. Food intake was measured one hour and 24 hours after refeeding.

For fluoxetine experiment, mice were fasted from 1PM to 2PM, and fluoxetine was injected at 2PM. Food was reintroduced 30 minutes after fluoxetine injection and food intake was measured during one hour. For biochemical analysis, a second injection of fluoxetine was done after 1 hour of feeding and mice were sacrificed 30 minutes later.

Histology

Fixed brains were include in 6% agar (Sigma, St Louis, MO, USA) and cut from Bregma 0.02mm to Bregma -2.90mm into 40µm coronal sections on a vibratome. Arcuate nucleus was identified according to Paxinos Brain Atlas. POMC immunohistochemistry was performed on half of selected brain sections. YFP immunohistochemistry was performed on 1 section per animal. Immunohistochemistry was performed on floating sections using standard histological techniques. Endogenous peroxidases were inactivated using 3% H_2O_2. For POMC immunohistochemistry, permeabilization and saturation of nonspecific sites were done with 0.25%(v/v) Triton (Sigma, St Louis, MO, USA) and 50mg/ml Bovine Albumin Serum (BSA, Sigma, St Louis, MO, USA). For GFP immunohistochemistry, permeabilization and saturation of nonspecific sites were done with 0.5%(v/v) Triton (Sigma, St Louis, MO, USA) and 5%(v/v) Horse serum (Gibco, Life Technologies, Carlsbad, CA, USA). Rabbit anti-POMC primary antibody (Phoenix Peptide, Burlingame, CA, USA; 1:2000) or rabbit anti-GFP primary antibody (Invitrogen, Life Technologies, Carlsbad, CA, USA, 1:1000) were incubated for overnight at room temperature. Biotinilated donkey anti-Rabbit secondary antibody (Jackson, West Grove, PA, USA; 1:500) was incubated during 90 minutes. Staining was performed using Vectastain Elite ABC kit (Vector, Burlingame, CA, USA). After revelation with 3,3'-Diaminobenzidine (DAB, Sigma, St Louis, MO, USA; 0.5mg/ml), sections were mounted and images of all sections were taken. Total numbers of POMC positive cell bodies in the arcuate nucleus were determined by animal by an operator in a blinded manner. The number of POMC positif cell bodies were normalised by the number of selected brain sections for each animal. Innervation score of YFP staining were determined by animal by an operator in a blinded manner.

RNA extraction and quantitative RT-PCR

RNA was extracted from mouse hypothalami using TRIZOL reagent (Life Technologies, Carlsbad, CA, USA). After reverse transcription with iScript reverse transcription Supermix for RT-qPCR (BioRAD, Hercules, CA, USA), cDNA was obtained from 1 µg of RNA. POMC and AgRP mRNA

level were obtained by quantitative PCR using Sso Advanced Universal SYBR Green Supermix (BioRAD, Hercules, CA, USA) with Agrp and POMC sense and antisense primers. Standard curves were constructed by amplifying serial dilutions of cDNA. Starting quantities of samples were calculated with Biorad software. mRNA levels of Agrp and Pomc were normalized to expression levels of the 18S ribosomal, TBP and pol2 RNA housekeeping genes using GeNorm (Vandesompele *et al.*, 2002). Primer sequences were the following:

POMC: F-AGTGCCAGGACCTCACCA, R-CAGCGAGAGGTCGAGTTTG

AgRP: F-CAGGCTCTGTTCCCAGAGTT, R-TCTAGCACCTCCGCCAAA

18S: F-TCTGATAAATGCACGCATCC, R-GCCATGCATGTCTAAGTACGC

TBP: F-CCAATGACTCCTATGACCCCTA, R-CAGCCAAGATTCACGGTAGAT

POL2: F-GCTGGGAGACATAGCACCA, R-TTACTCCCCTGCATGGTCTC

Serotonin levels

Hypothalamic serotonin levels were measured using HPLC, as previously described (Dentel *et al.*, 2013).

Statistical analysis

For statistical analyses in ALS patients, group comparisons were performed using mixed effects regression model analysis by the Institute of Epidemiology and Medical Biometrics at the University of Ulm using the statistical software package SAS Version 9.2 under Windows.

For animal experiments, comparison of two groups was performed using unpaired Student's t-test, except for experiments with pioglitazone in which paired t-test was used. Comparison of three or four groups was performed using One-way ANOVA and Tukey *post-hoc* test. Statistics in animal experiments were performed using Prism version 6.0.

All results from analysis were regarded as hypothesis generating only. All statistical tests were carried out two-sided at a significance level of 5%.

Results

Normal peripheral response to pioglitazone in ALS patients

We took advantage of data collected during the pioglitazone GERP-ALS trial to investigate energy metabolism in ALS patients in response to pioglitazone. The metabolic effects of thiazolinediones (TZDs), including pioglitazone are well understood in models and their effects are largely described in patients (Fig. 1A). Pioglitazone treatment is known to increase levels of adiponectin, an adipose-derived hormone through direct transcriptional activation of the adiponectin gene in adipocytes (Maeda *et al.*, 2001). Consistently, pioglitazone treatment multiplied by four the levels of circulating adiponectin in ALS patients after six months of treatment, and this was maintained after 12 months of treatment (Fig. 1B). Pioglitazone decreases glycemia through hepatic and skeletal muscle PPARγ. In ALS patients, pioglitazone decreased glycaemia (Fig. 1C), although this effect was milder than observed in other populations, including non-diabetic patients (Belfort *et al.*, 2006, Sanyal *et al.*, 2010, DeFronzo *et al.*, 2011). Consistent with a direct action on liver, pioglitazone decreased levels of ASAT and more robustly levels of ALAT (Fig. 1D-E). In all, pioglitazone displayed the expected metabolic effects on adipocytic, muscular, and hepatic biomarkers, and was likely able to activate PPARγ in these tissues.

Pioglitazone does not lead to weight gain in ALS patients

TZDs are also known to act in hypothalamic melanocortin neurons to promote feeding (Diano *et al.*, 2011, Long *et al.*, 2014), and this activation of PPARγ in melanocortin neurons is responsible for the robust weight gain associated with TZDs treatment (Lu *et al.*, 2011, Ryan *et al.*, 2011, Long *et al.*, 2014). Thus, the evolution of body weight upon pioglitazone treatment represents a reliable proximal marker of PPARγ action in hypothalamic melanocortin neurons. In ALS patients, pioglitazone had no effect on weight loss (Fig. 2A), or BMI (Fig. 2B). Increased weight in response to pioglitazone is due to increased food intake, and a subset of ALS patients experience dysphagia. However, pioglitazone had also no effect on BMI and weight loss when considering spinal onset patients (Fig. 2C-D), or patients with preserved everyday life during at least 6 months (results from EuroQoL EQ-5D questionnaire, Fig. 2E-F). Last, patients with preserved bulbar function during at least 6 months after inclusion (as assessed using ALS-FRS R bulbar subscale) did not lose weight, yet pioglitazone had no effect on their BMI (Fig. 2G-H). Thus, pioglitazone did not increase weight in ALS patients, and this appeared unrelated with dysphagia.

Pioglitazone does not increase food intake in mutant SOD1 mice

We hypothesized that the lack of weight gain for ALS patients under pioglitazone was due to defects in stimulating food intake. To test this hypothesis, we turned to transgenic mice expressing mutant SOD1(G86R) (SOD1m mice) as a model of ALS and set up an experimental protocol to study food intake in response to pioglitazone. In rodents, pioglitazone has various effects on food intake depending on genetic background, dose, route and associated diet (Diano *et al.*, 2011, Ryan *et al.*, 2011, Long *et al.*, 2014). Using a protocol (Fig. 3A) adapted from Ryan and collaborators (Ryan *et al.*, 2011), we observed that a single oral dose of pioglitazone (40mg/kg) increased food intake by 10-15% in wild type FVB/N mice (Fig. 3 B-C). However, food intake was not increased in littermate SOD1m mice either one month before motor symptoms (Fig. 3B) or at disease onset (Fig. 3C). Thus, pioglitazone was not able to increase food intake in SOD1m mice.

Defects in melanocortin neurons in mutant SOD1 mice

Hypothalamic melanocortin neurons constitute the primary target of TZDs to promote food intake (Diano *et al.*, 2011, Long *et al.*, 2014). The melanocortin system is mainly constituted of two antagonistic neuronal types located in the arcuate nucleus: pro-opiomelanocortin (POMC) neurons, that secrete the anorexigenic peptide αMSH, and AgRP neurons, that promote food intake, mostly through production of AgRP, an endogenous αMSH antagonist. POMC mRNA levels were two-fold lower in SOD1m mice, either at 75 days of age (Fig. 4A) or at onset (Fig. 4B), while AgRP mRNA levels were higher in non-symptomatic mice (Fig. 4A). Consistent with decreased POMC expression, we observed about 30% less POMC-positive neurons in the arcuate nucleus of SOD1m mice as compared with their wild type littermates at 75 days of age and almost 50% less at onset (Fig. 4C).

Multiple ALS mouse models display functional and molecular alterations in hypothalamic melanocortin system

We then asked whether the observed melanocortin defects translated into functional abnormalities. Indeed, the combination of decreased POMC mRNA levels with increased AgRP mRNA is usually found in situations of promotion of food intake, such as during fasting or in case of leptin deficiency (Mizuno *et al.*, 1998, Mizuno *et al.*, 1999, Ziotopoulou *et al.*, 2000), and compromised melanocortin system is likely to affect food intake behaviour, in particular during refeeding (Perez-Tilve *et al.*, 2010). Thus, we measured food intake after short term fasting in SOD1m mice. Consistent with decreased POMC levels, one hour food intake of SOD1m mice was two fold higher after seven hours (Fig. 5A) or one hour (Fig. 5B) of fasting. Mutations in SOD1 only account for

20% of familial ALS cases, and alterations in hypothalamic melanocortin pathways could be SOD1-specific. However, POMC mRNA levels were decreased in transgenic mice expressing A315T mutant TDP-43 (Wegorzewska *et al.*, 2009) (Fig. 6A), and these mice also displayed transient hyperphagia in response to fasting (Fig. 6B). Last, POMC mRNA levels tended to be lower in 10 months old knock-in mice expressing a truncated FUS protein retained in the cytoplasm ($Fus^{\Delta NLS/+}$ mice) (Fig. 6C) (Scekic-Zahirovic, in preparation), and $Fus^{\Delta NLS/+}$ mice displayed increased food intake after short term fasting as compared with their littermates (Fig. 6D). Thus, abnormal food intake behaviour and defects in the melanocortin system is a hallmark of ALS mouse models.

Involvement of serotonin loss in melanocortin defects associated with ALS

We then sought to understand the mechanisms underlying melanocortin defects in ALS. POMC neurons are affected by multiple stressors that could ultimately underlie the observed defects. We did not observe changes in expression of a series of genes related with oxidative or endoplasmic reticulum stress (*eg* gp47, splicing of XBP1 mRNA), peroxisome biogenesis (Gpx1, catalase) or mitochondrial function (Mfn2) (not shown) indirectly suggesting that neither overt oxidative stress, nor ER stress nor defective peroxisomal biogenesis nor mitochondrial abnormalities might account for decreased POMC neuronal counts. We hypothesized that the previously observed serotonin neuron degeneration (Turner *et al.*, 2005, Dentel *et al.*, 2013) could contribute to the observed melanocortin defects. Indeed, serotonin is known to promote POMC expression in arcuate nucleus through the 5-HT_{2C} receptor (Heisler *et al.*, 2006, Lam *et al.*, 2008). Interestingly, serotonin levels tended to decrease at onset in the hypothalamus of SOD1m mice (Fig. 7A). To determine whether loss of serotonin axons occurred earlier in the arcuate nucleus, we crossed SOD1m mice with Tph2-YFP mice, expressing YFP under the control of the Tph2 promoter targeting expression only in central serotonin neurons (Zhao *et al.*, 2011). We observed a sharp and profound decrease in the density of YFP positive fibers in the arcuate nucleus of SOD1m mice, as compared with their littermates (Fig. 7B). Hypothalamic 5-HT_{2C} expression was increased suggesting that the hypothalamus sought to compensate for loss of serotonergic innervation (Fig. 7C). To probe for serotonergic involvement in defects of the melanocortin system, we used fluoxetine, a selective serotonin reuptake inhibitor to rescue serotonin signaling, using previously published doses and protocols (Kaur and Kulkarni, 2002, Liou *et al.*, 2012). Interestingly fluoxetine pre-treatment completely abrogated the increased food intake in response to short term fasting (Fig. 7D) and increased POMC mRNA levels back to normal in SOD1m mice (Fig. 7E). Fluoxetine had no effect on AgRP upregulation (Fig. 7E). Thus, loss of serotonin innervation is contributing to the melanocortin defects observed in SOD1m mice.

Discussion

In this combined mouse and man study we showed that ALS is associated with defects in the melanocortin system, the major hypothalamic circuit controlling food intake and energy expenditure. Pioglitazone did not increase weight in ALS patients, thus providing indirect evidence of altered hypothalamic melanocortin pathway, and pathological and functional deficits of melanocortin system were found in ALS mouse models directly demonstrating these defects. These findings further extend the spectrum of defects in ALS and provide a mechanistic explanation for a subset of metabolic signs observed in these patients. Our study has also important implications for the design of therapies to target weight loss in this disease.

We first observed that pioglitazone did not increase body weight nor slowed down weight loss in ALS patients. This was a surprising observation since progressive weight gain has been repeatedly observed in all clinical trials of pioglitazone in multiple non-neurological diseases (Promrat *et al.*, 2004, Belfort *et al.*, 2006, Sanyal *et al.*, 2010, DeFronzo *et al.*, 2011). Despite this lack of weight gain, ALS patients under pioglitazone displayed all other biomarkers of efficacy, including decreased glycemia, decreased circulating liver enzymes or increased adiponectin, thus ruling out that ALS patients simply did not respond to the drug. Interestingly, a series of recent studies dissected out how TZDs lead to weight gain through activation of PPARγ in hypothalamic POMC neurons leading to increased food intake (Diano *et al.*, 2011, Lu *et al.*, 2011, Ryan *et al.*, 2011, Long *et al.*, 2014). Consistent with the notion that pioglitazone hypothalamic response was blunted in ALS patients, pioglitazone was not able to promote food intake in SOD1m mice. Indeed, the melanocortin system is dramatically affected in these mice with decreased POMC expression and loss of POMC positive neurons; similar alterations were observed in TDP43 and FUS based mouse models pointing out that such defects are a general feature in ALS. Since pioglitazone decreases the activity of POMC neurons thus increasing food intake (Diano *et al.*, 2011), we propose that the already decreased melanocortin tone in ALS prevents the silencing of POMC neurons by pioglitazone. Consistent with this, SOD1 mice displayed hyperphagia in response to short term fasting, an orexigenic stimulus that also leads to decreased POMC neuronal activity (Perez-Tilve *et al.*, 2010, Diano *et al.*, 2011). Thus, our results point to a general decrease in melanocortin tone in ALS, leading to both a lack of response to TZDs, and abnormal food intake behaviour in response to fasting.

What is the contribution of impaired melanocortin system to the metabolic phenotypes associated with ALS? The melanocortin system exerts multiple actions on energy metabolism, either

dependent on or independent on food intake. First, an expected consequence of decreased melanocortin tone is increased energy intake, especially in response to an orexigenic stimulus such as food deprivation. This is indeed what has been observed in multiple transgenic mouse models of ALS, suggesting that the defect in melanocortin system translates into a functional deficit. Furthermore, consistent with the observed melanocortin defect, we previously observed slightly increased cumulative food intake in SOD1m mice (Dupuis *et al.*, 2004). The situation in ALS patients is less clear with respect to energy intake due to a relative lack of studies reporting dietary intake accurately and to confounding effects of dysphagia in advanced ALS patients. However, two case-control studies reported that increased dietary fat intake was associated with ALS (Nelson *et al.*, 2000, Huisman *et al.*, 2015). Moreover, Huisman and collaborators observed that presymptomatic daily energy intake was increased in ALS patients as compared with controls (Huisman *et al.*, 2015), and this would be consistent with both melanocortin impairment and lack of weight gain under pioglitazone. Second, the melanocortin defect could be responsible for alterations in peripheral metabolic pathways. Indeed, the melanocortin system regulates peripheral lipid metabolism in rodents, by activating cholesterol re-uptake by the liver (Perez-Tilve *et al.*, 2010) and reduces hepatic lipogenesis (Leckstrom *et al.*, 2011) independently of food intake. In the same line, the melanocortin system is controlling glucose metabolism and insulin response (Obici *et al.*, 2001). Interestingly, ALS patients have been reported to display increased circulating cholesterol levels (Dupuis *et al.*, 2008), and glucose intolerance (Pradat *et al.*, 2010). Third, the melanocortin defect could impair regulation of the autonomic nervous system (Sohn *et al.*, 2013), and autonomic abnormalities have been sometimes found in ALS patients (Baltadzhieva *et al.*, 2005). The relationships between these different phenotypes and melanocortin defects are unclear and will have to be clarified in further studies. Importantly, the observed melanocortin defect is unable to explain the weight loss associated with ALS, as, on the contrary, the increased orexigenic drive triggered by POMC deficiency likely compensates for weight loss by increasing food intake. Other mechanisms, either peripheral or central have still to be identified to explain weight loss.

What causes the melanocortin defect in ALS? A first obvious potential mechanism is energy deficit. Indeed, SOD1m mice display weight loss due to hypermetabolism, leading to decreased fat mass and decreased circulating leptin levels (Dupuis *et al.*, 2004). Ablation of leptin in *ob/ob* mice or fasting is indeed sufficient to cause decreased POMC mRNA (Mizuno *et al.*, 1998, Mizuno *et al.*, 1999, Ziotopoulou *et al.*, 2000). However, leptin levels are only decreased by 30% in 75 days old mice (Dupuis *et al.*, 2004), an age at which we already observe strong POMC mRNA decreases. We and others had previously observed serotonin loss in ALS (Turner *et al.*, 2005, Dentel *et al.*, 2013), and we hypothesized that this contributed to melanocortin impairment in SOD1m mice. Indeed,

serotonin is a major activator of POMC neurons through the 5-HT_{2C} receptor, and this occurs through direct electrical stimulation (Heisler *et al.*, 2002) but also trough transcriptional activation (Zhou *et al.*, 2007, Lam *et al.*, 2008, Xu *et al.*, 2008). Consistently, loss of 5-HT_{2C} receptor leads to decreased POMC mRNA in the hypothalamus (Wang and Chehab, 2006). Our observation of restoration of POMC mRNA levels, as well as reversal of transient hyperphagia in SOD1m mice by fluoxetine argues for serotonin loss being a primary cause of melanocortin defect. This however does not exclude that direct modulation of electrical activity by either decreased leptin or other cues either extrinsic or intrinsic further exacerbate the observed defect. Consistent with this notion, decreasing leptin, whose major action is on the melanocortin system, was able to revert partially weight loss and increased energy expenditure in SOD1m mice (Lim *et al.*, 2014), suggesting that the melanocortin system can be further inhibited by leptin ablation.

What are the consequences of our current findings in ALS? There are at least two consequences of our finding for ALS research. First, the observation of melanocortin impairment further extends the notion of systemic involvement in ALS. That melanocortin impairment appears downstream of serotonin loss, also brings about the notion that circuitry dysfunction might contribute to aspects of ALS phenotype. How these serotonin and melanocortin defects might be related with the spreading of TDP-43 aggregates (Brettschneider *et al.*, 2013) remain to be resolved. Second, these results have consequences for the design of pharmacological strategies to combat weight loss in ALS. Indeed, many drugs that could be used to prevent weight loss, including atypical anti-psychotics (*eg* olanzapine) inhibit POMC neurons (Kirk *et al.*, 2009, Weston-Green *et al.*, 2012, Lian *et al.*, 2014). Drugs targeting the cannabinoid system increase body weight by increasing beta-endorphin release from POMC neurons (Koch *et al.*, 2015). Since beta-endorphin is derived from POMC which is decreased in ALS mice, it appears likely that cannabinoids might not be able to promote food intake through this mechanism in ALS. Thus, our current study provides a note of caution for the use of these drugs to counteract weight loss in the specific context of ALS patients, and suggest that disease progression might impair responsiveness of ALS patients to classical drugs leading to weight gain.

In all, our *post-hoc* analysis of the pioglitazone trial revealed that the melanocortin system is profoundly altered in ALS, and that this might be important for understanding and preventing impairment of energy metabolism in ALS patients.

Acknowledgements

We acknowledge the technical help of Marie Jo Ruivo, Annie Picchinenna, Coraline Kostal, Marc Antoine Goy and Paul Rochet.

Funding

This work was supported by Association de recherche sur la SLA (ARSLA) and Fondation Thierry Latran (SpastALS, to LD). Work in our laboratories is supported by ALS Association Investigator Initiated Award (grants 2235, 3209 and 8075; to LD); the Frick Foundation (award 2013 to LD); Association Française contre les Myopathies (grant #18280; to LD); Virtual Helmholtz Institute "RNA dysmetabolism in ALS and FTD" (WP2, to LD, AW, ACL and AH); Fondation « recherche sur le cerveau » (call 2015, to LD).

References

Baltadzhieva R, Gurevich T, Korczyn AD. Autonomic impairment in amyotrophic lateral sclerosis. Curr Opin Neurol. 2005;18(5):487-93.

Belfort R, Harrison SA, Brown K, Darland C, Finch J, Hardies J, et al. A placebo-controlled trial of pioglitazone in subjects with nonalcoholic steatohepatitis. N Engl J Med. 2006;355(22):2297-307.

Bouteloup C, Desport JC, Clavelou P, Guy N, Derumeaux-Burel H, Ferrier A, et al. Hypermetabolism in ALS patients: an early and persistent phenomenon. J Neurol. 2009;256(8):1236-42.

Brettschneider J, Del Tredici K, Toledo JB, Robinson JL, Irwin DJ, Grossman M, et al. Stages of pTDP-43 pathology in amyotrophic lateral sclerosis. Ann Neurol. 2013;74(1):20-38.

Cirulli ET, Lasseigne BN, Petrovski S, Sapp PC, Dion PA, Leblond CS, et al. Exome sequencing in amyotrophic lateral sclerosis identifies risk genes and pathways. Science. 2015;347(6229):1436-41.

DeFronzo RA, Tripathy D, Schwenke DC, Banerji M, Bray GA, Buchanan TA, et al. Pioglitazone for diabetes prevention in impaired glucose tolerance. N Engl J Med. 2011;364(12):1104-15.

Dentel C, Palamiuc L, Henriques A, Lannes B, Spreux-Varoquaux O, Gutknecht L, et al. Degeneration of serotonergic neurons in amyotrophic lateral sclerosis: a link to spasticity. Brain. 2013;136(Pt 2):483-93.

Desport JC, Preux PM, Magy L, Boirie Y, Vallat JM, Beaufrere B, et al. Factors correlated with hypermetabolism in patients with amyotrophic lateral sclerosis. Am J Clin Nutr. 2001;74(3):328-34.

Desport JC, Preux PM, Truong TC, Vallat JM, Sautereau D, Couratier P. Nutritional status is a prognostic factor for survival in ALS patients. Neurology. 1999;53(5):1059-63.

Diano S, Liu ZW, Jeong JK, Dietrich MO, Ruan HB, Kim E, et al. Peroxisome proliferation-associated control of reactive oxygen species sets melanocortin tone and feeding in diet-induced obesity. Nat Med. 2011;17(9):1121-7.

Dorst J, Dupuis L, Petri S, Kollewe K, Abdulla S, Wolf J, et al. Percutaneous endoscopic gastrostomy in amyotrophic lateral sclerosis: a prospective observational study. J Neurol. 2015;262(4):849-58.

Dorst J, Kühnlein P, Hendrich C, Kassubek J, Sperfeld AD, Ludolph AC. Patients with elevated triglyceride and cholesterol serum levels have a prolonged survival in Amyotrophic Lateral Sclerosis. J Neurol. 2011;258:613-7.

Dupuis L, Corcia P, Fergani A, Gonzalez De Aguilar JL, Bonnefont-Rousselot D, Bittar R, et al. Dyslipidemia is a protective factor in amyotrophic lateral sclerosis. Neurology. 2008;70(13):1004-9.

Dupuis L, Dengler R, Heneka MT, Meyer T, Zierz S, Kassubek J, et al. A randomized, double blind, placebo-controlled trial of pioglitazone in combination with riluzole in amyotrophic lateral sclerosis. PLoS One. 2012;7(6):e37885.

Dupuis L, Oudart H, Rene F, Gonzalez de Aguilar JL, Loeffler JP. Evidence for defective energy homeostasis in amyotrophic lateral sclerosis: benefit of a high-energy diet in a transgenic mouse model. Proc Natl Acad Sci U S A. 2004;101(30):11159-64.

Dupuis L, Pradat PF, Ludolph AC, Loeffler JP. Energy metabolism in amyotrophic lateral sclerosis. Lancet Neurol. 2011;10(1):75-82.

Fergani A, Oudart H, Gonzalez De Aguilar JL, Fricker B, Rene F, Hocquette JF, et al. Increased peripheral lipid clearance in an animal model of amyotrophic lateral sclerosis. J Lipid Res. 2007;48(7):1571-80.

Freischmidt A, Wieland T, Richter B, Ruf W, Schaeffer V, Muller K, et al. Haploinsufficiency of TBK1 causes familial ALS and fronto-temporal dementia. Nat Neurosci. 2015;18(5):631-6.

Gallo V, Wark PA, Jenab M, Pearce N, Brayne C, Vermeulen R, et al. Prediagnostic body fat and risk of death from amyotrophic lateral sclerosis: the EPIC cohort. Neurology. 2013;80(9):829-38.

Gurney ME, Pu H, Chiu AY, Dal Canto MC, Polchow CY, Alexander DD, et al. Motor neuron degeneration in mice that express a human Cu,Zn superoxide dismutase mutation. Science. 1994;264(5166):1772-5.

Heisler LK, Cowley MA, Tecott LH, Fan W, Low MJ, Smart JL, et al. Activation of central melanocortin pathways by fenfluramine. Science. 2002;297(5581):609-11.

Heisler LK, Jobst EE, Sutton GM, Zhou L, Borok E, Thornton-Jones Z, et al. Serotonin reciprocally regulates melanocortin neurons to modulate food intake. Neuron. 2006;51(2):239-49.

Huisman MH, Seelen M, de Jong SW, Dorresteijn KR, van Doormaal PT, van der Kooi AJ, et al. Lifetime physical activity and the risk of amyotrophic lateral sclerosis. J Neurol Neurosurg Psychiatry. 2013;84(9):976-81.

Huisman MH, Seelen M, van Doormaal PT, de Jong SW, de Vries JH, van der Kooi AJ, et al. Independent associations of presymptomatic body mass index, and consumption of fat and alcohol with amyotrophic lateral sclerosis. JAMA Neurology. 2015;in press.

Kaur G, Kulkarni SK. Evidence for serotonergic modulation of progesterone-induced hyperphagia, depression and algesia in female mice. Brain Res. 2002;943(2):206-15.

Kirk SL, Glazebrook J, Grayson B, Neill JC, Reynolds GP. Olanzapine-induced weight gain in the rat: role of 5-HT2C and histamine H1 receptors. Psychopharmacology. 2009;207(1):119-25.

Koch M, Varela L, Kim JG, Kim JD, Hernandez-Nuno F, Simonds SE, et al. Hypothalamic POMC neurons promote cannabinoid-induced feeding. Nature. 2015;519(7541):45-50.

Lam DD, Przydzial MJ, Ridley SH, Yeo GS, Rochford JJ, O'Rahilly S, et al. Serotonin 5-HT2C receptor agonist promotes hypophagia via downstream activation of melanocortin 4 receptors. Endocrinology. 2008;149(3):1323-8.

Lattante S, Ciura S, Rouleau GA, Kabashi E. Defining the genetic connection linking amyotrophic lateral sclerosis (ALS) with frontotemporal dementia (FTD). Trends Genet. 2015.

Leblond CS, Kaneb HM, Dion PA, Rouleau GA. Dissection of genetic factors associated with amyotrophic lateral sclerosis. Exp Neurol. 2014;262 Pt B:91-101.

Leckstrom A, Lew PS, Poritsanos NJ, Mizuno TM. Central melanocortin receptor agonist reduces hepatic lipogenic gene expression in streptozotocin-induced diabetic mice. Life sciences. 2011;88(15-16):664-9.

Lian J, Huang XF, Pai N, Deng C. Betahistine ameliorates olanzapine-induced weight gain through modulation of histaminergic, NPY and AMPK pathways. Psychoneuroendocrinology. 2014;48:77-86.

Lim MA, Bence KK, Sandesara I, Andreux P, Auwerx J, Ishibashi J, et al. Genetically altering organismal metabolism by leptin-deficiency benefits a mouse model of amyotrophic lateral sclerosis. Hum Mol Genet. 2014;23(18):4995-5008.

Lindauer E, Dupuis L, Muller HP, Neumann H, Ludolph AC, Kassubek J. Adipose Tissue Distribution Predicts Survival in Amyotrophic Lateral Sclerosis. PLoS One. 2013;8(6):e67783.

Liou YJ, Chen CH, Cheng CY, Chen SY, Chen TJ, Yu YW, et al. Convergent evidence from mouse and human studies suggests the involvement of zinc finger protein 326 gene in antidepressant treatment response. PLoS One. 2012;7(5):e32984.

Long L, Toda C, Jeong JK, Horvath TL, Diano S. PPARgamma ablation sensitizes proopiomelanocortin neurons to leptin during high-fat feeding. J Clin Invest. 2014;124(9):4017-27.

Lu M, Sarruf DA, Talukdar S, Sharma S, Li P, Bandyopadhyay G, et al. Brain PPAR-gamma promotes obesity and is required for the insulin-sensitizing effect of thiazolidinediones. Nat Med. 2011;17(5):618-22.

Maeda N, Takahashi M, Funahashi T, Kihara S, Nishizawa H, Kishida K, et al. PPARgamma ligands increase expression and plasma concentrations of adiponectin, an adipose-derived protein. Diabetes. 2001;50(9):2094-9.

Marin B, Desport JC, Kajeu P, Jesus P, Nicolaud B, Nicol M, et al. Alteration of nutritional status at diagnosis is a prognostic factor for survival of amyotrophic lateral sclerosis patients. J Neurol Neurosurg Psychiatry. 2011;82(6):628-34.

Mizuno TM, Kleopoulos SP, Bergen HT, Roberts JL, Priest CA, Mobbs CV. Hypothalamic pro-opiomelanocortin mRNA is reduced by fasting and [corrected] in ob/ob and db/db mice, but is stimulated by leptin. Diabetes. 1998;47(2):294-7.

Mizuno TM, Makimura H, Silverstein J, Roberts JL, Lopingco T, Mobbs CV. Fasting regulates hypothalamic neuropeptide Y, agouti-related peptide, and proopiomelanocortin in diabetic mice independent of changes in leptin or insulin. Endocrinology. 1999;140(10):4551-7.

Nelson LM, Matkin C, Longstreth WT, Jr., McGuire V. Population-based case-control study of amyotrophic lateral sclerosis in western Washington State. II. Diet. Am J Epidemiol. 2000;151(2):164-73.

O'Reilly EJ, Wang H, Weisskopf MG, Fitzgerald KC, Falcone G, McCullough ML, et al. Premorbid body mass index and risk of amyotrophic lateral sclerosis. Amyotrophic lateral sclerosis & frontotemporal degeneration. 2013;14(3):205-11.

Obici S, Feng Z, Tan J, Liu L, Karkanias G, Rossetti L. Central melanocortin receptors regulate insulin action. J Clin Invest. 2001;108(7):1079-85.

Otto M, Bowser R, Turner MR, Berry J, Brettschneider J, Connor J, et al. Roadmap and standard operating procedures for biobanking and discovery of neurochemical markers in ALS. Amyotroph Lateral Scler. 2011;in press.

Paganoni S, Deng J, Jaffa M, Cudkowicz ME, Wills AM. Body mass index, not dyslipidemia, is an independent predictor of survival in amyotrophic lateral sclerosis. Muscle Nerve. 2011;44(1):20-4.

Palamiuc L, Schlagowski A, Ngo ST, Vernay A, Dirrig-Grosch S, Henriques A, et al. A metabolic switch toward lipid use in glycolytic muscle is an early pathologic event in a mouse model of amyotrophic lateral sclerosis. EMBO Mol Med. 2015;7(5):526-46.

Perez-Tilve D, Hofmann SM, Basford J, Nogueiras R, Pfluger PT, Patterson JT, et al. Melanocortin signaling in the CNS directly regulates circulating cholesterol. Nat Neurosci. 2010;13(7):877-82.

Pradat PF, Bruneteau G, Gordon PH, Dupuis L, Bonnefont-Rousselot D, Simon D, et al. Impaired glucose tolerance in patients with amyotrophic lateral sclerosis. Amyotroph Lateral Scler. 2010;11(1-2):166-71.

Promrat K, Lutchman G, Uwaifo GI, Freedman RJ, Soza A, Heller T, et al. A pilot study of pioglitazone treatment for nonalcoholic steatohepatitis. Hepatology. 2004;39(1):188-96.

Ripps ME, Huntley GW, Hof PR, Morrison JH, Gordon JW. Transgenic mice expressing an altered murine superoxide dismutase gene provide an animal model of amyotrophic lateral sclerosis. Proc Natl Acad Sci U S A. 1995;92(3):689-93.

Ryan KK, Li B, Grayson BE, Matter EK, Woods SC, Seeley RJ. A role for central nervous system PPAR-gamma in the regulation of energy balance. Nat Med. 2011;17(5):623-6.

Sanyal AJ, Chalasani N, Kowdley KV, McCullough A, Diehl AM, Bass NM, et al. Pioglitazone, vitamin E, or placebo for nonalcoholic steatohepatitis. N Engl J Med. 2010;362(18):1675-85.

Sohn JW, Harris LE, Berglund ED, Liu T, Vong L, Lowell BB, et al. Melanocortin 4 receptors reciprocally regulate sympathetic and parasympathetic preganglionic neurons. Cell. 2013;152(3):612-9.

Turner MR, Rabiner EA, Hammers A, Al-Chalabi A, Grasby PM, Shaw CE, et al. [11C]-WAY100635 PET demonstrates marked 5-HT1A receptor changes in sporadic ALS. Brain. 2005;128(Pt 4):896-905.

Turner MR, Wotton C, Talbot K, Goldacre MJ. Cardiovascular fitness as a risk factor for amyotrophic lateral sclerosis: indirect evidence from record linkage study. J Neurol Neurosurg Psychiatry. 2012;83(4):395-8.

Vandesompele J, De Preter K, Pattyn F, Poppe B, Van Roy N, De Paepe A, et al. Accurate normalization of real-time quantitative RT-PCR data by geometric averaging of multiple internal control genes. Genome Biol. 2002;3(7):research0034.1–.11.

Wang B, Chehab FF. Deletion of the serotonin 2c receptor from transgenic mice overexpressing leptin does not affect their lipodystrophy but exacerbates their diet-induced obesity. Biochem Biophys Res Commun. 2006;351(2):418-23.

Wegorzewska I, Bell S, Cairns NJ, Miller TM, Baloh RH. TDP-43 mutant transgenic mice develop features of ALS and frontotemporal lobar degeneration. Proc Natl Acad Sci U S A. 2009;106(44):18809-14.

Weston-Green K, Huang XF, Deng C. Alterations to melanocortinergic, GABAergic and cannabinoid neurotransmission associated with olanzapine-induced weight gain. PLoS One. 2012;7(3):e33548.

Wills AM, Hubbard J, Macklin EA, Glass J, Tandan R, Simpson EP, et al. Hypercaloric enteral nutrition in patients with amyotrophic lateral sclerosis: a randomised, double-blind, placebo-controlled phase 2 trial. Lancet. 2014.

Xu Y, Jones JE, Kohno D, Williams KW, Lee CE, Choi MJ, et al. 5-HT2CRs expressed by pro-opiomelanocortin neurons regulate energy homeostasis. Neuron. 2008;60(4):582-9.

Zhao S, Ting JT, Atallah HE, Qiu L, Tan J, Gloss B, et al. Cell type-specific channelrhodopsin-2 transgenic mice for optogenetic dissection of neural circuitry function. Nature methods. 2011;8(9):745-52.

Zhou L, Sutton GM, Rochford JJ, Semple RK, Lam DD, Oksanen LJ, et al. Serotonin 2C receptor agonists improve type 2 diabetes via melanocortin-4 receptor signaling pathways. Cell Metab. 2007;6(5):398-405.

Ziotopoulou M, Erani DM, Hileman SM, Bjorbaek C, Mantzoros CS. Unlike leptin, ciliary neurotrophic factor does not reverse the starvation-induced changes of serum corticosterone and hypothalamic neuropeptide levels but induces expression of hypothalamic inhibitors of leptin signaling. Diabetes. 2000;49(11):1890-6.

Figures legends

Figure 1: effects of pioglitazone on peripheral biomarkers in ALS patients

A: summary of metabolic effects of pioglitazone (and TZDs) in humans

B-E: Changes in plasma adiponectin (% from the baseline) (B), glycaemia (% from the baseline, C), circulating aspartate amino-transferase (ASAT, changes in U/L from the baseline, D), and alanine amino-transferase (ALAT, changes in U/L from the baseline, E). Number of patients per time point is indicated in the table. Pioglitazone treated patients are significantly different from placebo treated patients for these items as assessed using a mixed effects regression model analysis. Data are presented as mean and standard error.

Figure 2: effects of pioglitazone on weight loss in ALS patients

Weight loss (kg loss per month, A, C, E, G) and changes in BMI from the baseline (B, D, F, H) in in the whole ALS population (A, B), spinal onset patients (C, D), in patients with relatively preserved quality of life (E, F) and in patients with preserved bulbar function (G, H). To select the patients with preserved quality of life, we used the results from the EuroQoL questionnaire to identify patients that had no or only few problems with their everyday-life. Selected patients answered that they had either no or few problems in their everyday life during at least 6 months after their allocation to a group. To select the patients with preserved bulbar function, we used the results from ALS-FRS-R bulbar subscale and selected patients with a score equal or superior to 10 (maximum: 12) six months after inclusion. The number of patients per time point is indicated on each panel. No significant difference is noted for these items. Data are presented as mean and standard error.

Figure 3 : No effect of piogliotazone on SOD1m mice food intake.

A: Experimental scheme: pioglitazone was provided *per os* after 6 hours of fasting. Food was reintroduced 1 hour after gavage, and food intake recorded for the next 24 hours.

B,C: food intake after pioglitazone treatment in SOD1(G86R) mice (SOD1m) and control littermates (wt) at 75 days of age (n=12, left panel) and symptom onset (n=13, right panel), either treated with vehicle (blue columns) or pioglitazone 40mg/kg body weight (red columns).*$p< 0.05$, Paired Student's t-test for the drug. Data are presented as mean and standard error.

Figure 4: Defect in melanocortin neurons in SOD1m mice.

A: mRNA levels of POMC and AgRP in the hypothalamus of SOD1(G86R) mice (black columns, SOD1m) and control littermates (white columns, wt) at 75 days of age (n= 15, left panel) and symptom onset (n=11, right panel). *p<0.05. **p<0.005. ***p<0.0005, Student's t-test.

B: Quantification of POMC neurons in the arcuate nucleus. POMC immunohistochemistry was performed on whole brain sections, and arcuate nucleus was identified according to Paxinos Brain Atlas (scheme of identified regions, in red, a). The whole region was sectioned and half of these sections were stained for POMC immunohistochemistry. Representative images are shown for SOD1(G86R) mice and control littermates at 75 days of age at two magnifications (scale bar 200 µm (middle row), 20µm (lower row)). Total numbers of POMC positive cell bodies in the arcuate nucleus were determined in SOD1m mice at 75 days of age (n=8, b-f) and at symptom onset (n=7, b) as compared with their wt littermates. **p<0.005, ****p<0.0001, One-way ANOVA followed by Tukey post-hoc test. Data are presented as mean and standard error.

Figure 5: Transient hyperphagia after fasting in SOD1m mice.

A-B: Food intake was measured during one hour, after either seven hours (A) or one hour (B) of fasting in SOD1(G86R) mice (black columns, SOD1m) and control littermates (white columns, wt) at 75 days of age (n= 10 and n=14 respectively for A and B). *p<0.05, Student's t-test. Data are presented as mean and standard error.

Figure 6:. Multiple ALS mouse models display functional and molecular alterations in hypothalamic melanocortin system

A: mRNA levels of POMC and AgRP in the hypothalamus of transgenic mice expressing A315T TDP-43 mutation (black columns, TDP43m) and control littermates (white columns, wt) at non symptomatic stage (n=6). Unpaired t-test. *p<0.05. -B: Food intake was measured one hour after refeeding in TDP43m mice (n=8). *p<0.05, **p<0.01, Multiple t-test.

C: mRNA levels of POMC and AgRP in the hypothalamus of transgenic mice *Fus* ΔNLS/+ knock-in mice) (black columns, ΔNLS/+) and control littermates (white columns, +/+) at 10 months of age (n=4).

D: Food intake was measured one hour after refeeding in ΔNLS/+ mice (n=10) at 10 months of age. *p<0.05, Student's t-test. Data are presented as mean and standard error.

Figure 7:. Involvement of serotonin loss in melanocortin defects of mutant SOD1 mice

A: Serotonin levels in the hypothalamus of SOD1(G86R) mice (black columns, SOD1m) and control littermates (white columns, wt) (n=5 at 75 days and n=5 at onset). One- way ANOVA followed by Tukey *post hoc* test.

B: Serotonergic innervation in the arcuate nucleus. GFP immunohistochemistry was performed on Tph2-YFP mice on arcuate nucleus cuts after identification on Paxinos Brain Atlas (scheme of identified regions, in red, in the upper left column, a). Representative images are shown for SOD1(G86R) Tph2-YFP mice and control littermates at onset at two magnifications (scale bar 200 µm (middle row), 20µm (lower row)) Serotonergic innervation in the arcuate nucleus were scored by a blind observer in SOD1m mice at symptom onset (b-f, n=4) as compared with their wt littermates. **p<0.005, Student's t-test.

C: mRNA levels of $5HT_{2C}$ receptor in the hypothalamus of SOD1(G86R) mice (black columns, SOD1m) at 75 days of age and onset and in control littermates (white column, wt) (n=8). **p<0.01, One-way ANOVA

D: Food intake was measured one hour after refeeding in SOD1(G86R) mice (SOD1m) at 80 days of age and control littermates (wt) after fluoxetine 20mg/kg body weight (red columns) or vehicle (blue columns) injection (n=38). **p<0.005, Multiple t-test.

E: mRNA levels of POMC and AgRP in the hypothalamus of SOD1(G86R) mice (SOD1m) and control littermates (wt) at 85 days of age after fluoxetine 20mg/kg body weight (red columns) or vehicle (blue columns) injection (n=20). *p<0.05, One-way ANOVA.

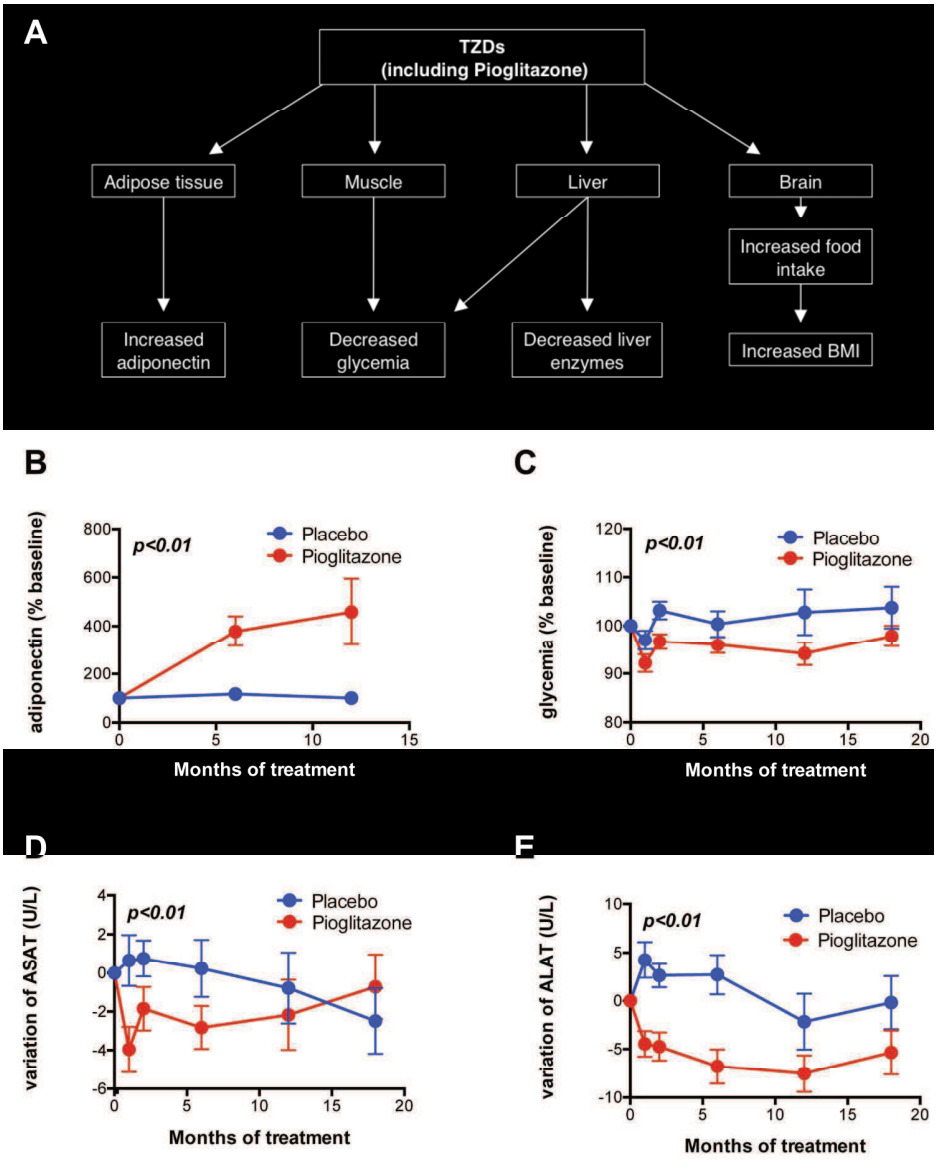

Figure 1: effects of pioglitazone on peripheral biomarkers in ALS patients
A: summary of metabolic effects of pioglitazone (and TZDs) in humans
B-E: Changes in plasma adiponectin (% from the baseline) (B), glycaemia (% from the baseline, C), circulating aspartate amino-transferase (ASAT, changes in U/L from the baseline, D), and alanine amino-transferase (ALAT, changes in U/L from the baseline, E). Number of patients per time point is indicated in the table. Pioglitazone treated patients are significantly different from placebo treated patients for these items as assessed using a mixed effects regression model analysis. Data are presented as mean and standard error.

158x199mm (300 x 300 DPI)

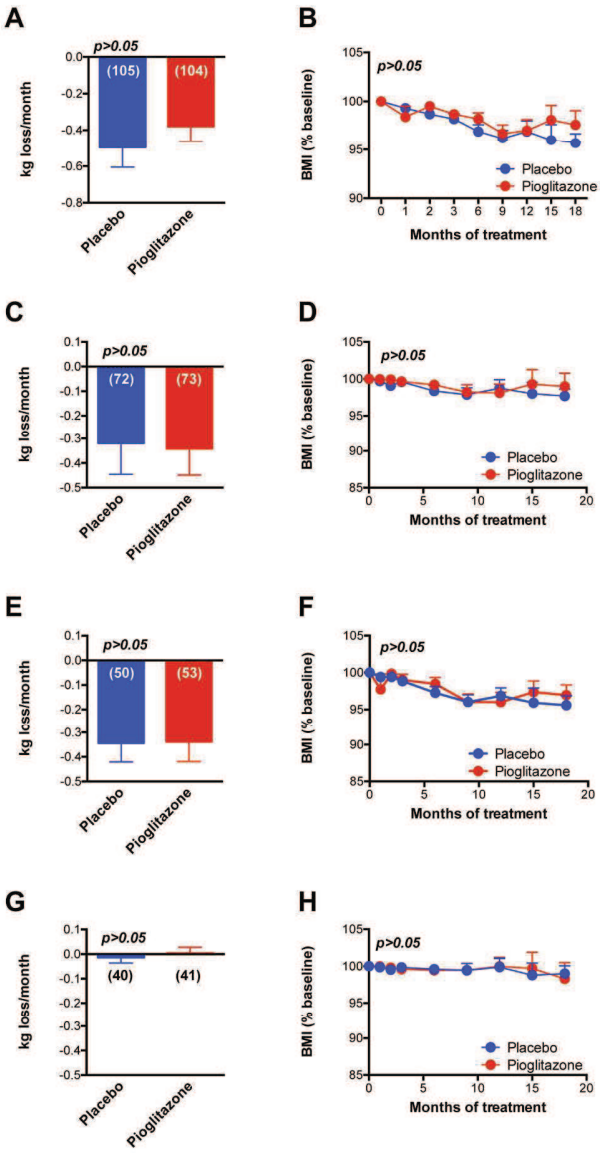

Figure 2: effects of pioglitazone on weight loss in ALS patients
Weight loss (kg loss per month, A, C, E, G) and changes in BMI from the baseline (B, D, F, H) in in the whole ALS population (A, B), spinal onset patients (C, D), in patients with relatively preserved quality of life (E, F) and in patients with preserved bulbar function (G, H). To select the patients with preserved quality of life, we used the results from the EuroQoL questionnaire to identify patients that had no or only few problems with their everyday-life. Selected patients answered that they had either no or few problems in their everyday life during at least 6 months after their allocation to a group. To select the patients with preserved bulbar function, we used the results from ALS-FRS-R bulbar subscale and selected patients with a score equal or superior to 10 (maximum: 12) six months after inclusion. The number of patients per time point is indicated on each panel. No significant difference is noted for these items. Data are presented as mean and standard error.

132x243mm (300 x 300 DPI)

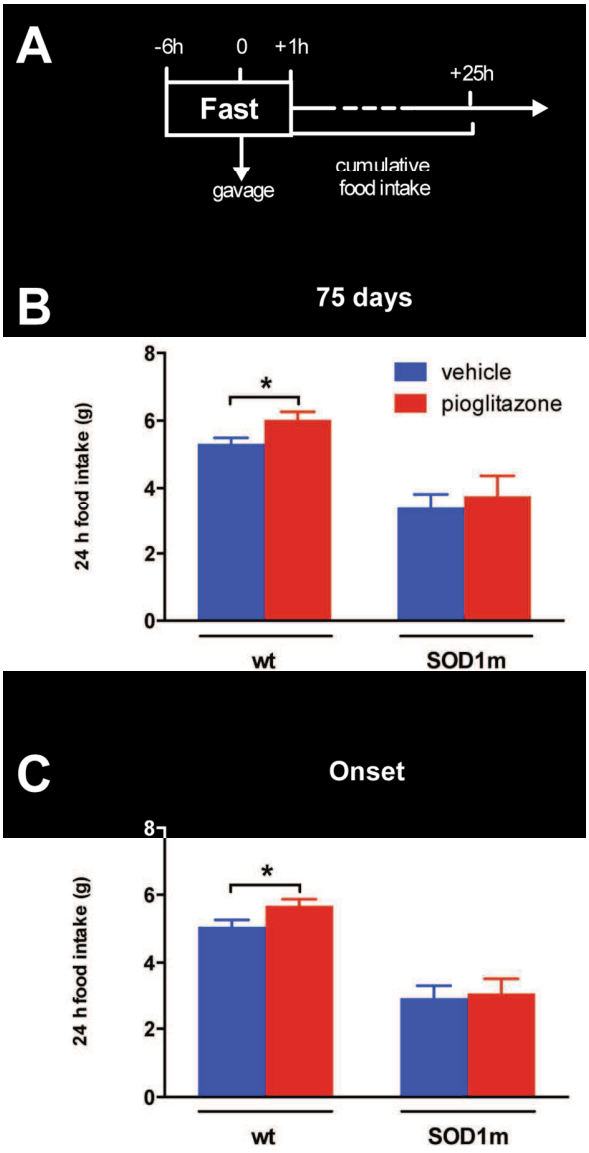

Figure 3 : No effect of piogliotazone on SOD1m mice food intake.
A: Experimental scheme: pioglitazone was provided per os after 6 hours of fasting. Food was reintroduced 1 hour after gavage, and food intake recorded for the next 24 hours.
B,C: food intake after pioglitazone treatment in SOD1(G86R) mice (SOD1m) and control littermates (wt) at 75 days of age (n=12, left panel) and symptom onset (n=13, right panel), either treated with vehicle (blue columns) or pioglitazone 40mg/kg body weight (red columns).*p< 0.05, Paired Student's t-test for the drug. Data are presented as mean and standard error.

76x153mm (300 x 300 DPI)

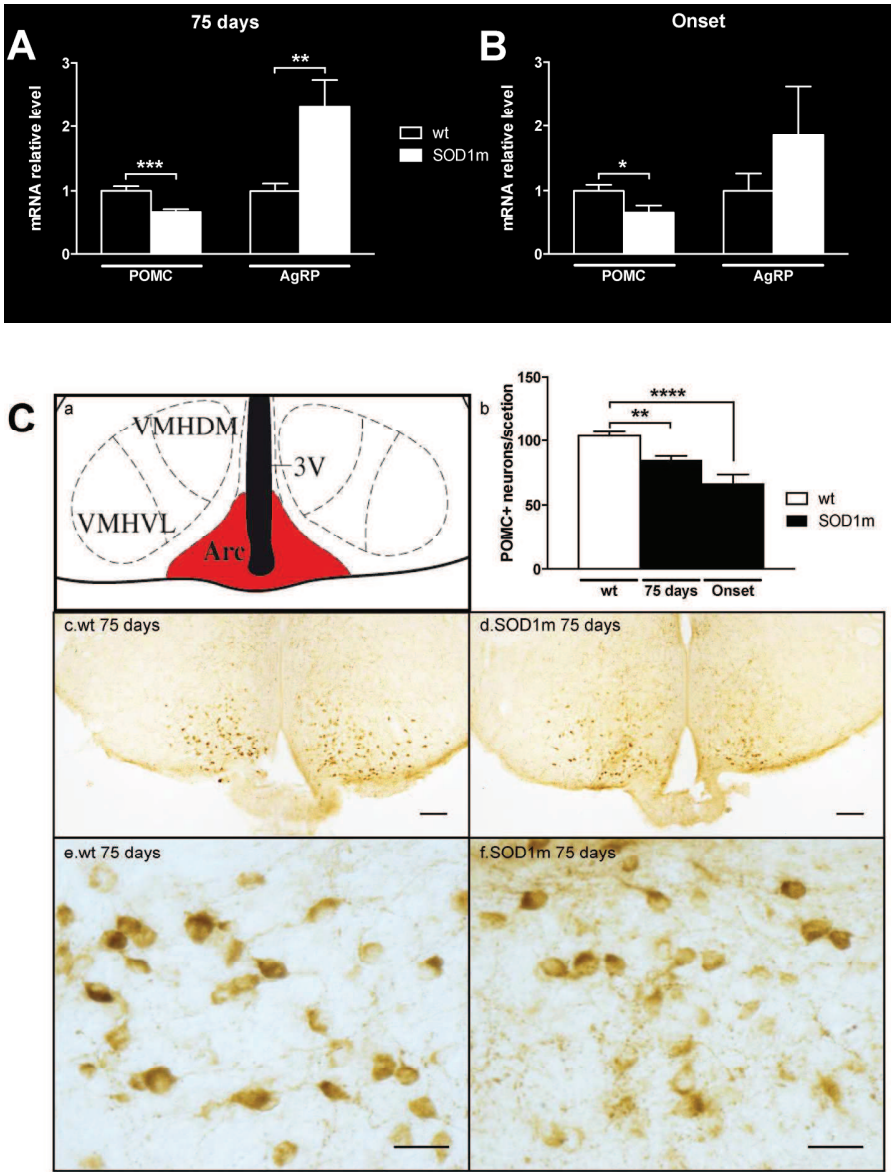

Figure 4: Defect in melanocortin neurons in SOD1m mice.
A: mRNA levels of POMC and AgRP in the hypothalamus of SOD1(G86R) mice (black columns, SOD1m) and control littermates (white columns, wt) at 75 days of age (n= 15, left panel) and symptom onset (n=11, right panel). *p<0.05. **p<0.005. ***p<0.0005, Student's t-test.
B: Quantification of POMC neurons in the arcuate nucleus. POMC immunohistochemistry was performed on whole brain sections, and arcuate nucleus was identified according to Paxinos Brain Atlas (scheme of identified regions, in red, a). The whole region was sectioned and half of these sections were stained for POMC immunohistochemistry. Representative images are shown for SOD1(G86R) mice and control littermates at 75 days of age at two magnifications (scale bar 200 µm (middle row), 20µm (lower row)). Total numbers of POMC positive cell bodies in the arcuate nucleus were determined in SOD1m mice at 75 days of age (n=8, b-f) and at symptom onset (n=7, b) as compared with their wt littermates. **p<0.005, ****p<0.0001, One-way ANOVA followed by Tukey post-hoc test. Data are presented as mean and standard error.

191x251mm (300 x 300 DPI)

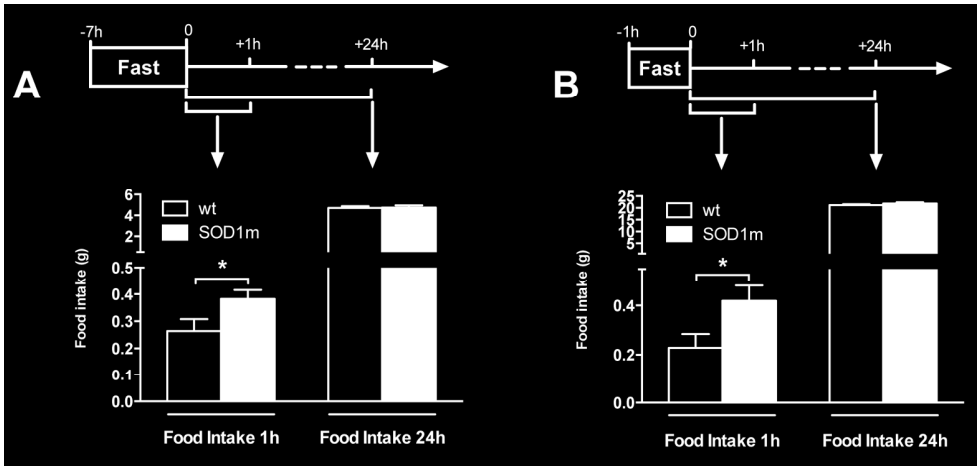

Figure 5: Transient hyperphagia after fasting in SOD1m mice.
A-B: Food intake was measured during one hour, after either seven hours (A) or one hour (B) of fasting in SOD1(G86R) mice (black columns, SOD1m) and control littermates (white columns, wt) at 75 days of age (n= 10 and n=14 respectively for A and B). *p<0.05, Student's t-test. Data are presented as mean and standard error.

168x80mm (300 x 300 DPI)

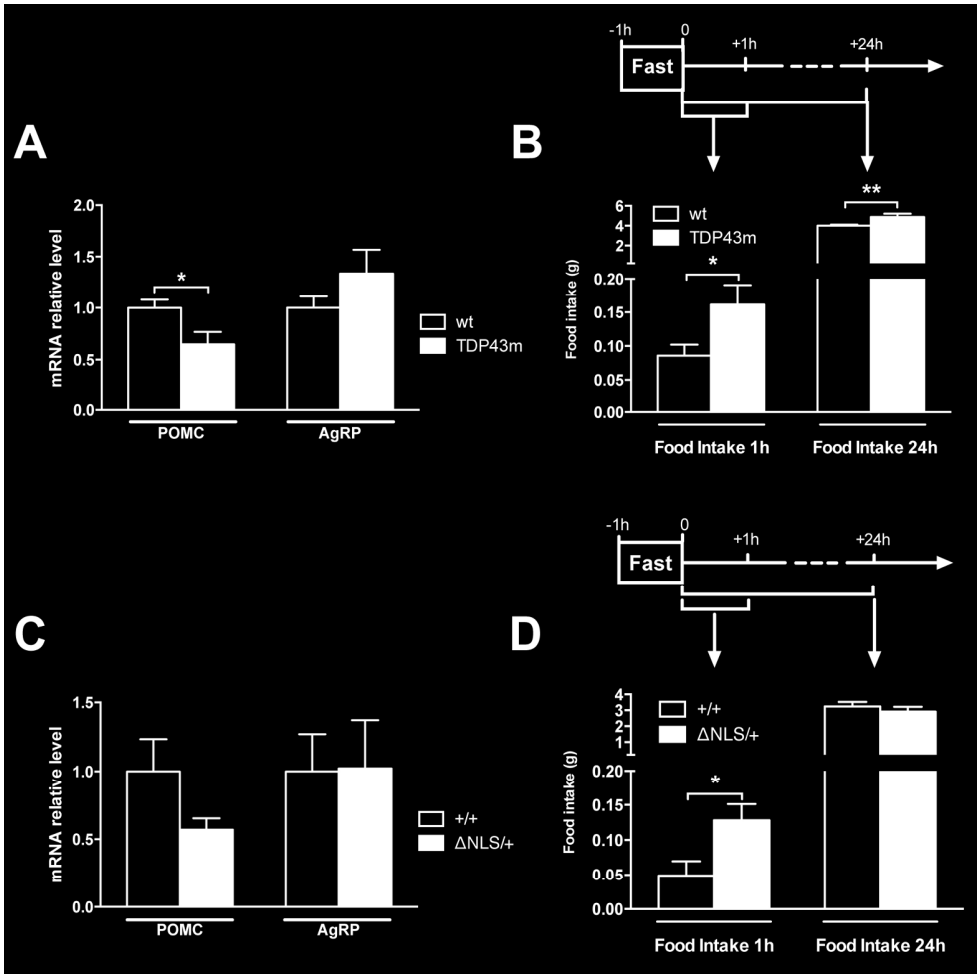

Figure 6:. Multiple ALS mouse models display functional and molecular alterations in hypothalamic melanocortin system

A: mRNA levels of POMC and AgRP in the hypothalamus of transgenic mice expressing A315T TDP-43 mutation (black columns, TDP43m) and control littermates (white columns, wt) at non symptomatic stage (n=6). Unpaired t-test. *p<0.05. -B: Food intake was measured one hour after refeeding in TDP43m mice (n=8). *p<0.05, **p<0.01, Multiple t-test.

C: mRNA levels of POMC and AgRP in the hypothalamus of transgenic mice Fus ΔNLS/+ knock-in mice) (black columns, ΔNLS/+) and control littermates (white columns, +/+) at 10 months of age (n=4).

D: Food intake was measured one hour after refeeding in ΔNLS/+ mice (n=10) at 10 months of age. *p<0.05, Student's t-test. Data are presented as mean and standard error.

170x169mm (300 x 300 DPI)

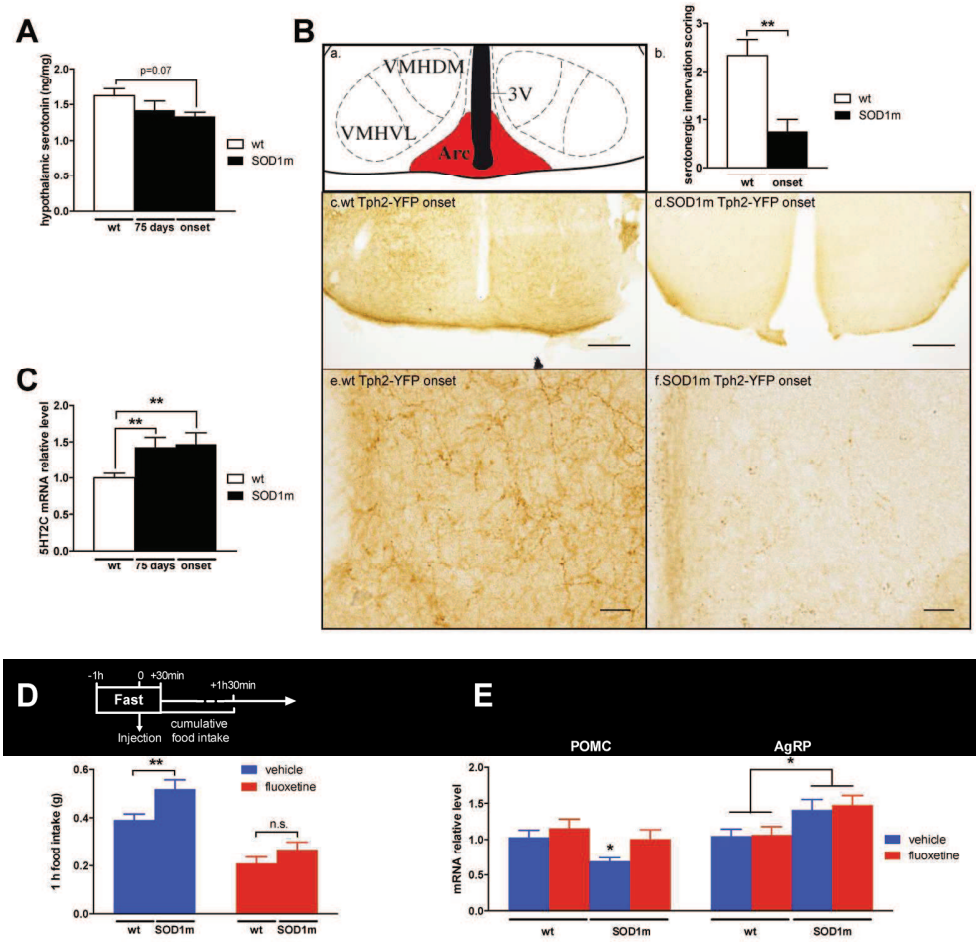

Figure 7:. Involvement of serotonin loss in melanocortin defects of mutant SOD1 mice
A: Serotonin levels in the hypothalamus of SOD1(G86R) mice (black columns, SOD1m) and control littermates (white columns, wt) (n=5 at 75 days and n=5 at onset). One- way ANOVA followed by Tukey post hoc test.
B: Serotonergic innervation in the arcuate nucleus. GFP immunohistochemistry was performed on Tph2-YFP mice on arcuate nucleus cuts after identification on Paxinos Brain Atlas (scheme of identified regions, in red, in the upper left column, a). Representative images are shown for SOD1(G86R) Tph2-YFP mice and control littermates at onset at two magnifications (scale bar 200 µm (middle row), 20µm (lower row)) Serotonergic innervation in the arcuate nucleus were scored by a blind observer in SOD1m mice at symptom onset (b-f, n=4) as compared with their wt littermates. **p<0.005, Student's t-test.
C: mRNA levels of 5HT2C receptor in the hypothalamus of SOD1(G86R) mice (black columns, SOD1m) at 75 days of age and onset and in control littermates (white column, wt) (n=8). **p<0.01, One-way ANOVA
D: Food intake was measured one hour after refeeding in SOD1(G86R) mice (SOD1m) at 80 days of age and control littermates (wt) after fluoxetine 20mg/kg body weight (red columns) or vehicle (blue columns) injection (n=38). **p<0.005, Multiple t-test.
E: mRNA levels of POMC and AgRP in the hypothalamus of SOD1(G86R) mice (SOD1m) and control littermates (wt) at 85 days of age after fluoxetine 20mg/kg body weight (red columns) or vehicle (blue columns) injection (n=20). *p<0.05, One-way ANOVA.

202x200mm (300 x 300 DPI)

Table 4. FUS knockout and knockdown models

MODEL	GENETIC MODIFICATION	REMINISCENT TRUBCATED PROTEIN	SURVIVAL	ALS PHENO-TYPE	FTLD PHENO-TYPE	OTHER PHENOTYPE	REFERENCES
FUS KO	TLS gene interrupted inside exon 8	TLS–NEO fusion protein encoded by the targeted allele expressed at very low levels	Inbred 129svev background - early lethality Outbred background (with equal contribution of genes from the 129svev and CD1 strains - reduced size but developmentally normal	/	/	Sterile ; Increased sensitivity to ionizing irradiation; Loss ofhomologous DNA pairing and recombination	Kuroda M et al., EMBO J. 2000;19(3):453–62.
FUS KO	Provirus disrupted exon 12 of Fus, resulting in a null mutation	Low levels of a truncated Fus protein were also present	Mice homozygous for the Fus mutation fail to suckle, and die within 16 hours of birth; Only one Fus–/– mouse survived 2.5 days	/	/	The smallest in the litter, Develop normally; B lymphocyte deficiency; Genomic instability	Hicks GG, et al. Nat Genet. 2000;24(2):175–9.
FUS KO	Gal-neo cassette in between exon 2 and 3 of Fus gene	?	?	?	?	Loss of Gem formation and spliceosome integrity	Tsuiji Het al., EMBO Mol Med. 2013;5(2):221–34.

MODEL	GENETIC MODIFICATION	REMINISCENT TRUBCATED PROTEIN	SURVIVAL	ALS PHENO-TYPE	FTLD PHENO-TYPE	OTHER PHENOTYPE	REFERENCES
FUS KO	Hicks' black-6 animals crossed with another strain – white ICR mice	?	2 years	NO	Histological and behavioral alteration including vacuolation in hippocampus hiperreactivityand reduction in anxiety-like behavior:	Smaller size: Boldness	Kino Y et al, Acta Neuropathol Commun 2015;3(1):1–11.
FUS KD	Adeno-associated viruses (AAVs) expressing shFUS were stereotactically injected into the mouse hippocampus	FUS depletion	?	?	Behavioural phenotypes related to novelty-induced hyperactivity and disinhibition; Preserved learning and memory	?	Udagawa T et al., Nat Commun 2015;6(May):7098.

Table 5. Models with overexpression of wild type or mutant FUS

GENE	GENETIC MODIFICATION	EXPRESSION	TISSUE EXPRESSION	FUS LOCALIZATION	ALS-LIKE PHENOTYPE	FTD-LIKE PHENOTPYE	INCLUSIONS/ aggregation	COLOCALIZATION WITH FUS	NEUROINFLAMATION	REFERENCES
hWTFUS	RATS FUS, under tight control by Doxycycline (Dox)+CAG-tTA transgenic line	↑↑↑	Ubiquitinosly	Nuclear	NO	Loss of neurons in the cortex and hippocampus deficit in spatial learning and memory	Ubiquitin aggregation NO typical FUS inclusion	NO	Glial reaction in the brain and spinal cord	Huang C et al. PLoS Genet. 2011;7(3).,
hFUSR521C		↑↑↑		Nuclear and minimaly cytoplasmic	Preserved motor neurons progressive paralysis, denervation atrophy of skeletal muscles	Loss of neurons in the cortex and hippocampus				

GENE	GENETIC MODIFICATION	EXPRESSION	TISSUE EXPRESSION	FUS LOCALIZATION	ALS-LIKE PHENOTYPE	FTD-LIKE PHENOTPYE	INCLUSIONS/ aggregation	COLOCALIZATION WITH FUS	NEUROINFLAMATION	REFERENCES
hWTFUS	MICE FUS, under tight control of the mouse prion protein (PrP) promoter	↑↑↑ Loss of endogenous murine FUS	Ubiquitinosly	Nuclear and increased cytoplasmic	Loss of large motor neurons progressive paralysis, denervation atrophy of skeletal muscles	/	Cytoplasmic FUS inclusions ubiquitin-negative	/	Astroglial and microglial in spinal cord and to lesser extent in brain	Mitchell JC et al. Acta Neuropathol. 2013;125(2):273–88.
hWTFUS	MICE Somatic brain transgenesis (SBT)	↑↑↑	Cerebral cortex and the hippocampus with no detectable glial expression	Nuclear	NO Lack of a motor phenotype or neurodegeneration	NO Lack of a motor phenotype or neurodegeneration	NO		NO	Verbeeck C et al. Molecular Neurodegeneration; 2012;7(1):53.
hFUSR521C		↑↑↑		Increased FUS protein in the neuronal cytoplasm			NO			
FUS Δ14		↑↑↑		Increased FUS protein in the neuronal cytoplasm			FUS cytoplasmic inclusions positive for ubiquitin, p62/SQSTM1	YES		

GENE	GENETIC MODIFICATION	EXPRESSION	TISSUE EXPRESSION	FUS LOCALIZATION	ALS-LIKE PHENOTYPE	FTD-LIKE PHENOTPYE	INCLUSIONS/ aggregation	COLOCALIZATION WITH FUS	NEUROINFLAMATION	REFERENCES
hFUSR521C Camk2a-tTA	RATS	↑↑↑	Restrictedly in neurons of the forebrain No glia expression	Gradual development of FUS mislocalization	/	Impaired rats' spatial memory; severe loss of neurites and dendritic spines; progressive loss of neurons in the superficial layers II and III of cortex	Ubiquitin aggregation NO typical FUS inclusion	NO	Reactive microglia and astrocytes firsty detected in the layers II and III of frontal cortex	Huang C et al. Hum Mol Genet. 2012;21(21):4602–14.
hFUS1-359 truncated	MICE Thy-1 promoter ,,nervous system specific,,	Lower level than the endogenous mouse FUS	Spinal cord, brainstem and cortex	Nuclear and increased cytoplasmic	Spinal motor neuronal loss and selective loss of LMN in the brainstem and denervation of NMJ; Gait impairment asymmetrical pareses and eventual complete paralyzes of limbs, musle atrophy	/	FUS-positive inclusions sometimes ubiquitinated lower and upper motor neuron cell bodies, axons and in the nucleus	YES/NO	Profound neuroinflammation	Shelkovnikova T et al.J Biol Chem. 2013;288(35):25266–74.

GENE	GENETIC MODIFICATION	EXPRESSION	TISSUE EXPRESSION	FUS LOCALIZATION	ALS-LIKE PHENOTYPE	FTD-LIKE PHENOTPYE	INCLUSIONS/ aggregation	COLOCALIZATION WITH FUS	NEUROINFLAMATION	REFERENCES
FLAG-tagged FUS-R521C	Syrian hamster prion promoter	↑↑↑ hFUSR521C ↑↑↑ endogenous mouse FUS	?	Dominantly nuclear but with presence in cytoplasm Reduction of endogenous FUS In neuronal nuclei and in punctate synaptic structures	Progressive, age-dependent loss of spinal cord motor neurons; No cortical layer specific motor neurons loss; Partial and complete denervation of NMJ; Severe dendritic and synaptic defects in spinal motor neurons and cortical neurons; Gait and motor coordination defects;	/ Severe dendritic and synaptic defects in cortical neurons	NO	NO	Prominent microgliosis and modest astrogliosis	Qui H et al. J Clin Invest. 2014;124(3):981-99

Résumé étendu de la thèse en français

Troncation conditionnelle de la protéine FUS chez la souris: un nouveau modèle animal du continuum sclérose latérale amyotrophique/démence fronto-temporale

Jelena Scekic-Zahirovic

Thèse soutenue le 11 janvier 2016

Contexte du travail de thèse

Sclérose latérale amyotrophique et démence fronto-temporale

La sclérose latérale amyotrophique (SLA) est une maladie neurodégénérative caractérisée par la perte des motoneurones spinaux et bulbaires, ainsi que des neurones moteurs supérieurs. Elle se traduit par une atrophie et une paralysie progressives des muscles squelettiques, et au décès des patients 3 a 5 ans apres le diagostic initial. Les premiers symptômes de SLA apparaissent généralement entre 50 et 60 ans, mais les formes les plus précoces peuvent débuter avant 20 ans.

Une partie des cas de SLA (10-20%) est d'origine familiale (SLAf), tandis que la majeure partie des cas ne présente pas d'histoire familiale (SLA sporadique). Des mutations de cinq gènes principaux (*Sod1*, *Fus*, *Tardbp, Tbk1* et *C9orf72*) sont responsables de plus de la moitié des cas de SLAf.

La démence fronto-temporale (DFT) est un autre type de maladie neurodégénérative qui se caractérise par des pertes neuronales au niveau des lobes frontaux et temporaux du cortex cerebral, et par l'atrophie de ces régions du cerveau. Les symptômes cliniques de la DFT sont des atteintes cognitives et des changements du comportement et de la personnalité. Les premiers symptômes de la DFT apparaissent vers la soixantaine, et les patients progressent vers une apathie à un stade terminal de la maladie entre 3 et 5 ans après les premiers symptômes.

La DFT présente une composante génétique plus forte que la SLA, puisque près de la moitié des patients DFT présentent une histoire familiale. Deux gènes identifiés initialement, ceux de la protéine associée aux microtubules TAU et de la la progranuline (PGRN) sont associés à 10 à 20% des cas de DFT. Plus récemment des mutations dans les gènes *C9ORF72* et *TBK1* ont été mises en évidence dans des formes familiales de DFT.

La SLA et la DFT ont été traditionnellement considérées comme deux maladies neurologiques distinctes, en raison de symptômes cliniques différents. Cependant, des données cliniques, anatomo-pathologiques et génétiques récentes montrent une convergence entre ces deux maladies. Premièrement, SLA et DFT se présentent sous la forme d'un continuum : 15% des patients SLA développent une DFT typique, et la même proportion de patients DFT développe des signes d'atteinte du motoneurone. SLA et DFT sont donc deux phénotypes extrêmes d'un continuum clinique. Deuxièmement, SLA et DFT se caractérisent toutes les deux par des dépôts protéiques insolubles, caractéristiques et similaires. En effet, plus de 90% des cas de SLA et plus de 50% des cas de DFT présentent des inclusions pathologiques dont les principaux composants sont les protéines TDP43 (TAR DNA binding protein, encodé par le gène *Tardbp*) et FUS (Fused in sarcoma), deux protéines de liaison à l'ARN et régulant de nombreuses étapes du métabolisme de l'ARN. SLA et DFT représentent donc deux maladies avec des signatures anatomo-pathologiques identiques. Enfin, les mutations des gènes *Fus*, *Tardbp, Tbk1* et *C9orf72* ont été associées aussi bien à des formes familiales de SLA que des formes familiales de DFT. Au sein d'une même famille, une mutation identique peut provoquer un tableau clinique de SLA, de DFT ou de SLA associée à une DFT. Par delà ces mutations communes, il est intéressant de noter que la protéine FUS, qui est retrouvée dans des agrégats protéiques chez certains patients atteints de SLA ou de DFT, régule le métabolisme de l'ARN messager de la protéine TAU, qui est elle aussi impliquée dans la DFT. Les différentes causes de SLA et de DFT sont donc reliées entre elles dans un réseau de gènes cohérent.

Ces découvertes récentes suggèrent donc que SLA et DFT peuvent être considérées comme deux extrêmes d'un continuum clinico-pathologique unique, appelé "SLA/DFT", causé par des altérations du métabolisme de l'ARN.

Les mutations de FUS : mécanismes de toxicité

Les mutations des gènes *Fus* et *Tardbp* résultent typiquement en une perte de la localisation nucléaire des protéines correspondantes (FUS et TDP43), et une séquestration de ces protéines au sein d'agrégats cytoplasmiques.

Les observations anatomo-pathologiques montrent que les agrégats de protéine TDP-43 ou FUS sont observés dans le cytoplasme des neurones. Dans ces mêmes neurones, la protéine n'est plus observée dans le noyau, sa localisation physiologique. Ceci montre que deux événements accompagnent l'agrégation de ces protéines : (i) une augmentation de la localisation cytoplasmique, (ii) une clairance de la localisation nucléaire. Il n'est pas connu si la cause de la neurodégénérescence est l'augmentation de la concentration cytoplasmique de FUS ou TDP-43 ou la perte de la protéine dans le noyau.

L'effet des mutations géniques de TDP-43 sur la localisation cytoplasmique de la protéine n'est pas clair, et les études sur ce point contradictoires. Au contraire, il est clairement démontré que les mutations de FUS diminuent l'entrée de la protéine dans le noyau. Plus spécifiquement, les mutations les plus sévères, qui peuvent amener à des SLA débutant à l'adolescence, sont provoquées par des mutations de FUS provoquant la troncation C-terminale de la protéine. Les 15 derniers acides aminés de FUS sont cependant critiques pour l'import nucléaire de FUS, et constituent une séquence de localisation nucléaire (NLS) atypique (PY-NLS). Les mutations de FUS associées à une SLA présentent une excellente corrélation entre phénotype et génotype, avec un phénotype clinique d'autant plus sévère que la mutation est proche ou affecte la PY-NLS.

Au cours de ce travail de thèse, je me suis intéressée plus particulièrement au gène *Fus* et à la protéine qu'il encode. En conditions physiologiques, la protéine FUS circule entre le noyau et le cytoplasme grâce à un signal de localisation nucléaire atypique (NLS) situé dans la partie C-terminale de la protéine. La redistribution sub-

cellulaire de FUS, d'une forme soluble et nucleaire à une forme insoluble et cytoplasmique constitue la « FUSopathie », qui caractérise aussi bien de nombreux cas de SLA et de DFT, sans pour autant résulter d'une mutation de *Fus*. En effet, les si mutations de *Fus* sont bien représentées dans les cas de SLAf, elles sont très rares chez les patients DFT. Il est à présent bien établi que la « FUSopathie » est directement liée à la neurodégénérescence. Cependant, il reste à déterminer de quel aspect de la FUSopathie découle l'événement pathogénique primaire : une perte de la fonction nucléaire de FUS, un gain de fonction cytoplasmique, ou une combinaison des deux ?

Modélisation animale de la SLA FUS

Pour modéliser la SLA liée à FUS, différentes lignées de souris génétiquement modifiées ont été créées.

Deux lignées de souris knock-out pour *Fus* ont été générés mais les résultats qui en découlent sont contradictoires. Un modèle est associé à un décès périnatal des souris, tandis que l'autre modèle n'a pas observé de mort prématuré. De plus, ces deux modèles ne permettent pas de conclure sur le rôle de la perte de fonction nucléaire de *Fus* dans la maladie car ils expriment tous deux une protéine résiduelle tronquée qui pourrait être toxique.

Par ailleurs, plusieurs modèles surexprimant des formes sauvages ou mutées de *Fus* ont été produits. Ces modèles animaux développent des maladies rapides, qui pourraient ressembler à la SLA. Cependant, la forme sauvage de FUS semble aussi, voire plus toxique que la forme mutée quand elle est surexprimée. Ceci suggère que le phénotype de ces animaux résulte d'une toxicité liée à la surexpression, sans lien direct avec la maladie. Par ailleurs, la surexpression ne modifie pas la localisation sub-cellulaire de FUS, qui demeure majoritairement nucléaire et ne reproduit pas la FUSopathie observée chez les patients. Enfin, il est important de noter également que la surexpression de la forme sauvage de *Fus* est en tant que telle extrêmement toxique et provoque des phénotypes variés, peu pertinents pour la SLA ou la DFT.

Au début de ce travail de thèse, les contributions respectives de la perte de fonction nucléaire et du gain de fonction cytoplasmique de FUS dans la SLA et la DFT étaient inconnues et la relation entre FUSopathie et neurodégénérescence peu clairs.

Problématique de la thèse

L'objectif de mon travail de thèse a été de comprendre en quoi la localisation cytoplasmique de FUS pouvait avoir une importance dans la physiopathologie de la maladie. Pour cela, nous avons développé et caractérisé un nouveau modèle murin et répondu aux deux questions suivantes:

1) quelles sont les contributions respectives de la perte de fonction nucléaire de FUS d'une part, et du gain de fonction cytoplasmique de FUS d'autre part, au déclenchement d'une maladie SLA/DFT ?

2) la perte partielle de localisation nucléaire de FUS serait-elle suffisante pour provoquer une SLA/DFT ?

Résultats principaux

Pour dépasser les problèmes liés aux modèles animaux existants basés sur *Fus*, nous avons généré, par recombinaison homologue, une lignée de souris exprimant une forme tronquée de *Fus*, dépourvue de la séquence de localization nucléaire : les souris *Fus-ΔNLS*. Pour ce faire, nous avons créé un allèle conditionnel de *Fus* n'exprimant pas la séquence NLS encodée par l'exon 15. Précisémment, nous avons inséré, au sein de l'intron 13, un ADNc codant pour les exons 13 et 14, ainsi que 3 cassettes "STOP". Cet ADNc a été flanqué de sites loxP, permettant en outre un retour à l'expression sauvage de *Fus,* en presence de recombinase Cre. La stratégie génétique est présentée en figure 1A.

Les deux publications principales de ma thèse sont basées sur la caractérisation des souris homozygotes, $Fus^{\Delta NLS/\Delta NLS}$, et hétérozygotes, $Fus^{\Delta NLS/+}$, respectivement.

Publication N°1 (publiée dans EMBO Journal, Scekic-Zahirovic, 2016)

Les souris $Fus^{\Delta NLS/+}$ sont viables et fertiles, alors que les souris homozygotes $Fus^{\Delta NLS/\Delta NLS}$ meurent à la naissance (Figure 1B). L'ARN porteur de la mutation *ΔNLS* est facilement détecté par RT-PCR chez les souris $Fus^{\Delta NLS/+}$et $Fus^{\Delta NLS/\Delta NLS}$, et l'ARN de *Fus* n'est pas diminué, ce qui montre que l'allèle *ΔNLS* n'est pas haplo-insuffisant (Figure 1C). A l'appui de ces résultats, un fort signal FUS est observé en western blot dans des extraits protéiques de cerveau de souris $Fus^{+/+}$, $Fus^{\Delta NLS/+}$ et $Fus^{\Delta NLS/\Delta NLS}$ lorsque l'on utilise des anticorps ciblant la partie N-terminale de FUS (Figure 1D). A l'inverse, nous n'avons observé aucun signal dans des extraits de tissus de souris $Fus^{\Delta NLS/\Delta NLS}$ en utilisant des anticorps qui ciblent la NLS de FUS (partie C-terminale). Ceci démontre que l'allèle $Fus^{\Delta NLS}$ encode bien une protéine FUS tronquée de sa NLS. De façon cohérente avec l'ablation de la NLS, le signal obtenu pour FUS en immunocytochimie ou immunohistochimie est entièrement cytoplasmique chez les $Fus^{\Delta NLS/\Delta NLS}$, et totalement nucléaire pour les souris $Fus^{+/+}$ (Figure 1E).

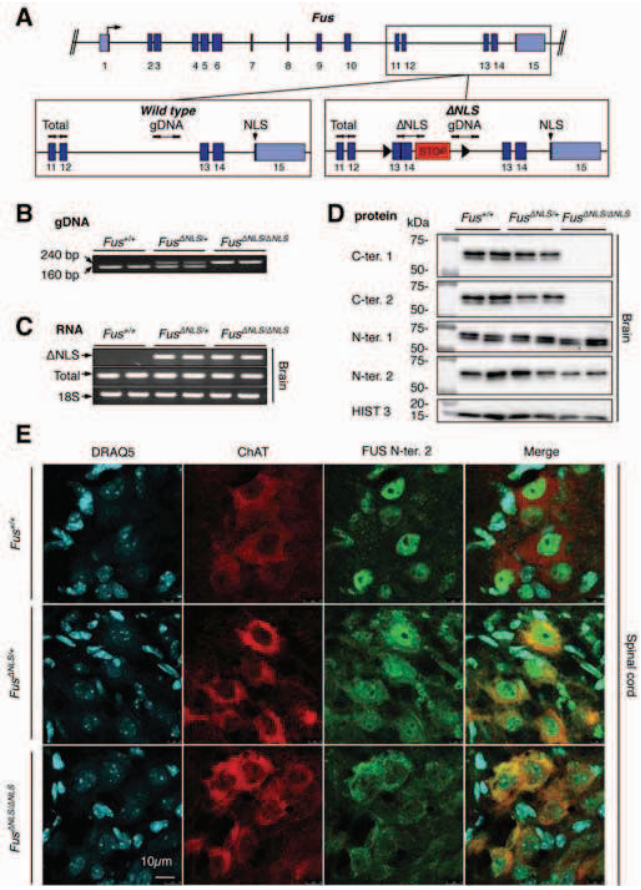

Figure 1 : caractérisation des souris Fus ΔNLS

A : stratégie génétique
B : résultats typiques de génotypage
C : RT-PCR montrant l'expression de la forme tronquée de FUS.
D : résultats typiques d'immunoempreinte pour FUS dans le cerveau des souris des génotypes indiqués.
E : double immunofluorescence montrant la ChAT (rouge) et FUS (vert) dans la partie ventrale de la moelle épinière des souris de génotypes indiqués.

Les souris *Fus*$^{\Delta NLS/\Delta NLS}$ meurent quelques minutes après la naissance (Figure 2A). Elles sont plus légères (Figure 2B) et plus petites (Figure 2C). La cause du décès est une insuffisance respiratoire, car les poumons ne se gonflent pas à la naissance (Figure 2D).

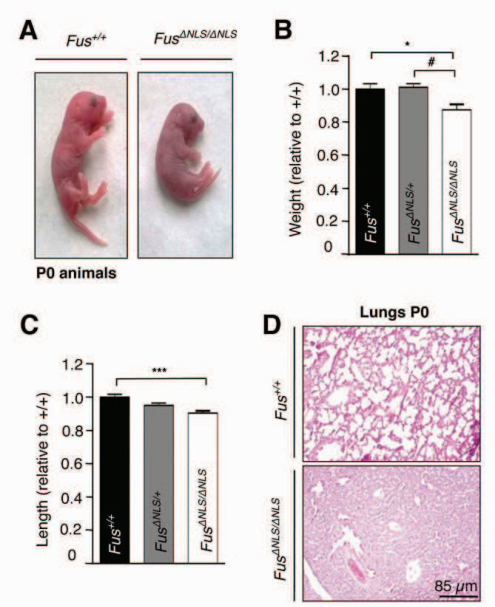

Figure 2 : les souris Fus ΔNLS homozygotes meurent à la naissance

A : phénotype des souris de génotypes indiqués
B : poids des souris de génotype indiqué
C : taille des souris de génotype indiqué
D : histologie pulmonaire des souris de génotype indiqué.

Nous avons cherché à comprendre si une perte complète de FUS pouvait reproduire ce phénotype. Pour cela, nous avons créé une nouvelle lignée de souris Fus knock-out (stratégie en Figure 3A). Ces souris n'expriment pas de protéine ou d'ARN FUS (Figure 3B-E), et meurent à la naissance avec un phénotype similaire aux souris homozygotes ΔNLS (Figure 3F-G).

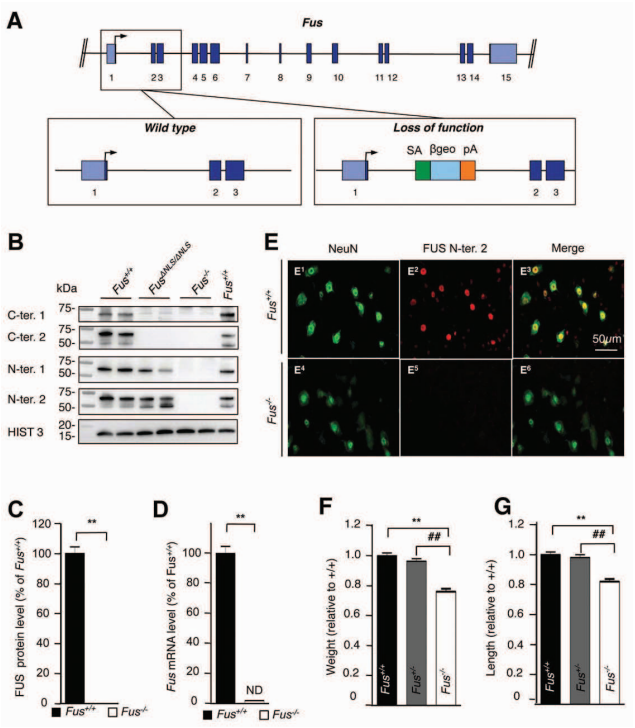

Figure 3 : caractérisation des souris Fus knock out

A : stratégie génétique
B: résultats typiques d'immunoempreinte pour FUS dans le cerveau des souris des génotypes indiqués.
C : niveaux protéiques
D : niveaux d'ARNm
E : double immunofluorescence montrant NeuN (vert) et FUS (rouge) dans la partie ventrale de la moelle épinière des souris de génotypes indiqués.
F : poids des souris de génotype indiqué
G : taille des souris de génotype indiqué

Pour déterminer si cette analogie phénotypique se doublait d'une analogie moléculaire, nous avons réalisé une étude par RNAseq (Figure 4 Scekic-Zahirovic et al. EMBO J) et RASLseq (Figure 5 Scekic Zahirovic et al., EMBO J) des deux souches de souris. Nous avons constaté qu'une grande partie des altérations de niveaux d'ARNm étaient communes aux deux souches, ce qui montre que la délocalisation cytoplasmique de FUS provoque une perte de sa fonction de régulation de la transcription et de l'épissage.

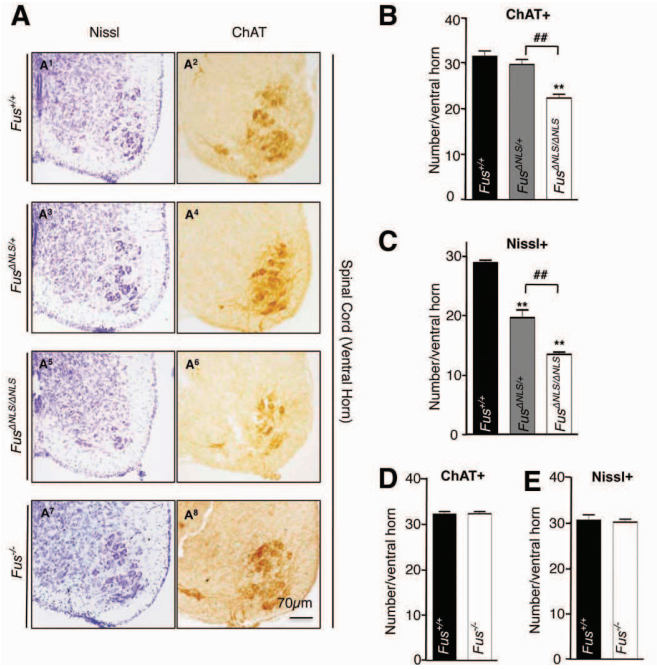

Figure 6 : caractérisation des motoneurones des souris Fus ΔNLS et Fus knock out

A : coloration au Nissl (gauche) ou immunohistochimie pour la ChAT (droite) dans la moelle épinière des souris de génotype indiqué
B-E : quantifications du nombre de motoneurones.

Les souris *Fus*$^{\Delta NLS/\Delta NLS}$ présentent un phénotype neuromusculaire marqué, caractérisé par une perte de jonctions neuromusculaires et une perte de motoneurones spinaux. Les jonctions neuromusculaires des souris *Fus*$^{\Delta NLS/\Delta NLS}$ sont moins nombreuses et plus petites. La plupart des jonctions restantes demeurent positives pour le marqueur axonal SV2. Cependant, au niveau ultra-structural, ces jonctions présentent des signes évidents de dégénérescence. Les défauts des jonctions neuromusculaires sont en outre associés à une diminution du nombre de motoneurones (Figure 6), et à une augmentation du nombre de motoneurones présentant des signes d'apoptose (Figure 7). Il est important de noter que les souris *Fus*$^{-/-}$, par contre, ne présentent pas de perte de motoneurones.

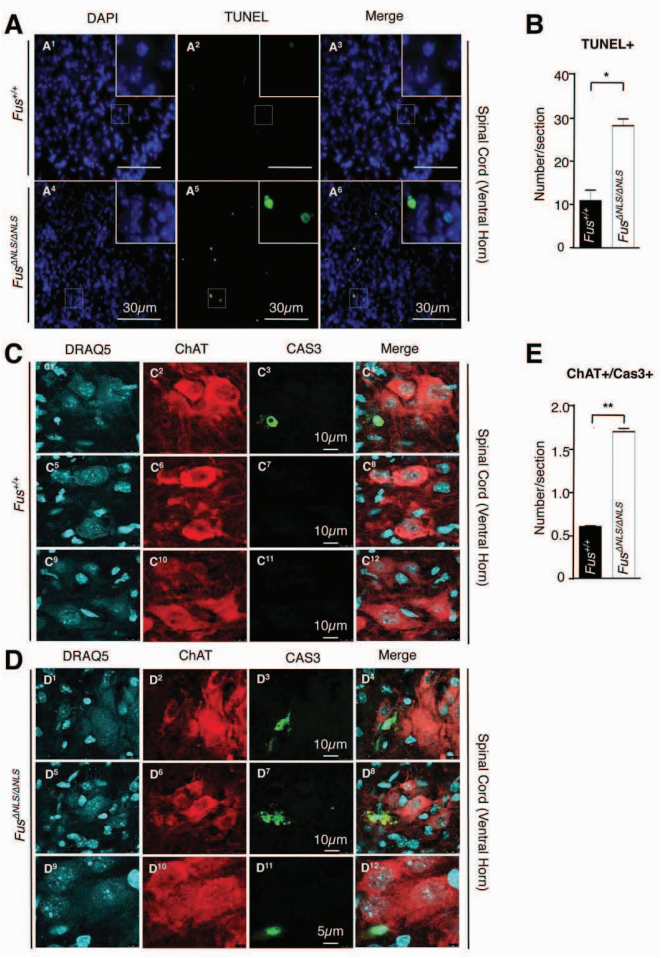

Figure 7 : apoptose des motoneurones des souris Fus ΔNLS

A B : coloration TUNEL

C-E : immunofluorescence pour la Chat (rouge) et la caspase 3 active (vert) dans la moelle épinière des souris de génotypes indiqués.

La localisation cytoplasmique de FUS dans les souris *Fus*$^{\Delta NLS/\Delta NLS}$ peut être réversée par action de la CRE recombinase. Nous avons donc cherché à déterminer si le phénotype motoneuronal observé chez nos souris était lié à une action de la protéine tronquée dans le motoneurone lui-même. Pour cela, nous avons croisé nos souris *Fus*$^{\Delta NLS/\Delta NLS}$ avec des souris *ChAT-CRE* exprimant la CRE dans les neurones cholinergiques (dont les motoneurones). La localisation de FUS a été restaurée dans les motoneurones, mais pas dans les neurones de la corne dorsale de la moelle épinière, non cholinergiques. De façon intéressante, la présence de l'allèle *ChAT-CRE* a réversé la perte de motoneurones et l'atteinte des jonctions neuromusculaires (Figure 9).

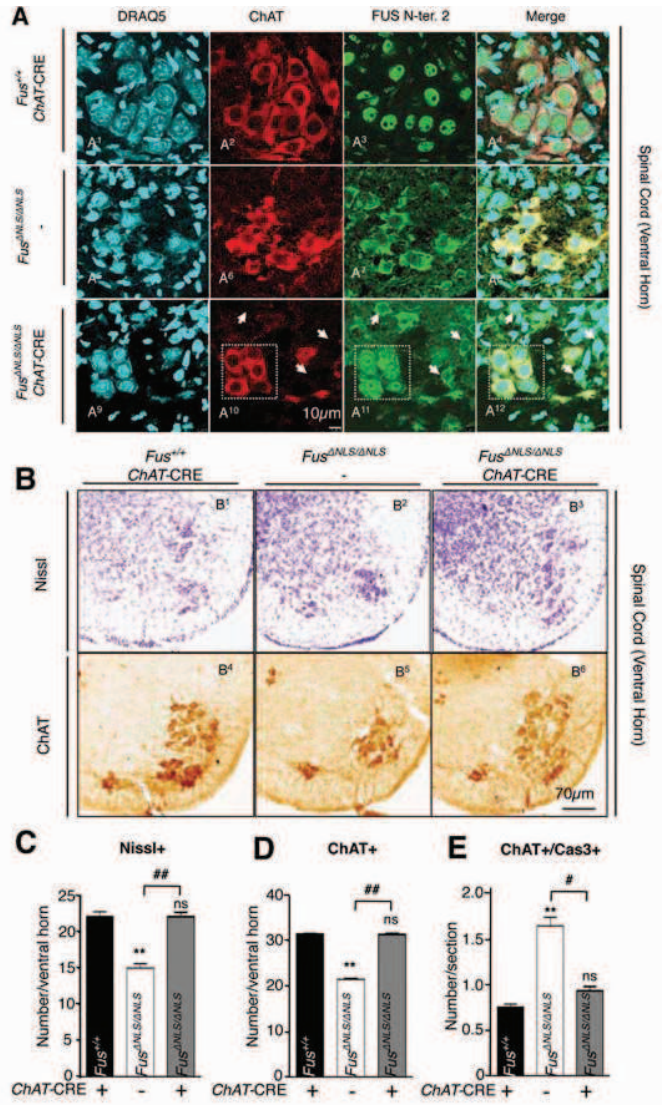

Figure 9 : effet de l'expression de la CRE dans les motoneurones sur la dégénérescence chez les Fus ΔNLS

A : immunofluorescence pour la Chat (rouge) et FUS (vert) dans la moelle épinière des souris de génotypes indiqués.
B : coloration au Nissl (haut) ou immunohistochimie pour la ChAT (bas) dans la moelle épinière des souris de génotype indiqué
C-E : quantifications du nombre de motoneurones et des motoneurones caspase 3 +.

Nos données rassemblées dans cette publication montrent que la localisation cytoplasmique de FUS amène à la mort des motoneurones *via* un gain de fonction dans les motoneurones eux-mêmes.

Publication N°2 (en préparation)

Nous avons ensuite cherché à déterminer si une localisation cytoplasmique partielle de FUS était suffisante pour développer un phénotype pertinent pour la SLA et/ou la DFT. Pour cela, nous avons étudié une grande cohorte de souris hétérozygotes *Fus*$^{\Delta NLS/+}$. Nous avons suivi longitudinalement ces animaux pendant près de deux ans. Nous avons observé un déficit moteur léger (inverted grid test) à partir de 10 mois d'âge. L'analyse de la démarche par Catwalk confirme ces anomalies motrices légères. Les souris *Fus*$^{\Delta NLS/+}$ présentent également une diminution de la surface des jonctions neuromusculaires et une apparition d'activités spontanées de dénervation par eletromyographie, ce qui démontre un phénotype neuromusculaire léger mais significatif. Ce phénotype s'accompagne d'une perte des motoneurones à 22 mois. Les souris *Fus*$^{\Delta NLS/+}$ reproduisent donc les caractéristiques principales atténuées d'une SLA-FUS.

La protéine FUS est également impliquée dans une fraction des cas de DFT. Pour tester l'hypothèse d'une potentielle atteinte fronto-temporale des souris *Fus*$^{\Delta NLS}$*/+,* nous avons procédé à une série de tests comportementaux adaptés. Les souris *Fus*$^{\Delta NLS/+}$ se comportent normalement dans la piscine de Morris, suggèrant qu'elles n'ont pas de défauts majeurs de fonctionnement de l'hippocampe. Cependant, le rappel à long terme (18 jours) de cette mémoire est déficient, ce qui suggère une altération du « dialogue » entre l'hippocampe et le cortex frontal. De façon cohérente avec ces données, les souris *Fus*$^{\Delta NLS/+}$ présentent des anomalies dans le cadre de différents tests d'interaction sociale. Enfin, le cortex fronto-temporal de ces souris apparait visiblement atrophié. En résumé, les souris *Fus*$^{\Delta NLS/+}$ récapitulent un certain nombre de symptômes de DFT.

Conclusions

Les résultats obtenus au cours de cette thèse ont démontré que la localisation cytoplasmique de FUS est plus toxique pour les motoneurones que la perte de fonction compète de la protéine. Ceci démontre que la maladie liée à FUS implique, au moins en partie, un gain de fonction toxique de la protéine lorsqu'elle est retenue dans le cytoplasme. Par ailleurs, nous avons caractérisé un nouveau modèle de souris qui présente à la fois des phénotypes d'atteinte du motoneurone et du cortex fronto-temporal. Ces différents modèles permettront des études mécanistiques pour comprendre les bases des FUSopathies et pourront permettre de développer des stratégies thérapeutiques pour ces maladies dévastatrices.

Production scientifique

Publications directement liées au travail de thèse

1. **Scekic-Zahirovic J**., Sendscheid O., El Oussini H., Jambeau M., Ying S., Mersmann S., Wagner M., Dieterlé S., Sinniger J., Dirrig-Grosch S., Drenner K., Birling M.C., Qiu J., Zhou Y., Li H., Fu X.D., Rouaux C., Shelkovnikova T., Witting A., Ludolph A.C., Kiefer F., Storkebaum E., Lagier-Tourenne C. & Dupuis L.

   Toxic gain of function from mutant FUS protein is crucial to trigger cell autonomous motor neuron loss

   EMBO Journal DOI 10.15252/embj.201592559

1. **Scekic-Zahirovic J et al.**

   Partial cytoplasmic mislocalization of truncated FUS protein in mice recapitulates the phenotypes of ALS and FTD.

   in preparation

Publication annexe au travail de thèse

Vercruysse P, Sinniger J, El Oussini H, **Scekic-Zahirovic J**, Dieterlé S, Dengler R, Meyer T, Zierz S, Kassubek J, Fischer W, Dreyhaupt J, Grehl T, Hermann A, Grosskreutz J, Witting A, Van Den Bosch L, Spreux-Varoquaux O, Ludolph A.C. & Dupuis L.

Alterations in the hypothalamic melanocortin pathway in amyotrophic lateral sclerosis**,**

Brain. 2016, in press

El Oussini H, Bayer H, **Scekic-Zahirovic J**, Vercruysse P, Sinniger J, Dirrig-Grosch S, Dieterlé S, Echaniz-Laguna A, Larmet Y, Müller K, Weishaupt JH, Thal DR, van

Rheenen W, van Eijk K, Lawson R, Monassier L, Maroteaux L, Roumier A, Wong PC, van den Berg LH, Ludolph AC, Veldink JH, Witting A & Dupuis L.

Serotonin 2B receptor slows disease progression and prevents degeneration of spinal cord mononuclear phagocytes in amyotrophic lateral sclerosis

Acta Neuropathol. 2016, 131(3):465-80

Han SM, El Oussini H, **Scekic-Zahirovic J**, Vibbert J, Cottee P, Prasain JK, Bellen HJ, Dupuis L, Miller MA.

VAPB/ALS8 MSP ligands regulate striated muscle energy metabolism critical for adult survival in caenorhabditis elegans. PLoS Genet. 2013;9(9):e1003738. doi: 10.1371/journal.pgen.1003738. Epub 2013 Sep 5.

Communications orales

1. Modelling amyotrophic lateral sclerosis in mice using gene targeting in ALS8/VAPB and ALS6/FUS. **Ecole Doctorale Day**. Janvier, 2012

2. Abolishing nuclear import of FUS leads to motor neuron loss and axonal degeneration in a novel knock-in mouse model. 12th annual **ENCALS Meeting**, Mai, 2014 – (premier prix, meilleure présentation orale du congrès)

3. Consequences of loss of nuclear import of FUS on motor neurons: insight from conditional knock-in mice. **Echange Franco-Quebecois**, Octobre, 2014

4. A new mouse model of amyotrophic lateral sclerosis and fronto-temporal dementia based on the *Fus* gene. **Journées Scientifiques de la Fédération de Médecine Translationnelle de Strasbourg** - FMTS, Avril, 2015, prix de la meilleure présentation orale.